Ionic complexes of biodegradable polyelectrolytes

Ph.D. Thesis presented by Ainhoa Tolentino Chivite
Directed by Prof. Sebastián Muñoz Guerra
Barcelona, March 2014

Tesis presentada para obtener el título de Doctor por la Universitat Politècnica de Catalunya
Doctorado en Polímers i Biopolímers

Departament d'Enginyeria Química
Escola Tècnica Superior d'Enginyeria Industrial de Barcelona (ETSEIB)
Universitat Politècnica de Catalunya (UPC)

Summary

Biopolymers are polymers produced by living organisms. According to the chemistry of the monomer, a basic classification of biopolymers includes polysaccharides (sugars), polypeptides (proteins), polynucleotides (nucleic acids), polyterpenes, and microbial polyesters and polyamides. A more comprehensive classification would embrace also those polymers synthesized from renewable sources which are able to display biodegradable properties.

The demand of biopolymers has been continuously growing along these last decades at a rate even higher than that of petrochemical polymers. The main reason for such exceptional increasing interest is their sustainability; the renewable origin of biopolymers makes them inexhaustible in contrast with the uncertain accessibility at medium-term of synthetic polymers produced from fossil sources. Biodegradability is a second advantage afforded by biopolymers; due to the presence in the nature of enzymes able to degrade them under environmental conditions and within relatively short periods of times to give non-toxic products, their impact on the environment is essentially negligible. Finally, to point out the great attention that is being currently given to more or less modified biopolymers in the use as biomaterials, which is undoubtedly due to their distinguishing properties of biocompatibility and biodegradability. As a result of all these driving considerations, great efforts in the research of biopolymers including chemical modification, characterization and property evaluation are today being carried out to develop new materials able to replace traditional plastics in a wide diversity of applications.

In the present Thesis, a selection of carboxylic biopolymers has been studied for their capacity to form stable ionic complexes with cationic surfactants suitable to render new materials with advanced properties. Previous studies on polyelectrolyte-surfactant complexes carried out in our group have demonstrated that these coupled systems tend to be self-assembled in well-ordered structures that can be exploited for building films and particles with singular properties as biomaterials.

The main goal of this Thesis is the study of polyelectrolyte-ionic complexes based on naturally occurring polyacids and cationic surfactants. One part of the work is devoted to deep into the complexes of poly(γ-glutamic acid), a system that has been object of continuous research in our group for more

than one decade. The aim is to progress in the development of poly(glutamic acid) complexes by making them “greener” through coupling with bio-based surfactants, and by improving their basic properties through blending with nanoclays. The other part is dedicated to explore the ionic complexes made from poly(uronic acid)s and cationic surfactants. This is the first time that such complexes are examined and their structural features and properties compared to those displayed by complexes based on poly(glutamic acid).

From the experimental point of view, the Thesis embodies a multidisciplinary task work that includes the preparation, structural characterization and evaluation of thermal properties of a series of ionic complexes, as well as a preliminary assessment of the suitability of some of them to be used as drug delivery systems.

Hence, the specific objectives in this Thesis are enumerated as follows:

1. Synthesis and chemical characterization of ionic complexes of poly(uronic acid)s (pectinic, alginic and hyaluronic acids), with trimethylalkylammonium surfactants of ***n***= 18, 20 and 22. Structural and thermal analysis of these complexes and critical comparison of results with those available for complexes made of poly(glutamic acid).

2. Synthesis and characterization of choline-based surfactants for the preparation of fully bio-based polyglutamic complexes as an alternative to complexes based on trimethylalkylammonium surfactants in their potential use as biomaterials. Structural and thermal analysis of these complexes and their preliminary evaluation as nano-particulated drug delivery systems.

3. Preparation of composites of poly(glutamic acid)-cationic surfactant complexes with organo-modified nanoclays, their extensive structural characterization and the evaluation of their thermal and mechanical properties compared to those displayed by the neat complexes.

The Thesis is organized in five Chapters. After a very brief summary of the whole work with explicit definition of the objectives, Chapter I is an introduction to the subject, in which an extensively referenced account of the main hints previously achieved in the field is provided and the state-of-art is described.

The following three Chapters correspond to the three specific objectives enumerated above. Chapter II gathers the synthesis, characterization and properties evaluation study carried out on ionic complexes of poly(uronic acid)s. Chapter III is focused on the study of ionic complexes of polyglutamic and alkanoylcholines, the synthesis and characterization of the surfactants, the preparation of their complexes with poly(glutamic acid) and their possibilities as potential biomaterials. Chapter IV covers the preparation of the composites made of Cloisite 30B and poly(glutamic acid) complexes along with a detailed study of their structure by X-ray diffraction, electron microscopy and modeling, and a correlative analysis of their structure with their thermal and mechanical properties.

Chapter V contains the whole collection of conclusions that have been drawn from the Thesis. The author's profile and published scientific production coming out from the Thesis constitute the body of the closing part.

Glossary

ACh	Alkanoylcholine
ATMA	Alkyltrimethlyammonium
ATR	Attenuated total reflectance
C14TAB	Tetradecyl trimethylammonium bromide
C16TAB	Hexadecyl trimethylammonium bromide
CAC	Critical aggregation concentration
CBZ	Carbamazepine
CEC	Cation exchange capacity
CL	Cloisite
cmc	Critical micelle concentration
coPGuMnA	Alginic acid
CP/MAS	Cross-Polarization Magic-Angle Spinning Nuclear Magnetic Resonance
CS	Chitosan
$\mathbf{d_{001}}$	Interplanar Bragg spacing
DDS	Drug delivery system
DMAE	Dimethylamino ethanol
DMAEA	Poly(dimethylaminoethyl acrylate)
DMF	*N,N*-Dimethylformamide
DMSO	Dimethyl sulfoxide
DNA	Deoxyribonucleic acid
DOX	Doxorubicin
DSC	Differential scanning calorimetry
ε	Elongation at break
E	Elastic modulus
ED	Esterification degree
EtOH	Etanol
FTIR	Fourier transform infrared spectroscopy
G	Guluronic acid unit
GAG	Glycosaminoglycans group
GlcA	Glucuronic acid
GlcNAc	Acetylglucosamine
GPC	Gel permeation chromatography
HFIP	1,1,1,3,3,3-hexafluoroisopropanol
HG	Homogalacturonan
HMPA	Hexamethylenphosphoramide
HyalA	Hyaluronic acid
IPEC	Interpolyelectrolyte complex
IR	Infrared spectroscopy
L or $\mathbf{L_0}$	Lamellar spacing
l	Alkanoyl tail length

LC	Liquid crystalline
M	Mannuronic acid unit
MeOH	Methanol
MMT	Montmorillonite
M_n	Number-average molecular weight
M_w	Weight-average molecular weight
n	Number of carbons in hydrocarbon chain
n.d.	Not determined
N6	Nylon 6
n_c	Number of crystallized methylenes
NMP	*N*-methyl-2-pyrrolidone
NMR	Nuclear magnetic resonance
OMLS	Organically modified layered silicate
P(D)GGA	Poly(γ,D-glutamic acid)
P(L)GGA	Poly(γ,L-glutamic acid)
PAE	Phenylalanine ethyl ester
PBS	Phosphate buffered saline
PBS	Poly(butylene succinate)
PC	Phosphatidylcholine
PCL	Poly(ε-caprolactone)
PE	Polyethylene
PEO	Poly(ethylene oxide)
PET	Poly(ethylene terephthalate)
PGaA	Poly(α,D-galacturonic acid)
PGGA	Poly(γ-glutamic acid)
PHA	Polyhydroxyalkanoate
PHB	Polyhydroxybutyrate
Ph-II	Structural phase at medium temperature
Ph-III	Structural phase at high temperature
Ph-Iα or Ph-Iβ	Structural phase at low temperature
PLA	Poly(lactic acid)
PMLA	Poly(b,L-malic acid)
PMMA	Poly(methyl methacrylate)
POM	Polarizing optical microscopy
PP	Polypropylene
PS	Polystyrene
PUrA	Poly(uronic acid)
PVA	Poly(vinyl alcohol)
PVP	Poly(vinyl pyrrolidone)
RG	Rhamnogalacturonan
Rha	Rhamnose
σ	Tensile strength
SAXS	Small angle X-ray scattering
SEM	Scanning electron microscopy

SI	Supporting information
T_c	Crystallization temperature
T_d or $^{m}T_d$	In TGA, temperature for maximum decomposition rate
$^{n}T_d$	In TGA, temperature for n decomposition step
$^{I/II}T_h(\alpha)$ or (β)	Temperature of phase I to II transition at heating
$^{II/III}T_h$	Tempearture of phase II to III transition at heating
$^{II/I}T_c(\beta)$	Temperature of phase II to I transition at cooling
$^{III/II}T_c$	Temperature of phase III to II transition at cooling
$^{o}T_d$	Onset decomposition temperature
TEM	Transmission electron microscopy
TFA	Trifluoroacetic acid
T_g	Glass transition temperature
TGA	Termogravimetric analysis
THEO	Theophylline
T_{Krafft}	Krafft temperature
T_m	Melting temperature
TMS	Tetramethylsilane
TXL	Paclitaxel
υ	Wavenumber (cm^{-1})
W	In TGA, remaining final weight
WAXS	Wide angle X-ray scattering
XRD	X-Ray diffraction
ΔH_c	Crystallization enthalpy
ΔH_m	Melting enthalpy

Index

Chapter I: Introduction

1. Carboxylic biopolymers

Chemical modification of functionalized biopolymers increases the number of possibilities that these compounds have by themselves. Polyacids are one of the most common classes of biopolymers bearing active functional groups; these compounds have pending carboxylic side groups that can be protonated or ionized according to pH. One interesting modification of carboxylic biopolymers that has been object of much attention in the recent years is ionic coupling with organic cations, mostly alkylammonium salts. The study of ionic complexes of some polyacids, specifically poly(γ-glutamic acid) and polyuronic acids, with alkylammonium surfactants constitute the subject of this Thesis.

1.1. Poly(γ-glutamic acid)

Poly(γ-glutamic acid) (PGGA) is a naturally occurring polyelectrolyte that is produced by different species of *Bacillus* bacteria.[1,2] This γ-polypeptide has the chemical structure of nylon 4 with a carboxylic group substituted in C4 (Figure 1.1). Poly(γ-glutamic acid) was first described by Ivánovics and Bruckner[3] in 1937 as the main component of the *Bacillus anthracis* capsule. PGGA has been present in the Japan gastronomy since long time ago; indeed the mucilage of "Natto", a traditional food made of soybean fermented by *Bacillus nattosawamura,*[4] is a mixture of a fructan polysaccharide and PGGA, from which the latter was isolated by Fujii[5] in 1963.

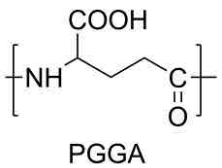

PGGA

Figure 1.1 Chemical structure of poly(γ-glutamic acid).

1.1.1. Sources, synthesis and production

Thorne et al.[6] made the first studies of the mechanisms involved in the synthesis of PGGA. They disclosed that *B. anthracis* produced an active

transaminase that catalyzed the synthesis of γ-glutamic acid from aspartic acid and α-ketoglutaric acid,[7] which was then polymerized into PGGA.

Due to the pathogenic nature of *B. anthracis* other *Bacillus* species such as *licheniformis*, *subtilis* or *megaterium*, were studied and used for the production of PGGA. However, only the *anthracis* specie is able to synthesize the enantiomerically pure poly(D,γ-glutamic acid), P(D)GGA, whereas all the other species afford polymers made of mixtures of the two enantiomeric forms with a more or less racemic composition.[2] On the other hand, it was reported in the last decade that *Natrialba aegyptiaca*, an extremely halophilic archaeon bacteria, was able to produce pure L-enantiomeric form P(L)GGA. This bacteria however seems to be unsuitable for the industrial fabrication of PGGA because the high complexity required by its cultures.[8]

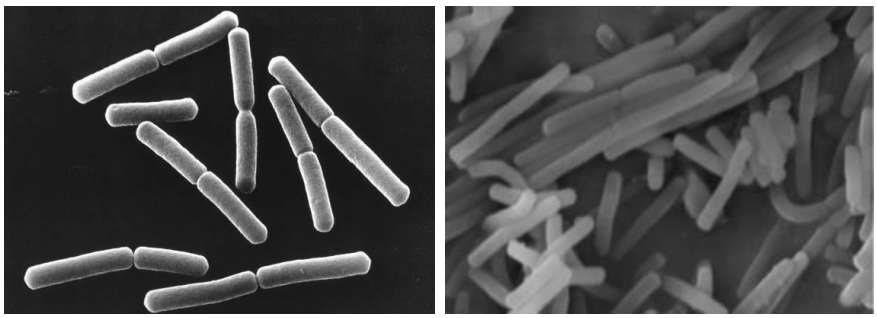

Figure 1.2 *Bacillus subtilis* (left) and Bacillus licheniformis (right) by SEM. (Credit: NASA)

Bacillus subtilis[9] (Figure 1.2) and *Bacillus licheniformis*[10] are the bacteria species mostly used for production of PGGA. Kunioka[11] suggested a complete mechanism (Figure 1.3) for the biosynthesis of PGGA in these bacteria species. The mechanism is based on the L-glutamic acid that is generated in the tricarboxylic acid cycle (TCA cycle). A partial stereochemical inversion leading to D-glutamic acid takes place by the action of pyruvic/keto-glucaric acid with the interactive concourse of the pair D/L-alanine. Polymerization of the glutamic acid D/L-enantiomeric mixtures finally occurs by the action of PGGA polymerase.

Nowadays production of PGGA at big scale is carried out by biosynthetic processes under aerobic conditions.[1] Different nutrient media and bacteria species have been used.[12,13] Kubota[14] described a procedure using *Bacillus subtilis* F-2-01 strain; the aerobic fermentation of the bacteria is accomplished in a growth medium composed of glucose, peptone, urea, and phosphate and nitrate salts. This medium is fed with L-glutamic acid (7-15%) to improve the

polymer productivity so a yield around 50 g·L^{-1} is attained. As it was pointed out by Kunioka,[11] L-glutamic acid takes part in the biosynthesis of PGGA increasing productiveness whereas the effect of D-glutamic is negligible. Moreover the presence of Mn (II) affects significantly the yield,[13] molecular weight and enantiomeric ratio of the formed biopolymer. Pérez-Camero *et al*.[15] found that an optimum concentration of Mn (II) can be set at which enantiomerically pure poly(γ,D-glutamic acid) is obtained with high molecular weight and in good yield.

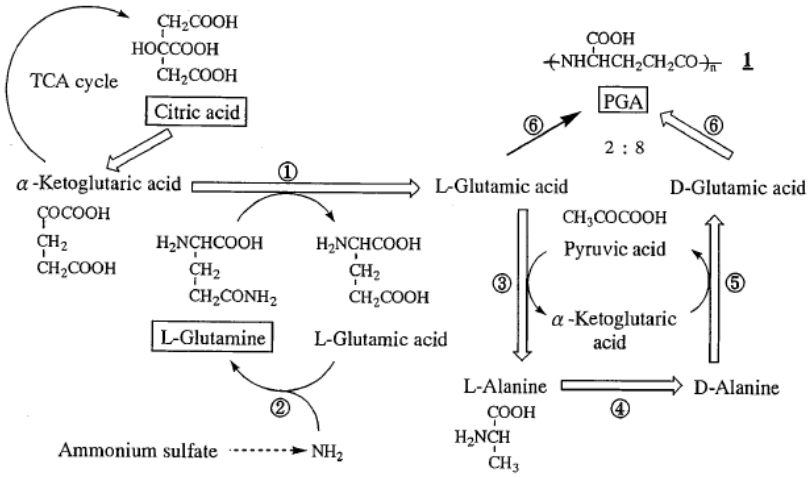

Figure 1.3 Biochemical mechanism of PGGA production by *Bacillus subtitlis*. Scheme reported by Kunioka *et al*.[9]

The chemical synthesis of PGGA from γ-glutamic acid is also feasible but through a so complex procedure that the method is not suitable for its production at industrial scale. The first attempts of the chemical synthesis of PGGA were reported by Waley[16] and Bruckner[17] and were based on the polycondensation of glutamic acid with protected α-carboxyl groups and activated γ-carboxyl groups. However, glutamic acid derivatives tend predominantly to cyclize into pyroglutamate by intramolecular condensation;[18] thus the use of γ-glutamyl-glutamic acid dimers is required in order to avoid undesirable cyclization (Figure 1.4). The γ-ester is activated with pentachlorophenol[19] and the α-carboxyl group is protected with alkyl esters such as methyl[18-20], ethyl, *tert*-butyl or benzyl.[21] Generally, these syntheses involve the polycondensation of the derivative ester of glutamic acid and subsequent hydrolysis to afford the PGGA. Nevertheless, Sanda et al.[20,22] have developed a new route to obtain the polymer that includes a previous transesterification followed by hydrogenation. In these last years new bio-

synthetic procedures have been studied, such as the enzymatic synthesis[23] using poly-γ-glutamate synthetase.[24]

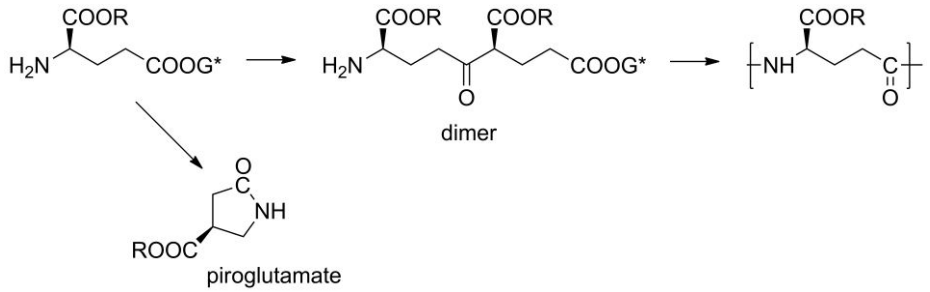

Figure 1.4 Chemical synthesis of PGGA.

1.1.2. Chemical modification of PGGA

In spite of the interesting properties of PGGA, such as non-toxicity and water affinity, the production and spreading of this polyacid is severely limited mainly due to its poor stability in humid environments and its incapacity for being processed. For this reason, diverse chemical modifications of PGGA have been explored with the purpose of increasing the potential industrial applications of its derivatives. The different approaches applied to date for the modification of PGGA regarding its use as a platform for the development of bioplastics suitable for active packaging and biomaterials have been recently reviewed by Muñoz-Guerra et al.[25]

First modifications of polyglutamic acid were centered on esterification reactions to get alkyl esters of PGGA with improved properties.[26] Those reactions consisted of a direct esterification with alkyl bromides in the presence of sodium hydrogen carbonate and in an organic solvent media such as NMP or DMSO. Kubota,[27,28,29] Borbély[30] and Gross[31,32] developed several modifications of this reaction with the purpose of obtaining higher conversion and yields. Nevertheless, as Gonzales et al.[33] studied, the unavoidable reversible hydrolysis of the formed ester group, as a result of kinetic equilibrium at higher conversions, makes difficult to achieve a full esterification of the carboxylate moieties in PGGA.

In the Chemical Engineering Department of UPC (ETSEIB) the chemical modification of PGGA was firstly investigated by Melis[34] and Morillo[35] in their respective Ph.D. theses. These researchers carried out the synthesis of poly(α-alkyl-γ-glutamate)s from both poly(D-glutamic acid) and poly(D,L-

glutamic acid and also their thermal and structural characterization. The synthetic approach followed in this case consisted of a two-steps esterification process. First PGGA was ethylated with EtBr in basic medium and then the ethyl polyglutamate was subjected to transesterification with the alcohol of choice in the presence of titanium tetrabutoxide to afford the desired poly(α-alkyl-γ-glutamate), PAAG, with 100% conversion (Figure 1.5). This technique was also used by Pérez-Camero *et al*. in for the transesterification of poly(α-methyl-γ-glutamate) with mono-, di- and triethyleneglycol methyl ethers with the purpose of obtaining polyglutamates with adjusted hydrophilicity.[36]

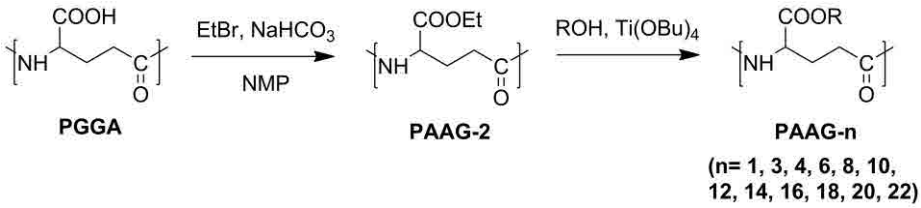

Figure 1.5 Scheme reaction for the synthesis of PAAG esters by transesterification.

Since the alkyl esters of PGGA are well stable to thermal degradation [27,37] and may be molten without appreciable decomposition, they are promising as thermoplastics materials able to replace traditional polymers coming from petrochemical feedstock. In fact most of these polyglutamates can be comfortably handled and many of them are able to form films and fibers from the melt with suitable mechanical properties. However they are still far from industrial applications due to the relative high production costs arising from the high price of PGGA itself as well as from the chemical procedure required for modification.

Given the capacity of polyelectrolytes to form stable complexes with oppositely charged compounds, PGGA has been also modified by coupling with alkyltrimethylammonium surfactants.[38,39] These complexes, which are obtained by simple mixing of polymer and surfactant aqueous solutions, showed properties comparable to those displayed by their homologous PGGA alkyl esters but they afford the remarkable advantage of being much more easily prepared. The alkyl chain of the surfactant increases the hydrophobicity of the complex and make the complex non-water soluble but soluble in organic solvents. Also the thermal processing of the resulting material is improved.

Other modifications deserving attention for their interest in the biomedical field are amidation and coupling with cationic naturally occurring polyelectrolytes.

Amidated graft copolymers of PGGA obtained by reaction with natural amino acids are particularly interesting for their use as protein carriers. Specifically PGGA derivatives prepared by amidation with the ethyl ester of L-phenylalanine (L-PAE) have attracted the attention of different authors.[25,40,41] PGGA-L-PAE copolymers are fully bio-based and sensitive to biodegradation; they display the capacity for self-assembling in structured nanoparticles useful for encapsulation and delivery of proteins[41] and vaccines.[42] The ionic coupling of PGGA with chitosan leads to biocompatible hydrogels with distinguishing properties[43] useful for diverse applications in biomedicine[44] and gene therapy.[45] The recent biomedical interest for biodegradable and bio compatible hydrogels[46] has stimulated lately the study of materials based on crosslinked PGGA.[47,48,25]

1.1.3. Structure, properties and applications

Chemical structure and conformation

PGGA produced by biosynthesis entirely consists of amide 1→4 linkages. The C4 of the γ-glutamyl residue is asymmetric and therefore two enantiomeric units, D and L may occur in the polymer. Usually biosynthetic PGGA contains a variable D/L monomer ratio that oscillates between 1/1 and 2/1 depending on the organism and conditions employed in the process. Enantiomerically pure D and L homopolymers are obtained from *B. anthracis* and *Natrialbaa egyptiaca*, respectively with the maximum percentage of D units contained in P(D)GGA being around 90-96%.[15,31] The stereochemical microstructure of racemic polyglutamic acid produced by *B. subtilis* has been shown to consist of a mixture of both PG(D)GA and PG(L)GA homopolymers and a block stereocopolymer PG(DL)GA;[49] the latter being the main component (≈90%) of the mixture.[50,51]

PGGA is a polyelectrolyte with pK_a= 2.27 so either the protonated (PGGA-H) or the ionized ($PGGA^-$) form would be present according to the pH of the medium, and its conformation in solution is therefore pH-dependent.[52] At low pH values, the PGGA-H form is predominant and the polymer adopts in such conditions a helical structure; in fact a left-handed 3_{19} α-helix has been described for PG(D)GA.[52,53] Increasing the pH, and therefore the ionization degree, the transition from the α-helix to the β-sheet is promoted.[54] Once that PGGA becomes completely ionized, which takes places at pH values above 5.1, the polymer adopts the random coil arrangement (Figure 1.6).

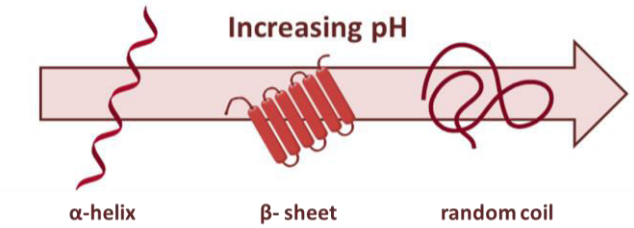

Figure 1.6 pH depending transitions of PGGA, from α-helix to β-sheet and to random coil conformations.

Solubility and degradation

The solubility of PGGA largely depends on its ionization grade. The protonated form is soluble in organic solvents such as DMSO (dimethylsulfoxide),[27] HMPA (hexamethylenphosphoramide),[32] or warm DMF (dimethylformamide) and NMP (*N*-methylpyrrolidone).[55] Nevertheless, the solubility of PGGA-H in water is a complex phenomenon that varies with the age of the material; when freshly prepared it readily dissolves in water, whereas at ageing in the solid state it becomes fully insoluble due to the occurrence of molecular rearrangements. On the other hand, the ionized form of PGGA, either as metallic salts (Na, K, Mg...) or as ammoniun salt, is completely soluble in water,[9] but non-soluble in MeOH, EtOH or DMSO. Heavy metals like Pb (II), Cd (II) and Cu (II) are chelated by PGGA to form precipitates in the form of complex aggregates.

As it is usual to occur in polypeptides, chemical degradation of PGGA is governed by the hydrolysis of the amide bonds. The presence of the pending carboxyl group in the PPGA main chain increases the accessibility of the water to the backbone. Hydrolysis of PGGA can be produced in either basic[56] or acidic[31] aqueous media through a random chain scission mechanism. Controlled hydrolysis of PGGA is a patented procedure that allows obtaining samples with Mw below 500,000.[57] The hydrolytic degradation rate can be raised by increasing the temperature; it has been reported that the hydrolysis rate dramatically changes according to temperature is above or below 60 ºC.[58,59] Ultrasound waves have been also employed to reduce the PGGA molecular weight with subsequent generation of low-molecular weight fractions displaying low dispersity.[15,60]

Digestion of the isomer poly(α-glutamic acid) is carried through by proteases such as pepsine, tripsine or quimotripsine but PGGA is insensitive to these enzymes.[28,61] On the contrary, PGGA is susceptible to degradation by γ-

glutamyldepolymerase,[62] which is inactive for the α-form. The susceptibility of PGGA to the degrading action of enzymes excreted by fungi and bacteria was pointed out in the 40's.[63] This investigation was completed by Oppermann *et al*.[64] several decades later, who made a deep study including 12 different bacteria able to carry out degradation of the polymer.

Regarding the thermal stability of PGGA, Kubota *et al.*[29] reported that this polymers is stable to heating up to 210 ºC, where melting and decomposition happen at same time. Portilla-Arias *et al.*[37] proposed an unzipping mechanism with generation of pyroglutamic acid for the thermal degradation of PGGA (Figure 1.7).

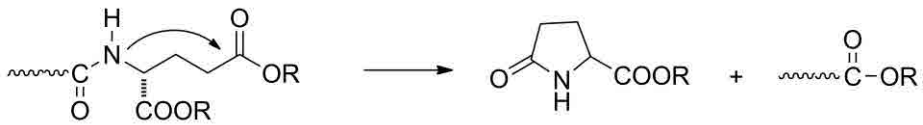

R= H (PGGA) or Me (PAAG-1)

Figure 1.7 Thermal decomposition mechanism of PGGA or PAAG-1.

Applications

An important property of PGGA regarding sequestering applications is its ability to interact with cations. Some studies revealed that binding of PGGA with cations such as Cu^{2+}, Al^{3+}, Cr^{3+} and Fe^{3+} induced flocculation of the polymer,[65] while interaction with heavy metals like Ur^{4+}can also occurs.[66] This property makes PGGA a suitable polymer for waste water treatment since both inorganic and organic suspensions can be removed by flocculation and coagulation.[67,68] Nowadays, inorganic flocculants such as poly(aluminum chloride)s or synthetic membranes like polyacrylamides are currently used. These flocculants present environmental and health problems derived from their production and resulting degradation products. The replacement of them using a bio-flocculant such as PGGA is a much desired alternative to minimize such problems. Nakano et al.[69] developed an interesting application of PGGA, in the treatment of the waste water of vinegar manufacture; a bacterium able to synthesize the polyacid is added so released acetic acid is consumed as nutrient and at the same time pollutants are removed by flocculation.

The high density of hydrogen bonds in the structure of PGGA causes high water sorption and makes PGGA a material suitable for applications that

require hydrogels. Some hydrogels have been developed from PGGA by cross-linking through other hydrophilic polymers like PEG[70] or by direct crosslinking using γ-irradiation.[71] PGGA is a humectant that releases moisture to the media, including soil or skin. This property confers to the polymer a potential for applications in agriculture and, taking into account its biocompatibility, in cosmetics or dermatology.[72] Some studies carried out in this direction concluded that in contact with the skin water release was efficient, no skin irritation was produced,[73]and wrinkles appearance was reduced.[74]

Another interesting outcome of this polymer is in the food field, not only as thickener but also as forming part of the food diet since it is easily biodegraded into the proteinogenic glutamic acid, which has a history of safe use in food products (Figure 1.8). Moreover it has been reported that the addition of PGGA to foods increases the uptake in the small intestine of those physiological active substances, like vitamins, carotenoids or polyphenols, eventually present in the digesting mass.[75]

Figure 1.8 PGGA is present in "Natto", a traditional Japanese fermented food made from soybeans by *Bacillus subtilis*.

Most promising applications of PGGA are however in the biomedical field. Micro and nanoparticles formed from PGGA have been used as drug, vaccine or gene carriers.[76] Besides PGGA itself, some of their derivatives have been found to be effective for the encapsulation of different therapeutic agents. The side carboxyl group can be conveniently modified given place to different derivatives with altered properties. Several amphipilic poly(α-alkyl γ-glutamate)s copolymers[77] have been developed with a potential as drug and protein delivery devices (Figure 1.9). Some graft copolymers made by grafting with phenylalanine ethyl ester (PAE)[78] or chitosan-PGGA (CS-PGGA) polyelectrolyte complexes obtained by ionic gelation[79] are claimed to be suitable to form nanoparticles for unique drug delivery applications. CS-PGGA complexes have found to be suitable carriers for transmucosal delivery of drugs or proteins, due to their pH dependence.[80,81] Furthermore, the

incorporation of PGGA to CS-DNA complexes improves significantly the cellular uptake and transgene expression of DNA,[45] presumably due to the interaction of PGGA with γ-glutamyl transpeptidase present in the cell membranes.

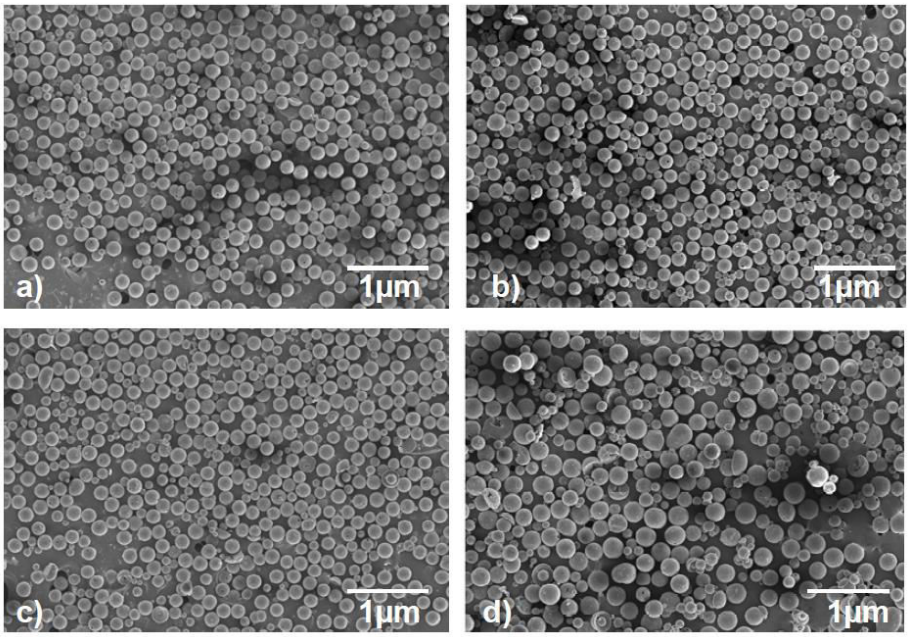

Figure 1.9 SEM images of nanoparticles made of α-alkyl esters of PGGA made from different alcohols and with different esterification degrees: a) *co*PAAG-(Et75H25), b) coPAAG-(Hex50H50), c) coPAAG-(Dod50H50) and d) *co*PAAG-(Octd50H50). From Portilla et al.[74]

The carboxyl groups offer attachment points for the conjugation of active agents as well, thereby rendering the drug more soluble and easier to administer. Indeed, the tactic of direct ionic coupling of Doxorubicin, an anthracycline antibiotic used as chemotherapeutic agent, with PGGA has recently been explored.[82] The effect of PGGA matrices for drug encapsulation was also studied showing an enhanced effect when amphiphilic trimethylammonium cations were used as compatibilizers. In such case three-component nanoparticles were obtained upon precipitation from the aqueous mixture.[83] Ionic complexes of PGGA and alkylammonium surfactants were previously explored as forthcoming drug delivery systems.[84] Paclitaxel (TXL) is another chemotherapeutic agent with high antitumor activity, including breast and ovarian tumors, but its insolubility in water is a severe shortcoming for its clinical use. The encapsulation of Paclitaxel into galactosamine

conjugates of PGGA-polylactide nanoparticles offers an alternative to drug delivery that distinguishes by showing specific interaction and inhibition of tumor growth.[85]

1.2. Polyuronic acids

Polyuronic acids are polysaccharides derived from uronic acids. In the uronic acid the primary hydroxyl group of the aldose or ketose from which it derives is oxidized into a carboxylic group. The nomenclature for uronic acids is as follows: the ending *–ose* from the parent aldose or ketose is replaced by *–uronic*, i.e. the uronic acid derived from glucose is named glucuronic acid and the polyuronic acid will be therefore polyglucuronic acid.

The uronic acids present in nature in isolate form are glucuronic, galacturonic, iduronic and mannuronic acids. These acids in addition to guluronic acid, which is not found as monosaccharide in the nature, are part of some naturally occurring polymeric structures. (Figure 1.10)

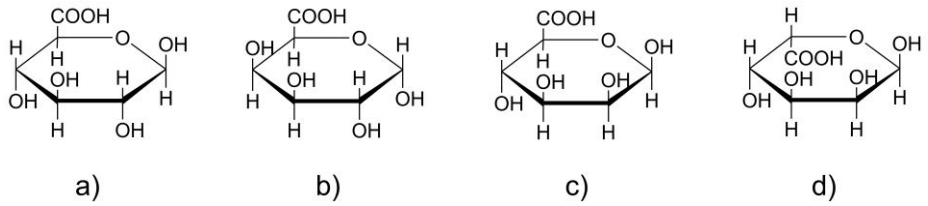

Figure 1.10 Haworth structures of a) D-glucuronic acid, b) L-galacturonic acid, c) D-mannuronic acid and d) L-guluronic acid.

In the present work, the following polyuronic acids have been studied: a) polygalacturonic acid, which is the homopolymer from α,D-galacturonic acid; b) alginic acid, a copolymer from β,D-mannuronic acid and α,L-guluronic acid, and c) hyaluronic acid, an alternating copolymer composed of β,D-glucuronic acid and acetyl β,D-glucosamine.

1.2.1. Pectins and polygalacturonic acid

Pectins are a family of heteropolysaccharides generated in primary cell walls of plants.[86] Pectins have a complex structure where the major component is a partially methylated polygalacturonic acid, a lineal copolymer of 1→4 linked

mixture of methyl α,D-galacturonate and α,D-galacturonic acid. Homopolymer polygalacturonic acid is obtained by chemical or enzymatic hydrolysis of pectins. It was first isolated and described by Bracannot in 1825.

Sources, synthesis and production

Plant cells are surrounded by a wall consisting of a mixture of polysaccharides, as the most abundant part, proteins and occasionally lignin. These polysaccharides in the wall are usually cellulose, hemicellulose and pectin,[87] which have functions in plant growth, development, morphology and to act as a plant defense.

Pectin is located commonly in most of the plant tissues, mainly in some fruits peels and pomaces; however, since the amount, structure and chemical composition of pectin differs between different plants,[88] the sources used for its commercial manufacture are selected according to the specific needs. Nowadays, main applications of these polysaccharides are in food and pharmaceutical industries. Typical requirement for pectin used in these fields is a 65% minimum content of galacturonic acid in the moisture-free material. Thus, commercial pectins are currently obtained from either citrus peel or apple pomace, that contain 20-30% and 15-20% or pectin respectively on a dry matter basis.[89] There is a wide number of alternative sources that have been studied, including beet waste from sugar manufacturing;[90] fruits such as berries, cherries, kakis, peaches and olives; flower plants like amaranths and sunflower; vegetables including soy beans and spinaches; tuber of the potato and different kind of plants or trees, i.e. some species of cactus and argane tree.[91]

Synthesis of pectins takes place at the Golgi vesicles, with a large number of enzymes involved.[92] Due to the complex structure of pectins, it has been estimated that in addition to gylcosyltransferases more than 50 different enzymatic activities are needed for their synthesis.[93]

Although the main procedure for isolating pectin is water extraction by direct boiling, new methods have been considered in the last years, such as microwave or ultrasonic techniques.[94] All the procedures are based on the hydrolysis and extraction of pectin from plant cell walls and its solubilization under the influence of different factors like pH, temperature and time. The water based industrial process extracts the pectin using hot aqueous solutions of mineral acids (pH up to 2). There is a compromise between the yield of extraction and solid separation and operation cost; the higher is the pectin concentration or its molecular weight, the higher is the viscosity, and more

difficult will be the separation of the aqueous phase from the solid waste. Powdered pectin can be produced by mixing the concentrated liquid from either apple or citrus with an alcohol (usually isopropanol). Following this procedure, pectins with an esterification degree (ED) of 70% approximately are obtained.

Direct boiling is a conventional method that takes around two hours to obtain pectin in a good yield but the long heating treatment unavoidably causes some thermal degradation of the polymer.[95] On the other hand, microwave heating extraction only needs around fifteen minutes to extract a satisfactory amount of pectin.[96] Another alternative processing technique is ultrasonic irradiation in the 16KHz-100 MHz range of frequencies, which has proven to increase yield and quality of pectin compared to the standard procedure.[97] A procedure avoiding aggressive conditions is that based on the enzymatic extraction assisted by endo-polygalacturonases from *Aspergillus niger*.[98] Polygalacturonic acid homopolymer is obtained either as a fraction along the extraction process or later from the liquid phase by hydrolysis of the methyl ester groups.[89]

Structure and properties

The characteristic structure of pectin is quite complex (Figure 1.11). This polysaccharide is polydisperse and is present in a broad Mw range; furthermore, its composition varies with the source and conditions applied for isolation. Pectins are the mixture of three different main structures varying in length and chemical composition of the polysaccharide chains.[86]

The main component is a linear homogalacturonan (HG),[99] with D-galacturonic acid subunits joined by $\alpha(1\rightarrow4)$ glycosidic linkages. There, some of the carboxylic acid groups are partially methylated according to the esterification grade (DE) or forming salts with monovalent cationic metals such as sodium. HG comprises ~65% of pectin total weight. Rhamnogalacturonan I (RG-I) is another existing structure representing 20-35% of pectin[100] and contains a backbone of the repeating disaccharide galacturonic-rhamnose, (1,4)-α-D-GaA-(1,2)-α-L-Rha.[101] In this structure, between 20-80% of rhamnose (Rha) residues are substituted at C4 with saccharides such as L-arabinose or D-galactose.[102] The most complex structure, Rhamnogalacturonan-II (RG-II), amounts up to the 10% of pectin and consists of a low molecular weight poly-D-galacturonic acid backbone highly branched with neutral sugar units.[100,103]

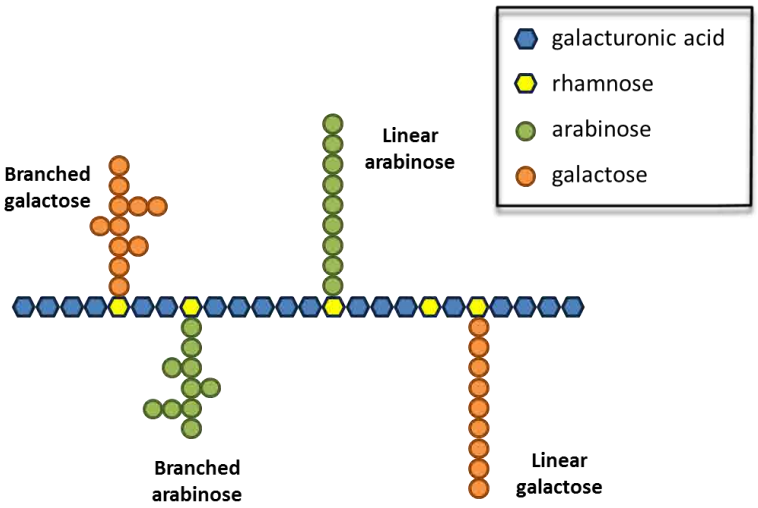

Figure 1.11 Schematic chemical representative structure of pectin.

In the solid state the homogalacturonan backbone adopts a threefold helical structure with a 1.32 nm pitch.[104] A later study suggested for the sodium salt a 3_1 helical conformation packed in a hexagonal lattice with an orthogonal unit cell of dimensions of *a*= 0.84, *b*= 1.43 and *c*(fibre axis)= 1.34 nm in the space group $P2_1$.[105] Sodium salt and acidic form of polygalacturonic acid differ in the unit cell dimensions and arrangement; helical pectinic acid molecules pack in a parallel arrangement, whereas the salt form consists of corrugated sheets made of antiparallel helices.[106]

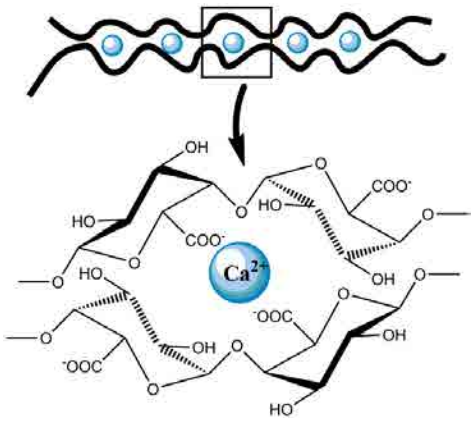

Figure 1.12 Representation of egg-model of pectins.

Applications and pectin derivatives

As other polyuronic acids, pectins are very versatile polymers with applications in a broad range of uses. They have been widely used as gelling agents, stabilizers of solutions and thickeners. Another more specific application in the food industry is their use as colloid solutions and gels able to carry and deliver aromas.[107]

In the pharmaceutical field, pectins are of interest since they display a wide spectrum of physiological activities. They are usable as mucoadhesive patches[108] due to their capacity to form robust bio-adhesive bonds with tissues. In addition, pectins have a gastroprotective action against toxic cations facilitating the removal of lead and mercury from the gastrointestinal tract and respiratory organs; a preventive effect of pectins on colitis has been also appraised.[109] There is even evidence that pectins have beneficial effect in the control of the cholesterol level in the blood stream with a significant reduction observed for uptakes of at least 6g per day.[110] Anticarcinogenic and antimetastatic responses have been also found for these polysaccharides. It has been shown that pectin, in particular that coming from apple source, induces apoptosis of intestinal carcinomas, as well as some modified pectins from citrus are able to suppress the growth and metastasizing of cancer cells.[91]

Pectins cannot be degraded in the upper gastrointestinal tract due to its insolubility at acidic pH and lack of gastric and intestinal degradable enzymes. On the contrary they will be degraded in the colon by pectinolitic enzymes providing a pharmaceutical carrier for drugs to be specifically deliver at the low intestinal track.[113] Strategies to avoid the solubility of the polymer in the organs preceding colon, which have alkaline pH, involve among others crosslinking, gelation with calcium or complexation with other biopolymers.[111,112]

1.2.2. Alginates and alginic acid

Alginates are natural linear polysaccharides that occur both as a structural component of marine brown algae and as capsular constituent in soil bacteria. These polymers were first described and isolated from brow algae by Stanford in 1881.[113] They are mainly composed of a linear copolymer made of 1→4 linked β-D-mannuronic acid (M) and α-L-guluronic acid (G) (Figure 1.13).

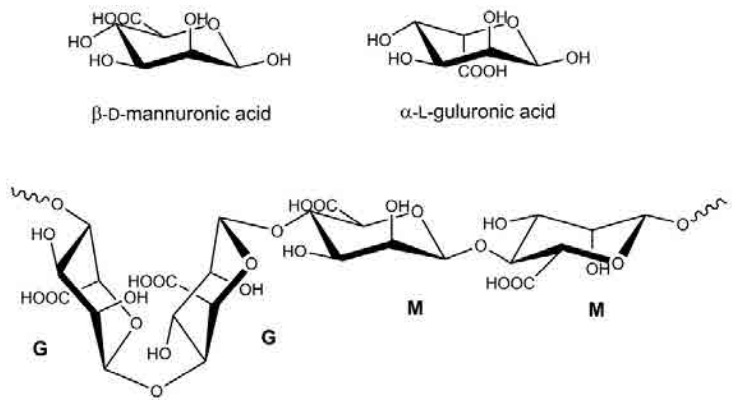

Figure 1.13 Chemical structure of β-D-mannuronic acid (M), α-L-guluronic acid (G) and alginic acid.

Sources, synthesis and production

Seaweeds contain alginates in the cell wall. This polysaccharide is found in the form of a gel containing cationic ions like sodium, calcium or magnesium and comprises up to 40% of the dried weight of those organisms.[114,115] Its main function is skeletal, giving strength and flexibility to the algal tissue. The composition of alginates varies greatly between different species of algae, since every habitat of every specie demands specific requirements of stiffness, elasticity or water-binding, being these properties related to the monomeric composition and block distribution in the polymer.[116] The alginates are also present in two families of heterotrophic bacteria, *Pseudomonas* and *Azetobacter* as capsular components. The main difference between algal and bacterial alginate is that some of M-units in the bacterial alginates are *O*-acetylated at the 2 and/or 3 positions adding a new variable that makes distinction in the properties of those polymers.[117]

Biosynthesis mechanism of alginate in cells starts with D-fructose-6-phosphate and involves isomerization to mannose and further oxidization to GPD-D-mannuronic acid, which is then polymerized to mannuronan. The C-5-epimerase enzyme epimerizes mannuronic acid residues into guluronic acid.[118]

The industrial production of this polymer is carried out by extraction from algal material. First of all, acidification of the insoluble alginate is accomplished by extracting the powdered tissue of algae with diluted mineral acid solutions. Subsequently, neutralization of the alginic acid is carried out with alkali, and algal materials are removed by separation methods such as centrifugation,

filtration or flotation. Finally, the alginate salt is precipitated in alcohol, dried and milled.[117] Commercial alginates are produced mainly from *Laminaria*, *Macrocystis* and *Ascophyllum* genus.[119] Nonetheless, commercial production by bacterial fermentation is still under development;[118] although these biotechnological procedures are technically possible, they are not from an economical point of view.

Structure and properties

The chemical structure of alginates is simple compared to pectins. They are linear block copolymers with three regions: homogeneous sequences of G or M combined with alternating regions.[119] As mentioned above, the composition varies with the source.[120] For instance, in *Laminaria hiperboria* alga guluronic monomer represents 70% of the copolymer; whereas *Pseudomonas aeruginosa* bacteria produces almost 100% of mannuronic residues. As expected, the conformation of the polymer chain varies with composition. The homogeneous segments of mannuronic acid adopt a $^4C_1$ double helix conformation and are set in an extended ribbon conformation with diequatorial linkages and a pitch of 1.04 nm. On the other hand, the GG sequences are arranged in a $^1C_4$ double helix set by diaxial linkages generating a structure more compact than for MM blocks, with a pitch of 0.87 nm. (Figure 1.14).[119]

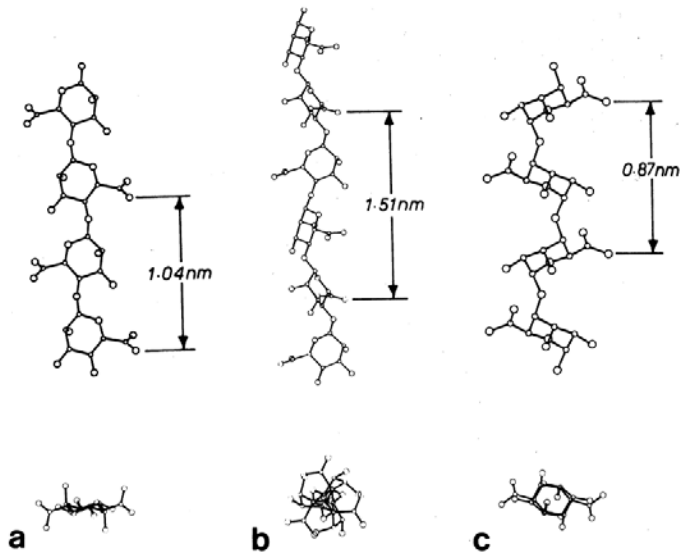

Figure 1.14 Chain conformations of a) polymannuronic acid, b) sodium salt form of polymannuronic c) polyguluronic acidd in directions parallel and perpendicular to the chain axis. From Atkins.[122]

The more the content of G homosequences, the higher the stiffness of the polymer due to the hindered rotation around the glycosidic linkage.[120] Related to this special arrangement, polyguluronic chains are able to be aligned in parallel and harbor calcium cations to form firm and brittle gels[121] as a result of chelation. This phenomenon has been also explained by means of the well-known egg-box model of polysaccharides.[109,122] (Figure 1.12)

The presence of electrostatic charges on the uronic acid residues will determine the solubility of the alginic acid, as it happens for other polycarboxylic acids previously described. Alginate salts of monovalent cations such as sodium are soluble in water but they precipitate and form gels when pH is lower than the pK_a of the polyelectrolyte[123] (3.38 and 3.65 respectively for homopolymers of manuronic and guluronic acids). Another critical parameter is the content of gelling ions in the media. The hardness of the water (i.e. the concentration of Ca^{2+}) affects drastically the solubility because of the formation of gels by irreversible binding reaction.[119] These ionic crosslinked gels are tougher than those coming from acidification.

Alginate solutions are in general highly viscous. This is caused by the extended conformation of the alginate molecule which entails a huge hydrodynamic volume. The rheological behavior is usually pseudoplastic, therefore the apparent viscosity of the solution depends on alginate concentration, temperature and shear rate.[124]

Stability of alginic acid is relatively poor. Glycosidic linkages of alginates are susceptible to break in both acid and alkaline aqueous solutions,[125] and additionally they can be oxidized in solid state through free radical mechanisms.[126] Regarding thermal stability, these polysaccharides are stable up to around 150 ºC and 180 ºC for the acid and sodium salt form, respectively.[127] Variations in stability among alginates will be again depending on the mannuronic and guluronic contents.

Applications and alginate derivatives

The high viscosity and gelling capability characteristics of alginates confer them a huge range of applications in different fields. In technical applications, alginates are utilized for paper coating and for viscosity enhancement in textile printing.[119] Nonetheless, most of important applications of alginates are in food industry. Alginate and its salts are widely used for increasing the viscosity, emulsifying and stabilizing food mixtures.[117] Propylene glycol alginate (PGA), the unique commercial derivative of alginate,[128] is also used as food additive, to stabilize acid emulsions, to coat fresh fruit pieces, as

pesticide adjuvant or to stabilize beer foam. Nowadays, the fast and simple gelling technique based on Ca-alginate gels has caught attention by the haute cuisine and spherification of different liquid preparations has been developed (Figure 1.15).[129]

Figure 1.15 Spherification of green tea with Ca-alginate.

As it happens with pectins, non-toxic and biocompatibility properties of alginates allow their use not only in food industry, but also in pharmaceutical applications as binder or disintegrating agent in tablets.[117] The G and M unit contents determine the grade of biocompatibility; in general, guluronic rich polymers are more compatible than mannuronic rich ones.[130] Fibers of calcium and sodium alginates are used for moist exudating wound dressings owing to their water absorption capacity, and also for surgical guts and dental impressions.[131]

One of the most advanced pharmaceutical applications of alginates is the entrapment of living cells or DNA. Several types of cells, from bacteria to animal cells, and also from fungi or algae, have been immobilized by calcium alginate gels prepared by the drop formation method.[117,119] Encapsulated cells are protected against mechanical stress, while diffusion of nutrients and metabolites is allowed through the semipermeable capsule.[132] This technique has a great potential use in cell transplantation, since alginate acts as a barrier between the immune system and transplant. Type I diabetes has been treated by immobilization of insuline producing cells, *langerhans islets*, in alginate capsules;[117] some studies have revealed that polyelectrolyte complexes with poly-L-lysine polycation can even reverse diabetes. This fact is possible due to the control of the porous size that permits free diffusion of glucose/insuline but at the same time protects the cells from immune system.[133] Continuing with the pharmaceutical uses, drug delivery systems (DDS) based on alginates have been widely employed[134] taking advantage of the diffusion barrier provided by the hydrocolloidal alginate.

In addition to poly-L-lysine, some other cationic polyelectrolytes have been considered for enhancement of intrinsic properties of alginates.[135] Complexes with chitosan have been reported to show a significant increase in bioadhesion with a strong affinity for the human stomach mucosa. Acrylic polymers like DMAEA (dimethylaminoethyl acrylate), thoroughly used in biological applications, form complexes with alginates that permit a modulation of erosion time and drug release rate, as well as to increase their adhesion to substrates.

1.2.3. Hyaluronic acid (hyaluronan)

Hyaluronic acid (HyalA) is a linear polysaccharide belonging to the glycosaminoglycans group (GAG) with a repeating disaccharide structure of 1→3 β,D-*N*-acetylglucosamine (GlcNAc) and 1→4 β,D-glucuronic acid (GlcA) alternatively linked[136] (Figure 1.16). The term hyaluronan refers to the general polymer, whether it is in the acid form (hyaluronic acid) or salt form (hyaluronate). It is naturally occurring in different animal tissues. Hyaluronic acid was already known in the second half of the 19th century, but was in 1934 when Karl Mayer and John Palmer first reliably isolated and described it from bovine vitreous humor.[137]

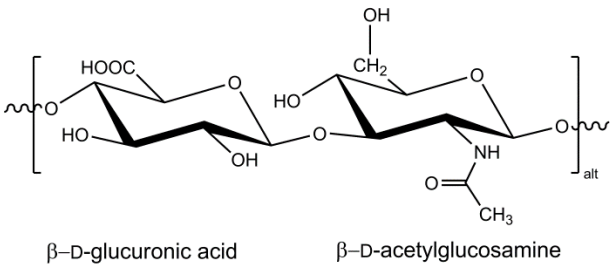

Figure 1.16 Chemical structure of hyaluronic acid.

Sources, synthesis and production

Hyaluronic acid is present in vertebrates and in the capsules of some bacteria, but is absent in fungi, plants and insects. The largest content of this polysaccharide is found in rooster combs.[138] In the human body different tissues such as skin, umbilical cord,[139] cartilage and vitreous humor contain HyalA.[141] This polymer occurs primarily in the extracellular and pericellular matrix, but it has been shown to occur also intracellularly. The role played by

hyaluronic acid in tissues is always related with hygroscopicity with implications in structural, rheological, physiological and biological functions; i.e. maintenance of viscoelasticity of liquid connective tissues or hydration control or water transport.[140]

Industrial production of hyaluronic acid has been traditionally based on the extraction from rooster combs. HyalA is usually linked to other biopolymers in animal tissues, thus several separation procedures have to be applied in order to obtain a pure compound. These techniques include protease digestion, ion-pair precipitation (e.g. with cetylpyridinium chloride), membrane ultrafiltration, and precipitation or lyophilization of hyaluronic acid.[141] Balazs developed a chemical procedure to produce pure hyaluronan,[142] using a chloroform extraction method for eliminating the accompanied proteins avoiding then inflammatory response and other secondary problems derived from their presence. Nowadays, microbial production by fermentation is gathering strength for commercial production, especially in pharmaceutical field, since these preparations meet the demand for a wide range of molecular weights, according to the specific applications, and will avoid the allergy responses usually provoked by products coming from animal sources.[142] Thus hyaluronic acid has been successfully produced on an industrial scale using several bacteria of the *Streptococcus*;[143,144] Shiseido Co. performed in the 80s the first industrial scale bacterial production of hyaluronic acid for cosmetic industry.[145] Nevertheless, the risk of mutation of bacteria strains with possible toxins production has hampered the development of hyaluronic acid from bacteria. Other alternative sources have been sought, one of the most promising based on the use of a genetically-modified *Bacillus subtilis* strain carrying the hasA gene from *Streptococcus equisimilis* that encodes the enzyme hyaluronic acid synthase.[146]

Structure and properties

The primary structure of hyaluronic acid, as previously mentioned, consists of an unbranched polymer of D-glucuronic acid and *N*-acetyl-D-glucosamine units linked by alternating 1→3 β and 1→4 β glycosidic bonds (Figure 1.16).[139] Further studies have provided evidence that the coiling of hylauronan is not necessarily random and that a secondary structure is adopted. Scott et al. determined that hydrophobic faces formed by the axial hydrogen atoms of about eight C-H groups on the alternating sides of the molecule are present along the chain.[147] Such hydrophobic patches are responsible for the stabilizing interactions that energetically favor the formation of a network-like β-sheet tertiary structure, which is additionally supported by intermolecular

hydrogen bonds. This specific molecular arrangement leads to the characteristic stiffness displayed by hyaluronic acid. (Figure 1.17)

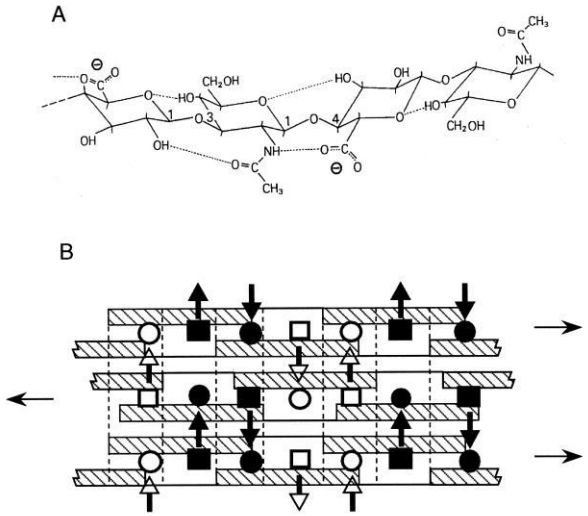

Figure 1.17 Schematic illustrations of primary, secondary and tertiary structures of hyaluronan in solution. a) Primary structure of two disaccharide units where five intra-molecular hydrogen bonds maintain the twofold helical secondary structure. b) Three twofold Hyal helices arranged in a β-sheet tertiary structure stabilized by H bonds between acetamido (■ and □) and carboxylate (● and ○) groups. From Scott et al.[150]

A newtonian to non-Newtonian transition of Hyal in solution has been reported; when molecular weight, shear rate or concentration is increased, an enhancement of the viscoelasticity behavior is observed for hyaluronan solutions.[148] The pK_a of this polysaccharide is around 3.0 and changes in the pH will provide different ionization grades[149] which will affect rheological properties due to the alterations caused between chain interactions in the tertiary structure.

Hyaluronic acid in the solid state is a flaky substance but its aqueous solutions show high viscosity and elasticity. Hyal is able to retain water quantities up to thousand times of its own weight. An 1% aqueous solution of Hyal still retains its characteristic viscosity and elasticity, becoming an interesting biomaterial.[150] It was found that both solutions made of raw hyaluronic acid containing proteins and those made of purified polymer maintain the high viscosity as well as the high molecular weight (it can reach 10^6-10^7 Daltons)[141] characteristic of this polysaccharide.[151]

Regarding the crystallographic conformation of hyaluronan, a variety of structures, separated ones from others by small energy differences, have been reported.[153] Hyaluronan fibers together with others made of other uronic polysaccharides were investigated by Atkins in the 70s.[122] Possible conformations involve single, two, three or four-fold helices besides the quasi-extended conformation analogous to the proteins β-sheet structure described above.[150] By changing the environmental parameters such as pH, ionic strength, nature of the counter-cation or humidity during crystallization, the hyaluronate may arrive to exhibit such a plethora of structures.[122,153] Nowadays it is not well understood yet the correlation existing between structural properties of hyaluronan and its biological functions.

Applications and hyaluronan derivatives

Most of the applications of hyaluronan are focused on cosmetic and biomedical fields. Distinguishing properties such as biocompatibility, non-immunogenicity, biodegradability and viscoelasticity make hyaluronic acid a suitable biomaterial for a large range of applications in such fields.[141,143]

As highlighted earlier, viscoelasticity is one of the main properties of this polymer. Hyaluronic acid matrices can act as stiff support biomaterials and have been employed as scaffolds in surgery, wound healing and embryology.[152] Cosmetic uses of hyaluronan involve dermal filler in cosmetic surgery reducing facial lines and wrinkles of skin. This polymer is also employed as skin cream, as a result of its water binding and moisturizing ability, elasticity and anti-wrinkle effect, as well as its radical scavenging capability that provides a protective effect against UV radiation.[153]

In those biomedical applications HyalA is used alone, in combination with other polymers or slightly crosslinked. This polysaccharide suffers rapid enzymatic degradation due to its sensitivity to hyaluronidase.[154] However, stabilization by crosslinking reduces solubility giving not only more durable materials but also better mechanical effects, which are appropriate for filling applications. Comparing to collagen, which is also employed as filler, hyaluronic acid hydrogels are more elastic, longer lasting and show better tolerability,[155] and a huge number of commercial products are today available. Shu et al.[156] recently developed a novel injectable and in-situ crosslinkable hyaluronic acid hydrogel that not needing surgical implantation has potential uses for tissue engineering. Furthermore Hyal has started to become an alternative to silicone implants[157] in plastic surgery due to its better biocompatibility and visual effect.

The first application of hyaluronan in medicine was in ophthalmology. The major component of the vitreous body of the eye is hyaluronic acid, thus, it is used as substitute or replacement for the vitreous fluid during procedures to protect delicate eye tissues.[141] The second major application of HyalA is in visco-supplementation in the joints affected by arthritis where it acts as a lubricant and provides mechanical support. The infiltration of joints with Hyal restores the desirable rheological properties and alleviates the symptoms.[158] Another interesting property of this polysaccharide is the inhibition of platelet adhesion and consequently thrombus formation, in addition to have an angiogenesis response[159] (formation of new vessels) which validate it as an interesting biomaterial for vascular applications.[143] As other polysaccharides, hyaluronic acid is a suitable component for drug delivery systems both as an inert matrix or by HyalA-drug covalently or ionically attached conjugates.[141,155,160]

Some chemical modifications of hyaluronic acid have been performed to get new derivatives that broaden its range of applications. As previously mentioned crosslinked hyaluronan is used for filling applications, and other hydrogels obtained by chemical modification are suitable for drug-releasing formulations.[163,161] Chemical modifications of hylauronan, like amidation, etherification or hemiacetal formation, and the applications of those derivatives have been recently reviewed.[163] For example, ionic complexes obtained by the interaction of the carboxyl group of HyalA and a tumor necrosis factor-related apoptosis-inducing ligand (TRAIL), which is a cationic compound, (Figure 1.18) have been found to prolong blood circulation of TRAIL *in vivo*, enhancing its anti-cancer therapeutic effect.[162] On the other hand hyaluronic acid-placlitaxel conjugate has found to show antitumor activity in vivo.[163]

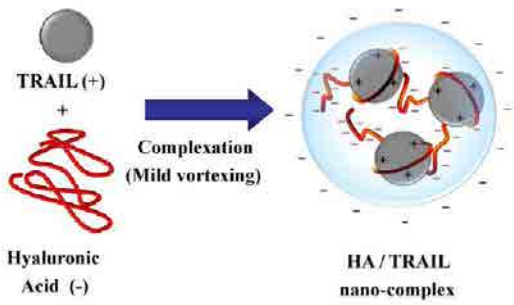

Figure 1.18 Schematic illustration of hyaluronic acid-TRAIL ionic nanocomplex formation. From Na et al.[165]

2. Self-assembled polymeric structures

Self-assembly of the matter is a required step for the existence of life. The specific combination and arrangement of different atoms into complex molecular systems were the basis for spontaneous origin of life, according to Oparin's assertions.[164] The ability of biomolecules to self-organize into different architectures in living systems such as micelles, vesicles, bilayers or helical biopolymers has been taken as an emerging model to mimic and develop new synthetic chemical structures.

The interactions that provide the stability necessary to form those structures are secondary forces such as Van Der Waals, ionic interactions, amphiphilic associations or H-bonding,[165] which will define the geometry and, therefore, the functionality of the biochemical structures. By controlling the chemistry and interactions of the mimetic synthetic molecules, a huge variety of different self-organized materials can be obtained with designed functions. These supramolecular organic materials involve from simple molecules such as surfactants up to complex ones like polyelectrolytes, including more or less sophisticated combinations of them.

2.1. Surfactants

The term surfactant is an abbreviation of "surface active agent". Surfactants or tensioactive agents tend to adsorb at surfaces and interfaces of immiscible phases. That adsorption is produced due to the lowering of the free energy in the phase boundary caused by the surfactant. The surfactant reduces the surface tension, i.e. the amount of energy required to break the intermolecular bounds that are covering the surface.[166]

Surfactants are generally organic molecules that are amphiphilic or amphipathic, i.e molecules consisting of two counter-parts, one which is soluble in a specific fluid (lyophilic part) and other one which is insoluble in such fluid (lyophobic phase).[167] Most frequently, the fluid is water and those two parts refer to hydrophilic (head group) and hydrophobic (tail) groups, respectively.

2.1.1. Classification and structure of surfactants

The hydrophobic tail of the surfactants is generally an alkyl chain, and less often a halogenated or oxygenated hydrocarbon or siloxane chain. The chain length is usually comprised in the C_8-C_{20} range as far as surfactants to be used in aqueous systems are concerned. These are long enough for displaying surface activity but still maintaining the solubility of the whole surfactant in the aqueous phase; longer chains would be suitable for non-aqueous systems. The hydrophilic head consists of an ionic or highly polar group. Regarding to the nature of that hydrophilic head, surfactants can be classified as:[168]

1. Anionic. The cationic counterion is usually an alkaline metal or ammonium group. (e.g. carboxyl acid salts of fatty acids).
2. Cationic. The anionic counterion is generally a halide. (e.g. alkylamines or quaternary ammonium salts).
3. Zwitterionic. It is a neutral molecule than has both positive and negative electrical charges at different locations within the molecule. (e.g. amino acids, betaines and phospholipid derived surfactants).
4. Nonionic. The head is a neutral polar group free of charge and without dissociation in water. (e.g. polyethylene oxide based surfactants).

Tensioactives can set up different kinds of structures in aqueous media depending on the concentration. Very diluted systems are dissolved in water below a certain concentration, called CMC (critical micelle concentration), above which micelles start to form. In those aggregations, the hydrophobic tails are directed towards the inner part of the micelle and the polar head remains in contact with the water phase; in this manner the free energy of the system is reduced. Moreover, emulsions of two different phases (i.e. water-oil mixtures) can be obtained by using surfactants due to the lowering of the interfacial tension.[171]

Israelachvili *et al*. defined the "packing parameter" in their micelle theory[169] to describe the tendency of the surfactant to form aggregates with a defined shape according to the v/v ratio of the hydrophobic and hydrophilic parts. The geometry of the micellar shape is determined by the factors including in the expression of the packing parameter, *p*:

$$p = \frac{v_H}{a_0 l}$$

where v_H is the volume occupied in the micellar core by the hydrophobic groups, l is the length of the hydrophobic tails, and a_0 is the cross-sectional

area of the hydrophilic group at the micelle–solution interface. Different values of that parameter give rise to several possible micelle structures such as those depicted in Table 2.1.

Table 2.1. Micelle structures depending on the packing parameter.

Value of $\frac{v_H}{a_0 l}$	Structure of the micelle	
0 - ⅓	Spheroidal in aqueous media	
⅓ - ½	Cylindrical in aqueous media	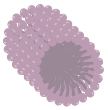
½ - 1	Lamellar in aqueous media	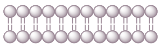
>1	Inverse micelles in nonpolar media	

The size, shape or aggregation number of micelles may change with surfactant concentration, temperature, or by addition of compounds to the liquid phase so that the morphology of the structure varies from spherical to cylindrical or lamellar shape.[170]

When the number of micelles in aqueous phase is high enough, they start to pack together in a higher structural level with a specific geometric arrangement. These structures have molecular order characteristic of crystals; however the molecular mobility is preserved and thereby they are called liquid-crystals. Depending upon the shape of the individual micelles, the arrangement geometry differs.[171] Hence the spherical micelles give rise to cubic liquid crystals, the cylindrical micelles pack together into hexagonal liquid crystals, and the lamellar micelles form lamellar liquid crystals (Figure 2.1).

As mentioned before, concentration along with temperature plays an important role in the structural morphology of surfactants. When temperature increases, usually the solubility of the surfactants increases too, and liquid crystals convert into micellar solutions. On the other hand, at high concentration and low temperatures, the surfactant can precipitate creating solid quasi-crystal structures. Liquid crystals would be present in the intermediate range of concentrations, where the phases moves from

hexagonal packing to continuous cubic structures and further to lamellar assembly, as concentration steadily increases.

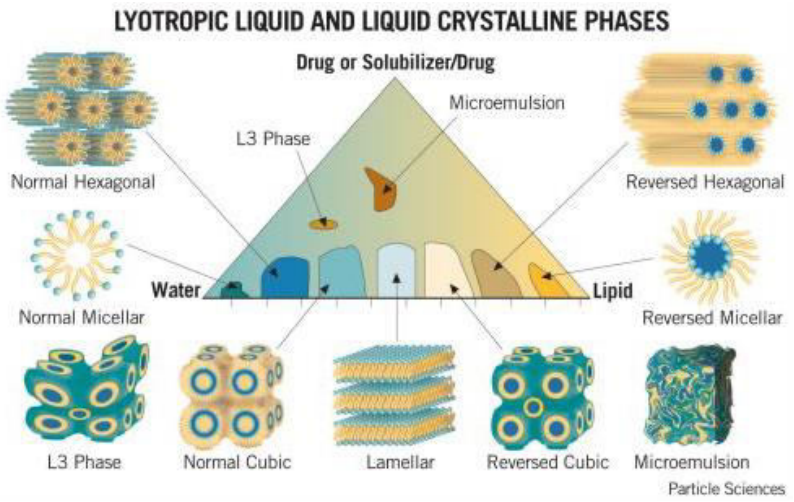

Figure 2.1 Liquid crystal structures of surfactants (from www.particlesciences.com).

2.1.2. Choline derivative surfactants

In the present thesis the surfactants used are alkanoylcholine iodides. Those compounds are derivatives from naturally occurring phospholipids like lecithin, that belongs to one of the bio-surfactants groups.

Bio-surfactants are some biological molecules that show surface activity and which are produced by living organisms, usually microorganisms such as bacteria or fungi. Different types of bio-surfactants are classified according to their chemistry nature; glycolipids, rhamnolipids, tehalolipids, lipoproteins, fatty acids, phospholipids and polymeric biosurfactants would encompass the principal groups.[171] In the present case, as previously stated, the surfactants employed in this work are derivatives from phospholipids, so we will focus on that group, specifically on choline derivatives.

Phospholipids are amphoteric or zwitter-ionic molecules and most of them consist of a phosphate diester of a diglyceride and choline. The phosphate group is anionically charged whereas the positive charge is located on the choline nitrogen. Lecithin, with phosphatidylcholine (PC) as major compound (Figure 2.2), was the first phospholipid identified and isolated in biological tissues by Gobley in 1847.[172] The biological importance of phospholipids

resides in their capacity for self-assembling in lamellar structures that integrate the biological membranes.

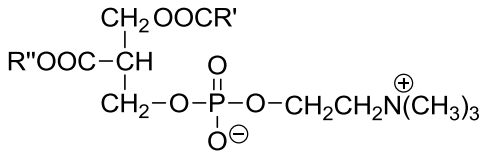

Figure 2.2 Chemical structure of phosphatidylcholine.

Apart from the mentioned structural functions, the role of phosphatidylcholines as nutraceutical complements in the human diets has been studied.[173] It was found that liver failure coincides with a 50% decrease in hepatic PC content.[174] In connection with this, several studies showed the recovery effect on the damaged liver and the healing effect of hepatitis A, B or C that is attained by PC administration.[175] Phosphatidylcholines and choline itself play an important role in the correct development of the brain;[176] and some authors have attributed them capacity to improve the mental function in dementia diseases.[177]

Some derivatives of the phosphatidylcholines, such as alkanoylcholines, i.e. the alkyl esters of choline (Figure 2.3), have been used in the detergent field. It is widely known that amphiphilic quaternary ammonium compounds are appropriate as cationic detergents for disinfection due to their antimicrobial activity.[178] This effect is based on the membrane disruptive reaction of those surface active substances in a broad variety of microorganisms, including gram-positive and negative bacteria, fungi or viruses. Nevertheless this affinity for biological membranes is not selective, and consequently a possible damage to human or mammalian cells can be caused. This side effect of toxicity may be avoided by incorporating labile moieties to the molecule that led to biodegradability of the substance into biocompatible fragments. Thus, the alkanoylcholine compounds have an ester bond between the ammonium and the long alkyl chain making the molecule sensible to certain hydrolytic enzymes such as butyrylcholine estearase.[179] Some studies reveal that the microbicidal activity of alkanoylcholines is comparable to that of non-biodegradable quaternary ammonium surfactants with the advantage of being hydrolysable into biocompatible products once that the antimicrobial effect has been exerted.[180]

Moreover, alkanoylcholines, as it is covered by several patents, have proven to display therapeutic effect in brain and cognitive related illnesses such as Alzheimer disease,[181,182] showing also a better penetration through the Blood

Brain Barrier (BBB). The enhancement in drug absorption by different human tissues provided by the ester group,[183] makes alkanoylcholines promising compounds for biomaterials. Nevertheless further studies are needed for the development of their all potential.

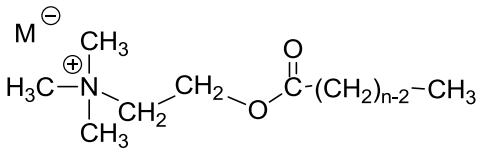

Figure 2.3 Chemical structure of *n*-alkanoylcholine.

2.2. Polyelectrolyte-surfactant complexes

Ionic complexes made of polyelectrolytes and oppositely charged surfactants generate well-defined self-assembled structures that show interesting mechanical, electrical or optical properties. The capacity of surfactants to become structured and even to crystallize and the capacity of polymers for being processed and to display mechanical properties are combined in these complexes. This synergic combination gives rise to new materials with unusual properties that have grown with increasing interest. The assortment of liquid crystalline structures of polyelectrolyte-surfactant complexes covers lamellar[184] (planar, undulated or perforated subphases),[185] columnar discotic morphologies[186] or cylinders[187] and hierarchical structure-within-structure morphologies (Figure 2.4).[188] The type of mesophase structure is determined by the surfactant, whereas the polyelectrolyte mainly plays a framework role although with significant effect on the structure due to its charge density.[189] At any case, it is the polyelectrolyte which has the major influence on the mechanical properties of the complex.[190]

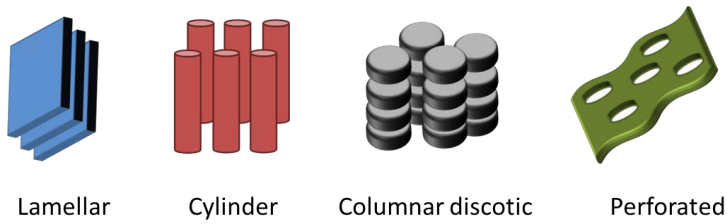

Figure 2.4 Schematic illustration of some mesophases of polyelectrolyte-surfactant complexes.

The cooperative binding of surfactant to the polyelectrolyte occurs because the surfactant is aggregated by the oppositely multicharged polyelectrolyte.[191] That binding starts at a narrow concentration range (CAC, critical aggregation concentration) that is usually some orders of magnitude below the CMC (critical micellar concentration) of the free surfactant.[169] Therefore, the linkage to the polymer, with a major contribution of electrostatic forces and reinforced by hydrophobic self-associations, is stronger than both surfactant-counterion and surfactant-surfactant bonds dominated by electrostatic and hydrophobic interactions, respectively.[168] The surfactant aggregates formed in polyelectrolyte solutions, which are similar to free micelles, follow the "pearl-necklace model", where micellar-like clusters of surfactant are ionically bound to the polymer chain.[169]

2.2.1. Structure of polyelectrolyte-surfactant complexes

The complexes obtained in aqueous solution can be more or less stoichiometric depending on the polymer to surfactant ratio used. In the case that a significant charge surplus is present due to an excess of either polymer or surfactant, water soluble complexes are generated. These non-stoichiometric complexes containing an excess of polyelectrolyte form are named "mixed micelles", in which the polyelectrolyte main chain surrounds the hydrophobic surfactant aggregate. Such clusters are able to solubilize hydrophobic organic molecules in water, allowing several technological applications.[192] In the biotechnological field, stiff and highly anionic charged double-helix of DNA changes its native extended coil conformation to compact globule by adding a cationic surfactant.[193,194] In gene therapy DNA chains need to be compacted to be transferred into the cells; non-stoichiometric complexation of nucleic acids with cationic surfactants has a great interest in this regard.

The simplest way to obtain polyelectrolyte-surfactant nanoparticles is mixing the two components in non-stoichiometric quantities whereas a solid complex is formed when equal number of anionic and cationic charges are used. As an example, the complex made of poly(ethylene imine) and dodecanoic acid renders 80-150 nm diameter nanoparticles in suspension when a 50% of polyelectrolyte excess is used.[195] The optimum ratio of polyelectrolyte-surfactant that forms nanospheres depends on the nature of both species and parameters such as packing parameter of surfactant, concentration or rigidity of the polymer backbone.

On the contrary, stoichiometric complexes obtained from equimolecular solutions of polyelectrolytes and surfactants, are not soluble in water but in common organic solvents. 1:1 ratio leads to organized self-assemblies with lamellar morphologies in the solid state,[188] similar to comb-like structures[196] where the surfactant molecules are bonded perpendicularly to the main polymer chain (Figure 2.5). This interesting assembly and simple preparation together with the huge number of possibilities for different polyelectrolytes available has led to the development of the study of stoichiometric polyelectrolyte-surfactants structure, properties and applications in the last two decades.[188,189,197,198,199]

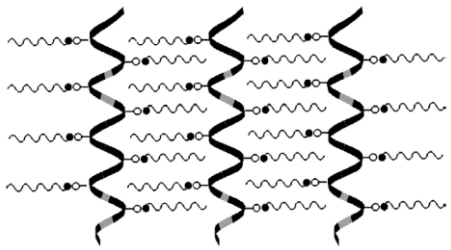

Figure 2.5 Lamellar biphasic structure characteristic of comb-like ionic complexes of poly(glutamic acid).

The study of equimolecular comb-like type surfactant-polyelectrolyte complexes has been mainly focused on two polymer families: conventional synthetic charged polymers, such as modified polystyrene[188] or poly(acrylic acid),[200] and bio-polyelectrolytes, such as polypeptides. Ponomarenko *et al*.[199,201] reported the preparation and structural characterization of complexes of poly(α,L-glutamate) and dodecyl- and cetyl-trimethylammonium bromides. They found that the polypeptide in these complexes adopts the α-helical conformation, and that the long alkyl chains of the surfactant are able to crystallize separately in a hexagonal lattice, whereas the shorter ones (below 16 carbon atoms) remain in a disordered state. A similar behavior is displayed by the long alkyl esters of poly(α,L-glutamic acid); [202] although in these cases the minimum number of alkyl carbons required to crystallize is lower. Alkyl side chain crystallization in the complexes might be hampered due to the spatial restriction imposed by the surfactant headgroups.[204] The system formed by poly(L-lysine) and dodecyl sulfate anions is known to take up a similar layered structure.[203]

In the Chemical Engineering Department of the ETSEIB (UPC) ionic-comb like complexes started to be investigated two decades ago. Pérez-Camero et al.[38] and García-Álvarez et al.[39] prepared and studied series of stoichiometric

or quasi-stoichiometric complexes made from poly(γ,D-glutamic acid) or poly(γ,DL-glutamic acid) and alkyltrimethylammonium bromides. These complexes are obtained by precipitation when aqueous solutions of Na·PGGA and alkyltrimethylammonium bromides are mixed. Crystallization of hydrocarbon tails takes place for alkyl chains containing at least 18 carbon atoms for both D and D,L-PGGA enantiomorphs. The melting temperature of the crystallized paraffin phase oscillates between 50 and 80 ºC depending on the alkyl chain length. X-Ray measurements ascertained the presence of the biphasic layered structure typical for these types of complexes where sheets of aligned PGGA chains are alternating with the crystalline surfactant partially crystallized in a pseudo-hexagonal lattice. The spacing of the layered ranged between 3.0 and 4.5 nm depending on the length of the alkyl chain.

The melting-crystallization transition involving the paraffinic phase can be closely followed by SAXS/WAXS and is also detected by ^{13}C-NMR spectroscopy[204] as an anti-to-gauche interconversion of methylenes. The interlamellar spacing is expanded after heating in the case of D-PGGA complexes, whereas a shrinkage has been observed for those made of D,L-PGGA. Similar lamellar structures undergoing comparable thermal transitions had been later reported for the complexes made of poly(aspartic acid) with *n*ATMA·Br surfactants.[205] More recently Portilla-Arias et al. have described *n*ATMA·PMLA complexes made of poly(L-malic acid) and the same surfactants; these complexes display almost exactly the same structure and properties than those made of PGGA.[206]

2.2.2. Properties and applications of polyelectrolyte-surfactant complexes

The specific structure adopted by polyelectrolyte-surfactant systems brings to the polymer exceptional properties of potential interest for increasing the applications of these materials. Illustrative examples are the complexes formed by polyelectrolytes with fluorinated surfactants. Fluoropolymers, like poly(tetrafluoroethylene) (PTFE, Teflon ®), due to their low surface tension, distinguish in generating non-sticky surfaces that are repellent to both water and oily liquid phases. These materials however cannot be processed because their extreme insolubility and high flowing temperatures. Complexes of polyelectrolytes with fluorinated surfactants offer a solution to processing problems; the arrangement of fluorocarbon tails in layers results in even lower surface tension than PTFE whereas, thanks to the polar moieties of these ionic complexes, they are able to be processed and dissolved.[189,207]

Certain complexes of cationic polyelectrolytes and DNA are able to form highly organized structures[208] and have been object of attention in several studies related to gene therapy.[209] Nevertheless, the most promising outcome of these complexes is in drug-delivery. The self-assembly and amphiphilicity make polyelectrolyte-surfactant systems suitable biomaterials either as simple drug carriers or even as targeting systems with an active role. An example is retinoic acid, an anionic metabolite of vitamine A involved in proliferation and differentiation of epithelial tissues, and whose role for the treatment of malignant-tumors or brain function and dermatological disorders is being widely investigated. In order to preserve its genuine properties, non-damaging immobilization of retinoic acid is necessary during administration. One approach to achieve it is complexation with cationic polyelectrolytes, both synthetic and naturally occurring polyaminoacids such as poly(L-lisine), poly(L-arginine) and poly(L-histidine).[202] On the other hand, nanoparticles useful as potential drug delivery systems have been prepared using different techniques.[189,202] However, one important drawback hampering the development of polyelectrolyte-surfactant complexes as DDS is the lack of biocompatibility of the counterions. As mentioned in section 2.1.2., surfactants such as quaternary ammonium compounds[181] or sodium alkyl sulphates[210] are suspected to be more or less toxic for human or mammalian organisms.

2.3. Fully polymeric systems

Macromolecular systems offer a practically unlimited number of possible architectures depending on the type of interaction that governs their formation and on the nature of the polymers. Analogously to polymer-surfactant complexes, block or comb-like amphiphilic copolymers are able to form specific architectures due to the mutual interaction between hydrophobic and hydrophilic domains. Furthermore complexation can also occur between two oppositely charged polyelectrolytes with generation of characteristic self-assembled structures.

2.3.1. Interpolyelectrolyte complexes (IPEC)

The mixing of anionic and cationic polyelectrolytes in aqueous solutions gives rise to the spontaneous formation of self-assembled interpolymer complexes. An entropy gain occurs due to the release of the low molecular counterions, which act as driving force for complex formation together with hydrophobic interactions and hydrogen bonding. This complexation may even entail an

endothermic process; elastic energy contributions of polyelectrolyte chains will hinder chains adaptation during the transitions to the more compacted IPEC structures.[202]

In the case of strong polyelectrolytes, stoichiometric end-point ratio near to 1:1 is found to result in a precipitation of the complex. Conversely under appropriate conditions in the presence of salt, non-stoichiometric systems consisting of polyelectrolytes bearing weak ionic groups and largely differing in molecular weight, water-soluble complexes may be obtained by using appropriate preparation conditions.[211] Salt concentration is a primary factor in determining the solubility of non-stoichiometric complexes.[212] Temperature is another parameter that affects aggregation and solubility of the IPEC. The adequate design of the IPEC structure and selection of the medium conditions (salt concentration, temperature, pH) lead to systems acting like living systems, i.e. systems able to respond sensitively to changes in their environment.

In contrast to polyelectrolyte-surfactant complexes, IPECs do not show in the solid state nanostructurated periodical mesophases. Experimental studies[213] have shown that IPEC structures are between two models, the ladder and the scrambled-egg model,[214] with predominant tendency to adopt the later one. The ladder-like structure arises as consequence of the formation of the complex at molecular level following a zip propagation mechanism of the interacting polyelectrolyte ion-pair. The scrambled-egg conformation refers to a high number of polycharged chains interacting non-specifically within the particle in which both components are confined (Figure 2.6).

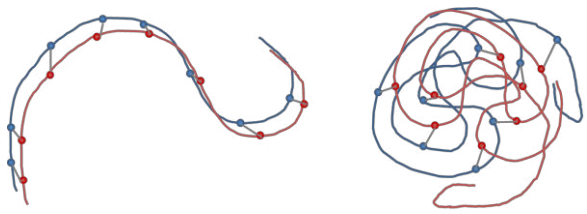

Figure 2.6 Ladder-like and scrambled-egg IPEC models.

When non-stoichiometric polyelectrolyte ratios are used, complex formation leads to stable dispersions of IPEC nanospheres in water at concentrations below 10^{-3} g·mL^{-1}. Static and dynamic light scattering studies suggested that the IPEC particles are constituted by a charge neutralized core surrounded by an electrostatic shell made of the exceeding component that stabilizes the

particle.[215] This ability of IPEC to form nanoparticles together with the aforementioned tailored properties encourages the interest for these compounds as biomaterials. Thus drug carriers and biomaterials[79] based on PGGA-chitosan porous IPECs have been widely studied and developed.[25] The active ingredient can also form directly a complex with the polyelectrolyte provided that it bears the suitable charge. Thus charged species such as enzymes[202] or DNA[45] can be directly integrated into the complex particles for a controlled administration.

2.3.2. Comb-like amphiphilic polymers

Polymers with an amphiphilic nature lead to a great variety of self-assembled structures, such as it happens with ionic complexes of polymer-surfactants. Three main types of amphiphilic polymers are described: graft copolymers, block copolymers and hydrophobically modified polymers.

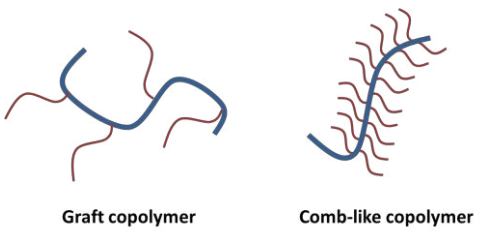

Figure 2.7 Schematic structures of graft and comb-like copolymers.

a) Graft copolymers are branched covalent polymers in which side chains have different chemical nature from the backbone (Figure 2.7). Interest in these copolymers arises because their conformation is determined by structural parameters such as grafting density or side chain and backbone lengths.[216,217]

b) Comb-like polymers are a specific kind of graft copolymer and are composed of a long flexible main chain and densely grafted side chains. Such a high density of grafting results in a copolymer molecular structure with a well-defined cylindrical shape due to the stiffness produced by the side chains. The interest of these compounds lies in their lyotropic behavior in dilute solution and the possibility of creating highly ordered biphasic structures in the solid state.[218]

Modification of poly(glutamic acid) on the carboxylic side group by esterification or amidation has given rise to a variety of graft and comb-like polyglutamates and copolyglutamates.[25] Given their relevance to the work carried out in this Thesis, attention is focused on the α-alkyl esters of poly(γ-glutamic acid), named henceforth as PAAG. The analogous esters of poly(α-glutamic acid) were developed first by Watanabe,[205] and Yamanobe[207] in the eighties of the last century. These authors concluded that above certain alkyl side length, (around 10 carbon atoms), the side chains were able to crystallize leading to the formation of a layered structure for the copolymer. This arrangement remained even after melting of the paraffinic phase with only slight changes in the characteristic spacing of the global structure.

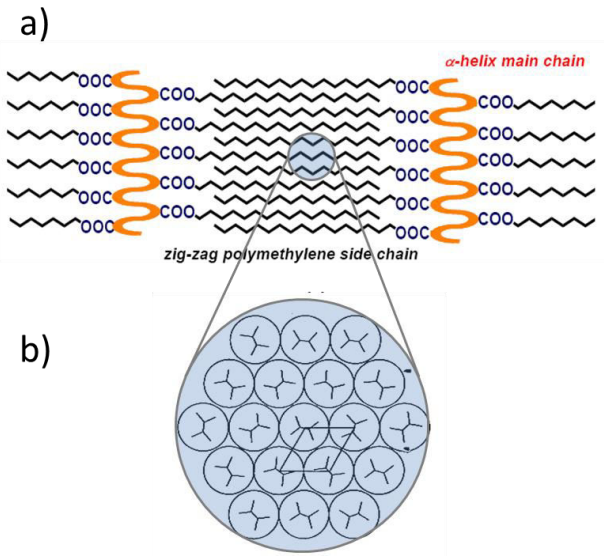

Figure 2.8 a) Layered structure of PAAG and b) perpendicular view of crystallized alkyl side chains in a hexagonal lattice.

In the last decade of the last century, Melis et al.[34,219] and Morillo et al.[35] described the preparation of a wide collection of alkyl esters of PGGA embracing from methyl to docosyl. They found that in most of cases, PGGA maintained the polypeptide backbone in α-helix conformation. According to the length of the alkyl side chain, poly(α-alkyl-γ-glutamate)s (PAAG) can be classified in two groups: "short" (from methyl to hexyl), and "long" (from dodecyl to docosyl) with the octyl and decyl derivatives remaining in a rather ambiguous position.[25] These two groups show a complete different behavior in terms of structure, thermal and mechanical properties. "Short" PAAG are semicrystalline and tend to crystallize in a three-dimensional close packing of

the α-helix polypeptide helices with the alkyl side chains integrated in the crystal lattice.[51,222] They melt at high temperatures, sometimes with decomposition and their Tg are in the 80-120 ºC range. They behave as typical semicrystalline materials showing good mechanical moduli and reduced extensibility. On the other hand, "long" PAAG display a comb-like characteristic structure with the polypeptide chains aligned in sheets and the flexible polymethylenic side chains crystallized in a separated phase[35] (Figure 2.8). These PAAG display reversible melting of the paraffinic phase in the 30-80 ºC range but they do not show T_g. The mechanical behavior of PAAG changed from hard and brittle to rubbery when the melting temperature is passed over. It has been recently shown that certain PAAG esters are able to form nanoparticles[77] and they have attracted attention as suitable materials for drug delivery applications.

3. Polymer-layered silicate nanocomposites

Polymeric materials are often filled with inorganic compounds, such as glass fiber or calcium carbonate, with the purpose of reducing costs of final material or enhancing their properties. Nanocomposites are a type of composites in which the reinforcing filler has at least one dimension in nanoscale. According to the number of nanodimensions, fillers can be *nanoparticles* with three nanometric dimensions, *nanotubes* or whiskers when two dimensions are of the nanometric order, and *layered clays or crystals* sheets with a thickness of nanometers. The filler materials mostly employed in nanocomposites are layered silicates due to their excellent availability and high aspect ratio and surface area.[220,221]

The addition of layered silicates into polymeric matrices has been study for over 60 years.[223] As a matter of fact; one of the earliest researches about this was carried out by Bower in 1949,[222] who described the absorption of DNA on montmorillonite. Although the systems made of polymers and layered silicates had been widely known, it was not until the 90s, when two major findings boosted the interest for these materials. On the one hand, Toyota researchers group disclosed a remarkable improvement in thermal and mechanical properties of Nylon 6 by adding small quantities of montmorillonite.[223] On the other hand, Vaia et al. reported that heating a mixture of polymer and silicate powder above T_g or T_m of the polymer, the chains are able to diffuse into the clay galleries leading to an intercalated structure of polymer and silicate.[224] The simplicity of the preparation method together with the possibility of

enhancing the properties by adding a few percents of filler encouraged the research on layered silicate nanocomposites.

3.1. Layered silicates

3.1.1. Structure and properties of layered silicates

Most common silicates used for the preparation of polymer-layered silicate nanocomposites belong to 2:1 phyllosilicates family. The crystal lattice of these silicates consists of a central octahedral sheet of aluminium hydroxide, which is fused to two external silica tetrahedral sheets by sharing oxygen atoms from octahedral and tetrahedral sheets (Figure 3.1). The thickness of the layers is around 1nm and the lateral dimensions may vary from 300 nm to several microns, depending on the specific silicate.[223,225]

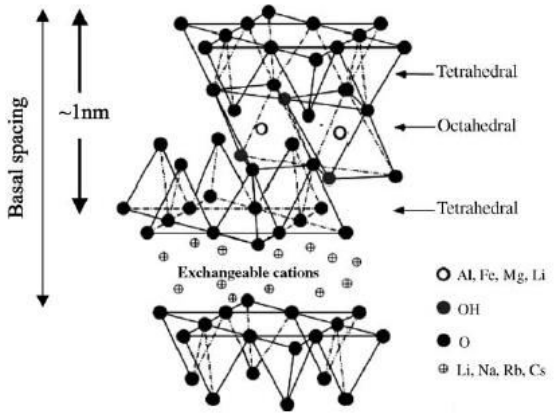

Figure 3.1 Layered structure of 2:1 phyllosilicate. (Image from Sinha Ray et al.)[228]

The basic structure of these compounds, with the silicon atom placed in the tetrahedral sites and the aluminium atom filling the octahedral ones without any substitution of the atoms is named as pyrophyllite. Isomorphic substitution of those atoms led to different types of silicates. When trivalent aluminium ion in the tetrahedral sheet is partially substituted by divalent magnesium an overall negative charge is created, which is counterbalanced in the interlayer by alkaline or alkaline earth cations like sodium or calcium.[226] This kind of phyllosilicate is called montmorillonite (MMT) and it is featured by its capacity

for exchanging (CEC) of the interlayer ions (measured as mequiv/100 mg) due to the relatively week forces holding the layers.[228,227]

Along with montmorillonite, hectonite and saponite are the most frequently used layered silicates in nanocomposite materials. The main characteristics of those clays are their ability of disperse into individual layers providing a high contact surface, the possibility of modifying their surface structure by ion exchange, their natural origin and the facility to obtain them in large quantities.

3.1.2. Organically modified layered silicates (OMLS)

Pristine layered silicates are hydrophilic, and therefore only miscible with hydrophilic polymers whereas most of engineering polymers are hydrophobic. In order to render clays compatible with hydrophobic polymers, it is necessary to modify properly the ionic interlayer space. This can be performed by exchange with cationic organic surfactants of surfactant-type able to replace the alkali counterions.[223,224,228,229] Alkylammonium ions are mostly employed, in addition to other "onium" salts such as phosphonium or sulfonium. The long organic chains of these surfactants not only provide hydrophobicity but also give rise to an increase of the interlayer distance of the clay with subsequent weakening of the interaction forces and improving diffusion of the polymer into the galleries.[228]

The cationic head group of the alkyl-onium molecule is preferentially tethered to the surface, leaving the organic tail protruding from the surface. Thus, ions can adopt monolayer, bilayer or paraffin-type aggregations in layered silicates.[229] Vaia et al. proposed a model where the interlayer structure of OMLS depends on the alkyl chain conformation, which varies from liquid-like to solid-like as the interlayer density or chain is made greater or temperature decreases.[230]

3.2. Characteristics of layered silicate nanocomposites

3.2.1. Phase structure

The affinity of the clay for the polymeric matrix is an essential factor in determining the structure of the composite. Inorganic and organic components that show poor physical attraction give rise to macrophase separation and

particle aggregation. The presence of those micro domains reduce the effect of the filler leading to a material with an overall behavior similar to traditional microcomposites and even with some properties impoverished.[223,231]

If the affinity between the filler and the matrix is good enough two different types of nanocomposites can be obtained according to the interactions between them. These two types of structures correspond to intercalated and exfoliated nanocomposites (Figure 3.2)

The intercalated structure is produced when a single or few polymer chains enter into the silicate galleries leading to an alternating polymer-silicate structure with a repeating spacing usually in a range of 2-3 nm. Conversely, in an exfoliated structure, individual clay sheets are well separated from each other and dispersed in the continuous polymeric matrix.[234] The interlayer distance between clay platelets becomes around 10 nm or more and the order is lost. The interlayer gap values are related to the gyration radius of the coil polymer or to the extended polymer chain for exfoliated and intercalated structures, respectively.[232] Generally, the clay content in exfoliated nanocomposite is much lower than in intercalated one.[228]

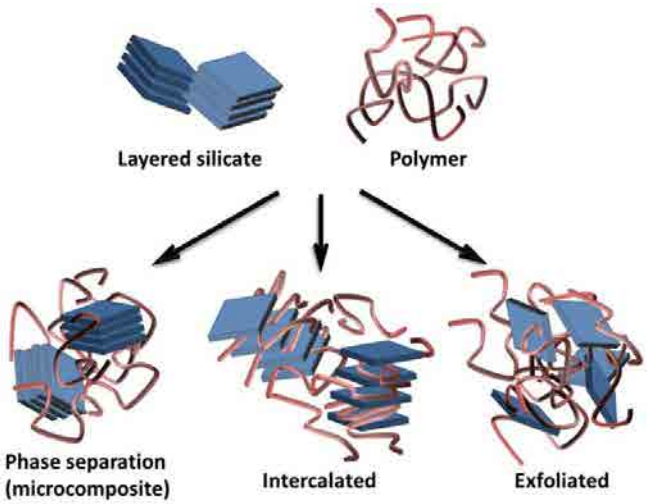

Figure 3.2 Scheme of intercalated and exfoliated structures of layered silicate nanocomposites.

Exfoliated systems present a much higher interaction between the polymer and the inorganic filler as a consequence of the better dispersion achieved in this case. The mechanical improvement observed in nanocomposites is due to the effective stress transfer from the polymer matrix to the filler through the

interphase area. Therefore, it is well accepted that exfoliated nanocomposites show better physical properties than intercalated ones due to their much larger interphase. Nevertheless, the achievement of totally exfoliated clay into a polymer matrix is difficult and most of reported polymer nanocomposites present an intercalated structure or a mixture of intercalated and exfoliated ones.[230]

3.2.2. Preparation methods

In addition to the nature of the components (polymer, silicate and modifier), the preparation method also plays an important role in succeeding to obtain an efficient nanocomposite. Currently, there are three main procedures to produce polymer-layered nanocomposites: intercalation of polymer in solution, *in-situ* intercalative polymerization, and melt intercalation.

Intercalation of polymer from solution

This method makes use of a suitable solvent which is able to dissolve the polymer and also to swell the clay or organoclay. The layered silicates are first dispersed in the solvent of choice, whose mutual interactions allow the clay layers to stay more separated and stacked by weak forces.[223,234] Delamination of the silicate can be also promoted by external shear forces, such as sonication.[233] Once the clay is swollen, the polymer is added to the dispersion and intercalation between the layers is produced. The driving force of the procedure is the exchange of intercalated solvent present in the clay gallery by polymer chains. In order to be a thermodynamically favored process, the entropy gained in the solvent molecules desorption has to compensate the loss of entropy produced by the constrained intercalated chains.[228] Upon removing the solvent, the structure of clay sheets remains and sandwiches the polymer leading to an intercalate nanocomposite.

Intercalation from solution technique was first used for water-soluble polymers such as polyethylene oxide (PEO), polyvinyl alcohol (PVA) or polyvinylpyrrolidone (PVP).[224,228,234] In fact Aranda and Ruíz-Hitzky[234] reported first PEO-MMT nanocomposites obtained by this method using different polar solvents. They found that polarity of the media was critical in promoting the insertion of the polymer chains in between the clay platelets. With regards to non-polar polymers, organic solvents are used to swell organically modified silicates and to dissolve the polymeric matrices. Intercalated nanocomposites

of polyethylene (PE), polystyrene (PS), polycaprolactone (PCL) or polylactic acid (PLA) have been obtained using this technique. [224,228,234]

However, the difficulty of finding the suitable polymer/solvent pair along with the environmental problems associated to the use of large amounts of non-aqueous solvents make this method inadequate for industrial applications.

In-situ intercalative polymerization

In this technique, the organoclay is swollen by a liquid monomer or monomer solution. The monomer resides into the layered silicates galleries and then, polymerization is carried out in the interlayer space of the clays provoking their delamination due to the restrictions imposed by the long chain macromolecules formed.[223]

Although *in-situ* polymerization is a known method that has been studied from the 1960s,[235] the researches performed by Toyota group[226] based on polyamide 6 have definitely stimulated its development. They reported that α,ϖ-amino acids modified montmorillonites were swollen by ε-caprolactam monomer and catalyzed the subsequent ring-opening polymerization of the monomer leading to N6/MMT nanocomposites (Figure 3.3). Related to the influence of the organically modified clay, they found that the longer was the carbon atom chain in the amino acids, the higher the extent of intercalation of the monomer that was achieved.[236]

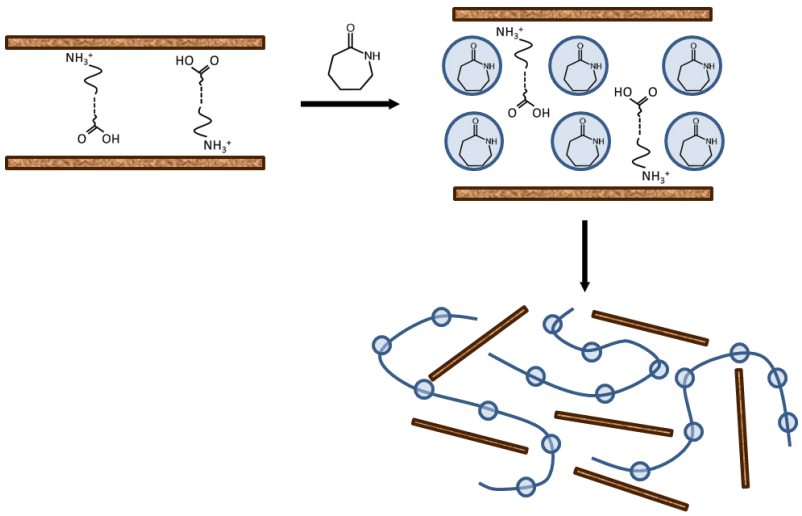

Figure 3.3 Swelling behavior of ε-caprolactam monomer in α,ϖ-amino acids modified montmorillonite and subsequent in-situ intercalative polymerization.

These findings were then used to obtain nanocomposites of PCL-based polymers[228,234] such as polyurethanes.[237] Besides the ring-opening polymerization method, this technique has been applied successfully to polymers synthesized by chain-growth mechanisms such as PMMA or PS.[228,230,234] On the other hand, its application to polymers obtained from direct condensation like PET result in low molecular weight nanocomposites.[238]

It is worth mentioning that, in spite of the success of the *in-situ* intercalative polymerization method; some disadvantages are associated to this procedure: it is a time-consuming route and, in some cases, exfoliation may be thermodynamically unstable producing a subsequent re-aggregation of clay platelets.[239] Despite these drawbacks, this method is the unique viable way to obtain nanocomposites of thermoset polymers, which obviously cannot be prepared neither from solution or by melt intercalation procedures.[234,240]

Related to *in-situ* polymerization, template synthesis is based on the synthesis of the clay minerals within the polymer matrix. In this technique, an aqueous solution of the polymer that contains the silicate building blocks is used in a sol-gel technology. The polymer acts as a nucleating agent for the growing of inorganic crystals and becomes trapped within the sheets during crystallization. Even though some successful works are reported, the high temperatures required for clays synthesis that would provoke the degradation of the polymers, might be an important drawback.[223,234]

Melt intercalation

This method consist of annealing a mixture of the polymer and the OMLS at a temperature above the softening point of the polymer, usually under shear.[227] The melt intercalation technique avoids the compatibility problems between clay and solvent or monomer that frequently appear in the solution or *in-situ* polymerization procedures, increasing therefore the number of feasible polymers for nanocomposite formation. Furthermore this procedure is suitable for industrial application since it can be performed at processing such as extrusion or injection molding.[228,235] The absence of organic solvents is another advantage that makes melt intercalation an environmentally friendly process.

Giannelis reported first this technique[227] and studied the thermodynamic of the process.[241,242] Intercalation consists of the diffusion of polymer chains from the bulk matrix into the galleries of the silicate. In contrast to intercalation of polymer from solution, where entropy is the driving force, in the molten

state the direct intercalation is driven by an enthalpic mechanism. Compared to solvent intercalation technique, specificity for polymer intercalation is improved by avoiding the competing host-solvent and polymer-solvent interactions.[227] The success in the formation of the intercalated nanocomposite depends on the structure of OMLS and the affinity of polymer with the organoclay.[244,245] The OMLS not only increases the interlayer gap but also acts as a compatibilizer between clay and polymer. Therefore, selection of the appropriate organoclay is an essential key to attain intercalation;[243] in some cases functionalization with appropriate organic groups would help for the purpose.[230]

The first nanocomposite obtained by this melt intercalation technique was based on a PS,[227] which was obtained upon melting under pressure. Studies on N6/octadecylammonium-MMT nanocomposite using a twin-screw extruder as shear force showed the presence of an exfoliated structure,[244] which established the importance of the shear applied for mixing.

3.2.3. Properties and applications

Layered silicate nanocomposites have proven to improve many properties when compared to the neat polymer, mainly mechanical and barrier properties, thermal stability and fire retardancy. The effect of the clay on properties is highly depending on the structure of the nanocomposite with dispersion of clay sheets playing the main role. Consequently, intercalated and exfoliated structures for the same system will display clearly different polymer properties.

Mechanical properties

Inorganic fillers used in composites are usually resistant to deformation and display high modulus; upon reinforcing they will confer improved mechanical properties to relatively soft polymer matrices. When the bonding between both phases is effective, the particle fillers restrain the movement of the surrounding chain polymers making the nanocomposite able to support higher efforts; therefore, the larger the interphase area between polymer and filler, the greater will be the reinforcing effect.[245]

Layered silicates are suitable materials for this purpose due to their extremely high surface area (around 800 $m^2 \cdot g^{-1}$) giving rise in some cases to a stunning enhancement of Young's modulus, tensile strength or toughness, even at low

concentrations.[223] Whereas in conventional composites the increase of the modulus is linear with the filler percentage, in nanocomposites a dramatic improvement is obtained for small quantities of silicate.[228] It is the high aspect ratio of layered silicates which makes possible such spectacular effects. Beyond the percolation limit, further added silicate sheets are incorporated in polymer areas that are already affected by other clay platelets and consequently, the modulus will not increase so vividly.[246] Generally, the best improvements are associated to the occurrence of exfoliated structures.[234]

Nonetheless, thermoplastic matrices usually lead to brittle materials when forming nanocomposites. In spite of the improved stiffness, the formation of microvoids created in the matrix/nanofiller interphase will coalesce with formation of larger cracks. This phenomena causes the embrittlement of the material with the consequent reduction in elongation at break and toughness.[230] For instance, 5% nylon 6 nanocomposites studied by Fornes et al.[247] showed double Young's modulus values compared to pure N6, whereas their elongation at break was around 100 times lower.

Micromorphology plays again an important role in ductility and toughness alterations. The interaction between silicate layers is somewhat retained in intercalated structures whereas it is definitely lost in the exfoliated systems. Such remaining interactions seem to be responsible for the better toughening properties found in intercalated nanocomposites compared to exfoliated ones.[248] A similar effect is sometimes observed on the elongation at break[249] despite it is very unusual as thermoplastic polymers are concerned. However, several authors have reported an enhancement in elongation in the case of elastomeric matrices.[230] It can be assumed that such behavior is due to the plasticizer effect provided by the gallery "oniums" in the polymer matrix and to their contribution in the formation of dangling chains, and also to conformational effects in the clay-matrix interphase.[234]

Thermal stability

The incorporation of clay layered sheets into the polymer matrix, generally lead to higher thermal stability of nanocomposites due to the insulator effect of the clay. Moreover the tortuous route imposed by dispersed platelets (Figure 3.4) and char formation hampers the mass transport of volatile compounds produced during degradation.[228,250] This effect was first reported by Blumstein for an intercalated nanocomposite of PMMA/MMT obtained by in-situ polymerization[251] which displays degradation temperatures 40-50 ºC higher than the neat polymer.

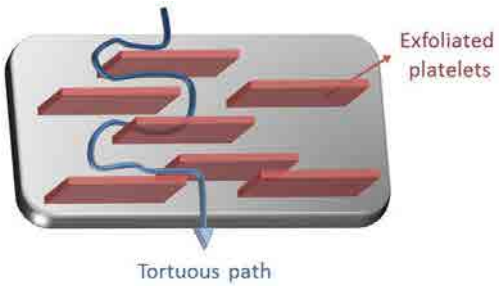

Figure 3.4 Proposed tortuous diffusion path model in layered silicate nanocomposites.

Notwithstanding contradictory results are reported in the literature for several systems and by different authors.[223,228] The two opposite effects might be the results of two different mechanisms operating in the dispersed clay. On the one hand, the higher thermal stability provided by the insulating barrier effect of platelets; on the other hand, the heat accumulation on the clay[228] together with its possible catalyst effect on polymer degradation. In OMLS heat originates instability in the organic part of the modified nanoclay (e.g. Hoffmann elimination reaction of alkyl ammonium salts).[252]

Gas barrier properties

Frequently a dramatic improvement of barrier properties is reported for layered silicate nanocomposites. As referenced above for thermal stability, it is due to the difficulty imposed to the circulation of small molecules by the presence of the impermeable nanolayers. The sheet-like morphology of the layered silicates is especially efficient in decreasing the permeability of nanocomposites due to their large aspect ratio. The effect is maximum in ordered nanocomposites with the silicate platelets stacked in a plane normal to the diffusion direction (Figure 3.4).[228] Nevertheless changes in matrix crystallinity or chain mobility caused by presence of the filler must be also taken into account to explain the loss of permeability. It is well known that an increase in either the crystalline-to-amorphous ratio or in T_g contribute to improve the barrier properties of polymers.[253]

Flame retardancy

Flame formation is a property related to thermal stability and gas barrier properties. The mechanism involved in the retardancy of flame creation is the formation of a char that acts as a barrier to both mass and energy

transport.[228,253,254,255] As long as clay fraction increases and thus the char does, it would lead to a decrease of heat releasing rate.

Nanocomposites can offer certain advantages when compared to conventional flame retardant polymers or flame retardant additives. Flame retardant polymers are frequently synthesized from halide polymers (usually fluorinated), with a harmful consequence in environmental contamination. In the case of additives, high amounts of them are needed to be loaded in the material in order to get the desired effect. This alters the intrinsic properties of the polymer; with an increase of the density and impoverishment of mechanical properties.[223] The substitution of conventional flame retardants by nanocomposites avoids the environmental impact as well as the detriment of the physical properties, which may be still improved.[258] Moreover, the presence of silicates provides physical integrity to the composite avoiding the dripping of flaming material which is the main cause of fire propagation to the surroundings.[256]

Crystallinity

Clay platelets are well known nucleating agents for polymer spherulites when forming composites. They promote heterogeneous nucleation in polymer crystallization with the consequent decrease in their sizes.[230] This nucleating effect is more pronounced for low loads of silicates, usually below 5%, so the higher the clay content, the more prevalent the opposite effect is observed. Furthermore melting temperatures of polymer decrease due to the reduction in crystal size provoked by the hindering of mobility of confined polymer chains in the presence of clay.[257] The predominance of this resulting effect will depend not only on the clay content but also on the polymer matrix nature, nanocomposite structure and crystallization conditions.[258]

Biodegradation

The influence of the silicate clay nanofillers in the biodegradability of nanocomposites is an interesting feature that is still under discussion. Frequently, an enhancement in the biodegradability of nanocomposite compared to neat polymer is reported.[223,228] First results on this issue were gathered for polycaprolactone nanocomposites,[259] which led to conclude that the presence of the organoclay improved the biodegradability of the polyester. The presence of terminal hydroxylated edge groups of silicate layers may be one of the responsible factors for this increased degradation rate. In the case

of PLA composite, it was observed that those hydroxyl groups contained in the clays tend to absorb water from the environment favoring the heterogeneous hydrolysis of the polymer.[260]

However, other studies show contradictory results which could be explained considering the role played by the barrier properties of the nanocomposite.[261,262] The tortuous path to transport imposed by the platelets can hamper the entrance and diffusion of microorganisms into the polymer matrix with the subsequent diminution in biodegradability.

Other properties

Nanocomposites display other specific characteristics when compared to conventional composites. One outstanding feature of nanocomposites is their transparency due to the lack of scattering by the nanometric clay particles Resistance to scratch and ablation are also properties that have been reported to be improved by nanocomposite formation.[223,230]

Applications

Nanocomposites offer superior properties to conventional composites. Since property improvement is attained at low amounts of clay, nanocomposites are much lighter than traditional composites, which makes them interesting competitive materials for a wide number of applications.

The current and potential applications for nanocomposites involve almost every technology fields as automotive sector, construction, aerospace, food packaging, electronics, biomedicine or textile.[223,263] The first commercial polymer material based on nanocomposite was developed for the automotive industry.[226] This material was a Nylon6 nanocomposite patented by Toyota and Ube in the 90s which was applied for timing belt cover because its good thermal resistance, rigidity and lightness. Later these nanocomposites were introduced in the building of engine covers, but their expensive prices limited their expansion and their applications were focused on high barrier materials.[264] Nanocomposites based on polyolefins and PP in particular have found use also in the automotive industry like materials for step assistant or structural seat backs.[266]

The improvement on the barrier properties exhibited by nanocomposites combined with their excellent optical transparency make them unique for beverage and food packing applications, in particular when gas containing

drinks are concerned. Bayer, Mitsubishi and Nanocor companies have developed materials with high barrier properties suitable for packaging films and bottles using clay nanocomposites.[223,266] The fire retardant behavior of nanocomposites together with their tailoring functionalities for conductivity, membranes or corrosion protection have been taken of advantage for preparing thin layers for electrochemical or electroanalytical devices.[265]

Several big automotive companies such as General Motors, Ford and Volvo as well as chemical companies such as Dow, Honeywell, Eastman, Clariant or Showa Denko maintain great efforts in the research and development of nanocomposites with the aim of expanding their market and technology by solving their shortcomings, in particular their high production costs.[223,266]

3.3. Bio-nanocomposites

Despite their high level performance, interesting properties and technology benefits, conventional petrochemical-based polymers constitute a big environmental concern as a consequence of the non-biodegradability of those materials and the use of toxics in their manufacture. Moreover, the fossil origin of the raw materials used for their fabrication presents a huge limitation at a mid-term future. Hence, the development and use of biodegradable or renewable sources based polymers replacing those environmentally unfriendly materials is more and more required. Although some biopolymers afford a potential for applications as plastics they suffer from severe drawbacks in properties such as brittleness, high gas permeability, low heat distortion temperature or low melt viscosity. Nevertheless, the formation of biopolymer nanocomposites leading to an enhancement of mechanical and other properties appears as a good option to overcome such problems.[228,266]

Strictly speaking, a biopolymer is a polymer produced by living organisms. Polysaccharides, polypeptides, gelatin or poly(3-hydroxybutyrate) (PHB) are among others common biopolymers of technological importance. Polysaccharides are difficult to process and biopolyesters are naturally available only in small amounts. Nonetheless, some of them as poly(hydroxyalakanoate)s (PHA, *Biopol* is as trade name for the copolymer PHB-PHV) are today biotechnologically produced at the industrial level.[267] However, the term “biopolymer” is also informally applied to those polymers produced by chemical synthesis but that have a bio-based origin as it is the case of poly(lactic acid) (PLA, *Natureworks* as a trademark) or poly(butylene succinate) (PBS), or even to synthetic polymers that display biodegradability as poly(caprolactone).[268,269]

The first studied nano-biocomposites were petroleum-based biodegradable polymers, which were developed by Messersmith and Giannelis group and date from early 1990s.[270] They consisted of PCL matrix composites with fluorohectorite as filler, a mica-type layered silicate, obtained by in-situ polymerization technique taking benefit from the catalytic effect of the layered silicates on the ring opening polymerization of ε-caprolacton. The same authors also reported the preparation of PCL composites by employing different kinds of OMLS,[271] being 12-aminolauric acid the most suitable one. PCL is a linear and semicrystalline polymer with low T_g and T_m values that shows high elongation at break but a quite low elastic modulus.[269] Thereby, the interest for PCL nanocomposites lies in their capacity for upgrading mechanical properties of the neat polymer with the purpose of broadening their possibilities.[272] The physical properties together with commercial availability make PCL a potential material not only as a commodity substitute but also for specific medicine or agricultural applications. Indeed, some new applications of these PCL-nanocomposites include tissue engineering or scaffolds[273] in biomedicine.

Within the petroleum-based biodegradable polymers, PVA constitutes a particularly interesting plastic due to its water solubility. This feature allows to obtaining PVA/MMT composites by casting from water,[269,274] with the consequent reduction in toxicity and VOC release, and simplicity in the production procedure. The obtained composites based on PVA matrix displayed an enhancement of 300% in strength modulus and an increase in thermal stability among other positive effects.[277]

PLA is synthesized by a biotechnological procedure using the lactic acid obtained from the fermentation of carbohydrates by fungi or bacteria such as *Lactobacillus.*[275] Due to its commercial availability and low price, this material is one of the most promising polymers, existing in a wide range of grades according to the specifications required for applications, mainly in biomedicine and food packaging (Figure 3.5).[272] PLA displays interesting features like satisfactory mechanical properties, thermal plasticity and biocompatibility. On the other hand, other properties such as gas permeability, flexural stress or heat distortion temperature are insufficient for some purposes. Several works have reported that such shortcomings of PLA may be overcome by making nanocomposites with either intercalated or exfoliated layered silicates.[263,269,272] Significant decrease in O_2 permeability down to half of the initial value or increase in strength up to of 130% are thus achieved.[276]

Figure 3.5 Plastic cup made from corn-based PLA.

Polyhydroxyalkanoates (PHA)s are produced by microorganisms in culture media containing an excess of carbon substrates, being poly(hydroxybutarate) (PHB) the main polymer of the family.[277] PHB is a relatively high crystalline polymer which is also produced in industrial amounts and commercialized, although in smaller scale than PLA.[272] Despite the fact that the PHB general properties are satisfactory it is too sensitive to processing conditions and its mechanical behavior needs upgrading for some applications.[278] The preparation of PHB-based nanocomposites regarding its mechanical and thermal stability improvement is stimulating.[280] Several intercalated nanocomposites using fluoromica instead of MMT have been reported to lead to an enhancement on the mechanical properties.[279] Moreover, an acceleration in thermal or biodegradation processes favored by the presence of organically modified MMT, due to the catalytic effect of Al and organomodifiers, has also been showed.[282,280]

Apart from those commercial biotechnology-based polymers, some nanocomposites of naturally occurring biopolymers have been developed for specific applications. Kevadiya et al. developed an alginate-based nanocomposite, where the MMT was organically modified by thiamine hydrochloride (Vitamin B1) and pyridoxine hydrochloride (Vitamin B6). This material was proposed to be used as carrier system for intestinal delivery of vitamins.[281]

The ion exchange capacity of layered clays can be used in order to obtain intercalated polyelectrolyte-clay nanocomposites. Biopolymers of polyelectrolyte nature become charged depending on the pH of the media. These bio-polyelectrolytes have been utilized to form nanocomposites based on polymer-filler electronic interactions. Polycationic chitosan and anionic MMT can interact to form intercalated nanocomposites with a robust and compact three-dimensional structure which displays some interesting functional properties.[282] First layer of chitosan is adsorbed in the clay through

a cationic exchange procedure, and depending on the chitosan:clay ratio a second layer of polymer can be adsorbed in acetate salt form. The $NH_3^+Ac^-$ moiety of this second layer may act as an anionic exchanger and in consequence, these nanocomposites can be applied as potential electrodes that are distinguished by an easy surface renewal, long-time stability and ruggedness. Finally, gelatin nanocomposites have been also prepared based on the amphoteric properties of gelatin. The pH of the media is determinant of the interaction type between gelatin and MMT, which takes place by cationic exchange of the metal cations of MMT and the $-NH_3^+$ of gelatin or by hydrogen bonding between $–COO^-$ of gelatin and the OH groups of MMT.[283]

4. References

1. Shih, I. L.; Van, Y. T. The production of poly-(gamma-glutamic acid) from microorganisms and its various applications. *Bioresource Technol.* **2001**, *79*, 207–225.

2. Buescher, J. M.; Margaritis, A. Microbial biosynthesis of polyglutamic acid biopolymer and applications in the biopharmaceutical, biomedical and food industries. *Crit. Rev. Biotechnol*. **2007**, *27*, 1–19.

3. Ivanovics, G.; Bruckner. V. Chemishe und immunologiche Studien uber den Mechanismus der milzbrandinfektin und Immunitat; die chemische Struktur der Kapselsubstanz des Milzbrandbazillus und der serologisch identischen spezifischen Subtanz des Bazillus mesentericus. Z. Immunitatsforsch. **1937**, *90*, 304–318.

4. Sawamura, S. On the Micro-organisms of Natto. *Bulletin of the College of Agriculture. Tokyo Imperial Univ.* **1913**, *7*, 107-110.

5. Fujii, H. Formation of mucilage by Bacillus natto.Effects of some cultural conditions on the chemical constituents of mucilage. *Nippon Kagaku Kaishi.* **1963**, *37*, 615-518.

6. Housewright, R. D.; Thorne, C. B. Synthesis of glutamic acid and glutamyl polypeptide by Bacillus Anthracis. I. Formation of glutamic acid by transamination. *J. Bacteriol*. **1950**, *60*, 89–100.

7. Herbst, R. M. The transamination reaction. *Adv. Enzymol*. **1944**, *4*, 75-97.

8. Hezayen, F. F.; Rehm, B. H.; Tindall, B. J.; Steinbüchel, A. Transfer of Natrialba asiatica B1T to Natrialba taiwanensis sp. nov. and description of Natrialba aegyptiaca sp. nov., a novel extremely halophilic, aerobic, non-pigmented member of the Archaea from Egypt that produces extracellular poly(glutamic acid). *Int. J. Syst. Evol. Micr.* **2001**, *51*, 1133–1142.

9. Ho, G.; Ho, T.; Hsieh, K.; Yang, J.; Yang, S. γ-Polyglutamic acid produced by Bacillus subtilis (natto): structural characteristics, chemical properties and biological functionalities. *J. Chin. Chem. Soc.* **2006**, *53*, 1363–1384.

10. Yoon, S.; Do, J.; Lee, S.; Chang, H. Production of poly-y-glutamic acid by fedbatch culture of Bacillus licheniformis. *Biotechnol. Lett.* **2000**, *22*, 585-588.

11. Kunioka, M. Biosynthesis and chemical reactions of poly(amino acid)s from microorganisms. *Appl. Microbiol. Biotechnol.* **1997**, *47*, 469–475.

12. Richard, A.; Margaritis, A. Poly(glutamic acid) for biomedical applications. *Crit. Rev. Biotechnol.* **2001**, *21*, 219–232.

13. Kedia, G.; Hill, D.; Hill, R.; Radecka, I. Production of poly-gamma-glutamic acid by Bacillus subtilis and Bacillus licheniformis with different growth media. *J. Nanosci. Nanotechnol*. **2010**, *10*, 5926-5934.

14. Kubota, H.; Matsunobu, T.; Uotani, K.; Takebe, H.; Satoh, A.; Tanaka, T.; Taniguchi, M. Production of poly(gamma-glutamic acid) by Bacillus-Subtilis F-2-01. *Biosci. Biotechnol. Biochem*. **1993**, *57*, 1212-1213.

15. Pérez-Camero, G.; Congregado, F.; Bou, J. J.; Muñoz-Guerra, S. Biosynthesis and ultrasonic degradation of bacterial poly(gamma-glutamic acid). *Biotechnol. Bioeng.* **1999**, *63*, 110–115.

16. (a) Waley, S. G. The structure of bacterial polyglutamic acid. Chem. Ind. **1956**, *37*, 1148-1149. (b) Waley, S. G. The structure of bacterial polyglutamic acid. *J. Chem. Soc.* **1955**, 517-522.

17. (a) Bruckner, V.; Kovacs, J.; Nagy, H.; Katjár, M. Synthesis of γ-polyglutamic acid. *Naturwissenshaften*. **1954**, *41*, 528-529. (b) Bruckner, V.; Wein, J.; Nagy, H.; Katjár, M.; Kovacs, J. Synthesis of γ-poly-L-glutamic acid. *Naturwissenshaften*. **1955**, *42*, 210.

18. Katjar, M.; Bruckner, V. Improved syntheses of stereoiomeric poly-gamma-glutamic acids. I. Syntheses via polymethylesters. *Acta Chim. Acad. Sci. Hung.* **1969**, *62*, 191-212.

19. Kovacs, J.; Smith, G. N.; Johnson, B. J. A new synthesis of poly-gamma-D- and L-glutamic acid. *Can. J. Chem.* **1969**, *47*, 3690–3693.

20. Sanda, F.; Fujiyama, T.; Endo, T. Chemical synthesis of poly- γ-glutamic acid by polycondensation of γ-glutamic acid dimer : Synthesis and reaction of poly-γ-glutamic acid methyl ester. *J. Polym. Sci. A Polym. Chem.* **2001**, *39*, 732–741.

21. Hollosi, M.; Kajtar, M.; Bruckner, V. Improved syntheses of stereoisomeric poly-gamma-glutamic acids. 2. Syntheses via polybenzyl and poly-t-butyl esters. *Acta Chim. Acad. Sci. Hung.* **1969**, *62*, 305.

22. Sanda, F.; Fujiyama, T.; Endo, T. Stepwise synthesis of gamma-glutamic acid 16-mer. *Macromol. Chem. Phys*. **2002**, *203*, 727-734.

23. Ashiuchi, M., Kamei, T., Baek, D. H., Shin, S. Y., Sung, M. H.; Soda, K.; Yagi, T.; Misono, H. Enzymatic synthesis of high molecular weight poly-

gamma-glutamate and regulation of its stereochemistry. *Appl. Environ. Microbiol*. **2004**, *70*, 4249–4255.

24. Ashiuchi, M.; Kamei, T.; Misono, H. Poly-gamma-glutamate synthetase of Bacilllus Subtilis. *J. Mol. Cat. B Enzym.* **2003**, *23*, 101-106.

25. Muñoz-Guerra, S.; García-Álvarez, M.; Portilla-Arias, J. A. Chemical modification of microbial poly(γ-glutamic acid): Progress and perspectives. *J. Renew. Mater.* **2013**, *1*, 42–60.

26. Pfeffer, P.; Silbert, L. S. Esterification by alkylation of carboxylate salts. Influence of steric factors and other parameters on reaction rates. *J. Org. Chem.* **1976**, *41*, 1373-1379.

27. Kubota, H.; Fukuda, H.; Takebe, H.; Endo, T. Poly-gamma-glutamic acid ester and shaped body thereof. US Patent 5118784, 1992

28. Kubota, H., Nambu, Y.; Endo, T. Convenient and quantitative esterification of poly(gamma-glutamic acid) produced by microorganism. *J. Polym. Sci. A Polym. Chem*. **1993**, *31*, 2877-2878.

29. Kubota, H.; Nambu, Y.; Endo, T. Convenient esterification of poly(γ-glutamic acid) produced by microorganism with alkyl halides and their thermal properties. *J. Polym. Sci. A Polym. Chem*. **1995**, *33*, 85-88.

30. Borbély, M.; Nagasaki, Y.; Borbély, J.; Fan, K.; Bhogle, A.; Sevoian, M. Biosynthesis and chemical modification of poly(γ-glutamic acid). *Polym. Bull.* **1994**, *32*, 127-132.

31. Shah, D. T.; McCarthy, S. P; Gross, R. A. New polymers derived from gamma-poly(glutamic acid). *Abs. Pap. Amer. Chem. Soc*. **1992**, *204*, 249.

32. Gross, R. A.; McCarthy, S. P.; Shah, D. T. Gamma-poly(glutamic) acid esters. US Patent 5378807, 1995.

33. Gonzales, D.; Fan, K.; Sevoian, M. Synthesis and swelling characterization of a poly(γ-glutamic acid) hydrogel. *J. Polym. Sci. A Polym. Chem. 1996,* **34**, 2019-2027.

34. Melis, J.; Morillo, M.; Martínez de Ilarduya, A.; Muñoz-Guerra, S. Poly (α-alkyl γ-glutamate) s of microbial origin : I. Ester derivatization of poly (γ-glutamic acid) and thermal degradation. *Polymer* **2001**, *42*, 9319–9327.

35. (a) Morillo, M.; Martínez de Ilarduya, A.; Muñoz-Guerra, S. Comblike alkyl esters of biosynthetic poly (γ-glutamic acid). 1. Synthesis and characterization. *Macromolecules* **2001**, *34*, 7868–7875. (b) Morillo, M.;

Martinez de Ilarduya, A.; Alla, A.; Muñoz-Guerra, S. Comblike alkyl esters of biosynthetic poly (γ-glutamic acid). 2. Supramolecular structure and thermal transitions. *Macromolecules* **2003**, *36*, 7567–7576.

36. Pérez- Camero, G.; Vazquez, B.; Muñoz-Guerra, S. Water-soluble esters of biosynthetic poly(γ-glutamic acid). *J. Appl. Polym. Sci*. **2001**, *82*, 2027-2036.

37. Portilla-Arias, J. A.; García-Alvarez, M.; Martínez de Ilarduya, A.; Muñoz-Guerra, S. Thermal decomposition of microbial poly (γ-glutamic acid) and poly (γ-glutamate)s. *Polym. Degrad. Stab.* **2007**, *92*, 1916–1924.

38. (a) Pérez-Camero, G.; Martínez de Ilarduya, A.; García-Álvarez, M., Muñoz-Guerra, S. Stoichiometric complexes made of naturally occurring poly (γ,D-glutamic acid) and cationic surfactants. *Abs. Pap. Amer. Chem. Soc.* **1999**, *218*, U532. (b) Pérez-Camero, G.; García-Alvarez, M., Martínez De Ilarduya, A.; Fernández, C., Campos, L., Muñoz-Guerra, S. Comblike complexes of bacterial poly(γ,D-glutamic acid) and cationic surfactants. *Biomacromolecules*. **2004**, *5*, 144–152.

39. García-Alvarez, M.; Alvarez, J.; Alla, A.; Martínez de Ilarduya, A.; Muñoz-Guerra, S. Comb-like ionic complexes of cationic surfactants with bacterial poly(γ-glutamic acid) of racemic composition. *Macromol. Biosci.* **2005**, *5*, 30–38.

40. Akagi, T.; Kaneko, T.; Kida, T.; Akashi, M. Preparation and characterization of biodegradable nanoparticles based on poly(γ-glutamic acid) with L-phenylalanine as a protein carrier. *J. Control. Release.* **2005**, *108*, 226–236.

41. Akagi, T.; Baba, M.; Akashi, M. Preparation of nanoparticles by the self-organization of polymers consisting of hydrophobic and hydrophilic segments: Potential applications. *Polymer* **2007**, *48*, 6729–6747.

42. Yoshikawa, T.; Okada, N.; Oda, A.; Matsuo, K.; Matsuo, K.; Kayamuro, H.; Ishii, Y.; Yoshinaga, T.; Akagi, T.; Akashi, M.; Nakagawa, S. Nanoparticles built by self-assembly of amphiphilic γ-PGA can deliver antigens to antigen presenting cells with high efficiency: A new tumor-vaccine carrier for eliciting effector T cells. *Vaccine* **2008**, *26,* 1303-1313.

43. Kang, H. S.; Park, S. H.; Lee, Y. G.; Son, T. I. Polyelectrolyte complex hydrogel composed of chitosan and poly(γ-glutamic acid) for biological application: Preparation, physical properties, and cytocompatibility. *J. Appl. Polym. Sci.* **2007**, *103*, 386-394.

44. Mi, F. L.; Wu, Y.Y.; Lin, Y. H.; Sonaje, K.; Ho, Y. C.; Chen, C. T.; Juang, J. H.; Sung, H. W. Oral delivery of peptide drugs using nanoparticles self-

assembled by poly(γ-glutamic acid) and a chitosan derivative functionalized by trimethylation. *Bioconjug. Chem.* **2008**, *19*, 1248-1255.

45. Peng, S. F.; Yang, M. J.; Su, C. J.; Chen, H. L.; Lee, P. W.; Wei, M. C.; Sung, H. W. Effects of incorporation of poly(γ-glutamic acid) in chitosan/DNA complex nanoparticles on cellular uptake and transfection efficiency. *Biomaterials* **2009**, *30*, 1797-1808.

46. Gonzales, D.; Fan, K. S.; Zevoian, M. Synthesis and swelling characterizations of a poly(γ-glutamic acid) hydrogel. *J. Polym. Sci. Pol. Chem.* **1996**, *34*, 2019-2027.

47. Radu, J. E. F.; Novak, L.; Hartmann, J. F.; Beheshti, N.; Kjoniksen, A. L.; Nystrom, B.; Borbely, J. Structural and dynamical characterization of poly-γ-glutamic acid- based cross-linked nanoparticles. *Colloid. Polym. Sci.* **2008**, *286*, 365-376.

48. Yoshida, H.; Klinkhammer, K.; Matsusaki, M.; Moller, M.; Klee, D.; Akashi, M. Disulfide-crosslinked electrospun poly(γ-glutamic acid) nonwovens as reduction-responsive scaffolds. *Macromol. Biosci.* **2009**, *9*, 568-574.

49. Cromwick, A. M.; Gross, R. A. Effects of manganese (II) on Bacillus licheniformis ATCC 9945A physiology and γ-poly(glutamic acid) formation. *Int. J. Biol. Macromol.* **1995**, *17*, 259–267.

50. Tanaka, T.; Fujita, K.-I.; Takeneshi, S.; Taniguchi, M. Existence of an optically heterogeneous peptide unit in poly(γ-glutamic acid) produced by Bacillus subtilis. *J. Ferment. Bioeng.* **1997**, *84*, 361–364.

51. de Ilarduya, A. M.; Ittobane, N.; Bermudez, M.; Alla, A.; El Idrissi, M.; Munoz-Guerra, S. Poly(α-alkyl γ-glutamate)s of microbial origin. 2. On the microstructure and crystal structure of poly (α-alkyl γ-glutamate)s. *Biomacromolecules* **2002**, *3*, 1078-1086.

52. Rydon. H. N. Polypeptides. Part X. Optical rotatory dispersion of poly- γ-D-glutamic acid. *J. Chem. Soc*. **1964**, 1328-1333.

53. Zanuy, D.; Aleman, C.; Muñoz-Guerra, S. On the helical conformation of unionized poly(γ-D-glutamic acid). *Int. J. Biol. Macromol*. **1998**, *23*, 175-184.

54. Edelhoch, H.; Bateman, J. B. The behavior of a bacterial polypeptide as a polyelectrolyte. *J. Amer. Chem. Soc.* **1957**, *79*, 6093-6100.

55. Kubota, H.; Nambu, Y.; Endo, T. Some properties of poly(γ-glutamic acid) produced by microorganism. *Nippon Kagaku Kaishi*, **1993**, *8*, 973-977.

56. Kubota, H.; Nambu, Y.; Endo, T. Alkaline Hydrolysis of poly(γ-glutamic acid) produced by microorganism. *J.Polym. Sci. A Polym. Chem.* **1996**, *34*, 1347–1351.

57. Hiruta, O.; Hasegawa, N.; Oonishi, Y. et al. Low-molecule weight γ-polyglutamic acid manufacture with acid or alkali. JP Patent 94/112332, 1994.

58. Goto, A.; Kunioka, M. Biosynthesis and hydrolysis of poly(γ-glutamic acid) from Bacilllus subtilis IFO3335. *Biosci. Biotech. Biochem*. **1992**, *56*, 1031-1035.

59. Kunioka, M.; Goto, A. Biosynthesis of poly(γ-glutamic acid) from L-glutamic acid, citric acid, and ammonium sulfate in Bacillus subtilis IF03335. *Appl. Microbiol. Biotech.* **1994**, *40*, 867-872.

60. Muñoz-Guerra, S.; Pérez-Camero, G.; Bou Serra, J. Obtención de ácido poli(γ-glutámico) (PGGA) y poli(α-metil-γ-glutamato) (PAMG) con pesos moleculares medios o bajos mediante irradiación con ultrasonidos. ES Patent 009801306, 2001.

61. Birrer, A. G.; Cromwick, A. M.; Gross, R. A. γ-poly(glutamic acid) formation by Bacillus licheniformis 9945a: physiological and biochemical studies. *Int. J. Biol. Macromol.* **1994**, *16*, 265-275.

62. Troy, F. A. Chemistry and biosynthesis of the poly(γ-D-glutamyl) capsule in Bacillus licheniformis. I. Properties of the membrane-mediated biosynthetic reaction. *J. Biol. Chem.* **1973**, *248*, 305–315.

63. Dabrowska, W.; Kazenko, A.; Laskowski, M. Concerning the specifity of chicken pancreas conjugase. *Science* **1949**, *110*, 95.

64. Oppermann, F. B.; Zickartz, S.; Steinbuchel, A. Biodegradation of polyamides. *Polym. Degrad. Stab.* **1998**, *59*, 337-344.

65. Mclean, R. J. C.; Beauchemin, D.; Clapham, L.; Beveridge, T. J. Metal-Binding characteristics of the metal-binding characteristics of the gamma-glutamyl capsular polymer of Bacillus licheniformis ATCC 9945t. *Appl. Environ. Microbiol.* **1990**, *56*, 3671–3677.

66. He, L. M.; Neu, M. P.; Vanderberg, L. A. Bacillus lichenformis γ-glutamyl expolymer: Physicochemical characterization and U(VI) interaction. *Environ. Sci. Technol.* **2000**, *34*, 1694-1701.

67. (a) Yokoi, H.; Natsuda, O.; Hirose, J.; Hayashi, S.; Takasaki, Y. Characteristics of a biopolymer flocculant produced by Bacillus SP PY-90. *J. Ferment. Bioeng.* **1995**, *79*, 378-380. (b) Yokoi, H.; Arima, T.; Hirose, J.;

Hayashi, S.; Takasaki, Y. Flocculation properties of poly(γ-glutamic acid) produced by Bacillus subtilis. *J. Ferment. Bioeng.* **1996**, *32*, 84-87.

68. Shih, I. L.; Van, Y. T.; Yeh, L. C.; Lin, H. G.; Chang, Y. N. Production of a biopolymer flocculant from Bacillus licheniformis and its flocculation properties. *Bioresource Technol.* **2001**, *78*, 267-272.

69. Nakano, N.; Miyatake, K.; Ueda, M.; Azuma, Y.; Urano, K. *Treatment of plum vinegar waste and fermentative manufacture of poly(γ-glutamic acid) from the waste*; Kokai Tokyo Koho: Japan, 2000.

70. Markland, P.; Zhang, Y.; Amidon, G. L.; Yang, V. C. A pH- and ionic strength-responsive polypeptide hydrogel: synthesis, characterization, and preliminary protein release studies. *J. Biomed. Mater. Res.* **1999**, *47*, 595–602.

71. Choi, H. J. Preparation conditions and swelling equilibria of hydrogel prepared by γ-irradiation from microbial poly (γ-glutamic acid). *Radiat. Phys. Chem.* **1995**, *46*, 175-179.

72. Fukazu, F.; Taguchi, Z*. Cosmetics containing crosslinked poly(γ-glutamic acid);* Kokai Tokyo Koho: Japan, 2003

73. Sung, M. H.; Park, C.; Kim, C. J; Park, J. S.; Uyama, H.; Poo, H. R.; Song, J. J. Poly-gamma-glutamic acid-vitamin complex and use thereof. Patent WO2006001567, 2006.

74. Ben-Zur, N.; Goldman, D. M. γ-Poly glutamic acid: a novel peptide for skin care. *Cosmet. Toiletries.* **2007**, *122*, 64–72.

75. Kashim, N.; Furuta, K.; Tanabe, I. Permeability enhancer. US Patent 20060025346, 2006.

76. Bajaj, I.; Singhal, R. Poly (glutamic acid) – An emerging biopolymer of commercial interest. *Bioresource Technol.* **2011**, *102*, 5551–5561.

77. Portilla-Arias, J.A.; Camargo, B.; García-Álvarez, M.; Martínez de Ilarduya, A.; Muñoz-Guerra, S. Nanoparticles made of microbial poly(γ-glutamate)s for encapsulation and delivery of drugs and poteins. *J. Biomater. Sci.* **2009**, *20*, 1065-1079.

78. Akagi, T.; Kaneko, T.; Kida, T.; Akashi, M. Preparation and characterization of biodegradable nanoparticles based on poly(γ-glutamic acid) with L-phenylalanine as a protein carrier. *J. Control. Release.* **2005**, *108*, 226–236.

79. Lin, Y.-H.; Mi, F.-L.; Chen, C.-T.; Chang, W.-C.; Peng, S.-F.; Liang, H.-F.; Sung, H.-W. Preparation and characterization of nanoparticles shelled with chitosan for oral insulin delivery. *Biomacromolecules* **2007**, *8*, 146–152.

80 . (a) Mi, F. L.; Wu, Y. Y.; Lin, Y. H.; Sonaje, K.; Ho, Y. C.; Chen, C. T.; Juang, J. H.; Sung, H. W. Oral delivery of peptide drugs using nanoparticles self-assembled by poly(γ-glutamic acid) and a chitosan derivative functionalized by trimethylation. *Bioconjug. Chem.* **2008**, *19*, 1248-1255. (b) Sonaje, K.; Chen, Y. J.; Chen, H. L.; Wey, S. P.; Juang, J. H.; Nguyen, H. N.; Hsu, C.W.; Lin, K. J.; Sung, H. W. Enteric-coated capsules filled with freeze-dried chitosan/poly(γ-glutamic acid) nanoparticles for oral insulin delivery. *Biomaterials* **2010***, 31*, 3384-3394.

81. Tang, D. W.; Yu, S. H.; Ho, Y. C.; Mi, F. L.; Kuo, P. L.; Sung, H. W. Heparinized chitosan/poly(γ-glutamic acid) nanoparticles for multifunctional delivery of fibroblast growth factor and heparin. *Biomaterials* **2010**, *31*, 9320-9332.

82. Manocha, B.; Margaritis, A. Controlled release of doxorubicin from doxorubicin/ γ-polyglutamic acid ionic complex. *J. Nanomater.* **2010**, 9, DOI:10.1155/2010/780171.

83. Akao, T.; Kimura, T.; Hirofuji, Y.; Matsunaga, K.; Imayoshi, R.; Nagao, J.; Cho, T.; Matsumoto, H.; Ohtono, S.; Ohno, J.; Taniguchi, K.; Kaminishi, H. A poly(γ-glutamic acid)-amphiphile complex as a novel nanovehicle for drug delivery system. *J. Drug Target.* **2010**, *18*, 550-556.

84. Portilla-Arias, J. A; García-Alvarez, M.; Martínez de Ilarduya, A.; Muñoz-Guerra, S. Ionic complexes of biosynthetic poly(malic acid) and poly(glutamic acid) as prospective drug-delivery systems. *Macromol. Biosci.* **2007**, *7*, 897–906.

85. Liang, H. F.; Chen, C. T.; Chen, S. C.; Kulkarni, A. R.; Chiu, Y. L.; Chen, M. C.; Sung, H. W. Paclitaxel-loaded poly(gamma-glutamic acid)-poly(lactide) nanoparticles as a targeted drug delivery system for the treatment of liver cancer. *Biomaterials* **2006**, *27*, 2051-2059.

86. Ridley, B. L.; Neill, M. A. O.; Mohnen, D. Pectins: structure, biosynthesis, and oligogalacturonide-related signaling. *Phytochemistry* **2001**, *57*, 929–967.

87. Scheller, H. V.; Jensen, J. K.; Sørensen, S. O.; Harholt, J.; Geshi, N. Biosynthesis of pectin. *Physiol. Plant.* **2006**, *129*, 283–295.

88. Thakur, B. R.; Singh, R. K.; Handa, A.K. Chemistry and uses of pectin – A review. *Crit. Rev. Food Sci. Nutr.* **1997**, *37*, 47-73.

89. May, C. D. Industrial Pectins : Sources, production and applications. *Carbohydr. Polym.* **1990**, *12*, 79–99.

90. Rolin, C. Pectin. In *Industrial gums*, 3rd Edition; Academic Press: New York, 1993.

91. Ovodov, Y. S. Current views on pectin substances. *Russ. J. Bioorg. Chem.* **2009**, *35*, 269–284.

92. Scheller, H. V.; Jensen, J. K.; Sørensen, S. O.; Harholt, J.; Geshi, N. Biosynthesis of pectin. *Physiol. Plant.* **2006**, *129*, 283–295.

93. Mohnen, D. Biosynthesis of pectins and galactomannans. In *Comprehensive natural products chemistry, carbohydrates and their derivatives including tannins cellulose and related lignins*; Barton, D.; Nakanishi, K.; Meth-Cohn, O.; Pinto, B. M., Eds., Elsevier: Oxford, 1999; Vol. 3, pp 497–527.

94. Bagherian, H.; Ashtiani, F. Z.; Fouladitajar, A.; Mohtashamy, M. Comparisons between conventional, microwave and ultrasound-assisted methods for extraction of pectin from grapefruit. *Chem. Eng. Process.* **2011**, *50*, 1237-1243.

95. Marsha, C.; Chow, K. Pectin extraction from pectin and sugar beets. *Agr. Res.* **2007**, *2*, 16-17.

96. Fishman, M. L., Chau, H. K. Extraction of pectin by microwave heating under pressure. US Patent 6143337, 2000.

97. Panchev, I. N., Kirtchev, N. A., Kratchanov, G. On the production of low esterified pectins by acid maceration of pectic raw materials with ultrasound treatment. *Food Hydrocolloids*. **1994**, *8*, 9–17.

98. Contreras-Esquivel, J. C.; Voget, C.E.; Vita, C.E.; Espinoza-Perez, J.D.; Renard, C. M. G. M. Enzymatic extraction of lemon pectin by endo-polygalacturonase from Aspergillus niger. *Food Sci. Biotechnol.* **2006**, *15*, 163-167.

99. Mukhiddinov, Z. K.; Khalikov, D. K.; Abdusamiev, F. T.; Avloev, C. C. Isolation and structural characterization of a pectin homo and ramnogalacturonan. *Talanta* **2000**, *53*, 171-176.

100. Mohnen, D. Pectin structure and biosynthesis. *Curr. Opin. Plant Biol.* **2008**, *11*, 266–277.

101. McNeil, M.; Darvill, A. G.; Albersheim, P. Structure of plant-cell walls. 10. Rhamnogalacturonan-I, a structurally complex pectic polysaccharide in the

walls of suspension-cultured sycamore cells. *Plant physiol.* **1980**, *66*, 1128-1134.

102. Oakenfull, D. G. The chemistry of high-methoxylpectins.In *The chemistry and technology of pectin*; Walter, R. H., Ed., Academic Press: New York, 1991.

103. Darvill, A. G.; McNeil, M.; Albersheim, P. Structure of plant-cell walls. 8. New pectic polysaccharide. *Plant Physiol.* **1978**, *62*, 418-422.

104. Palmer, K. J.; Hartzog, M. B.. An X-Ray diffraction investigation of Sodium Pectate. *J. Amer. Chem. Soc.* **1945**, *67*, 2122-2127.

105. Walkinshaw, M. D.; Arnott, S. Conformations and interactions of pectins. I. X-Ray diffraction analyses of sodium pectate in neutral and acidified forms. *J. Molec. Biol.* **1981**, *153*, 1055-1073.

106. Walkinshaw, M. D.; Arnott, S. Conformations and interactions of pectins. II. Models for junction zones in pectinic acid and calcium pectate gels. *J. Molec. Biol.* **1981**, *153*, 1075-1085.

107. Hansson, A.; Leufvén, A.; Van Ruth, S. Partition and release of 21 aroma compounds during storage of a pectin gel system. *J. Agr. Food Chem.* **2003**, *51*, 2000-2005.

108 P. Srivastava, R. Malviya. Sources of pectin, extraction and its applications in pharmaceutical industry − An overview. Indian J. Nat. Prod. Res. **2011**, *2*, 10–18.

109 S.V Popov, P.A Markov, I.-R.Nikitina, S. Petrishev, V. Smirnov, Y.S. Ovodov. Preventive effect of a pectic polysaccharide of the common cranberry Vacciniumoxycoccos L. on acetic acid-induced colitis in mice. World J. Gastroenterol. **2006**, *12*, 6646–6651.

110. Sriamornsak, P. Chemistry of Pectin and Its Pharmaceutical Uses : A Review. *Silpakorn Univ. Int. J.* **2003**, *3*, 206–228.

111. Liu, L.; Fishman, M. L.; Kost, J.; Hicks, K. B. Pectin-based systems for colon-specific drug delivery via oral route. *Biomaterials* **2003**, *24*, 3333–3343.

112. Xu, C.; Zhang, J. S.; Mo, Y.; Tan, R. X. Calcium pectinate capsules for colon-specific drug delivery. *Drug Dev. Ind. Pharm.* **2005**, *31*, 127–34.

113. (a) Stanford, E. C. C. Improvements in the manufacture of useful products from seaweeds. BR Patent, 142, 1881. (b) Stanford, E. C. C. New substance obtained from some of the commoner species of marine algae; Algin. *Chem. News.* **1883**, *47*, 254-257 (c) and 267-269.

114. Sabra, W.; Deckwer, W.-D. Alginate — A polysaccharide of industrial interest and diverse biological functions. In *Polysaccharides: Structural diversity and functional versality*; Dimitriu, S., Ed.; Marcel Dek: New York, 2005; pp. 515–533.

115, Ertesvag, H. Biosynthesis and applications of alginates. *Polym. Degrad. Stab.* **1998**, *59*, 85–91.

116. Draget, K. I.; Smidsrod, P. O.; Skjåk-braek, P. G. Alginates from Algae. In *Polysaccharides and polyamides in the food industry. Properties, production, and patents;* Steinbüchel, A.; Rhee, S. K., Eds.; Wiley-VCH: Weinheim, 2005; pp. 1–30.

117. Skjåk-braek, G.; Grasdalen, H.; Larsen, B. Monomer sequence and acetylation pattern in some bacterial alginates. *Carbohydr. Res.* **1986**, *154*, 239-250.

118. Hay, I. D.; Rehman, Z. U.; Ghafoor, A.; Rehm, B. H. A. Bacterial biosynthesis of alginates. *J. Chem. Technol. Biotechnol.* **2010**, *85*, 752-759.

119. Atkins, E. D. T. Conformations of uronic acid containing pollysaccharides. *Pure Appl. Chem.* **1977**, *49*, 1135–1149.

120. Smidsrod, O. Relative extension of alginates having different chemical composition. *Carbohydr. Res.* **1973**, *27*, 107-118.

121. Stokke, B. T.; Draget, K. I.; Smidsrod, O.; Yuguchi, Y.; Urakawa, H.; Kajiwara, K. Small-angle X-ray scattering and rheological characterization of alginate gels. 1. Ca-alginate gels. *Macromolecules* **2000**, *33*, 1853-1863.

122. (a) Braccini, I.; Grasso, R. P.; Pérez, S. Conformational and configurational features of acidic polysaccharides and their interactions with calcium ions: a molecular modeling investigation. *Carbohydr. Res.* **1999**, *317*, 119–130. (b) Braccini, I.; Pérez, S. Molecular basis of Ca2+ induced gelation in alginates and pectins: The egg-box model revisited. *Biomacromolecules* **2001**, *2*, 1089-1096.

123. Haug, A.; Larsen, B. The solubility of alginate at low pH. *Acta Chem. Scand.* **1963**, *17*, 1653–1662.

124. Mancini, M.; Moresi, M.; Sappino, F. Rheological behaviour of aqueous dispersions of algal sodium alginates. J. *Food Eng.* **1996**, *28*, 283–295.

125. Haug, A.; Smidsrod, O.; Larsen, B. Degradation of alginates at different pH values. *Acta Chem. Scand.* **1963**, *17*, 1466-1468.

126. Smidsrod, O.; Larsen, B.; Haug, G. Degradation of alginate in presence of reducing compounds. Acta Chem. Scand. **1963**, *17*, 2628-2637.

127. Soares, J. P.; Santos, J. E.; Chierice, G. O.; Cavalheiro, E. T. G. Thermal behavior of alginic acid and its sodium salt. *Eclet. Quim.* **2004**, *29*, 57–64.

128. (a) Stainer, A. B. Manufacture of glycol alginates. US Patent 2426215, 1947. (b). Stainer, A. B.; McNeilly, W. H. High stability glycol alginates and their manufacture. US Patent 2494911, 1950.

129. Ivanovic, S.; Mikinac, K.; Perman, L. Molecular gastronomy in function of scientific implementation in practice. *UTMS J. Econ.* **2011**, *2*, 139–150.

130. Gombotz, W. R.; Wee, S. F. Protein release from alginate matrices. *Adv. Drug Deliver. Rev*. **1998**, *31*, 267-285.

131. Picquadio, D.; Nelson, D. B. Alginates a new dressing alternative. *J. Dermatol. Surg. Onc.* **1992**, *18*, 992–998.

132. Ertesvag, H.; Valla, S. Biosynthesis and applications of alginates. *Polym. Degrad. Stab.* **1998**, *59*, 85–91.

133. Kulseng, B.; Thu, B.; Espevik, T.; SkjakBraek, G. Alginate polylysine microcapsules as immune barrier: Permeability of cytokines and immunoglobulins over the capsule membrane. *Cell Transplant.* **1997**, *6*, 387-394.

134. Tønnesen, H. H.; Karlsen, J. Alginate in drug delivery systems. *Drug Dev. Ind. Pharm.* **2002**, *28*, 621–30.

135. d'Ayala, G. G.; Malinconico, M.; Laurienzo, P. Marine derived polysaccharides for biomedical applications: Chemical modification approaches. *Molecules* **2008**, *13*, 2069–2106.

136. Weissmann, B.; Meyer, K. Structure of hyaluronic acid – The glucuronidic linkage. *J. Amer. Chem. Soc.* **1952**, *74*, 4729.

137. Meyer, K.; Palmer, J. W. The polysaccharide of the vitreous humor. *J. Biol. Chem.* **1934**, *107*, 629-634.

138. Kogan, G.; Soltés, L.; Stern, R.; Gemeiner, P. Hyaluronic acid: a natural biopolymer with a broad range of biomedical and industrial applications. *Biotechnol. Lett.* **2007**, *29*, 17–25.

139. Jeanloz, R. W.; Forchielli, E. Studies on hyaluronic acid and related substances. I. Preparation of hyaluronic acid and derivatives from human umbilical cord. *J. Biol. Chem.* **1950**, *9*, 495–511.

140. Necas, J.; Bartosikova, L.; Brauner, P.; Kolar, J. Hyaluronic acid (hyaluronan): a review. *Vet. Med.-CZECH* **2008**, *53*, 397–411.

141. Mendichi, R.; Soltes, L. Hyaluronan molecular weight and polydispersity in some commercial intra-articular injectable preparations and in synovial fluid. *Inflamm. Res.* **2002**, *51*, 115-116.

142. Balazs, E. A. Ultrapure hyaluronic acid and the use thereof. US Patent 4141973, 1979.

143. Liu, L.; Liu, Y.; Li, J.; Du, G.; Chen, J. Microbial production of hyaluronic acid: current state, challenges, and perspectives. *Microb. Cell Fact.* **2011**, *10*, 99.

144. Izawa, N.; Hanamizu, T.; Iizuka, R.; Sone, T.; Mizukoshi, H.; Kimura, K.; Chiba, K. Streptococcus thermophilus produces exopolysaccharides including hyaluronic acid. *J. Biosci. Bioeng.* **2009**, *107*, 119–123.

145. Hidemichi, A.; Hisayuki, K.; Mitsuo, Y. Shiseiso Co LTD. Preparation of hyaluronic acid. JP Patent 58056692, 1983.

146. Widner, B.; Behr, R.; Von Dollen, S. Hyaluronic acid production in Bacillus subtilis. *Appl. Environ. Microbiol.* **2005**, *71*, 3747-3752.

147. Scott, J. E.; Heatley, F. Hyaluronan forms specific stable tertiary structures in aqueous solution: a C-13 NMR study. *P. Natl. Acad. Sci. USA* **1999**, *96*, 4850–4855.

148. Gribbon, P.; Heng, B. C.; Hardingham, T. E. The analysis of intermolecular interactions in concentrated hyaluronan solutions suggest no evidence for chain–chain association. *Biochem. J.* **2000**, *350*, 329–335.

149. Kobayashi, Y.; Okamoto, A.; Nishinari, K. Viscoelasticity of hyaluronic-acid with different molecular-weights. *Biorheology* **1994**, *31*, 235–244.

150. Hargittai, I.; Hargittai, M. Molecular structure of hyaluronan: an introduction. *Struct. Chem.* **2008**, *19*, 697–717.

151. Balazs, E. A.; Sundblad, L. Viscosity of hyaluronic acid solutions containing proteins. *Acta Soc. Med. Ups.* **1959**, *64*, 137–146.

152. Brown, M. B.; Jones, S. a Hyaluronic acid: a unique topical vehicle for the localized delivery of drugs to the skin. *J. Eur. Acad. Dermatol. Venereol.* **2005**, *19*, 308–318.

153. Trommer, H.; Wartewig, S; Bottcher, R.; Poppl, A., Hoentsch, J., Ozegowski, J. H.; Neubert, R. H. H. The effects of hyaluronan and its fragments on lipid models exposed to UV irradiation. *Int. J. Pharm*. **2003**, *254*, 223–234.

154. Volpi, N.; Schiller, J.; Stern, R.; Soltés, L. Role, metabolism , chemical modifications and applications of hyaluronan. *Curr. Med. Chem.* **2009**, *16*, 1718–1745.

155. Duranti, F.; Salti, G.; Bovani, B.; Calandra, M., Rosati, M. L. Injectable hyaluronic acid gel for soft tissue augmentation – a clinical and histological study. *Dermatol. Surg.* **1998**, *24*, 1317–1325.

156. Shu, X. Z.; Liu, Y.; Palumbo, F. S.; Luo, Y.; Prestwich, G. D. In situ crosslinkable hyaluronan hydrogels for tissue engineering. *Biomaterials* **2004**, *25*, 1339–1348.

157. Lin, K.; Bartlett, S. P.; Matsuo, K.; Livolsi, V. A.; Parry, C.; Hass, B. Hyaluronic acid-filled mammary implants – an experimental study. *Plast. Reconstr. Surg.* **1994**, *94*, 306–315.

158. Balazs, E. A.; Denlinger, J. L. Clinical uses of hyaluronan. Ciba F Symp. 1989, 143, 265–280.

159. West, D. C.; Hampson, I. N.; Arnold, F.; Kuman, S. Angiogenesis induced by degradation products of hyaluronic acid. *Science* **1985**, *228*, 1324–1326.

160. Schanté, C. E.; Zuber, G.; Herlin, C.; Vandamme, T. F. Chemical modifications of hyaluronic acid for the synthesis of derivatives for a broad range of biomedical applications. *Carbohydr. Polym.* **2011**, *85*, 469–489.

161. Coviello, T.; Matricardi, P.; Marianecci, C.; Alhaique, F. Polysaccharide hydrogels for modified release formulations. *J. Control. Release.* **2007**, *119*, 5–24.

162. Na, S. J.; Chae, S. Y.; Lee, S.; Park, K.; Kim, K.; Park, J. H.; Kwon, I. C.; Jeong, S. Y.; Lee, K. C. Stability and bioactivity of nanocomplex of TNF-related apoptosis-inducing ligand. *Int. J. Pharm.* **2008**, *363*, 149–154.

163. Auzenne, E.; Ghosh, S. C.; Khodadadian, M.; Rivera, B.; Farquhar, D.; Price, R. E.; Ravoori, M.; Kundra, V.; Freedman, R. S.; Klostergaard, J.

Hyaluronic acid–paclitaxel: Antitumor efficacy against CD44(+) human ovarian carcinoma xenografts. *Neoplasia* **2007**, *9*, 479–486.

164. Oparin, A. I. The origin of life. *Izd. Moskovshii Rabochii*, Moscow, 1924. English translation in A.I. Oparin. *The origin of life*; Bernal, J. D.; Ed.; Weidenfeld & Nicolson: London, 1967; pp. 199–234.

165. Faul, C. F. J.; Antonietti, M. Ionic Self-Assembly: Facile synthesis of supramolecular materials. *Adv. Mater.* **2003**, *15*, 673–683.

166. Holmberg, K.; Jönsson, B.; Kronberg, B.; Lindman, B. *Surfactants and polymers in aqueous solution*; John Wiley & Sons, LTD: Chichester, England, 2003.

167. Winsor, P. A. Hydrotropy, solubilisation, and related emulsification processes. *Trans. Faraday Soc.* **1948**, *44*, 376 – 382.

168. Rosen, M. J. *Surfactants and interfacial phenomena*; 3rd Edition; Wiley-Interscience: New Jersey, 2004.

169. Israelachvili, J. N.; Mitchell, D. J.; Ninham, B. W. Theory of self-assembly of hydrocarbon amphiphiles into micelles and bilayers. *J. Chem. Soc.-Faraday Trans. II.* **1976**, *72*, 525-1568.

170. Winsor, P. A. Binary and multicomponent solutions of amphiphilic compounds. Solubilization and the formation, structure, and theoretical significance of liquid crystalline solutions. *Chem. Rev.* **1968**, *68*, 1–38.

171. Pattanathu, K. S.; Gakpe, E. Production, characterisation and applications of biosurfactants. Rev. *Biotechnol.* **2008**, *7*, 360–370.

172. Gobley, M. Examen comparatif du jaune d'oeufe et de al matiere cerebrale. *J. Pharm. Chim.* **1847**, *11*, 409-412.

173. Zeisel, S. H.; Blusztajn, J. K. Choline and human nutrition. *Annu. Rev. Nutr.* **1994**, *14*, 269–96.

174. Walkey, C. J.; Yu, L. Q.; Agellon, L. B.; Vance, D. E. Biochemical and evolutionary significance of phospholipid methylation. *J. Biol. Chem.* **1998**, *273*, 27043–27046.

175. Cohn, J. S.; Wat, E.; Kamili, A.; Tandy, S. Dietary phospholipids, hepatic lipid metabolism and cardiovascular disease. *Curr. Opin. Lipidol.* **2008**, *19*, 257–262.

176. Zeisel, S. H. Choline: needed for normal development of memory. *J. Amer. Coll. Nutr.* **2000**, *19*, 528S–531S. S

177. Chung, S.Y.; Moriyama, T.; Uezu, E.; Uezu, K.; Hirata, R.; Yohena, N.; Masuda, Y.; Kokubu, T.; Yamamoto, S. Administration of phosphatidylcholine increases brain acetylcholine concentration and improves memory in mice with dementia. *J. Nutr.* **1995**, *125*, 1484-1489

178. Tischer, M.; Pradel, G.; Ohlsen, K.; Holzgrabe, U. Quaternary ammonium salts and their antimicrobial potential: targets or nonspecific interactions? *ChemMedChem* **2012**, *7*, 22–31.

179. Chelminska-Bertilsson, M.; Allenmark, S. Butyrylcholinesterase activity towards long-chain alkanoylcholines- Kinetics and mechanism. *Biochim. Biophys. Acta.* **1993**, *1202*, 56-60.

180. Ahlström, B.; Chelminska-Bertilsson, M.; Thompson, R. A; Edebo, L. Long-chain alkanoylcholines, a new category of soft antimicrobial agents that are enzymatically degradable. *Antimicrob. Agents Chemother.* **1995**, *39*, 50–55.

181. Carelli, V.; Liberatore, F.; Scipione, L.; Cardellini, M.; Rotiroti, D.; Rispoli, V. Choline derivative for the treatment of Alzheimer's disease. US Patent 0166721 A1, 2003.

182. Patel, H. Use of choline derivatives for memory, learning and cognition. US Patent 018631 A1, 2005.

183. (a) Alexander, J.; Fix, J. A. Enhancement of absorption of drugs from gastrointestinal tract using choline ester salts US Patent 4822773, 1989. (b) Alexander, J.; Fix, J. A.; Repta, A. J. Choline esters as absorption-enhancing agents for drug delivery through mucous membranes of the nasal, buccal, sublingual and vaginal cavities US Patent 4963556, 1990.

184. Thünemann, A. F.; Schnoller, U.; Nuyken, O.; Voit, B. Self-assembled complexes of diazosulfonate polymers with low surface energies. *Macromolecules* **1999**, *32*, 7414-7421.

185. Antonietti, M.; Conrad, J.; Thünemann, A. Polyelectrolyte-surfactant complexes: A new type of solid, mesomorphous material. *Macromolecules* **1994**, *27*, 6007–6011.

186. Thünemann, A. F. Polyelectrolyte – surfactant complexes (synthesis, structure and materials aspects). *Progr. Polym. Sci.* **2002**, *27*, 1473–1572.

187. Antonietti M.; Conrad, J. Synthesis of very highly ordered liquid-crystalline phases by complex-formation of polyacrylic-acid with cationic surfactants. *Angew. Chem. Int. Edit.* **1994**, *33*, 1869-1870.

188. Ruokolainen, J.; ten Brinke, G.; Ikkala, O. Supramolecular Polymeric Materials with Hierarchical Structure-within-Structure Morphologies. *Adv. Mater.* **1999**, *11*, 777-780.

189. Zhou, S. Q.; Burger, C.; Yeh, F. J.; Chu, B. Charge density effect of polyelectrolyte chains on the nanostructures of polyelectrolyte-surfactant complexes. *Macromolecules* **1998**, *31*, 8157-8163.

190. Antonietti, M.; Neese, M.; Blum, G. Dielectric and mechanic relaxation in polyelectrolyte-supported bilayer stacks: A model for the dynamics of membrans? *Langmuir* **1996**, *12*, 4426-4441.

191. Abuin, E. B.; Scaiano, J. C. Exploratory study of the effect of polyelectrolyte surfactant aggregates on photochemical behaviour. *J. Amer. Chem. Soc.* **1984**, *106*, 6274-6283.

192. Goddard, E. D.; Ananthapadmanabhan, K. P. *Interactions of surfactants with polymers and proteins*; CRC Press: Boca Raton, FL, 1993.

193. Mel'nikov, S. M.; Dias, R.; Mel'nikova, Y. S.; Marques, E. F.; Miguel, M. G.; Lindman, B. DNA conformational dynamics in the presence of catanionic mixtures. *FEBS Lett.* **1999**, *453*, 113–118.

194. Langevin, D. Complexation of oppositely charged polyelectrolytes and surfactants in aqueous solutions. A review. *Adv. Colloid. Interfac. Sci.* **2009**, *147-148*, 170–177.

195. Thünemann, A. F.; General, S. Nanoparticles of a polyelectrolyte-fatty acid complex: carriers for Q(10) and triiodothyronine. *J. Control. Release* **2001**, *75*, 237-247.

196. Platé, N. A.; Shibaev, V. P. Comb-like polymers – Structure and properties. J. Polym. Sci. D Macromol. Rev. 1974, 8, 117-253.

197. Macknight, W. J.; Ponomarenko, E. A.; Tirrell, D. A. Self-assembled polyelectrolyte-surfactant complexes in nonaqueous solvents and in the solid state. *Accounts Chem. Res.* **1998**, *31*, 781–788.

198. Kötz, J.; Kosmella, S.; Beitz, T. Self-assembled polyelectrolyte systems. *Progr. Polym. Sci.* **2001**, *26*, 1199–1232.

199. Thünemann, A. F.; Müller, M.; Dautzenberg, H.; Löwen, J. J. H. Polyelectrolyte complexes. *Adv. Polym. Sci.* **2004**, *166*, 113–171.

200. Antonietti M.; Conrad, J. Synthesis of very highly ordered liquid-crystalline phases by complex-formation of polyacrylic-acid with cationic surfactants. *Angew. Chem. Int. Edit.* **1994**, *33*, 1869-1870.

201. Ponomarenko, E. A.; Waddon, A. J.; Tirrell, D. A.; Macknight, W. J. Structure and properties of stoichiometric complexes formed by sodium poly (α,L-glutamate) and oppositely charged surfactants. *Langmuir* **1996**, *12*, 2169–2172.

202. Watanabe, J.; Ono, H.; Uematsu, I.; Abe, A. Thermotropic polypetides. 2. Molecular packing and thermotropic behavior of poly (L-glutamates) with long n-alkyl side chains. *Macromolecules* **1985**, *18*, 2141–2148.

203. Ponomarenko, E. A.; Tirrell, D. A.; Macknight, W. J. Stoichiometric complexes of synthetic polypeptides and oppositely charged surfactants in organic solvents and in the solid state. *Macromolecules* **1996**, *29*, 8751–8758.

204. Yamanobe, T.; Tsukahara, M.; Komoto, T.; Watanabe, J.; Ando, I.; Uematsu, I.; Deguchi, K.; Fujito, T.; Imanari, M. Conformation and dynamic aspects of poly(γ-n-octadecyl L-glutamate) in the solid state and liquid-crystalline State. *Macromolecules* **1988**, *21*, 48–50.

205. López-Carrasquero, F.; Báez, M. E.; García-Alvarez, M.; Martínez de Ilarduya, A.; Alla, A.; Fernández, C. E.; Muñoz-Guerra, S. Comblike complexes of poly(aspartic acid) and alkyltrimethylamonium cationic surfactants. *Macromol. Symp.* **2006**, *245-246*, 266–275.

206. Portilla-Arias, J. A.; García-Alvarez, M.; Martínez de Ilarduya, A.; Holler, E.; Muñoz-Guerra, S. Nanostructurated complexes of poly(β,L-malate) and cationic surfactants: synthesis, characterization and structural aspects. *Biomacromolecules* **2006**, *7*, 161–170.

207. Antonietti, M.; Henke, S.; Thünemann, A. Highly ordered materials with ultra-low surface energies: Polyelectrolyte surfactant complexes with fluorinated surfactants. *Adv. Mater.* **1996**, *8*, 41-45.

208. Radler, J. O.; Koltover, I.; Salditt, T.; Safinya, C. R. Structure of DNA-cationic liposome complexes: DNA intercalation in multilamellar membranes in distinct interhelical packing regimes. *Science* **1997**, *275*, 810-814.

209. Zhu, L.; Mahato, R. I. Lipid and polymeric carrier-mediated nucleic acid delivery. *Expert Opin. Drug Del.* **2010**, *7*, 1209–1226.

210. Leal, J. S.; Gonzalez, J. J.; Comelles, F.; Campos, E.; Ciganda, T. Biodegradability and toxicity of anionic surfactants. *Acta Hydrochim. Hydrobiol.* **1991**, *19*, 703-709.

211. Kabanov, V. A.; Zezin, A. B. Soluble interpolymeric complexes as a new class of synthetic polyelectrolytes. *Pure Appl. Chem.* **1984**, *56*, 343–354.

212. Zezin, A. B.; Kabanov, V. A. New form of the poly-electrolytes water-soluble complexes. *Usp. Khim.* **1982**, *51*, 1447-1483.

213. Philipp, B.; Dautzenberg, H.; Linow, K. J.; Koetz, J.; Dawydoff, W. Polyelectrolyte complexes - recent developments and open problems. *Progr. Polym. Sci.* **1989**, *14*, 91-172.

214. Michaels, A. S.; Miekka, R.G. Polycation-polyanion complexes – Preparation and properties of poly-(Vinyl benzyl trimethylammonium) poly-(Styrenesulfonate). *J. Phys. Chem.* **1961**, *65*, 1765-1773.

215. Dautzenberg, H.; Gao, Y. B.; Hahn, M. Formation, structure and temperature behavior of polyelectrolyte complexes between ionically modified thermosensitive polymers. *Langmuir* **2000**, *16***,** 9070-9081.

216. Cai, C.; Lin, J.; Chen, T.; Tian, X. Aggregation behavior of graft copolymer with rigid backbone. *Langmuir* **2010**, *26*, 2791–2797.

217. Wang, W.; Qu, X. Z.; Gray, A. I.; Tetley, l.; Uchegbu, I. F. Self-assembly of cetyl linear polyethylenimine to give micelles, vesicles, and dense nanoparticles. *Macromolecules* **2004**, *37*, 9114-9122.

218. Brinke, G.; Ikkala, O. Ordered Structures of Molecular Bottlebrushes. *Trends Polym. Sci.* **1997**, *5*, 213–217.

219. Melis, J.; Zanuy, D.; Aleman, C.; García-Álvarez, M.; Muñoz-Guerra, S. On the crystal structure of poly(α-benzyl-γ-D,L-glutamate)s. *Macromolecules* **2002**, *35*, 8774-8780.

220. Pavlidou, S.; Papaspyrides, C. D. A review on polymer-layered silicate nanocomposites. *Progr. Polym. Sci.* **2008**, *33*, 1119-1198.

221. Nguyen, Q. T.; Baird, D. G. Preparation of polymer – clay nanocomposites and their properties. *Adv. Polym. Technol.* **2007**, *25*, 270–285.

222. Bower, C. A. Studies on the form and availability of organic soil phosphorous. Ames, Iowa State College of Agriculture and Mechanic Arts, Agricultural Experiment Station: Iowa, 1949; 362 pp. 39-42.

223. Okada, A., Fukushima, Y.; Kawasumi, M.; Inagaki, S.; Usuki, A.; Sugiyama, S.; Kurauchi, T.; Kamigatio, O. (Toyota Motor Co., Japan). Composite material and its preparation. US Patent 4739007, 1987.

224. Vaia, R. A.; Ishii, H.; Giannelis, E. P. Synthesis and properties of two-dimensional nanostructures by direct intercalation of polymer melts in layered silicates. *Chem. Mater.* **1993**, *5*, 1694–1696.

225. Sinha Ray, S.; Okamoto, M. Polymer/layered silicate nanocomposites: a review from preparation to processing. *Progr. Polym. Sci.* **2003**, *28*, 1539–1641.

226. Zanetti, M.; Lomakin, S.; Camino, G. Polymer layered silicate nanocomposites. *Macromol. Mater. Eng.* **2000**, *279*, 1-9.

227. Tjong, S. C. Structural and mechanical properties of polymer nanocomposites. *Mater. Sci. Eng. R* **2006**, *53*, 73–197.

228. Kim, Y.; White, J. L. Formation of polymer nanocomposites with various organoclays. *J. Appl. Polym. Sci.* **2005**, *96*, 1888–1896.

229. Lagaly, G. Interaction of alkylamines with different types of layered compounds. *Solid State Ionics* **1986**, *22*, 43-51.

230. Vaia, R. A.; Teukolsky, R. K.; Giannelis, E. P. Interlayer structure and molecular environment of alkylammonium layered silicates. *Chem. Mater.* **1994**, *6*, 1017–1022.

231. Alexandre, M.; Dubois, P. Polymer-layered silicate nanocomposites : preparation , properties and uses of a new class of materials. *Mater. Sci. Eng. R* **2000**, *28*, 1–63.

232. Giannelis, E. P. Polymer layered silicate nanocomposites. *Adv. Mater.* **1996**, *8*, 29–35.

233. Poli, A. L.; Batista, T.; Schmitt, C. C.; Gessner, F.; Neumann, M. G. Effect of sonication on the particle size of montmorillonite clays. *J. Colloid Interfac. Sci.* **2008**, *325*, 386–390.

234. Aranda, P.; Ruiz-hitzky, E. Poly (ethylene oxide) - Silicate intercalation materials. *Chem. Mater.* **1992**, *4*, 1395–1403.

235. (a) Blumstein, A. Polymerization of adsorbed monolayers: II. Thermal degradation of the inserted polymers. *J. Polym. Sci. A Polym. Chem*. **1965**, *3*, 2665–2673. (b) Theng, B. K. G. *Formation and properties of clay–polymer complexes*; Elsevier: Amsterdan, 1979.

236. (a) Usuki, A.; Kawasumi, M.; Kojima, Y., Okada, A., Kurauchi, T.; Kamigaito, O. Swelling behavior of montmorillonite cation exchanged for ω-amine acid by ε-caprolactam. *J. Mater. Res*. **1993**, *8*, 1174–1178. (b) Usuki, A.; Kojima, Y.; Kawasumi, M.; Okada, A.; Fukushima, Y.; Kurauchi, T.; Kamigaito, O. Synthesis of nylon-6–clay hybrid. *J. Mater. Res.* **1993**, *8*, 1179–1183.

237. Chen, T. K.; Tien, Y. I.; Wei, K. H. Synthesis and characterization of novel segmented polyurethane/clay nanocomposite via poly(ε-polycaprolactone)/clay. *J. Polym. Sci. A Polym. Chem*. **1999**, *37*, 2225–2233.

238. Lee, S. S.; Ma, Y. T.; Rhee, H. W.; Kim, J. Exfoliation of layered silicate facilitated by ring-opening reaction of cyclic oligomers in PET-clay nanocomposites. *Polymer* **2005**, *46*, 2201-2210.

239. Sepehr, M.; Utracki, L. A.; Zheng, X. X.; Wilkie, C. A. Polystyrenes with macro-intercalated organoclay. Part I. Compounding and characterization. *Polymer* **2005**, *46*, 11557-11568.

240. Kornmann, X.; Lindberg, H.; Berglund, L. A. Synthesis of epoxy-clay nanocomposites: influences of the nature of the clay on structure. *Polymer* **2001**, *42*, 1303-1310.

241. Vaia, R. A.; Giannelis, E. P. Lattice model of polymer melt intercalation in organically-modified layered silicates. *Macromolecules* **1997**, *30*, 7990–7999.

242. Vaia, R. A.; Giannelis, E. P. Polymer melt intercalation in organically-modified layered silicates: model predictions and experiment. *Macromolecules* **1997**, *9297*, 8000–8009.

243. (a) Balazs, A. C.; Singh, C.; Zhulina, E. Modeling the interactions between polymers and clay surfaces through self-consistent field theory. *Macromolecules* **1998**, *31*, 8370–8381. (b) Balazs, A. C.; Singh, C.; Zhulina, E.; Lyatskaya, Y. Modeling the phase behavior of polymer/clay nanocomposites. *Accounts Chem. Res.* **1999**, *32*, 651-657.

244. Liu, L. M.; Qi, Z. N.; Zhu, X. G. Studies on nylon 6 clay nanocomposites by melt-intercalation process. *J. Appl. Polym. Sci.* **1999**, *71*, 1133-1138.

245. Fornes, T. D.; Paul, D. R. Modeling properties of nylon 6/clay nanocomposites using composite theories. *Polymer* **2003**, *44*, 4993-5013.

246. Shia, D.; Hui, C. Y.; Burnside, S. D.; Giannelis, E. P. An interface model for the prediction of Young's modulus of layered silicate-elastomer nancomposites. *Polym. Composite.* **1998**, *19*, 608-617.

247. Fornes, T. D.; Yoon, P. J.; Keskkula, H.; Paul, D. R. Nylon 6 nanocomposites: the effect of matrix molecular weight. *Polymer* **2001**, *42*, 9929-9940.

248. Zerda, A. S.; Lesser, A. J. Intercalated clay nanocomposites : Morphology, mechanics , and fracture behavior. *J. Polym. Sci. B Polym. Phys.* **2001**, *39*, 1137–1146.

249. Chen, B. Q.; Evans, J. R. G. Poly (ε-caprolactone)-clay nanocomposites: Structure and mechanical properties. *Macromolecules* **2006**, *39*, 747-754.

250. Zhu, J.; Uhl, F. M.; Morgan, A. B.; Wilkie, C. A. Studies on the mechanism by which the formation of nanocomposites enhances thermal stability. *Chem. Mater.* **2001**, *13*, 4649-4654.

251. Blumstein, A. Polymerization of adsorbed monolayers: II. Thermal degradation of the inserted polymers. *J. Polym. Sci. A Polym. Chem.* **1965**, *3*, 2665–2673.

252. Leszczynska, A.; Njuguna, J.; Pielichowski, K.; Banerjee, J. R. Polymer/montmorillonite nanocomposites with improved thermal Part I: Factors influencing thermal stability and mechanisms of thermal stability improvement. *Thermochim. Acta* **2007**, *453*, 75–96.

253. Osman, M. A.; Mittal, V.; Lusti, H. R. The aspect ratio and gas permeation in polymer-layered silicate nanocomposites. *Macromol. Rapid Comm.* **2004**, *25*, 1145-1149.

254. Gilman, J. W.; Jackson, C. L.; Morgan, A. B.; Harris, Jr. J.; Manias, E.; Giannelis, E. P.; Wuthenow, M.; Hilton, D.; Phillips, S. H. Flammability properties of polymer-layered silicate nanocomposites. Propylene and polystyrene nanocomposites. *Chem. Mater.* **2000**, *12*, 1866–1873.

255. Porter, D.; Metcalfe, E.; Thomas, M. J. K. Nanocomposite fire retardants – A review. *Fire Mater.* **2000**, *24*, 45-52.

256. Pandey, J. K.; Reddy, K. R.; Kumar, A. P.; Singh, R. P. An overview on the degradability of polymer nanocomposites. *Polym. Degrad. Stab.* **2005**, *88*, 234-250.

257. Di Maio, E.; Iannace, S.; Sorrentino, L.; Nicolais, L. Isothermal crystallization in PCL/clay nanocomposites investigated with thermal and rheometric methods. *Polymer* **1994**, *45*, 8893-8900.

258. Zhang, G. S.; Yan, D. Y. Crystallization kinetics and melting behavior of nylon 10,10 in nylon 10,10-montmorillonite nanocomposites. *J. Appl. Polym. Sci.* **2003**, *88*, 2181-2188.

259. Tetto, J. A.; Steeves, D. M.; Welsh, E. A.; Powell, B. E. Biodegradable poly(ε-caprolactone)/clay nanocomposites. *ANTEC* **1999**, 1628–1632.

260. Sinha Ray, S.; Yamada, K.; Okamoto, M.; Ueda, K. Polylactide-layered silicate nanocomposite: A novel biodegradable material. *Nano Lett.* **2002**, *2*, 1093–1096.

261. Lee, S. R.; Park, H. M.; Lim, H. L.; Kang, T.; Li, X.; Cho, W. J.; Ha, C. S. Microstructure, tensile properties, and biodegradability of aliphatic polyester/clay nanocomposites. *Polymer* **2002**, *43*, 2495–2500.

262. Maiti, P.; Batt, C. A., Giannelis, E. P. Renewable plastics: synthesis and properties of PHB nanocomposites. *J. Macromol. Sci. C Rev.* **2003**, *88*, 58-59.

263. Ray, S.; Easteal, A. J. Advances in Polymer-Filler Composites: Macro to Nano. *Mater. Manuf. Process.* **2007**, *22*, 741–749.

264. Walls, H. J.; Riley, M. W.; Singhal, R. R.; Spontak, R. J.; Fedkiw, P. S.; Khan, S.A. Nanocomposite electrolytes with fumed silica and hectorite clay networks: passive versus active fillers. *Adv. Funct. Mater.* **2003**, *13*, 710–717.

265. Aranda, P.; Darder, M.; Fernández, S. –R.; López, B. –M.; Ruiz, H. -E. Relevance of polymer and biopolymer– clay nanocomposites in electrochemical and electroanalytical applications. *Thin Solid Films* **2006**, *495*, 104–112.

266. Sinha Ray, S.; Bousmina, M. Biodegradable polymers and their layered silicate nanocomposites: In greening the 21st century materials world. *Progr. Mater. Sci.* **2005**, *50*, 962–1079.

267. Okamoto, M. Biodegradable polymer/layered silicate nanocomposites: A review. *J. Ind. Eng. Chem.* **2004**, *10*, 1156-1181.

268. Chandra, R.; Rustgi, R. Biodegradable polymers. *Progr. Polym. Sci.* **1998**, *23*, 1273-1335.

269. Bordes, P.; Pollet, E.; Averous, L. Nano-biocomposites: Biodegradable polyester/nanoclay systems. *Progr. Polym. Sci.* **2009**, *34*, 125–155.

270. Messersmith, P. B.; Giannelis, E. P. Polymer-layered silicate nanocomposites: in situ intercalative polymerization of ε-caprolactone in layered silicates. *Chem. Mater.* **1993**, *5*, 1064–1066.

271. Messersmith, P. B.; Giannelis, E. P. Synthesis and barrier properties of poly(e-caprolactone)-layered silicate nanocomposites. *J. Polym. Sci. A Polym. Chem.* **1995**, *33*, 1047–1057.

272. Di, Y. W.; Iannace, S.; Di Maio, E.; Nicolais, L. Nanocomposites by melt intercalation based on polycaprolactone and organoclay. *J. Polym. Sci. B Polym. Phys.* **2003**, *41*, 670–678.

273. Diba, M.; Kharaziha, M.; Fathi, M. H.; Gholipourmalekabadi, M.; Samadikuchaksaraei, A. Preparation and characterization of

polycaprolactone/forsterite nanocomposite porous scaffolds designed for bone tissue regeneration. *Compos. Sci. Technol.* **2013**, *72*, 716-723.

274. Strawhecker, K. E.; Manias, E. Structure and properties of poly(vinyl alcohol) / Na + montmorillonite nanocomposites. *Chem. Mater.* **2000**, *12*, 2943–2949.

275. Wee, Y. –J.; Kim, J. –N.; Ryu, H. -W. Biotechnological production of lactic acid and its recent applications. *Food Technol. Biotechnol.* **2006**, *44*, 163–172.

276. Chang, J. –H.; An, Y. U.; Sur, G. S. Poly(lactic acid) nanocomposites with various organoclays. I. Thermomechanical properties, morphology, and gas permeability. *J. Polym. Sci. B Polym. Phys.* **2003**, *41*, 94–103.

277. Philip, S.; Keshavarz, T.; Roy, I. Polyhydroxyalkanoates : biodegradable polymers with a range of applications. *J. Chem. Technol. Biotechnol.* **2007**, *247*, 233–247.

278. Ramkumar, D. H. S.; Bhattacharya, M. Steady shear and dynamic properties of biodegradable polyesters. *Polym. Eng. Sci.* **1998**, *38*, 1426–1435.

279. Maiti, P.; Batt, C. A.; Giannelis, E. P. Renewable plastics: synthesis and properties of PHB nanocomposites. *Polym. Mater. Sci. Eng.* **2003**, *88*, 58–59.

280. Hablot, E.; Bordes, P.; Pollet, E.; Avérous, L. Thermal and thermo-mechanical degradation of PHB-based multiphase systems. *Polym. Degrad. Stab.* **2008**, *93*, 413–421.

281. Kevadiya, B. D.; Joshi, G. V; Patel, H. A.; Ingole, P. G.; Mody, H. M.; Bajaj, H. C. Montmorillonite-alginate nanocomposites as a drug delivery system: intercalation and in vitro release of vitamin B1 and vitamin B6. *J. Biomater. Appl.* **2010**, *25*, 161–177.

282. Darder, M.; Colilla, M.; Ruíz-Hitzky, E. Biopolymer-clay nanocomposites based on chitosan intercalated in montmorillonite. *Chem. Mater.* **2003**, *15*, 3774-3780.

283. Xu, S. W.; Zheng, J. P.; Tong, L.; De Yao, K. Interaction of functional groups of gelatin and montmorillonite in nanocomposite. *J. Appl. Polym. Sci.* **2006**, *101*, 1556–1561.

Chapter II:
Ionic complexes of carboxylic biopolymers

Comb-like polymers present an amphiphilic nature that can lead to different types of structures due to the phase separation of main and side branches. Those comb-like polymers containing a rigid backbone and flexible side chains form self-assembled structures whit biphasic bilayers. Several authors have described and analyzed this structure; from the first polypeptide based comb-like structures consisting of long alkyl esters of polyglutamates, to poly(alkyl aspartates) and alkyl esters of poly(malic acid). It has been reported that in solid state, these polypeptide backbones are arranged in an alpha-helix conformation and long alkyl side chains are oriented perpendicularly giving rise to a layered structure. Furthermore, upon heating, the helical conformation of the main chain remains unaltered and fixed whereas the alkyl side chains are melted. Therefore, the layered structure is preserved, undergoing just slight contractions and expansions in the interlayer spacing.

This particular thermal response has been also reported for analogous comb-like systems obtained from ionic coupling between polyelectrolytes and oppositely charged ionic alkyl surfactants. Thereby, ionic complexes of poly(α-glutamates), poly(γ-glutamates) or poly(β,L-malates), among other polypeptides, with alkyltrimethylammonium surfactants (*n*ATMA) have been studied and showed the described thermal behavior. The main advantage of these systems, compared to covalently bonded esters, lies in the simpler preparation method. Ionic complexes are basically obtained by direct mixing of the aqueous solution of corresponding salts.

In this chapter, the study of ionic complexes of some polyuronic carbohydrates, such as pectinic, alginic and hyaluronic acids, with alkyltrimethylammonium surfacatants is detailed. Pectinic acid, is the homopolymer poly(1,4-α-D-galacturonic acid), named as PGaA; alginic acid, is the copolymer poly(1,4-α-L-guluronic-*co*-1,4,β-D-mannuronic acid), named as coPGuMnA, and hyaluronic acid is an alternating copolymer poly(β-1,3-N-acetyl glucosamine-*alt*-β-1,4-guluronic acid), abbreviated HyalA. These polyuronics show different types of helical conformations, making them interesting for the thermal and structural study of their ionic complexes with alkyltrimethylammonium surfactants. Besides this, the obtained ionic

complexes of these carbohydrates, generally named as *n*ATMA·PUr has been analyzed and compared to the well-known analogous complexes of polypeptides, such as alkyltrimethylammonium-poly(γ-glutamate)s, *n*ATMA·PGGA.

1. Comb-like ionic complexes of pectinic and alginic acids with alkyltrimethylammonium surfactants

Summary: Ionic coupling of both polygalacturonic and alginic acids with alkyltrimethylammoniun surfactants containing 18, 20 and 22 carbon atoms in the alkyl side chain was conducted in water solution to prepare non-soluble comb-like complexes. These amphiphilic complexes are arranged in a biphasic layered structure with the paraffinic phase made of alkyl side chains alternating with the hydrophilic phase made of polyuronic chains. The complexes displayed the thermal behaviour typical of comb-like systems carrying long polymethylene groups, which melt at temperatures between 40 and 80 ºC without significant disruption of the layered arrangement. Melting temperature, crystallinity and thermal stability were slightly higher for the polygalacturonic complexes and all they increased almost steadily with the length of the alkyl chain within each series. The melting-crystallization process was followed by combined WAXS/SAXS and ^{13}C CP/MAS NMR, which revealed that the transition involves an expansion-contraction of the structure that may attain up to 20% of the original dimension. The transition takes place without large conformational changes and is not fully reversible.

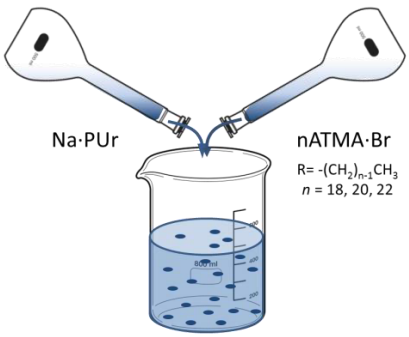

Publication derived from this work:

Tolentino, A.; Martínez de Ilarduya, A.; Alla, A.; Muñoz-Guerra, S. Ionic complexes of polyacids and cationic surfactants. *Macromolecular Symposia* **2010**, *296*, 265–271.

Tolentino, A.; Alla, A.; Martínez de Ilarduya, A.; Muñoz-Guerra, S. Comb-like ionic complexes of pectinic and alginic acids with alkyltrimethylammonium surfactants. *Carbohydrate Polymers* **2011**, *86*, 484–490.

1.1. Introduction

As it is widely known, a comb-like polymer is a highly branched polymer in which the main chain and the side chain have constitutions different enough as to form two separates phases. The structure adopted in the solid state by these systems varies between two limiting cases: a) A fully disordered globular arrangement typical of systems in which, both main and side chains are non-crystallizable, and b) a well-ordered layered structure with the two phases alternating periodically with a spacing that depends on the length of the side chain; this is the usual arrangement adopted by comb-like polymers in which the two phases are able to crystallize.[1,2]

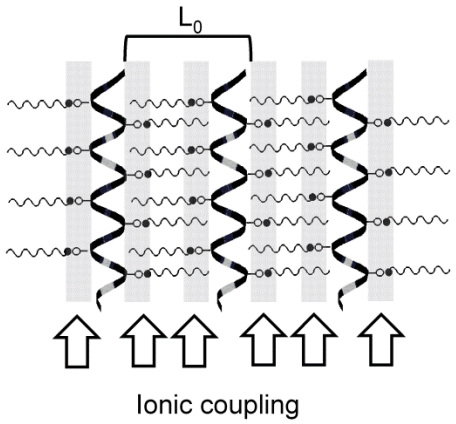

Figure 1. Side view of the layered structure adopted by comb-like ionic polymer complexes.

Different authors have reported extensively on the biphasic structure of poly(alkyl glutamate)s[3] and poly(alkyl aspartate)s[4] with long alkyl groups containing from 12 to 22 carbon atoms, in which the polypeptide chains in the alpha-helix conformation are arranged side-by-side in sheets with the alkyl side chain in fully extended conformation and crystallized with an orientation more or less normal to the sheet plane. When these systems are heated, the alkyl side chains melt but the conformation of the main chain remains essentially unaltered retaining the helical arrangement and keeping its position in the lattice. The layered structure is therefore preserved but the interlayer spacing slightly varies due to the conformational change undergone by the polymethylene chain.[2] Such thermal behaviour has interesting phenomenological consequences with potential technological applications such as thermoresponsive-permeoselective membranes and thermochromic sensors.[5,6]

Recently it has been shown that comb-like systems with structures and properties similar to those described above can be generated by coupling between ionic alkyl surfactants and charged polyelectrolytes (Figure 1). Alkyltrimethylammonium-poly(α-glutamate)s complexes were the systems firstly reported with such characteristics.[7] Similar complexes of poly(γ-glutamate)s[8]and poly(β,L-malate)s[9] have been later studied in great detail in our group with special attention paid to their structure and thermal properties. The clear advantage afforded by the systems based on ionic coupling respect to the covalent systems is their greater simplicity of preparation. Ionic complexes can be readily obtained by direct mixing of the corresponding components dissolved in aqueous medium and avoiding thus laborious synthetic work.

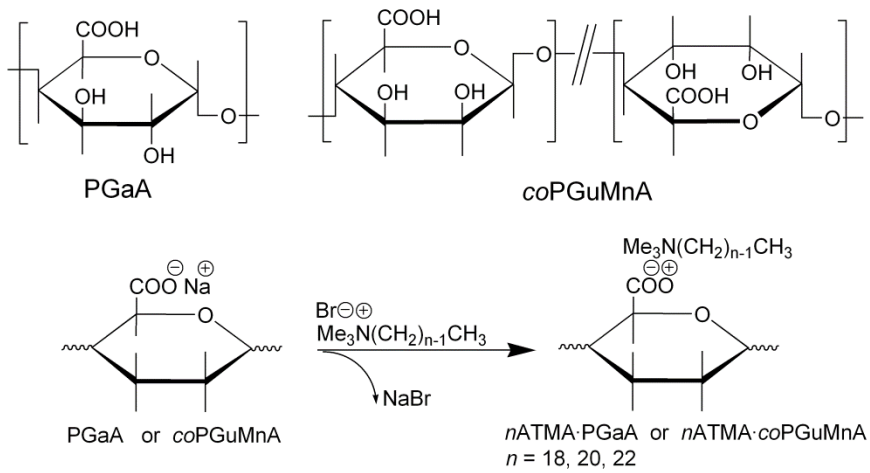

Figure 2. Top: Chemical structures of pectinic (PGaA) and alginic (coPGuMnA) acids. Bottom: Coupling reaction leading to alkyltrimethylammonium-polyuronic acid complexes (hydroxyl and glycosyl groups are not indicated).

In this paper a structure-property study of the complexes produced by ionic coupling of alkyltrimethylammonium surfactants (*n*ATMA, *n* is the number of carbon atoms contained in the alkyl chain with even values from 18 to 22) with polyuronic acids, specifically, pectinic and alginic acids (Figure 2), is reported. Pectinic acid is the homopolysaccharide poly(1,4-α-D-galacturonicacid), abbreviated PGaA, whereas alginic acid is the copolymer poly(1,4-α,L-guluronic-co-1,4-β-D-mannuronic acid), abbreviated coPGuMnA, with the two comonomericuronate units distributed in a blocky microstructure.[10] The interaction of both pectinic and alginic acids with different types of cationic surfactants has been object of several studies in these last years[11] and also the formation of nanoparticles with antimicrobial properties made of alginate

complexes has been described.[12] Nevertheless, the comb-like complexes formed from polyuronic acids and quaternary ammonium surfactants have not been studied so far. Worthy to notice that a rather close approach to these systems based on coupling of cationic surfactants and starch partially functionalized with carboxylic groups has been very recently reported.[13]A preliminary account of the present work was presented in the EPF2009 congress and made available in the corresponding published symposium account.[14]

1.2. Experimental Part

1.2.1. Materials

The alkyltrimethylammonium surfactant bromide salts of general formula $RMe_3N{\cdot}Br$ were either purchased from Aldrich (R= $-C_{18}H_{37}$ (stearyl)) or synthesized by us according to the procedure described in the literature (R= $-C_{20}H_{41}$ (eicosyl) and $-C_{22}H_{45}$ (docosyl)).[15]Thepolyuronic acids were purchased to Sigma-Aldrich. The pectinic acid sample with a Mw = 25,000-50,000 $g{\cdot}mol^{-1}$ was enzymatically produced, and the alginic acid sodium salt was obtained by extraction from brown algae with a Mw = 80,000-120,000 and has a L-Gu/D-Mn ratio of 39/61.

1.2.2. Complexes preparation

Complexes were prepared following the methodology described by us for the synthesis of complexes of *n*ATMA surfactants with poly(γ-glutamic acid)[8] and poly(β,L-malic acid).[9] In summary, an aqueous solution of the surfactant was added to an equimolecular solution of the sodium salt of the polyacid. The aqueous mixture was maintained under stirring at temperatures between 40-60 ºC for 4 hours. The formed precipitate was isolated from the sodium bromide solution by centrifugation, washed with water, and dried under vacuum.

1.2.3. Structure and thermal characterization methods.

Thermal analysis was performed with a Perkin-Elmer Pyris 1 DSC instrument and calibrated with indium. 2-4 mg samples were subjected to heating and

cooling rates of 10 ºC·min^{-1} under a nitrogen atmosphere in the -30-120 ºC temperature range. Time-resolved X-ray diffraction experiments were carried out at the A2 beamline of DORIS at HASYLAB in Hamburg. Non-isothermal treatments at heating and cooling rates of 5 ºC·min^{-1} were carried out within the 10-120 ºC temperature range. Small and wide angle X-ray scattering patterns (SAXS and WAXS) were acquired simultaneously every minute. Semicrystalline standard PET and Ag-behenate were used for calibrations. Other X-ray diffraction experiments were also recorded in a Siemens D5000 instrument from samples in powder form using a radiation of 0.154 nm wavelength. Solid state ^{13}C CP/MAS NMR spectra were recorded at 75.5 MHz in a Bruker AMX-300 instrument equipped with a CP/MAS accessory and an Eurotherm variable temperature controller. Samples of 100-200 mg weight were spun at 3.9-4.0 kHz in a cylindrical ceramic rotor. All spectra were acquired with contact and repetition times of 2 ms and 5 s, respectively, and 512 to 1024 scans were accumulated. The spectral width was 31.2 kHz, and the number of data points was 4K. Chemical shifts were externally calibrated against the methylene peak of glycine appearing at 43.3 ppm.

1.3. Results and discussion

1.3.1. Synthesis of complexes

As it is depicted in Figure 2, the procedure leading to the complexes is extremely simple. The complexes were readily formed and precipitated when equimolecular aqueous solutions of the sodium polyuronate and *n*ATMA·Br salt were mixed, and the mixture was left to stand at room temperature for a few hours. Yields approximated to 75 and 85% for pectinic and alginic complexes, respectively. The complexes were recovered as white hygroscopic powders that rapidly take up water in contact with the atmosphere. After an exhaustive exploratory testing, it was concluded that, at difference with complexes based on polypeptides, the polyuronic complexes are non-soluble in most of common organic solvents, although they become swollen in some chlorinated hydrocarbons and were soluble in warm m-cresol. The exceptional insolubility displayed by these complexes should be attributed to the occurrence of frequent intermolecular hydrogen-bonding tightly interlocking the polysaccharide chains. The NMR analysis of ionic complexes made of long alkyl surfactants that have been previously reported has shown all them to have a nearly stoichiomeric composition in the two counterparts. In the present case, a similar analysis is unfortunately not

feasible because the non-solubility of these polyuronic complexes; in the absence of any opposite evidence, it will be reasonable to assume that the composition of these complexes must be no far from stoichiometric composition.

1.3.2. Thermal properties

The thermal behaviour of *n*ATMA·PUrA complexes was examined by both TGA and DSC, and results are compared in Table 1. The TGA analysis showed that complexes start to decompose at temperatures above 200 ºC.

Decomposition took place along a multi-stage mechanism involving at least three successive stages which are defined by three maximum rate decomposition temperatures in the 210-230 ºC, 260-300 ºC and 380-410 ºC ranges, respectively, with no residual material left at the end of the last stage. According to $^{o}T_{d}$ and the first step decomposition temperature values, complexes of pectinic acid appear to be slightly resistant to heating than the alginic ones, and comparison of the temperatures for the second and third decomposition steps reveals that the thermal stability increases steadily with n in both series. The DSC analysis revealed that all complexes have a melting peak in the 50-80 ºC range showing a trend of increasing temperature and enthalpy with the increase in length of the alkyl side chain. An exothermic peak indicative of crystallization is observed upon cooling after melting although the crystallinity attained is much lower than originally attained, and crystallization could take place only if the overheating above melting is restricted to a few tens of degrees. The heating and cooling DSC traces registered from the 18ATMA complexes of both pectinic and alginic acids are depicted in Figure 3.

Thermal data of melting and crystallization for the three series of complexes afforded by DSC analysis are compared in Table 1. According to which is well known for polyglutamates and polymalates complexes,[8,9] the endothermic peak located in the 40-80 ºC range is interpreted to arise from the melting of the polymethylene segments. It can be inferred from the broaden shape displayed by the melting peaks that, compared to polypeptide and polyester chains, the polysaccharide chain hinders the crystalline packing of the alkyl side chains and reduces the efficiency of the system for being arranged in ordered structures. This effect is even more pronounced for the complexes made of alginic acid, where melting enthalpies of the recrystallized material only are able to reach tenths of a kcal·mol^{-1}. It does make sense to interpret that after melting, a fraction of hydrogen bonds is disrupted and their

Table 1. Thermal data of polyuronic complexes measured by TGA and DSC.

Complex	TGA			DSC								
				1st Heating					2nd Heating		Cooling	
	$^{o}T_d$[a] (ºC)	T_d[b] (ºC)	W[c] (%)	T_{m1} (ºC)	ΔH_{m1} (kcal·mol^{-1})	n_c^H	ΔS_{m1}[d] (cal·K^{-1}·mol^{-1})	n_c^S	T_{m2} (ºC)	ΔH_{m2} (kcal·mol^{-1})	T_c (ºC)	ΔH_c (kcal·mol^{-1})
*n*ATMA·PGaA												
18	211	229/270/381	70/18/0	70	4.2	6.0	12.2	6.1	52	2.5	50	-2.7
20	212	227/281/398	68/19/0	77	5.3	7.6	15.1	7.6	61	1.9	55	-3.5
22	207	219/301/411	73/23/0	73	7.0	10	20.2	10.1	66	3.8	59	-5.1
*n*ATMA·*co*PGuMnA												
18	204	210-217/266/381	66/15/0	58	2.2	2.6	6.6	2.8	47	0.8	41	-0.8
20	206	211-220/289/392	66/18/0	68	3.7	4.4	10.9	4.6	53	0.7	47	-0.7
22	202	209/301/400	73/22/0	76	5.6	6.6	16.0	6.8	64	2.8	57	-2.9

[a]Onset decomposition temperature calculated by the tangent method.
[b]Maximum rate decomposition temperature for each decomposition step.
[c]Remaining weights at the end of the respective decomposition stages.
[d]Values calculated from experimental enthalpy and temperature data; $\Delta H_m/T_m$.

rebuilding must require appropriate time and temperature conditions. It is worth noting that surfactants display melting peaks above 100 ºC clearly distinguishable from the melting of the alkyl side chain; the absence of such peaks in the DSC traces of complexes indicates that the excess of surfactant in these compounds, if any, must be small.

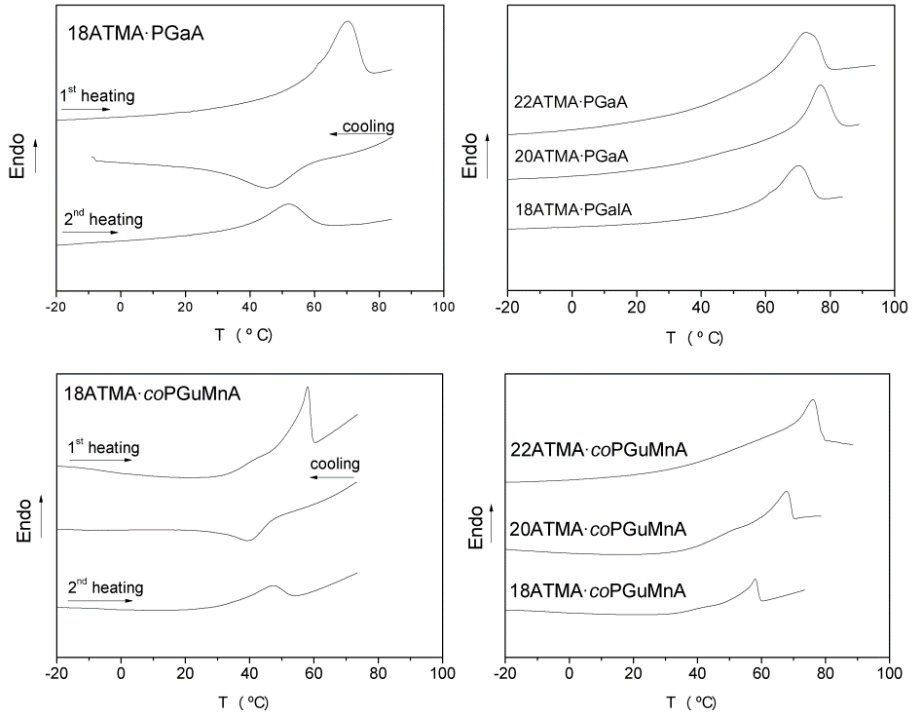

Figure 3.DSC traces of *n*ATMA·PGaA and *n*ATMA·coPGuMnA.

The plot of the melting enthalpy against the number of carbons contained in the alkyl surfactant group for pectinic and alginic acid complexes (Figure 4a) consists of two almost parallel straight lines with a slope of 0.7-0.8 kcal·mol^{-1}·CH2^{-1} indicating that the paraffinic crystal lattice must be similar in both cases. Conversely, a difference of nearly 5 kcal·mol-1 is observed between the two series as the y-intercept is concerned. The higher enthalpy values observed for *n*ATMA·PGaA complexes reveal a higher crystallinity of the paraffinic phase in this series. The number of crystallized methylenes, inferred from enthalpy data, is plotted against n in Figure 4b, which shows an almost exact linear dependence with the same slope for the two series. Specifically, n_c takes values between 6 and 10 for the *n*ATMA·PGaA complexes and between 2 and 6 for the *n*ATMA·coPGuMnA complexes. It is noteworthy that only a minor fraction of the methylenes contained in the paraffinic phase is

able to crystallize and that such fraction is significantly greater in the case of pectinic complexes. The lower crystallizability displayed by nATMA·coPGuMnA complexes can be attributed to the chain microstructure heterogeneity of the poly(guluronic-co-mannuronic) chain.

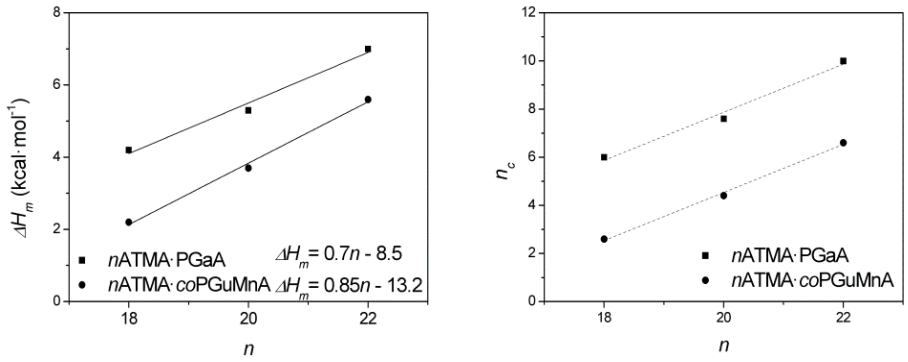

Figure 4. Methylene melting enthalpy, ΔH_m a), and number of crystallized methylene units, n_c, b), as a function of the number of methylenes, n, contained in the alkyl side chain.

1.3.3. The biphasic structure of the complexes

According to the DSC results described above, the X-ray diffraction analysis of the *n*ATMA·PUrA complexes revealed the existence of a considerable order, at both short and medium range. The powder X-ray diffraction diagram recorded from the 20ATMA·PGaA complex is depicted in Figure 5a for illustration. This X-ray scattering pattern, which is characterized by the presence of the two peaks at ~0.42 nm and ~3.5 nm is shared by all the complexes examined in this work; the precise spacing values appearing for all the complexes are listed in Table 2.

In all the complexes but in 18ATMA·coPGuMnA, the 0.42 nm reflection is the only one appearing in the wide-angle region. According to what is known for polyglutamates and polymalates complexes,[8,9] such reflection should be associated to the 100 interplanar spacing of a crystallized paraffinic phase with the alkyl chains packed in a pseudohexagonal phase with a ≈ 0.48 nm. The strong sharp peak appearing in the medium angle region, which is invariably accompanied by a second order peak, arises from a ~3-4 nm periodical spacing (L_0), which tends to increase with the value of *n* in both series. The L_0 values of the complexes together with values reported for the polyglutamate complexes (*n*ATMA·PGGA) are plotted against *n* in Figure 5b.

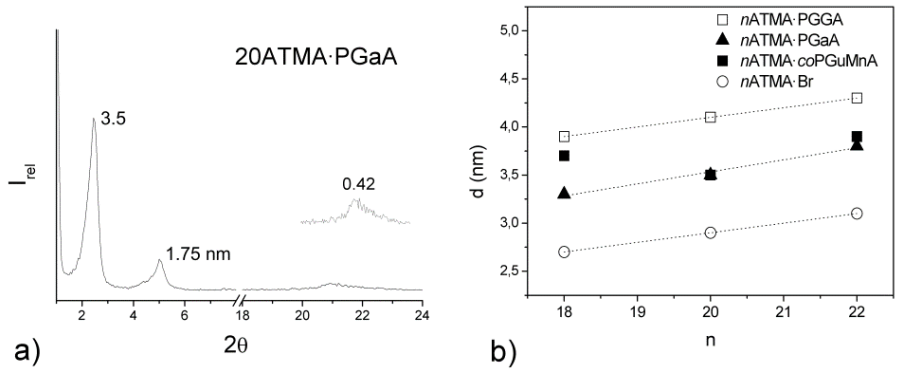

Figure 5. a) X-Ray diffraction profile of the indicated complex in the SAXS region. Inset: 19-23º region of WAXS displaying the 0.42 nm reflection characteristic of the crystallized paraffinic phase. b) Variation of the interlayer spacing with n for the indicated series of complexes and for the *n*ATMA·Br surfactant series.

Table 2. X-Ray data of polyuronic complexes subjected to heating.[a]

*n*ATMA·PUrA	SAXS		WAXS	
	$L_0^{20ºC}$	L_0^{Tm}	$d_{001}^{20ºC}$	d_{001}^{Tm}
PGaA				
18	3.3	3.4	0.41	0.46
20	3.5	3.7	0.41	0.46
22	3.8	4.1	0.41	0.46
*co*PGuMnA				
18[b]	3.7	4.2	0.42	0.46
	4.2		0.45	
20	3.5	4.3	0.42	0.46
22	3.9	4.3	0.42	0.46

[a]Lamellar spacings (L_0) and interplanar distances (d_{001}) at 20 ºC and at the melting temperature.
[b]Two spacings seen at 20 ºC due to partial melting of this complex at this temperature.

A straight line is obtained for the *n*ATMA·PGaA series with a slope of 0.125 nm·$CH2^{-1}$comparable to the 0.10 value observed for the *n*ATMA·PGGA. A 0.10-0.125 nm value is acceptable with the rise of the methylene unit of a chain in full-extended conformation. In the case of the *n*ATMA·coPGuMnA, the L_0 spacing changes unevenly with n although the overall trends seems to follow the other series. According to what is well known for comb-like systems, the L_0 spacing is associated to the periodicity of a biphasic layered

structure in which the paraffinic phase made of alkyl side chains alternates to the hydrophilic phase made of polysaccharide chains.

1.3.4. Thermal transitions

The structural changes accompanying the melting of the alkyl side chain were followed by powder X-ray diffraction recorded at real time with synchrotron radiation. The evolution of the scattering profile of 20ATMA·PGaA complex with temperature in both WAXS and SAXS regions is shown in Figure 6. Upon melting, i.e. at temperatures about 70 ºC, the 0.42 peak vanished and displaced to around 0.45 nm; the changes observed in the SAXS region reflect the dimensional variations of the interlayer spacing upon melting. The 3.5 nm peak moves slightly toward higher values indicating the occurrence of an expansion in the structure of 0.2 nm. This pattern of behaviour can be taken as representative of the *n*ATMA·PUrA complexes and it reflects the structural changes that take place in the layered arrangement.

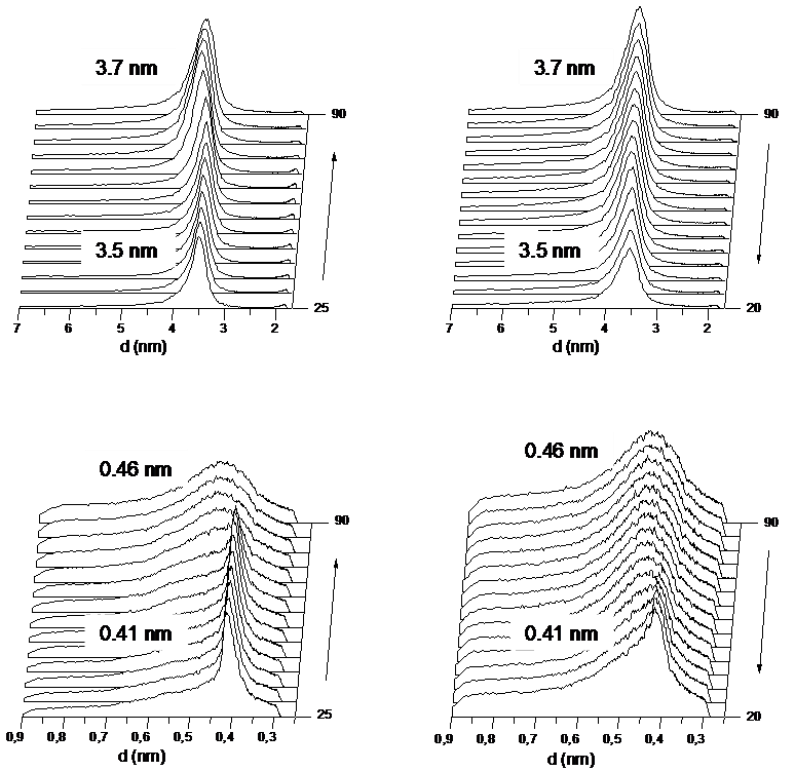

Figure 6. Real time SAXS (top) and WAXS (bottom) profiles of 20ATMA·PGaA at heating (left) and cooling (right).

The disruption of the pseudohexagonal paraffinic crystal lattice leads to a liquid phase in which the polymethylene chains are packed with an average chain-to-chain distance of 0.45 nm. Simultaneously, a slight rearrangement occurs involving a spacing out around 5% and 10% of the original value for the pectinic and alginic acid, respectively. The SAXS and WAXS values measured for the complexes below and above melting are compared in Table 2.

The heating effect on the structure is similar to that displayed by polyglutamates and polymalates, both esters and complexes, previously studied by us.[3,8,9] It should be noticed however that the changes taking place in L_0 with temperature, in both magnitude and sign, are depending on the chemical nature of the polymer chain as well as on the nature of the bond linking the alkyl side chain to the main chain. The evolution of the SAXS profiles at heating and cooling deserves special attention. The increasing in intensity and sharpness displayed by the 3-4 nm peak with temperature is really striking; such changes denote an improvement in the layered arrangement with temperature, which even continues above melting. Although it could be explained assuming that the main chain sheets can be accommodated better when the interlayer structure become more fluid, this is a complex point that required further attention. Furthermore, the full reversibility of the process suggests that the structural modification must be essentially dimensional without implying severe molecular rearrangements.

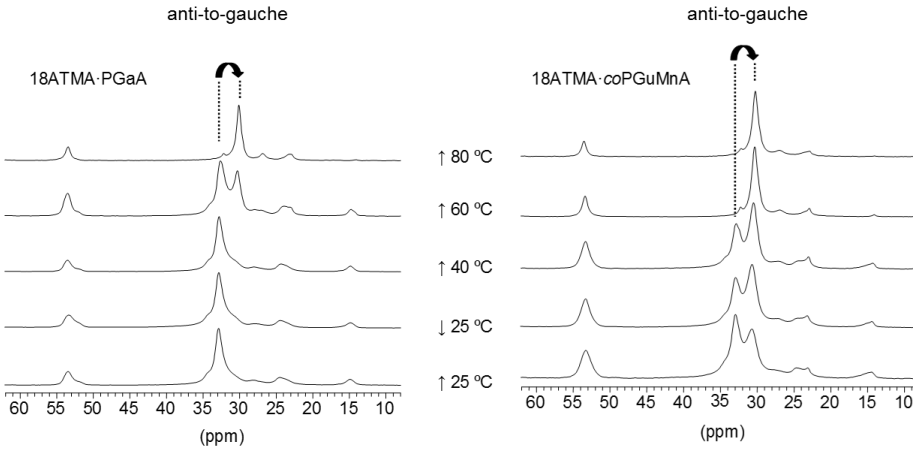

Figure 7. ^{13}C CP/MAS NMR spectra of polyuronic complexes revealing the anti-to-gauche transition of inner paraffinic methylenes that takes place upon heating and cooling.

The conformational changes involved in the melting of the alkyl side chain of *n*ATMA·PUrA were investigated by ^{13}C CP/MAS NMR since the application of this technique in the transitions happening in comblike polymers induced by heating effects is wealthy documented.[16] It is well known that melting of a paraffinic lattice implies a anti-to-gauche transition in the dihedrals of the polymethylene segments, which is reflected in changes in the shifts of the implicated carbon resonance peaks. The changes taking place in the ^{13}C NMR spectrum of 18ATMA·PGaA and 18ATMA·coPGuMnA upon successive heating and cooling are shown in Figure 7. In 18ATMA·PGaA at 25 °C, the peak arising from the inner methylenes of the alkyl side chain in *anti* conformation appeared near to 33 ppm, whereas at 80 °C, the peak is upfield displaced to 30 ppm which is the shift expected for a polymethylene chain undergoing a fast transition between the anti and gauche conformers. At intermediate temperatures, both peaks are present since the melting proceeds along a broad temperature range and upon cooling to 25 °C, the initial spectrum is fully recovered. In the case of 18ATMA·coPGuMnA, the changes are similar although the spectrum at 25 ºC shows the double peak indicating that the octadecyl chain is partially melted at this temperature in this complex. This observation is unique in the whole set of complexes here studied and accounts for the second spacing observed at 4.2 nm in the SAXS profile of 18ATMA·coPGuMnA (Table 2). The pattern of changes described for 18ATMA·PGaA is shared by all the complexes studied in this work and it is similar to that described for the A-B transition happening in comb-like polyaspartates and polyglutamates, both covalent and ionic, by effect of heating.[3,4,8] The NMR results not only give strong support to DSC and X-ray diffraction interpretations given above, but provided helpful information to understand the melting process at the molecular level. The fact that a good amount of methylenes remain at *anti* conformation after melting indicates that the polymethylene chain looses the crystalline order without abandoning the stretched conformation. This should be the reason for the small dimensional change involved in the transition and for the outstanding willingness of the system to recover the original structure.

1.4. Conclusions

Comb-like ionic complexes of polypectinic acid (polygalacturonic acid) and polyalginic acid were prepared by coupling with alkyltrimethylammonium surfactants bearing long alkyl chains of 18, 20 and 22 carbon atoms. The resulting complexes are not soluble in water neither in most of common organic solvents and are stable up to temperatures above 200 ºC. These complexes crystallize in a biphasic layered structure which displays melting

and recrystallization of the alkyl side chain at temperatures between 40 and 80 ºC. The transition temperatures and crystallinity increase with the length of the alkyl side chain and are higher for the pectinic acid complexes suggesting that a better molecular arrangement is reached in this case. The melting-recrystallization process is reversible, happens instantaneously and involves a significant dimensional change in the structure. This interesting behaviour confers to these complexes high interest as potential membranes with thermoresponsive properties.

1.5. References

1. Plate, N. A.; Shibaev, V. P.. Comb-like polymers - Structure and properties. *J. Polym. Sci. Macromol. Rev.* **1974**, *8*, 117-253.

2. Loos, K.; Muñoz-Guerra, S. Microstructure and crystallization of rigid coil comblike polymers and block copolymers. In *Supramolecular polymers, 2*nd Edition; Ciferri, A. Ed.; CRC Press: Boca Ratón, 2005; pp 393-442.

3. (a) Morillo, M.; Martínez de Ilarduya, A.; Muñoz-Guerra, S. Comblike alkyl esters of biosynthetic poly (γ-glutamic acid). 1. Synthesis and characterization. *Macromolecules* **2001**, *34*, 7868–7875. (b) Morillo, M.; Martinez de Ilarduya, A.; Alla, A.; Muñoz-Guerra, S. Comblike alkyl esters of biosynthetic poly (γ-glutamic acid). 2. Supramolecular structure and thermal transitions. *Macromolecules* **2003**, *36*, 7567–7576.

4. (a) Lopez-Carrasquero, F.; Montserrat, S.; Martinez de Ilarduya, A.; Muñoz-Guerra, S. Structure and thermal properties of new comblike polyamides: Helical poly(β-L-aspartate)s containing linear alkyl side chains. *Macromolecules* **1995**, *28*, 5535–5546. (b) Martínez de Ilarduya, A.; Alemán, C.; García-Alvarez, M.; López-Carrasquero, F.; Muñoz-Guerra, S. Helical poly (β-peptides): The helix-coil transition of poly (α-alkyl-β-aspartate)s in solution. *Macromolecules* **1999**, *32*, 3257–3263.

5. Muñoz-Guerra, S.; López-carrasquero, F.; Alemán, C.; Morillo, M.; Castelletto, V. Supramolecular layered structures of comb-Like poly(β-peptide)s showing thermochromic properties. *Adv. Mater.* **2002**, *14*, 203–205.

6. Compañ, V.; Zanuy, D.; Andrio, A.; Morillo, M.; Aleman, C.; Muñoz-Guerra, S. Permeation properties of the stereoregular nylon-3 analogue, poly (α-hexyl β-L-aspartate). *Macromolecules* **2002**, *35*, 4521–4530.

7. Ponomarenko, E. A.; Waddon, A. J.; Tirrell, D. A.; Macknight, W. J. Structure and properties of stoichiometric complexes formed by sodium poly (α,L-glutamate) and oppositely charged surfactants. *Langmuir* **1996**, *12*, 2169–2172.

8. (a) Pérez-Camero, G.; García-Alvarez, M.; Martínez De Ilarduya, A.; Fernández, C.; Campos, L.; Muñoz-Guerra, S. Comblike complexes of bacterial poly(γ,D-glutamic acid) and cationic surfactants. *Biomacromolecules* **2004**, *5*, 144–152. (b) García-Alvarez, M.; Alvarez, J.; Alla, A.; Martínez de Ilarduya, A.; Muñoz-Guerra, S. Comb-like ionic complexes of cationic surfactants with bacterial poly(γ-glutamic acid) of racemic composition. *Macromol. Biosci.* **2005**, *5*, 30–38.

9. Portilla-Arias, J. A.; García-Alvarez, M.; Martínez de Ilarduya, A.; Holler, E.; Muñoz-Guerra, S. Nanostructurated complexes of poly(β,L-malate) and cationic surfactants: Synthesis, characterization and structural aspects. *Biomacromolecules* **2006**, *7*, 161–170.

10. Dumitriu, S. Polysaccharides as biomaterials. In: *Polysaccharides*; Dumitriu, S. Ed.; Marcel Dekker: New York, 1998; pp 1-61.

11. Ropers, M.-H.; Meister, A.; Blume, A.; Ralet, M.-C. Pectin-lipid assembly at the air-water interface: Effect of the pectin charge distribution. *Biomacromolecules* **2008**, *9*, 1306–1312.

12. Asker, D.; Weiss, J.; McClements, D. J. Analysis of the interactions of a cationic surfactant (lauric arginate) with an anionic biopolymer (pectin): Isothermal titration calorimetry, light scattering, and microelectrophoresis. *Langmuir* **2009**, *25*, 116–122.

13. Balsamo, V.; López-Carrasquero, F.; Laredo, E.; Conto, K.; Contreras, J.; Feijoo, J. L. Preparation and thermal stability of carboxymethyl starch/quaternary ammonium salts complexes. *Carbohydr. Polym.* **2011**, *83*, 1680–1689.

14. Tolentino, A.; Martínez de Ilarduya, A.; Alla, A.; Muñoz-Guerra, S. Ionic complexes of polyacids and cationic surfactants. *Macromol. Symp.* **2010**, *296*, 265–271.

15. Hendrix, W. T.; von Rosenberg, J. L. The mechanism of the rearrangement of the hydrocobalt carbonyl catalyzed isomerization of 3-phenylpropene. *J. Am. Chem. Soc.* **1976**, *98*, 4850–4852.

16. Yamanobe, T.; Tsukahara, M.; Komoto, T.; Watanabe, J.; Ando, I.; Uematsu, I.; Deguchi, K.; Fujito, T.; Imanari, M. Conformation and dynamic aspects of poly(γ-*n*-octadecyl L-glutamate) in the solid state and liquid-crystalline state. *Macromolecules* **1988**, *21*, 48–50.

2. Thermal degradation of polyuronic acids and their complexes with alkylammonium surfactants

Summary: The thermal decomposition of complexes made of polyuronic acids (polygalacturonic and alginic acids) and alkyltrimethylammonium surfactants (*n*ATMA·PUr) bearing long alkyl chains (*n* = 18, 20 and 22) was examined by using a combination of TGA, FTIR and NMR techniques. Decomposition of neat polyacids happened in one single stage with almost quantitative decarboxylation and dehydration along with furfural and formic acid formation. Complexes decomposed along a three-stages process with initial dissociation of the complex and decomposition of the ammonium counterpart followed by decomposition of the polysaccharide favoured by the amines generated in the previous step. A mutual interaction between the polymer and the surfactant operated in the complex so that decomposition temperatures decreased respect to those shown by the separated components.

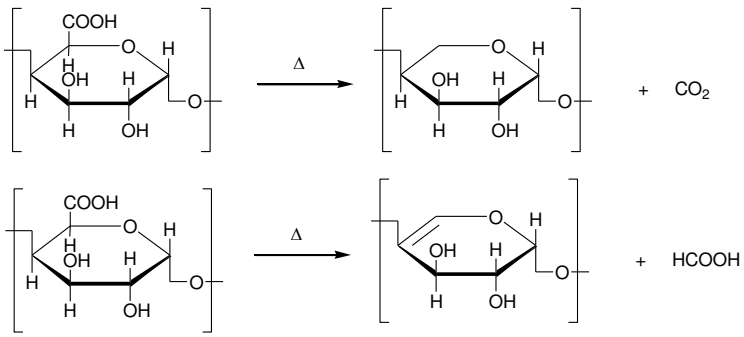

2.1. Introduction

In the last years, a considerable attention has been given to comb-like complexes generated by coupling naturally occurring polyelectrolytes with counter-ionic surfactants bearing long alkyl chains.[1] After pioneering examples described by Tyrrell et al. for basic poly(α-aminoacids) and alkylsulfonates,[2] a fair number of complexes made of microbial polyacids (poly(γ-glutamic)[3,4] and poly(β-malic)[5] acids) and alkyl trimethylammonium surfactants (ATMA) or alkanoyl cholines were reported (Chapter III.2). More recently anionically charged polysaccharides such as modified starch[6] containing carboxylic groups and several polyuronic acids (PUr)[7-9] (Chapter II.1 and II.2) have been also coupled with ATMA to produce similar complex structures. All these comb-like have in common the ability to self-assemble in a layered structure with the paraffinic phase made of alkyl chains alternating with a highly hydrophilic phase constituted by the polyelectrolyte chain. The suitability of these complexes to encapsulate different types of drugs and to deliver them as a result of the dissociation of the complex[10] (Chapter III.3) or the hydrolysis of the polymer[11] has been shown for several cases.

The study of the thermal degradation of these complexes is really challenging because a considerable number of decomposition reactions occur simultaneously. A detailed study on the pyrolysis of ATMA polyglutamic[12] and polymalic[13] complexes reported that decomposition of these compounds happened through several steps including complex dissociation, decomposition of the alkyltrimethylammonium counterpart and depolymerization of the polyelectrolyte. To our best knowledge no similar study on polysaccharide complexes has been carried out to date.

The pyrolysis of polysaccharides is an extremely complex process with more than 70 volatile compounds identified in the thermal decomposition of glucose.[14] Furthermore, furfural and furane-type compounds are invariably found in the volatiles released in the thermal decomposition of carbohydrates.[15] These compounds are assumed to be generated through a series of reactions embracing cleavage of glycosidic bonds and rearrangement of the pyranosyl structure into the 5-carbon ring in addition to β-eliminations leading to endocyclic double bonds.[16] It is also known that polyuronic acids at temperatures near 250 ºC undergo almost quantitative decarboxylation of the uronic moieties leaving a residue mainly composed of 5-carbon units.[17] Several works dealing with the analysis of volatiles released by different pectin-containing products have shown that carbon oxides, water, and furfural and furane derivatives are invariably present in addition to some aromatic hydrocarbons.[18,19] Sharma et al.[20] reported that the residue left by pectinic acid heated at 550 ºC contains H/C and O/C ratios decreasing

steadily with temperature in agreement with the progressive formation of polycyclic aromatic hydrocarbons. On the other hand, experimental evidence proving that furfural is the main volatile evolved in the heating of alginic acid at temperatures below 300 ºC has been also provided.[21] Furthermore, hydrolysis of the main chain glycoside bridge takes place concomitantly by the action of the water generated in the dehydration of the pyranosyl units.

In this work a preliminary study of the thermochemical decomposition of the complexes made of pectinic and alginic acids with alkyltrimethylammonium surfactants with *n* =18, 20 and 22 is carried out. The analysis is performed by combining TGA data obtained by heating under inert atmosphere with ^{1}H NMR data recorded from the degradation products collected by pyrolysis. The purpose is to disclose the mechanism underlying the first steps of decomposition of *n*ATMA·PUr complexes caused by heating between 200 and 300 ºC for the significance that the thermal degradation may have in the potential application of these compounds as biomaterials.

2.2. Experimental part

2.2.1. Materials

The two polyuronic acids used in this study were provided by Sigma-Aldrich. Polygalacturonic acid (PGaA) was synthesized with enzymes and has a molecular weight of 25,000-50,000. The alginic acid (*co*PGuMnA) from brown algae was supplied as the sodium salt with a molecular weight of 80,000-120,000 and a G/M ratio of 39/61. The alkyltrimethylammonium bromide (*n*ATMA·Br) with *n* = 18, 99% pure, was also provided by Sigma-Aldrich. The eicosyltrimethylammonium and docosyltrimethylammonium bromides (*n* = 20 and 22) were synthesized following the procedure described in the literature.[22] The complexes of polyuronic acids and alkyltrimethylammonium salts (*n*ATMA·PUr) were prepared by the method described by Pérez-Camero et al.,[3] for the preparation of similar complexes from poly(γ-glutamic acid). Features of these complexes relevant to the present work are given in Table 1.

Table 1. Relevant features of *n*ATMA·PUr complexes

	T_m[a] (ºC)	L_0[b] (nm)
*n*ATMA·PGaA		
18	70	3.3
20	77	3.5
22	73	3.8
*n*ATMA·*co*PGuMnA		
18	58	3.7; 4.2
20	68	3.5
22	76	3.9

[a]Melting temperature.
[b]Window width of the layered structure.

2.2.2. Methods

Thermogravimetry was performed on a Perkin-Elmer TGA6 thermobalance under an inert atmosphere. 15-30 mg samples were heated at a rate of 10 ºC·min^{-1} within the 30-800 ºC range. For isothermal experiments, samples were heated at the selected temperature and weight registered as a function of time. The onset temperature corresponding to 5% of weight loss was estimated by the tangent method. Infrared spectroscopy was carried out on powder samples using an FTIR 4100 Jasco spectrophotometer or a Perkin Elmer Spectrum One FTIR in both cases equipped with an ATR diamond accessory. Measurements covered the 600-4000 cm^{-1} frequency range and 32 scans were accumulated for each spectrum. ^{1}H RMN spectra were registered with a Bruker AMX300 instrument operating at 300.13 MHz. $CDCl_3$, $CDCl_3$/TFA or DMSO-d_6 solutions of samples at 3-10 mg·mL^{-1} concentrations and tetramethylsilane (TMS) added as reference were used for this analysis.

2.3. Results and discussion

Thermal data of PGaA and *co*PGuMnA acids and their ionic complexes afforded by TGA analysis are collected in Table 2. These data were recorded from samples coming directly from synthesis and subjected to heating at a rate of 10 ºC·min^{-1} along the 30-800 ºC range under a nitrogen atmosphere. A similar pattern consisting on three decomposition stages taking place within the 200-400 ºC range preceded by a minor weight loss at temperatures near

below 100 ºC is shared by all the studied compounds. A separated description of the thermal behavior of the polyacids and the complexes is given below.

Table 2. Thermal decomposition data of PGaA and *co*PGuMnA and their ionic complexes with *n*ATMA.

Compound	T^a (ºC)	$^oT_d^b$ (ºC)	$^mT_d^c$ (ºC)	W^d (%)
nATMA·Br				
18	-	236	268/297/451/497	0
20	-	245	266/292/310/450/488	0
22	-	240	259/305/460/493	0
PGaA	95 (90)	232	252	16
*n*ATMA·PGaA				
18	100 (93)	211	229/270/381	65/17/0
20	100 (97)	212	227/281/398	66/18/0
22	99 (97)	207	219/301/411	71/22/0
*co*PGuMnA	100 (90)	227	237	23
*n*ATMA·*co*PGuMnA				
18	84 (88)	204	210-217/266/381	58/13/0
20	94 (88)	206	211-220/289/392	58/16/0
22	82 (89)	202	209/301/400	65/20/0

[a]Water release temperature. In parenthesis, residual weight (%).
[b]Onset decomposition temperature obtained by tangent method.
[c]Maximum rate decomposition temperature for each decomposition step.
[d]Remaining weights at the end of the respective decomposition stages.

2.3.1. Polyuronic acids

The TGA traces of PGaA and *co*PGuMnA along with their corresponding derivative curves are shown in Figure 1. A weight loss of about 10% is observed to take place near 100 ºC, which is attributable to desorption of small amounts of water usually present in polyuronic samples. In fact, no weight change was observed at the reheated TGA trace of a polymer sample that has been previously heated at 170 ºC for 30 min whereas the same weight loss was repeated in the trace recorded from the sample left to

exposure to the environment overnight (inset of Figure 1). Degradation of both polyacids starts above 200 ºC and proceeds through a well-defined stage with an associate weight loss of about 40% and at a maximum decomposition rate at 252 and 237 ºC, respectively for PGaA and *co*PGuMnA. After this stage, decomposition further continues slowly and steadily to leave a final residue of approximately 20% of the initial weight when temperature is 800 ºC. The close similarity in the TGA profile displayed by PGaA and *co*PGuMnA suggests the occurrence of a common decomposition mechanism for the two polyacids with observed minor divergences likely due to their differences in molecular weight or even to configurational effects.

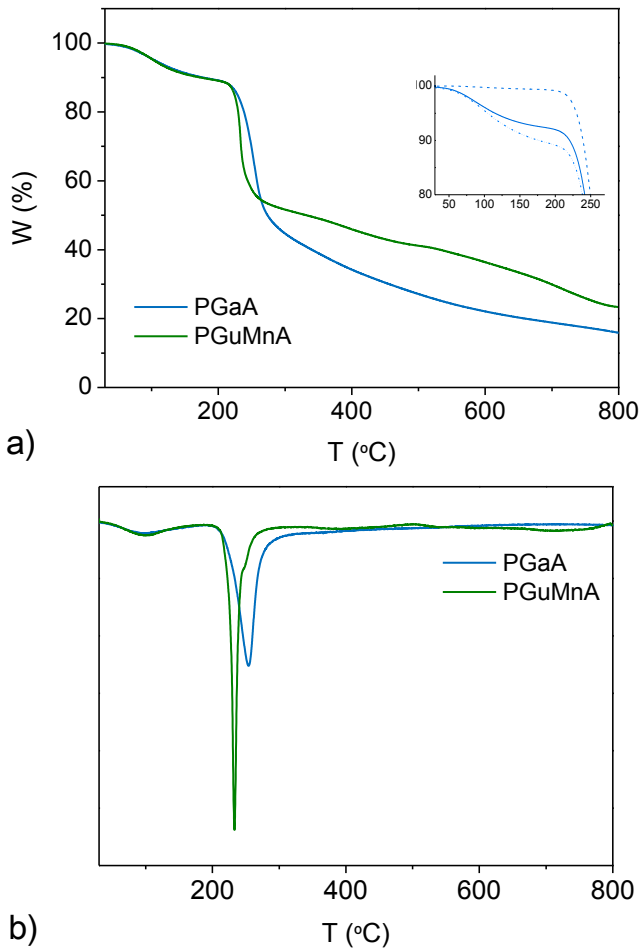

Figure 1. TGA traces of polyuronic acids (a) and their derivative curves (b). Inset: traces of 18ATMA·PGaA. Original sample (solid line) and after heating at 170 ºC, either exposed (dashed line) or not exposed (dotted line) to humid atmosphere.

To study the mechanism that laying under the decomposition of the polyacids, samples were subjected to several isothermal heating at increasing temperatures from 190 to 250 ºC and the volatiles were analyzed by NMR spectroscopy (Figure 2). Results were very similar for the two polyacids at all tested temperatures. Water was invariably the compound largely released followed by furfural and formic acid in comparable amounts, and other unidentified products in much minor amounts. On the other hand, the non-soluble residue left by samples that were isothermally heated at several temperatures within the 200-400 ºC range was analyzed by ATR-FTIR. The sets of spectra registered from both polyacids are depicted in Figure 3. It is observed that at increasing applied temperatures the original carbonyl peak at 1720 cm^{-1} disappears whereas a new absorption typical of double bond arises within the 1580-1600 cm^{-1}.

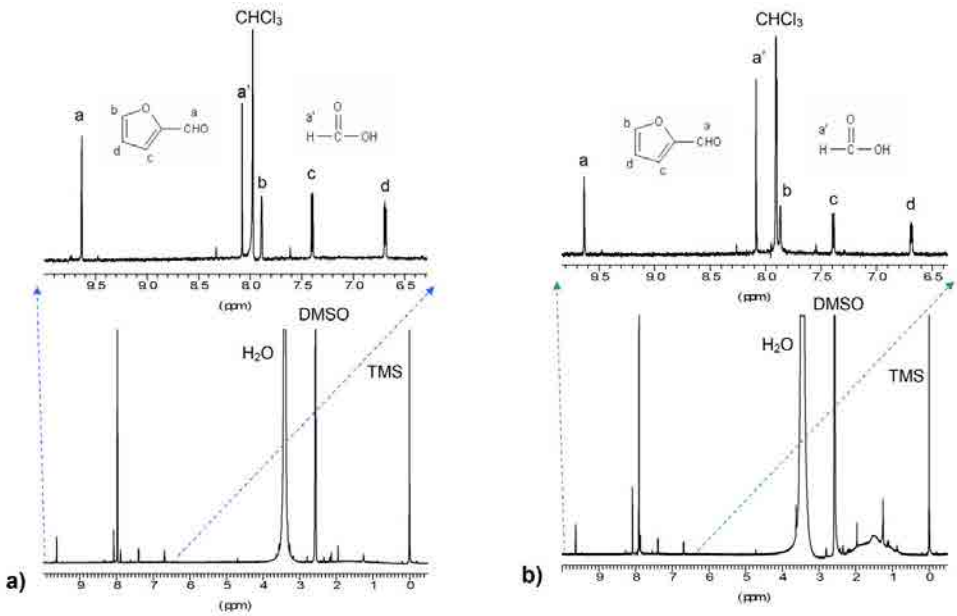

Figure 2. ^{1}H NMR in $CDCl_3$/DMSO of compounds released from PGaA (a) and *co*PGuMnA (b) heated at temperatures within 200-250 ºC range.

According to the available literature antecedents[16] these results asses that decarboxylation and elimination reactions with concomitant cleavage of the glycosyl bonds and rearrangement of the pyranosyl structure into furfural must be the main events occurring in the thermal decomposition of these two polyuronic acids. It should be stressed that the decarboxylation and dehydration reactions with elimination of two water molecules per each repeating unit would account for a weight about 45% of the molecular weight

of the polyuronic acid, an amount very close to the weight loss associated to the fall observed in the TGA curve (Figure 1). A possible interpretation arisen from FTIR-ATR spectra of PGaA and *co*PMnGuA pyrolysis residues could indicate a complex thermal degradation mechanism similar to that described by Sharma et al.[20] for pectins. By a ^{13}C-NMR study they determined an increased presence of aromatic groups with temperature, leading to polycyclic aromatic hydrocarbon compounds. The enlargement of double bond corresponding signs in detriment of C-O bands observed for higher pyrolysis temperatures of PGaA and coPMnGuA in Figure 3 would be in agreement with such suggested mechanism.

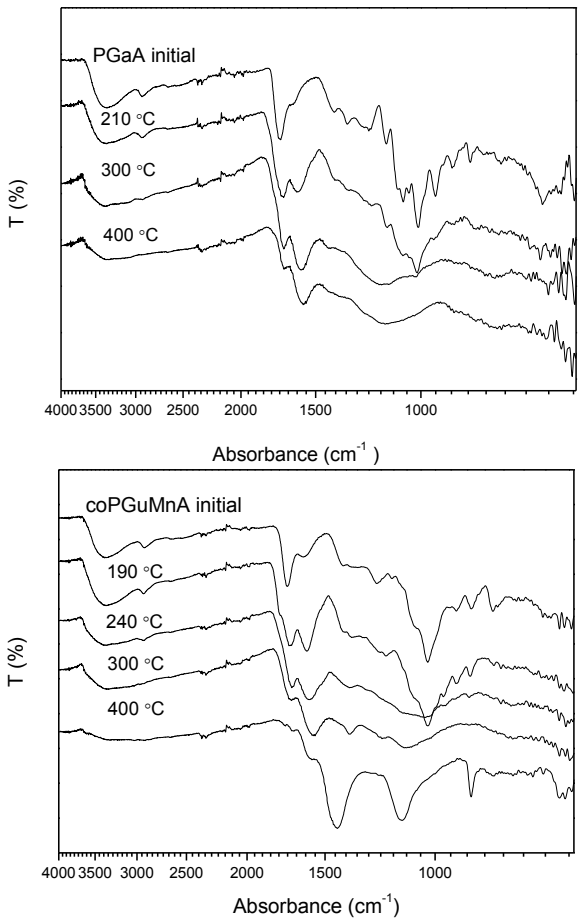

Figure 3. FTIR spectra of the residue left by polyuronic acids after isothermal heating at the indicated temperatures.

2.3.2. Alkyltrimethylammonium complexes of polyuronic acids

The TGA traces of some representative *n*ATMA·PUr complexes and their derivative curves are depicted in Figure 4. The thermal degradation profile of the complexes is very similar for the two families. In both cases they start to lose weight at around 200 ºC and further proceeds through a three-stage decomposition process that extends over the 200-400 ºC range of temperatures.

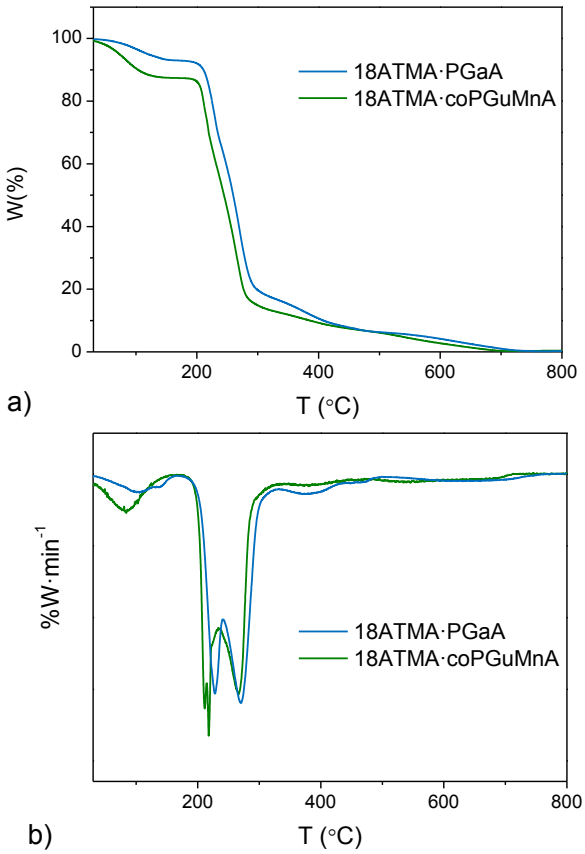

Figure 4. TGA traces of representative complexes (a) and their derivative curves (b).

The temperatures at which such stages present their maximum reaction rates are plotted as a function of *n* for the two families in Figure 5. This plot brings into evidence not only the almost linear dependence of T_d with *n* in the second and third stage but the extreme similar behavior displayed by the two families along the whole process.

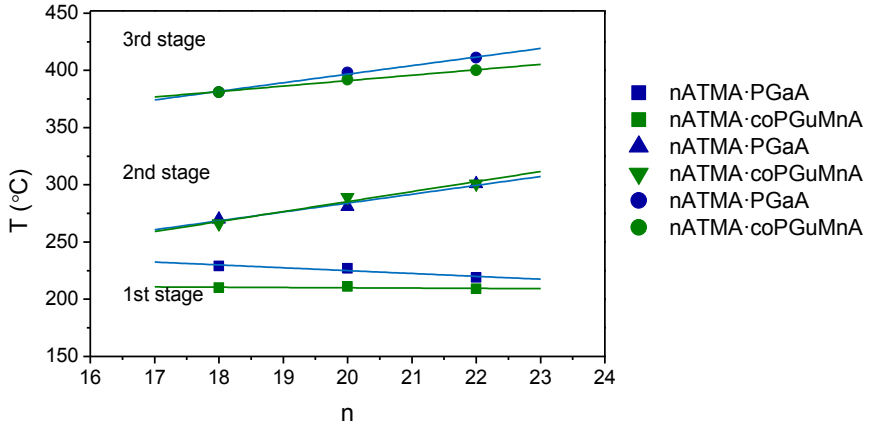

Figure 5. Maximum rate decomposition temperatures of the three decomposition stages of *n*ATMA·PUr complexes as a function of the alkyl chain length.

The first stage takes place around 220 ºC and seems to be independent of the length of the alkyl side chain. For studying this stage, genuine samples of 18ATMA·PUr complexes were subjected to constant heating at 200 ºC for one hour and both the released compounds and the remaining residue analyzed by NMR. The main components detected in the volatilized material were methanol and dimethyloctadecylamine accompanied by a lower amount of trimethylamine. This indicates that decomposition of the complex induced by the water released by the polyacid must be the chemical process happening in this stage. Trialkylamines were therefore formed as a consequence of the attack of water to the methyl or the α-carbon of the octadecyl group with subsequent formation of methanol or 1-octadecanol, respectively. The analysis of the residue revealed the presence of dimethyloctadecylamine together with unaltered complex in addition to a small amount of 1-octadecanol. Other minor peaks of uncertain assignment but likely arising from small molecular weight compounds were detected in the 3.5-4.5 ppm interval. The NMR spectra recorded in this study from both the volatiles and the solid residue with their corresponding peak assignments are shown in Figure 6. These results confirm the water-mediated decomposition of the complex in this stage although the reaction did not arrive to completion under the applied conditions.

The second stage takes place within the 250-300 ºC region at temperatures increasing with the value of *n* indicating its close dependence on the surfactant alkyl chain length. Further decomposition of amines generated in the first steps seems to take place in this second stage. Volatilization of the newly formed compounds will accounts for the linear dependence of temperature on *n*.

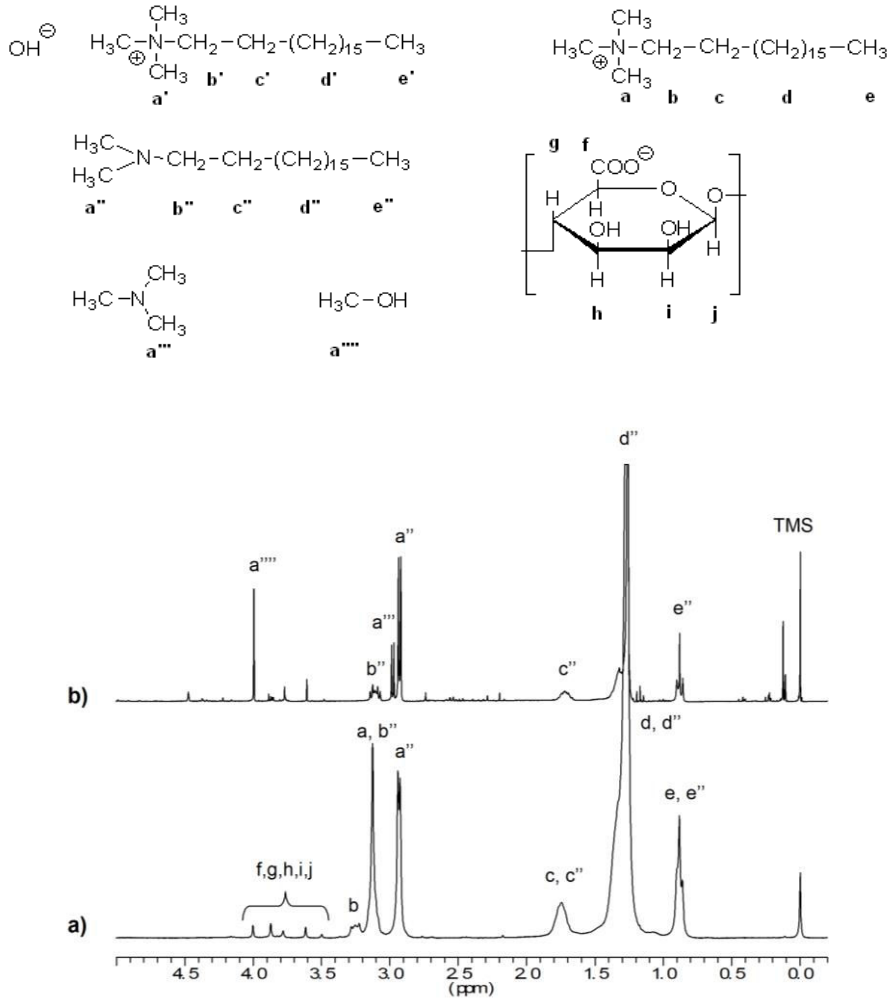

Figure 6. ^{1}H NMR spectra of the degradation products of 18ATMA·PGaA. a) Residue; b) Volatiles.

2.4. Conclusions

Comb-like ionic complexes made of polygalacturonic and alginic acids, and alkyltrimethylammonium surfactants display a thermal decomposition behaviour very similar for the two families and slightly depending on the length of the alkyl side chain. In agreement with results previously described by other authors, decomposition of neat polyacids happened in one single stage with almost quantitative decarboxylation and dehydration along with

furfural and formic acid formation. On the other side, complexes decomposed along a three-stages process with initial dissociation of the complex and decomposition of the ammonium counterpart in amines and alkanols. Decomposition of the polysaccharide takes place in the second stage with the concourse of the amines generated in the previous step. Remarkably, these two decomposition stages occur at temperatures considerably lower than those recorded for the separated components revealing that a certain mutual interaction between the polymer and the surfactant must operate. Data afforded in this work will be valuable for the processing of these complexes under heating.

2.5. References

1. Thünemann, A. F.; Müller, M.; Dautzenberg, H.; Löwen, J. J. H. Polyelectrolyte complexes. *Adv. Polym. Sci.* **2004**, *166*, 113–171.

2. Tyrrell, D. A.; Heath, T. D.; Colley, C. M.; Ryman, B. E. New aspects of liposomes. *Biochim. Biophys. Acta* **1976**, *457*, 259-302.

3. (a) Pérez-Camero, G.; García-Alvarez, M.; Martínez De Ilarduya, A.; Fernández, C.; Campos, L.; Muñoz-Guerra, S. Comblike complexes of bacterial poly(γ,D-glutamic acid) and cationic surfactants. *Biomacromolecules* **2004**, *5*, 144–152. (b) García-Alvarez, M.; Alvarez, J.; Alla, A.; Martínez de Ilarduya, A.; Muñoz-Guerra, S. Comb-like ionic complexes of cationic surfactants with bacterial poly(γ-glutamic acid) of racemic composition. *Macromol. Biosci.* **2005**, *5*, 30–38.

4. Tolentino, A.; León, S.; Alla, A.; Martínez de Ilarduya, A.; Muñoz-Guerra, S. Comblike ionic complexes of poly (γ-glutamic acid) and alkanoylcholines derived from fatty acids. *Macromolecules* **2013**, *46*, 1607-1617.

5. Portilla-Arias, J. A.; García-Alvarez, M.; Martínez de Ilarduya, A.; Holler, E.; Muñoz-Guerra, S. Nanostructurated complexes of poly(β,L-malate) and cationic surfactants: synthesis, characterization and structural aspects. *Biomacromolecules* **2006**, *7*, 161–170.

6. Balsamo, V.; López-Carrasquero, F.; Laredo, E.; Conto, K.; Contreras, J.; Feijoo, J. L. Preparation and thermal stability of carboxymethyl starch/quaternary ammonium salts complexes. *Carbohydr. Polym.* **2011**, *83*, 1680–1689.

7. Tolentino, A.; Martínez de Ilarduya, A.; Alla, A.; Muñoz-Guerra, S. Ionic complexes of polyacids and cationic surfactants. *Macromol. Symp.* **2010**, *296*, 265–271.

8. Tolentino, A.; Alla, A.; Martínez de Ilarduya, A.; Muñoz-Guerra, S. Comb-like ionic complexes of pectinic and alginic acids with alkyltrimethylammonium surfactants. *Carbohydr. Polym.* **2011**, *86*, 484–490.

9. Tolentino, A.; Alla, A.; Martínez de Ilarduya, A.; Muñoz-Guerra, S. Comb-like ionic complexes of hyaluronic acid with alkyltrimethylammonium surfactants. *Carbohydr. Polym.* **2013**, *92*, 691-696.

10. Tolentino, A.; Alla, A.; Martínez de Ilarduya, A.; Muñoz-Guerra, S. Complexes of polyglutamic acid and long-chain alkanoylcholines: nanoparticle formation and drug release. *Int. J. Biol Macromol.* **2014** (Accepted).

11. Portilla-Arias, J. A; García-Alvarez, M.; Martínez de Ilarduya, A.; Muñoz-Guerra, S. Ionic complexes of biosynthetic poly(malic acid) and poly(glutamic acid) as prospective drug-delivery systems. *Macromol. Biosci.* **2007**, *7*, 897–906.

12. Portilla-Arias, J. A.; García-Alvarez, M.; Martínez de Ilarduya, A.; Muñoz-Guerra, S. Thermal decomposition of microbial poly(γ-glutamic acid) and poly(γ-glutamate)s. *Polym. Degrad. Stabil.* **2007**, *92*, 1916–1924.

13. Portilla-Arias, J. A.; García-Alvarez, M.; Martínez de Ilarduya, A.; Holler, E.; Muñoz-Guerra, S. Thermal decomposition of fungal poly(β,L-malic acid) and poly(β,L-malate)s. *Biomacromolecules* **2006**, *7*, 3283–3290.

14. Heyns, K.; Stute, R.; Paulsen, H. Bräunungsreaktionen und fragmentierungen von kohlenhydraten: Teil I. Die flüchtigen abbauprodukte der pyrolyse von d-glucose. *Carbohydr. Res.* **1966**, *2*, 132–149.

15. Fagerson, I. S. Thermal degradation of carbohydrates. A review. *J. Agr. Food Chem.* **1969**, *17*, 747–750.

16. Byrne, G. A.; Gardiner, D.; Holmes, F. H. Pyrolysis of cellulose and action of flame-retardants. *J. Appl. Chem.* **1966**, 16, 81-88.

17. Perlin, A. S. Thermal decarboxylation of uronic acids. *Can. J. Chem.* **1951**, *30*, 278–290.

18. Demirbas, A. The influence of temperature on the yields of compounds existing in bio-oils obtained from biomass samples via pyrolysis. *Fuel Process. Technol.* **2007**, *88*, 591–597.

19. Fisher, T.; Hajaligol, M.; Waymack, B.; Kellogg, D. Pyrolysis behavior and kinetics of biomass derived materials. *J. Anal. Appl. Pyrolysis* **2002**, *62*, 331-349.

20. Sharma, R. K.; Wooten, J. B.; Baliga, V. L.; Hajaligol, M. R. Characterization of chars from biomass-derived materials: pectin chars. *Fuel* **2001**, *80*, 1825–1836.

21. Anastasakis, K.; Ross, A. B.; Jones, J. M. Pyrolysis behaviour of the main carbohydrates of Brown macro-algae. *Fuel* **2011**, *90*, 598-607.

22. Hendrix, W. T.; von Rosenberg, J. L. The mechanism of the rearrangement of the hydrocobalt carbonyl catalyzed isomerization of 3-phenylpropene. *J. Amer. Chem. Soc.* **1976**, *98*, 4850–4852.

3. Comb-like ionic complexes of hyaluronic acid with alkyltrimethylammonium surfactants

Summary: Stoichiometric complexes of hyaluronic acid with alkyltrimethylammonium surfactants bearing octadecyl, eicosyl and docosyl groups were prepared by ionic coupling in aqueous solution. The complexes were non soluble in water but soluble in organic solvents. In the solid state they self-assembled in a biphasic layered structure with the alkyl side chains forming a separate phase that melted in the 50-60 ºC range. They were stable to heating up to above 200 ºC.

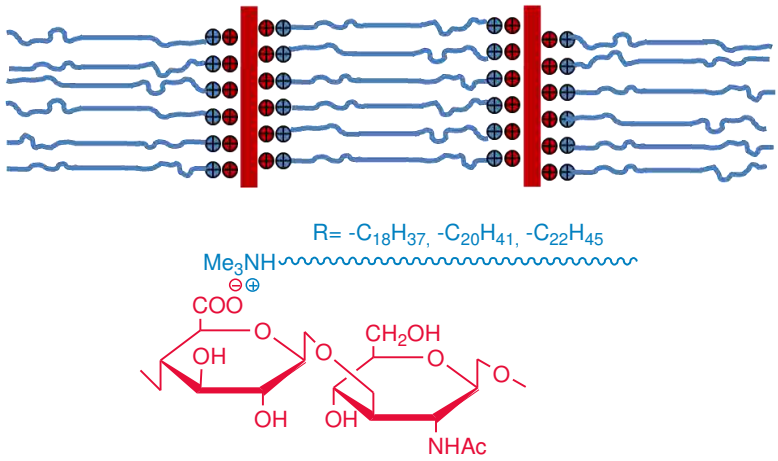

Publication derived from this work:

Tolentino, A.; Alla, A.; Martínez de Ilarduya, A.; Muñoz-Guerra, S. Comb-like ionic complexes of hyaluronic acid with alkyltrimethylammonium surfactants. *Carbohydr. Polym.* **2013**, *92*, 691-696.

3.1. Introduction

Hyaluronic acid (HyalA) is a linear polysaccharide ubiquitous in the human body. It is composed of repeating disaccharide units of β-1,3-N-acetyl glucosamine and β-1,4-glucuronic acid with a molecular weight up to 6 million Daltons. With excellent viscoelasticity, high moisture retention capacity, high biocompatibility and non-immunogenicity, HyalA finds a wide-range of applications in surgery, cosmetology, veterinary science, and hygiene medicine, where it has been used for over thirty years.[1,2] When chemically modified by reaction of the pendant reactive groups, HyalA can be transformed into a variety of new biomaterials with properties suitable for tissue repair and regeneration.[3,4,5] HyalA has been recently explored for its use in novel drug delivery systems with increasing enthusiasm because HyalA-binding receptors are believed to be involved in cancer metastasis.[6] Traditionally HyalA was extracted from rooster combs but now it is increasingly produced through microbial fermentation which has enhanced its application interest and commercial value.[7,8]

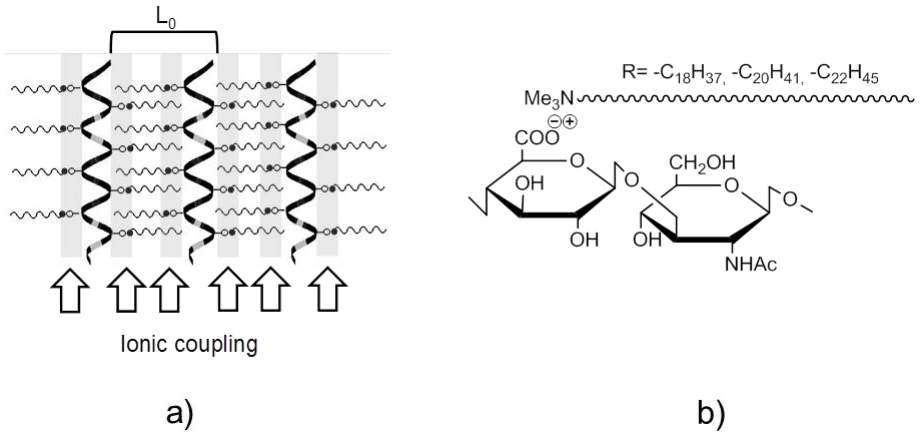

Figure 1. a) Side view of the layered structure usually adopted by comb-like ionic polymer complexes b) Chemical structure of *n*ATMA·HyalA ionic complexes.

In these last years it has been revealed that coupling of polyelectrolytes with ionic surfactants is a convenient method for the preparation of ionic complexes with remarkable structure and properties.[9,10] Specifically, coupling of polyacids with tetraalkylammonium surfactants bearing long alkyl chains is known to lead to amphiphilic comb-like systems displaying a layered biphasic structure (Figure 1a) able to lodge agents with chemical or biomedical activity.[11,12,13] In this communication we wish to report on the preparation,

structure and thermal behavior of complexes made of hyaluronicacid with alkyltrimethylammonium surfactants, abbreviated as *n*ATMA·HyalA, with alkyl chains containing 18, 20 and 22 carbon atoms (Figure 1b). Recently we have reported on similar complexes made of polyuronic acids (*n*ATMA·PUr), specifically, polygalacturonic and alginic acids[14,15] (Chapter II.1) and the binding of certain amphiphilic drugs to HyalA was investigated with regards to the flexibility of the polyanion.[16] The choice of Hyal as polyacid made in this work obeys to two reasons, to extend the ionic coupling method to this polysaccharide in order to broaden its potential as biomaterial, and to appraise how the alternating ionic structure of Hyal may affect the formation of these comb-like ionic complexes.

3.2. Experimental part

3.2.1. Materials

The sodium salt of hyaluronic acid (Na·HyalA), poly(sodium-β-D-glucuronate-[1-3]-β-N-acetyl-D-glucosamine-[1-4]), with a weight-average molecular weight of about 50,000 g·mol-1 used in this work was purchased from Enze Chemicals. Linear alkyltrimethylammonium bromide surfactants of general formula RMe_3NBr were purchased from Sigma-Aldrich (octadecyl, R=-$C_{18}H_{37}$) or synthesized by us according to a procedure described in the literature (eicosyl, R= -$C_{20}H_{41}$ and docosyl, R= -$C_{22}H_{45}$).[17]

3.2.2. Complexes preparation

The complexes were prepared following the methodology initially reported by Ponomarenko et al.[9] for poly(α-glutamate) complexes and later applied by us with some minor modifications to the preparation of other complexes.[11,12,15] In brief, an aqueous solution of *n*ATMA·Br surfactant was added dropwise to a solution of Na·HyalA in water under stirring at temperatures between 40 and 60 ºC depending on the surfactant. Equimolecular amounts of hyaluronic acid and surfactant were used in all cases. The complex precipitated upon standing for a few hours as a white fine powder that was isolated by centrifugation, washed several times in water and dried under vacuum.

3.2.3. Structure and thermal characterization methods

^{1}H-NMR spectra were recorded on a Bruker AMX-300 NMR instrument with samples dissolved in deuterated water (sodium hyaluronate) or MeOH-d4 (complexes) using TMS as internal reference. Calorimetric analysis was performed under a nitrogen atmosphere in the -30 to 120 ºC temperature range with a Perkin-Elmer Pyris 1 DSC instrument provided with an Intracooler device and calibrated with indium and zinc. Thermogravimetric analysis was performed at a heating rate of 10 ºC·min-1 within the 30-800 ºC interval under inert atmosphere using a Perkin-Elmer TGA6 thermobalance. X-ray diffraction studies were carried out using synchrotron X-ray radiation (WAXS and SAXS at A2 Hasylab beam line of DESY in Hamburg (Germany) with an energy corresponding to a 0.15 nm wavelength.

3.3. Results and Discussion

3.3.1. Synthesis of complexes

The complexes *n*ATMA·HyalA with *n* = 18, 20 and 22, were synthesized by mixing aqueous solutions of equimolecular amounts of polyacid and surfactant at the minimum temperature required to dissolve the surfactant. As a result of ionic coupling between the polyacid and the surfactant, complexes precipitated from the mixed aqueous solution after several hours of standing with release of sodium bromide. Complexes were readily isolated by centrifugation as white hygroscopic powders that were soluble in methanol but non-soluble either in chloroform or ethyl ether. The ^{1}H NMR spectra of the complexes displayed resolution enough as to ascertain the presence of the two counterparts. The spectra of Na·HyalA and 18ATMA·HyalA complex are comparatively depicted in Figure 2 with full assignment of their respective signals.[18] The composition of the complexes was accurately determined by 1H NMR on the basis of the area ratio of the hyaluronic acid methyl protons signal (CH_3, δ= 2.0 ppm) to the alkylammonium interior methylenes accumulative signal ($^{3\text{-}17}$CH2, δ= 1.2-1.5 ppm). The results afforded by this analysis revealed that all the *n*ATMA·HyalA complexes had essentially a stoichiometric composition showing an ATMA to HyalA ratio between 1 and 1.1.

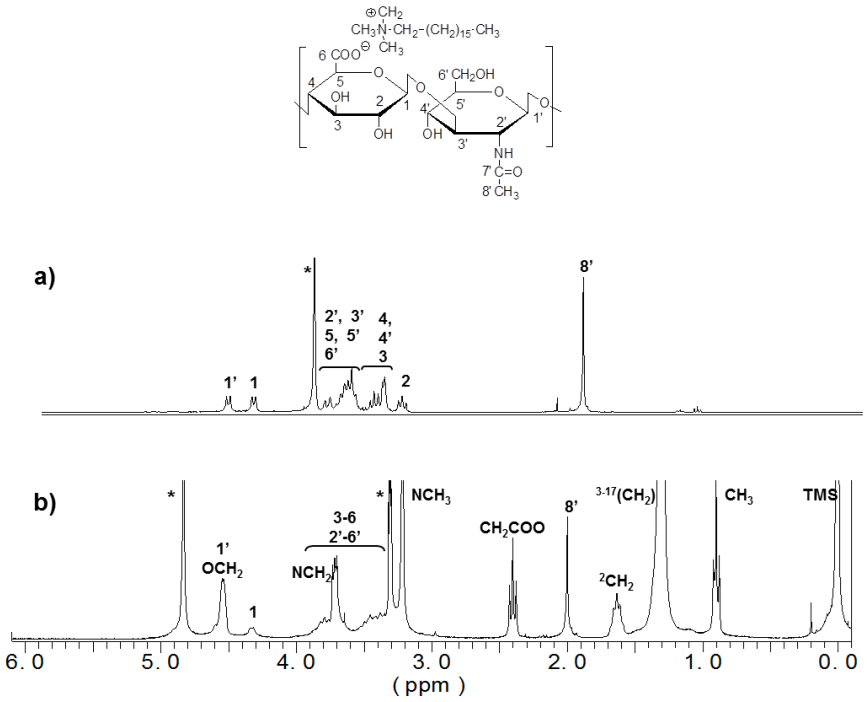

Figure 2. ^{1}H-NMR spectra of Na·HyalA (in D_2O) (a) and 18ATMA·HyalA (in MeOH-d) (b).

3.3.2. Thermal properties

The thermal behaviour of *n*ATMA·HyalA complexes was examined by both TGA and DSC, and data afforded by these analyses are gathered in Table 1. The TGA traces recorded from the complexes in the 25-800 ºC range are plotted in Figure 3 with their respective derivative curves displayed in the inset. These results indicated that *n*ATMA·HyalA complexes have a thermal stability similar to complexes of polygalacturonic and alginic complexes with onset temperatures near below 210 ºC (Chapter II.1).[15] In all cases, decomposition took place along a multi-stage process involving at least three successive stages with maximum rate decomposition temperatures in the 215-225 ºC, 265-300 ºC and in the proximities of 400 ºC, respectively. The weight lost in these three steps was 30-35, 40-50 and 10-15% of the original mass; no residue was left after heating at 800 ºC. The thermal decomposition mechanism of comb-like ionic complexes made from polyglutamic and polymalic acids has been studied by us in some detail;[12,13] in these complexes decomposition started by depolymerisation of the polypeptide chain along with

Table 1. Thermal properties and XRD data of *n*ATMA·HyalA complexes.

*n*ATMA·HyalA	TGA			DSC		SAXS[e]			WAXS[e]		
	$^{o}T_d$ [a] (ºC)	T_d [b] (ºC)	W [c] (%)	T_m [d] (ºC)	ΔH_m [d] (kcal·mol^{-1})	$L_0^{25ºC}$ (nm)	L_0^{Tm} (nm)	$L_0^{25ºC}$ (nm)	$d^{25ºC}$ (nm)	d^{Tm} (nm)	$d^{25ºC}$ (nm)
18	209	215-225	68	57	1.7	4.4	4.4	4.4	0.41	0.45	0.41
		265	21			*4.0*	*4.1*	*4.1*	*0.44*		*0.44*
		380-400	10								
		>800	~0								
20	208	215-225	67	66	1.2	4.5	4.6	4.5	0.41	0.45	0.41
		285	22			*4.1*	*4.1*	*4.1*	*0.44*		*0.44*
		380-400	7								
		>800	~0								
22	209	215-225	65	69	2.1	4.5	4.4	4.4	0.42	0.45	0.42
		300	27			*4.1*	*4.1*	4.1			0.44
		380-400	11								
		>800	~0								

[a]Onset decomposition temperature calculated by the tangent method.
[b]Maximum rate decomposition temperature for each decomposition step.
[c]Remaining weights at the end of the respective decomposition stages.
[d]Melting temperature and enthalpy recorded by DSC from pristine samples.
[e]Long (L_0) and short (d) spacings arising from the repeating interlayer distance and from the interplanar distance of the paraffinic phase at 25 ºC, at the melting temperature (70, 75 and 80 ºC for n=18, 20 and 22, respectively) and at 25 ºC after cooling.(In parenthesis, spacings arising from the initially disordered phase).

dissociation of the complex at temperatures slightly above 200 ºC followed by degradation of the alkyltrimethylammonium moiety in amines. The thermal decomposition of complexes of polyuronic acids *n*ATMA·PUr seems to happen through a rather more complex mechanism involving degradation of the polysaccharide chain in two stages within the 200-250 ºC followed by decomposition of the complex with release of alkylamines at temperatures steadily increasing with the length of the alkyl side chain.

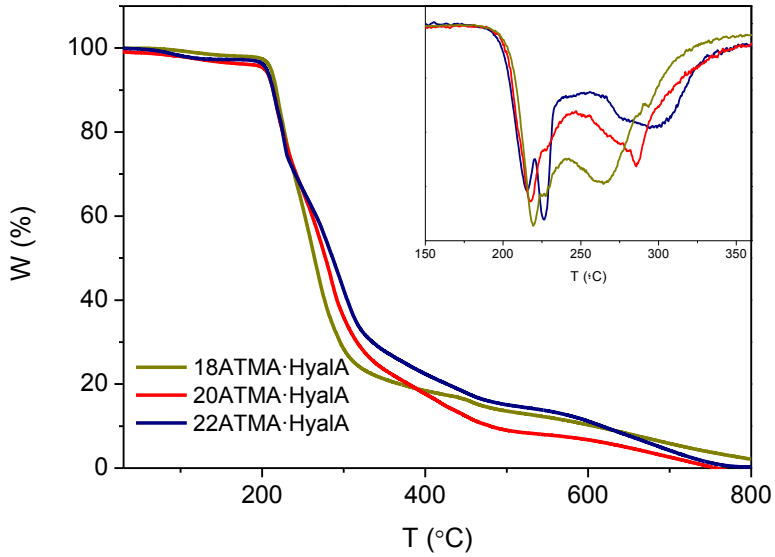

Figure 3. TGA traces of *n*ATMA·HyalA complexes. Inset: Derivative curves showing the maximum rate decomposition temperatures.

The DSC analysis revealed that *n*ATMA·HyalA complexes display melting peaks below 80 ºC (Figure 4a). By analogy with *n*ATMA·PUr complexes such peaks should be attributed to the melting of the paraffinic phase constituted by the long alkyl chains of the surfactant. Annealing of the complexes for a few hours at temperatures nearly below melting improved the crystallinity of the material as revealed by DSC (Figure 4b); peak multiplicity probably arising from the occurrence of crystallite size population heterogeneity, disappeared and the remaining melting peak became sharper and placed at temperatures steadily increasing with the value of *n* (Table 1). The melting enthalpy associated to melting also increased with the length of the alkyl side chain but with a slope much smaller than in the case of *n*ATMA·PUr. Furthermore the evolution of the enthalpy does not follow a monotonous trend as it happens in other complexes series with higher crystallinity previously studied by us.[11,12,15] The small differences in enthalpy (less than 1 kcal/mol) observed in this case may be critically affected by experimental errors probably distorting an actual

monotonous trend. Nevertheless, it can be concluded from these DSC results that the thermal behaviour of *n*ATMA·HyalA complexes essentially fits in the same pattern as *n*ATMA·PUr complexes which leads to infer that a similar structure must be adopted by all these complexes upon crystallization.

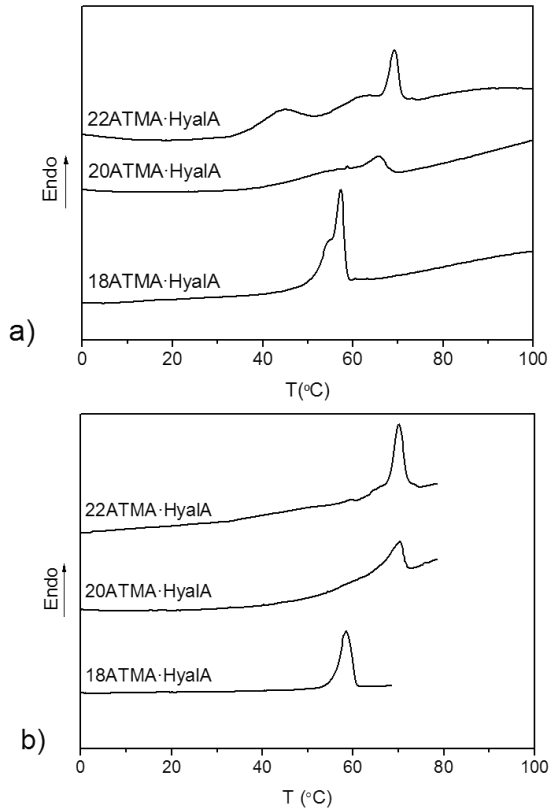

Figure 4. Heating DSC traces of *n*ATMA·HyalA complexes. a) Sample s coming from synthesis, b) samples annealed as indicated in the text.

3.3.3. Structural analysis

Films of these complexes prepared by casting were examined by X-ray diffraction in both wide and small angle regions at different temperatures in order to collect information from both the supramolecular structure and the packing of the alkyl side chains and to evaluate the effect of heating on the structure. The structural spacings recorded from this analysis are gathered in Table 1 and the SAXS profiles recorded from the whole series at 25 ºC are compared in Figure 5a. It was found that the three *n*ATMA·HyalA complexes

generated discrete scattering patterns which have in common the presence of a strong peak with a maximum at ~4.4 nm together with a second peak (*n* = 18) or shoulder (*n* = 20 and 22) at ~4.0 nm. In the WAXS angle range, all the complexes show a sharp peak at 0.41-0.42 nm accompanied by another broader one at ~0.45 nm for *n* = 18 and 20 (figures afforded as SI). According to diffraction data available for other comb-like ionic complexes previously studied by us, and for *n*ATMA·PUr in particular, the 4.4 nm peak should be associated to the periodical spacing L_0 of a biphasic layered structure consisting of sheets made of side-by-side arranged polyuronic chains and separated by a paraffinic phase made of the alkyl side chains. The 0.41-0.42 nm peak appearing in the WAXS region is assigned to d_{100} spacing of the lattice generated by the hexagonal packing of the alkyl side chains arranged in an almost fully extended conformation and oriented with the c-axis more or less normal to the plane of the sheets. Although the L_0 spacing in the comb-like ionic complexes usually increases almost linearly with the length of the polymethylene segment, in the present case the interlayer distance appears to be almost constant along the whole series (comparative plot in SI). Nonetheless, this rather exceptional behaviour is close to that observed for the complexes of alginic acid, which have been reported to display an increase in L_0 of only 0.2 nm when n increases from 18 to 22 (Chapter II.1).[15]

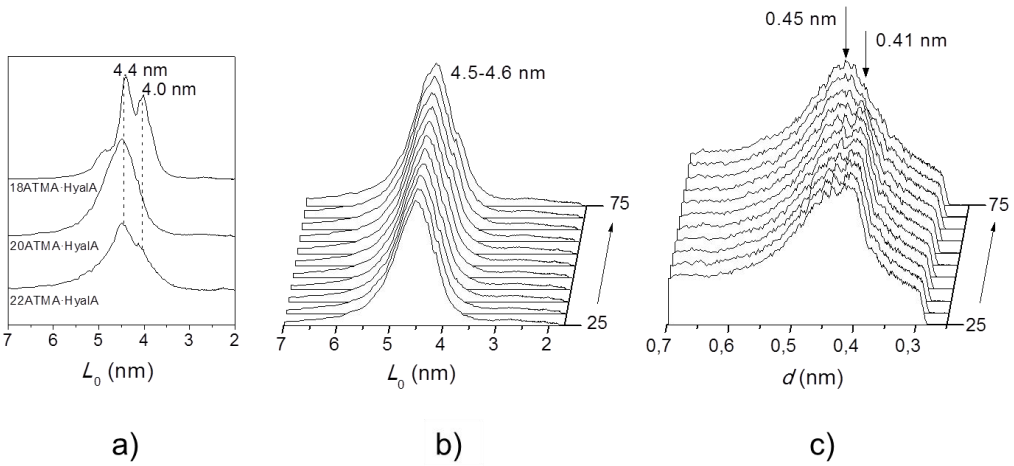

Figure 5. a) Compared SAXS profiles of complexes at 25 ºC. b) and c) Evolution of SAXS and WAXS profiles of 20ATMA·HyalA at heating from 25 ºC up to above melting.

The evolution of the scattering profile of 20ATMA·HyalA complex with temperature in both SAXS and WAXS regions is shown in Figure 5b-c. No significant changes were detected in the SAXS profiles after heating up to 75

ºC, a temperature well above melting. In fact, the 4.5 nm peak retained its position and intensity, and also its shape remained essentially unaltered. On the contrary, the 0.41 nm peak appearing in the WAXS region vanished at about 70 ºC and only the broad peak centered at 0.45 nm was present above that temperature. This process was reversed at cooling with the 0.41 nm peak reappearing at temperatures slightly below 70 ºC. The same diffraction pattern was displayed by 18ATMA·HyalA and 22ATMA·HyalA complexes with transition temperatures correspondingly changed (see SI material), the small deviations in spacings seen in Table 1 falling within the experimental error margins.

In agreement with the DSC results described above and according to previous studies made on other comb-like systems bearing long alkyl side chains, the changes taking place in WAXS region reflect the fusion of the paraffinic pseudohexagonal crystal lattice into a liquid phase in which the polymethylene chains, although disordered, are side-by-side packed with an average chain-to-chain distance of 0.45 nm. The enthalpy of the melting peak observed within the 50-70 ºC interval of the DSC traces is an indication of the methylene units fraction that is crystallized in the complex. The recorded melting enthalpy values were in the 1-2 kcal·mol^{-1} range, which are much lower than those reported for *n*ATMA·PUR which were in the 2-7 kcal·mol^{-1} range corresponding to 3-10 crystallized methylene units.[15] It can be concluded therefore that the fraction of crystallized alkyl side chains in *n*ATMA·Hyal must be very small, which would explain the invariance observed in the L_0 spacing upon heating. The low crystalline order attained in these complexes compared to others similar complexes like those made of polyglutamic,[11] polymalic,[12] polygalacturonic or alginic acids (Chapter II.1)[15] is likely due to the lower density of anionic charges in HyalA. Although no experimental data are available to ascertain what can be the conformation of HyalA in the complexes, it can be reasonably assumed that the polyacid chain must be in a more or less extended arrangement with the carboxylate ions openly exposed to the ammonium cations. The presence of the non-charged acetylglucosamine units in HyalA implies a larger separation between the carboxylate groups that will hinder the lateral packing of the alkyl chains attached to the coupled ammonium groups.

3.4. Conclusions

Stoichiometric ionic complexes of hyaluronic acid with cationic alkylammonium surfactants with alkyl side chains containing 18, 20 and 22 carbon atoms could be readily prepared. The complexes were non-water

soluble but they dissolved in organic solvents and are stable to heating up to above 200 ºC. These complexes self-organized in a biphasic layered structure characteristic of comb-like amphiphilic systems with the polyacid and the alkyl side chains phases alternating periodically with a repeating distance of ~4.5 nm. They displayed melting of the paraffinic phase in the 50-70 ºC range without appreciable changes in the layered spacing. The degree of order attained by the alkyl chains in these complexes is significantly lower than usually found in other similar comb-like ionic complexes.

3.5. References

1. Kogan, G.; Soltés, L.; Stern, R.; Gemeiner, P. Hyaluronic acid: A natural biopolymer with a broad range of biomedical and industrial applications. *Biotechnol. Lett.* **2007**, *29*, 17–25.

2. Necas, J.; Bartosikova, L.; Brauner, P.; Kolar, J. Hyaluronic acid (hyaluronan): a review. *Vet. Med.-CZECH* **2008**, *53*, 397–411.

3. Allison, D. D. ; Grande-Allen, K. J. Hyaluronan : A powerful tissue engineering tool. *Tissue Eng.* **2006**, *12*, 2131-2140.

4. Burdick, J. A. ; Prestwich, G. D. Hyaluronic acid hydrogels for biomedical applications. *Adv. Mater.* **2011**, *23*, 41-56.

5. Schanté, C. E.; Zuber, G.; Herlin, C.; Vandamme, T. F. Chemical modifications of hyaluronic acid for the synthesis of derivatives for a broad range of biomedical applications. *Carbohydr. Polym.* **2011**, *85*, 469–489.

6. Yadav, A. K.; Mishra, P.; Agrawal, G. P. An insight on hyaluronic acid in drug targeting and drug delivery. *J. Drug Target.* **2008**, *16*, 91-107.

7. Izawa, N.; Hanamizu, T.; Iizuka, R.; Sone, T.; Mizukoshi, H.; Kimura, K.; Chiba, K. Streptococcus thermophilus produces exopolysaccharides including hyaluronic acid. *J. Biosci. Bioeng.* **2009**, *107*, 119–123.

8. Liu, L.; Liu, Y.; Li, J.; Du, G.; Chen, J. Microbial production of hyaluronic acid: current state, challenges, and perspectives. *Microb. Cell Fact.* **2011**, *10*, 99.

9. Ponomarenko, E. A.; Waddon, A. J.; Tirrell, D. A.; Macknight, W. J. Structure and properties of stoichiometric complexes formed by sodium poly (α,L-glutamate) and oppositely charged surfactants. *Langmuir* **1996**, *12*, 2169–2172.

10. Macknight, W. J.; Ponomarenko, E. A.; Tirrell, D. A. Self-assembled polyelectrolyte-surfactant complexes in nonaqueous solvents and in the solid state. *Accounts Chem. Res.* **1998**, *31*, 781–788.

11. Pérez-Camero, G.; García-Alvarez, M., Martínez De Ilarduya, A.; Fernández, C., Campos, L., Muñoz-Guerra, S. Comblike complexes of bacterial poly(γ,D-glutamic acid) and cationic surfactants. *Biomacromolecules*. **2004**, *5*, 144–152.

12. Portilla-Arias, J. A.; García-Alvarez, M.; Martínez de Ilarduya, A.; Holler, E.; Muñoz-Guerra, S. Nanostructurated complexes of poly(β,L-malate) and

cationic surfactants: synthesis, characterization and structural aspects. *Biomacromolecules* **2006**, *7*, 161–170.

13. Portilla-Arias, J. A; García-Alvarez, M.; Martínez de Ilarduya, A.; Muñoz-Guerra, S. Ionic complexes of biosynthetic poly(malic acid) and poly(glutamic acid) as prospective drug-delivery systems. *Macromol. Biosci.* **2007**, *7*, 897–906.

14. Tolentino, A.; Martínez de Ilarduya, A.; Alla, A.; Muñoz-Guerra, S. Ionic complexes of polyacids and cationic surfactants. *Macromol. Symp.* **2010**, *296*, 265–271.

15. Tolentino, A.; Alla, A.; Martínez de Ilarduya, A.; Muñoz-Guerra, S. Comb-like ionic complexes of pectinic and alginic acids with alkyltrimethylammonium surfactants. *Carbohydr. Polym.* **2011**, *86*, 484–490.

16. Caram-Lelham, N.; Hed, F.; Sundelöf, L.-O. Adsorption of charged amphiphiles to oppositely charged polysaccharides. A study of the influence of polysaccharide structure and hydrophobicity of the amphiphile molecule. *Biopolymers,* **1997***, 41*, 765-772.

17. Hendrix, W. T.; Von Rosenberg, J. L. The mechanism of the rearrangement of the hydrocobalt carbonyl catalyzed isomerization of 3-phenylpropene. *J. Amer. Chem. Soc.* **1976**, *98*, 4850-4852.

18. Blundell, C.D.; Reed, M.A.C.; Almond, A. Complete assignment of hyaluronan oligosaccharides up to hexasaccharides. *Carbohydr. Res.* ***2006,*** *341*, 2803-2815.

3.6. Supporting information

SI Table 1. Synthesis data of hyaluronic complexes.

Complex	T^1 (ºC)	Composition[a]
*n*ATMA·HyalA		
18	40	1:1.1
20	50	1:1.0
22	60	1:1.0

T^1: reaction Temperature, Composition[a] Ratio of Hyal to ATMA, estimated by ^{1}H-NMR.

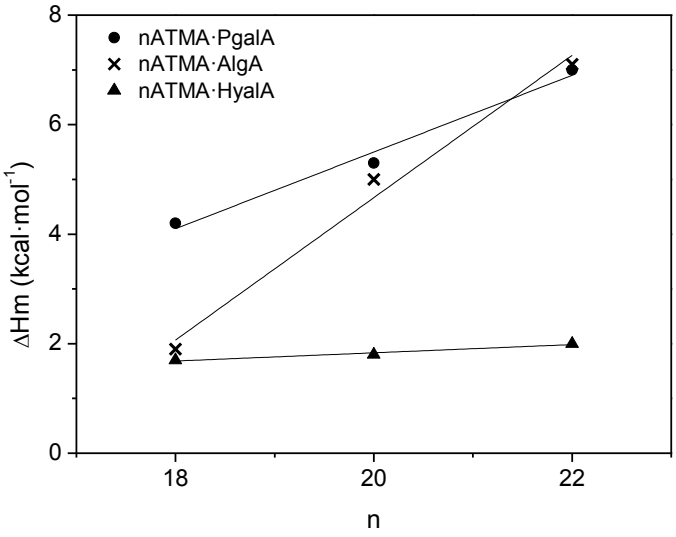

SI Figure 1. Melting enthalpy vs alkyl length of *n*ATMA complexes of polygalacturonic (PgalA), alginic (AlgA) and hyaluronic (HyalA) acids.

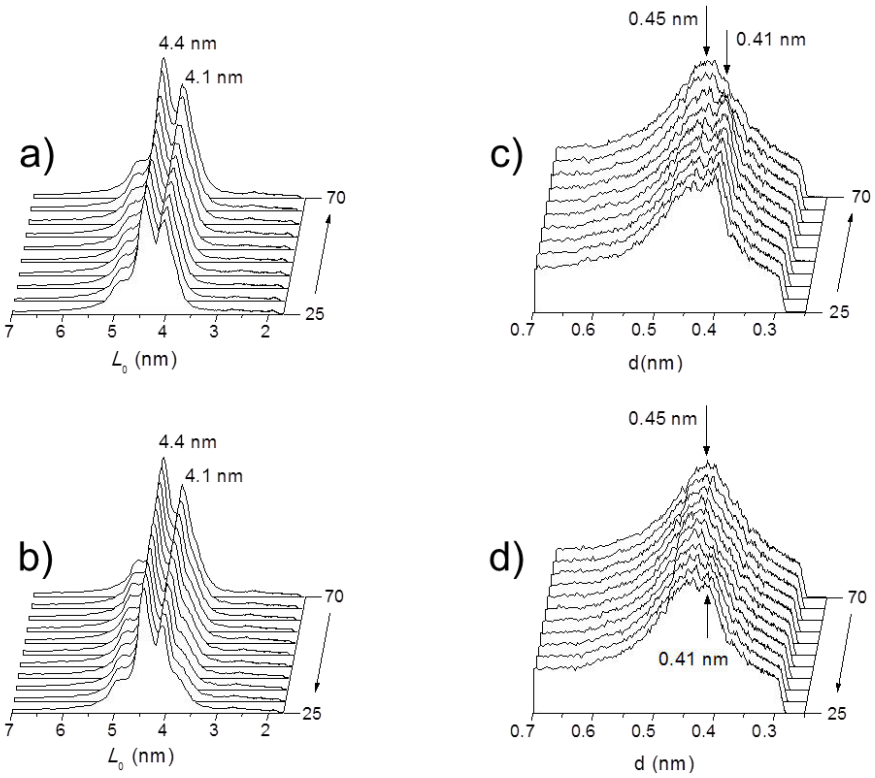

SI Figure 2. a) and b) Evolution of SAXS and WAXS profiles of 18ATMA·HyalA at heating from 25 ºC up to above melting .

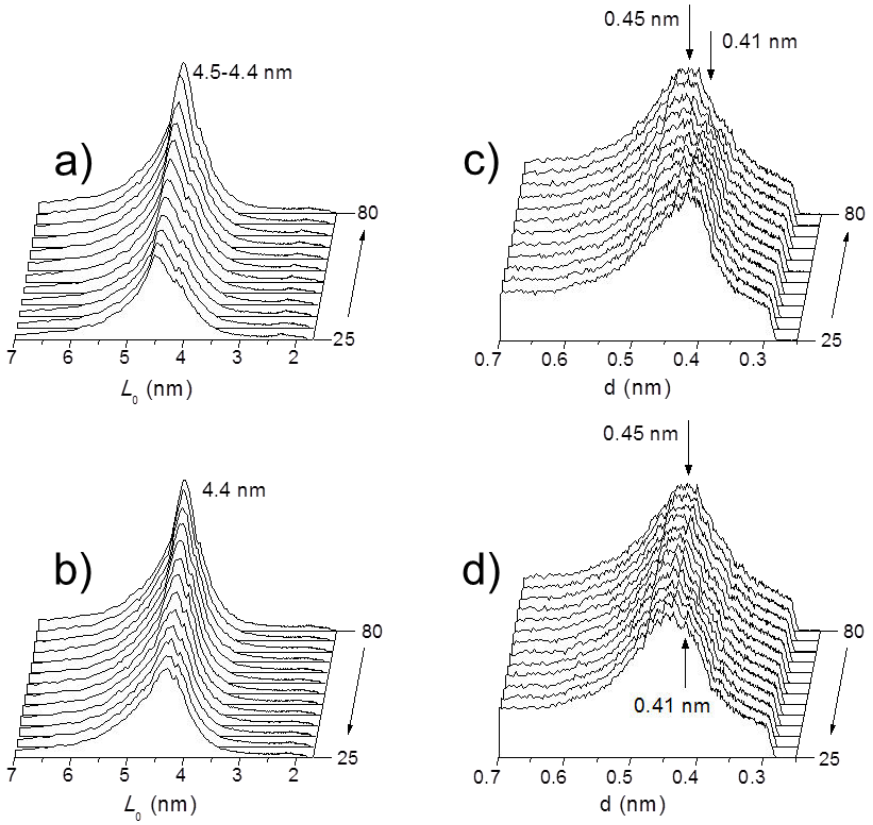

SI Figure 3. a) and b) Evolution of SAXS and WAXS profiles of 22ATMA·HyalA at heating from 25 ºC up to above melting .

Chapter III:
Ionic complexes of polyglutamic acid and alkanoylcholines

Surfactants or tensoactives are amphiphilic materials that contain a hydrophilic part, usually a polar head, and a hydrophobic part, generally a hydrocarbonated tail. The different nature of these parts allows the surfactant to form a variety of structures by self-assembling depending on factors such as the ratio and volume of either parts or concentration and temperature in the solvent.

Taking advantage of the structural behavior of surfactants, ionic complexes of polyelectrolyte-surfactant can display a new level of morphology. Tensoactives tend to form organized mesophases that able to crystallize; whereas polymers offer mechanical resistance and processability. This synergic combination leads to the formation of new materials that have drawn the attention.

Based on the self-assembly tendency of biopolymers, ionic complexes of bio-based polyelectrolytes, especially polypeptides, have been developed and studied in the last years. Poly(L-lisine) with dodecyl sulfate anions or poly(α,L-glutamate) and trimethylalkylammonium bromides are some of the first studied systems. Recently in our group, among other polypeptides, ionic complexes formed by coupling of poly(γ-glutamic acid) and alkyltrimethylammonium surfactants, i.e. *n*ATMA·PGGA, have been deeply studied and analyzed in terms of structure and thermal properties. Nevertheless, in spite of the potential applications of these ionic complexes as biomaterials, based on biological origin of PGGA and the well-defined lamellar structures formed, the lack of biocompatibility of the surfactants can be a problem for their use in biomedical applications.

Among the huge range of tensoactives, cationic surfactants, e.g. quaternary alkyl ammonium compounds, apart from various applications based on stability and structure, are often used as detergents due to their well-established anti-microbial effect. This activity against diverse microorganisms is produced because of the similarity to the cellular membranes. However, that affinity presents low selectivity and can affect the human membranes

representing a toxic effect. For this reason, the called biosurfactants have attracted the attention in the last years as an alternative to common detergents. These kinds of tensoactives display mimetic structures to those present in biomolecules of human body, and thereby the damage effect or toxicity is minimized. This is the case of alkanoylcholines, which are derivatives from phosphatidylcholines present in the lipid bilayer of cell membranes. Alkanoylcholines, named as ACh, are alkyl esters of choline analogous to previously mentioned alkylammmoniums, which introduce an ester bond between the ammonium moiety and the alkyl tail. This ester group is susceptible to hydrolysis by hydrolytic enzymes likebutirylcholineestearase, giving rise to biocompatible byproducts and eliminating the toxicity for humans. Moreover, alkanolylcholines have proven to offer a therapeutic activity in brain and cognitive diseases, as well as gastrointestinal illnesses.

Therefore, alkanolylcholines seem to be a good candidate to form ionic complexes by coupling with biopolymers such as PGGA. The assumable self-assembly trend of the system together with the biocompatibility of both compounds make the *n*ACh·PGGA ionic complexes a suitable biomaterial. Besides this, the diversity of morphologies provided by parameters such as the ratio or the length of counterionsallows to tailor the structure. Thus, playing around with those factors, arrangements from lamellar to spherical morphologies can be obtained depending on the functionality of the material.

In the present work, thermal properties, conformation and structures of alkanoylcholine, as well as their ionic complexes with PGGA, *n*ACh·PGGA have been analyzed. In addition, the application of these complexes as potential biomaterials and drug delivery systems has also been studied.

1. Thermal behavior of long-chain alkanoylcholine soaps

Summary: Long-chain alkanoylcholines prepared from fatty acids (*n*ACh) are fully sustainable cationic surfactants that are known for their biological and medicinal properties. In the present work the thermal behavior of the homologous series of alkanoylcholine iodides with *n* =12, 14, 16 and 18, has been examined along the 25-200 ºC range of temperatures. Up to three thermotropic phases have been identified, and the thermal transitions implied in their interconversion have been characterized by DSC and simultaneous WAXS and SAXS analysis carried out in real-time. The all three phases consist of a bilayered structure with alkanoyl chains confined in the space between the head group layers and interdigitated in a more or less extent. Melting-crystallization of either the polymethylene segments or the choline iodide groups is involved in such transitions. Additionally, a crystal phase consisting also of a bilayered structure but excluding side chain interdigitation was observed upon crystallization from solution and its structure was elucidated by single-crystal X-ray diffraction direct methods. The close correlation existing between thermal properties, phase structure and *n* has been brought into evidence.

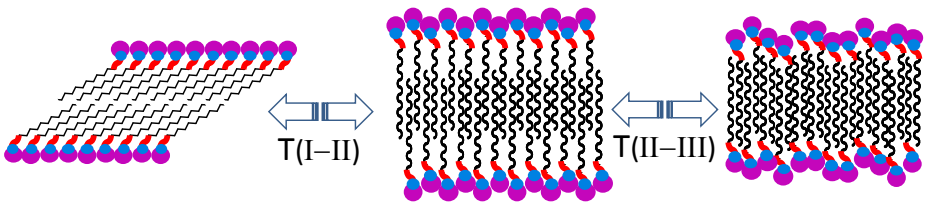

Publication derived from this work:

Tolentino, A.; Alla, A.; Martínez de Ilarduya, A.; Font-Bardía, M.; León, S.; Muñoz-Guerra, S. Thermal behavior of long-chain alkanoylcholine soaps. *RSC Adv.* **2014**, *4*, 10738-10750.

1.1. Introduction

Choline derivatives are extensively investigated due to multiple reasons. Choline itself, (2-hydroxyethyl)trimethyl ammonium salt, is a naturally occurring compound of extreme biological relevance as precursor of neurotransmissors and membrane constituents.[1,2] Choline is biocompatible and able to biodegrade both in living organisms[3] and in the environment,[4] a faculty that makes their derivatives very promising candidates for the preparation of sustainable eco-friendly materials. Such behavior has in fact incentivized the use of choline as additive for eutectic solvents[5] or as counter-ion in ionic liquids, to which it is able to bring down their melting points.[6] On the other hand, choline based ionic surfactants are distinguished by displaying low Krafft temperatures.[7,8] Recent works have shown that it is possible to have green surfactants with good water solubility from long-chain alkanoates by using choline as counterion.[9]

The work reported in this paper is related to the use of choline in the design of surfactants derived from fatty acids. The thermotropic behavior of alkanoate soaps has been studied in detail for long time.[10] It is well known that metallic salts of alkanoates display a complex behavior characterized by the occurrence of several thermal transitions involving crystalline, semicrystalline and liquid-crystalline phases.[11,12] The temperature, nature and number of transitions taking place in these systems are critically dependent on both the length of the alkyl chain and the size of the counter cation.[13] Cholinium alkanoate soaps are in line with the trend observed for metallic alkanoates according to the high voluminosity of the cholinium cation, *i.e.* they adopt a relatively low number of mesophases, and their melting transitions occur at so low temperature that they may be catalogued as ionic liquids.[9] The lyotropic behavior of these systems has been also examined in deep for both short and long alkyl chains.[14]

Surfactants based on fatty acid choline esters are of more recent interest for their potential as suitable components of novel green materials. This class of compounds however has been known for quite some time and shown to display certain biological activity,[15,16] as well as highly appreciated medical properties.[17-21] Long-chain alkanoylcholines are cationic lipids due to the quaternary ammonium functionality in the head-group and they are provided with a high molecular flexibility because the easy rotation of the inserted ester linkage. Although all choline salts are classified as health dangerous compounds just because they are quaternary ammonium ions, a recent toxicity and biodegradability study of choline carboxylate surfactants has proved the innocuity of these products.[22] Alkanoylcholines have in addition the

property of being hydrolyzed rapidly by the action of mammalian enzymes to produce fatty acids and choline, both compounds being common human metabolites. This property makes them potentially valuable to replace traditional tetraalkylammonium compounds in personal care products.[23] To our best knowledge, no study addressed to examine the thermotropic properties of alkanoylcholines has been reported to date. Notwithstanding, the Hofmeister anion effect on alkanoylcholines in the hydrated state has been evaluated as a function of the counter anion for their interest as bioactive surfactants.[24] Although this study was mainly centered in the gel behavior of the whole alkanoylcholine series, the crystal structure of hydrated stearoylcholine iodide was solved. It was reported to consist of a bilayered arrangement with alkanoyl chains aligned and interdigitated in a paraffinic phase that separates the polar layers integrated by the cholinium iodide head groups.

In this paper we study the thermal behavior of the homologous series of alkanoylcholine iodides (*n*ACh·I) derived from lauric, myristic, palmitic and stearic acids (*n* = 12, 14, 16 and 18, respectively), which are represented in Scheme I. The study examines the thermal transitions occurring in these compounds along the 20-200 ºC range both at heating and cooling. The diverse phases appearing or disappearing by effect of temperature are characterized by DSC, real-time XRD, solid-sate ^{13}C CP/MAS NMR and optical microscopy.

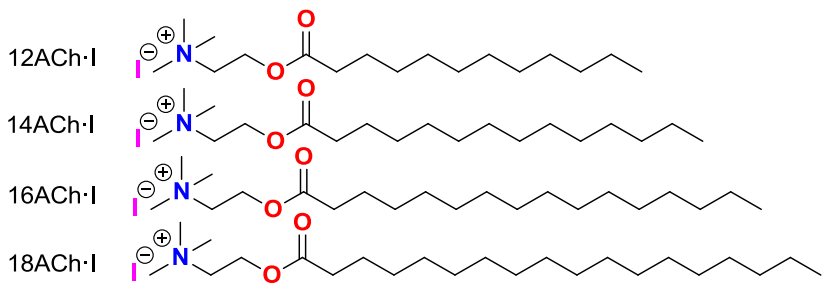

Scheme I. Chemical structure of the alkanoylcholine iodides *n*ACh·I studied in this work (*n* = 12, 14, 16 and 18).

It is worthy to mention that a good number of studies dealing with the thermal-structural behavior of a wide diversity of cationic surfactants, both in solution and in the pure state, are found in the literature. The occurrence of mesophases of smetic type is a very common feature of all these systems.[11] Among them, the ones closest to ours are those dealing with

tetralkylammonium halides bearing long alkyl groups. In these studies a transition taking place in the 70-130 ºC temperature range and leading to a layered semicrystalline structure with the alkyl chains in the molten state was described. The thermal instability of such compounds hampered the detailed study of high-temperature phases.[25] Attachment of longer alkyl or hydroxyalkyl groups to the nitrogen allowed to observing broad and stable smectic phases.[26]

The alkanoylcholine iodides series object of the present study has been recently used for ionic coupling with microbial poly(γ-glutamic acid) in order to obtain amphiphilic polymeric complexes (Chapter III.2).[27] These bio-based comb-like polymers are well stable and readily able to self-assemble in supramolecular structures with features similar to the lamellar arrangement described for cationic surfactants bearing long alkyl tails. The thermal transitions taking place in these complexes were found to involve semicrystalline phases and liquid-crystal phases while the thermotropic stuctural behavior of alkanoylcholines has not been examined so far. In addition to contributing to the basic knowledge on choline-based surfactants, the present work was undertaken with the aim of providing the information about alkanoylcholines necessary to evaluate their influence on the structural properties of the complexes that they generate upon coupling to anionic polyelectrolytes.

1.2. Experimental part

1.2.1. Materials

Lauroyl (98%), miristoyl (97%), palmitoyl (97%) and stearoyl (90%) chlorides, 2-(dimethylamino)ethanol (98%) and methyl iodide (99%) were supplied from Sigma-Aldrich and used as received. Chloroform, dichloromethane, pentane, hexane and acetone were supplied from Panreac and used without further purification.

1.2.2. Synthesis of alkanoylcholine iodides

The synthesis of the alkanoylcholine iodide surfactants (*n*ACh·I) was carried out from 2-(dimethylamino)ethanol, fatty acids of 12, 14, 16 and 18 carbon atoms, and methyl iodide through two concatenated reactions, esterification

and quaternization, without isolation of the intermediate aminoethyl ester. The procedure was the following: A solution of 0.06 mol of 2-(dimethylamino)ethanol (DMAE) in chloroform (50 mL) was added drop-wise to a solution (100 $g \cdot L^{-1}$) of 0.04 mol of the fatty acid chloride in the same solvent at a temperature between 0 and 20 ºC. After neutralization with aqueous $NaHCO_3$, the organic phase containing the 2-(dimethylamino)ethyl-alkanoate (DMAE-*n*A) was separated as oil. For quaternization, DMAE-*n*A was made to react with an excess of methyl iodide at room temperature. Upon standing overnight the resulting alkanoylcholine iodide (*n*ACh·I) was obtained as a white precipitate that was purified by reprecipitation from chloroform with acetone. Yields were around 90% except for $n = 12$, which was only 25% due to isolation/purification difficulties associated to the higher solubility displayed by this compound. The alkanoylcholine iodides were soluble in a variety of organic solvents such as chloroform, dichloromethane and methanol, and also in hot water. All they were obtained as white powders and their chemical constitution and purity were ascertained by NMR. A detailed account of the conditions used in the synthesis of each compound together with the NMR spectra of the whole series is provided in the SI subdivision.

1.2.3. NMR

^{1}H- and ^{13}C NMR spectra were registered at 300.1 and 75.5 MHz, respectively, on a Bruker AMX-300 NMR instrument equipped with a variable temperature unit. The samples were dissolved in chloroform and TMS was used as internal reference. 128 FIDs for ^{1}H NMR spectra were recorded with 2.3 μs (30º) pulse width, 3.4 s acquisition time, 20 s relaxation delay, and 4.9 KHz spectral width. For ^{13}C NMR spectra, 1000 to 10000 FIDs were recorded using pulse and spectral widths of 4.3 μs (90º) and 18 KHz, respectively. ^{13}C CP/MAS NMR spectra were recorded within the temperature range of 25 to 95 ºC. Samples were heated first at 190 ºC and then cooled to room temperature before spectral acquisition. Around 200-250 mg sample were spun at approximately 4 KHz in a cylindrical ceramic rotor. All the spectra were acquired with contact and repetition times of 2 ms and 5 s, respectively. Around 640 transients were accumulated. The spectral width was 31.2 KHz, and the number of data points was 4K. Chemical shifts were externally calibrated against the carbonyl peak of glycine appearing at 176 ppm relative to TMS.

1.2.4. Critical micelle concentration (cmc) and Krafft temperature determinations

The *cmc* of *n*ACh·I in D_2O was determined by ^1H NMR by following the evolution of the chemical shifts of specific signals of the surfactant with increasing concentration according to the procedure described in the literature.[28,29] Samples were dissolved in D_2O, and ^1H NMR spectra were recorded at the selected temperature using the sodium salt of the 3-(trimethylsilyl)-propanesulfonic acid as internal reference.

The Krafft temperatures (T_{Krafft}) were estimated both visually and conductimetrically. For visual estimation, 1% mixtures of *n*ACh·I in water were heated until dissolution and then cooled down to room temperature and kept in a refrigerator at 5 ºC for 24 hours. The cooled samples were then heated up in steps of 1 ºC every 15 min in a water bath provided with a magnetic stirring, and the temperature at which turbidity disappeared was taken as the T_{Krafft}. Conductimetry measurements were performed in a Mettler Toledo conductivity meter S30, provided with an Inlab720 sensor with a 0.06 cell constant. Dispersions were heated in a jacketed vessel with a heating rate of 0.5 ºC every 5 min and conductivity was measured. The T_{Krafft} was determined as the inflection point of the conductivity values versus temperature plot.

1.2.5. Thermal measurements

Decomposition temperatures (T_d) were measured using a Perkin-Elmer TGA6 thermobalance. Data were collected under a constant nitrogen flow at a heating rate of 10 ºC·min^{-1} within the 30 to 600 ºC temperature interval. Differential scanning calorimetry (DSC) measurements were performed on a Perkin-Elmer Pyris1 DSC instrument provided with an Intracooler device, and calibrated with indium and zinc. Sample weights of about 2-5 mg were examined within a temperature range of -30 to +200 ºC at heating and cooling rates of 10 ºC·min^{-1} under a nitrogen atmosphere. Several cycles were recorded for each compound and raw data were corrected in order to attain a flat baseline.

1.2.6. X-ray scattering

X-ray real time diffraction studies of powdered samples were carried out using X-ray synchrotron radiation in both WAXS and SAXS modes at the A2 beam-

line of light source DORIS III at DESY in Hamburg. Variable temperature experiments were performed at heating and cooling rates of 5 ºC·min^{-1}. The energy employed corresponded to a 0.15 nm wavelength, and spectra were calibrated with PET and rat tail tendon for WAXS and SAXS, respectively. X-ray diffraction patterns produced by using conventional light were recorded on the PANalytical X'Pert PRO MPD θ/θ diffractometer using the Cu-K_α radiation of wavelength 0.1542 nm.

1.2.7. Optical microscopy

Optical polarizing microscopy was performed on an Olympus BX51 Orthoplan microscope with an Olympus digital camera attached. A Linkham THMS-600 hot stage provided with a CS-196 nitrogen cooling system, and equipped with TMS90 temperature controller (± 0.5 ºC) was used for this study. Thin films of alkanoylcholines were prepared by casting and trapped between glass cover slides. Observations were carried out under a nitrogen atmosphere to avoid contact with air humidity, and at least two heating-cooling cycles were applied for each sample at a rate of 5 ºC·min^{-1}.

1.2.8. Stearoylcholine iodide (18ACh·I): single-crystal analysis

Crystallization of 18ACh·I addressed to grow crystals suitable for single-crystal X-ray diffraction analysis was performed by the vapor-diffusion technique. In brief, a solution of 0.5 mg of 18ACh·I in 0.5 mL of chloroform was placed in a capped 2 mL glass vial provided with a needle and the vial put inside a sealed glass flask containing 5 mL of hexane. The solution was then left undisturbed at 25 ºC for a few days until a fine crystalline precipitate was observed.

A prismatic crystal (aprox. 0.2 x 0.1 x 0.07 mm) was selected and mounted on a MAR345 diffractometer using graphite monochromatized Mo-Kα radiation (λ= 0.071073 nm) and provided with an image plate detector. Unit-cell parameters were determined from 1141 reflections located in the 3º < θ < 31º range, and refined by the least-squares method. Intensities of 6616 reflections in the range 1.33º ≤ θ ≤ 32.32º were collected and the structure was solved by direct methods and refined by using SHELXS computer programs. A fully detailed description of the methodology used for this analysis is provided in the Supplementary Information subdivision (SI) attached to this chapter.

1.3. Results and discussion

1.3.1. *cmc* and T_{Krafft} of *n*ACh·I

The changes taking place at 50 ºC in the 3.15-3.30 ppm region of the ^{1}H NMR spectra of 12ACh·I, which is the region in which the resonance of the methyl protons appears, as a function of concentration are depicted in Figure 1a, and the chemical shift of the methyl peak is plotted against the inverse of concentration in Figure 1b. This plot shows that the position of the methyl signal is independent of the amount of surfactant present in the solution until the *cmc* is reached, after which it moves upfield linearly with the inverse of concentration. It is interpreted that below *cmc* the observed resonance signal arises from free surfactant molecules whereas above *cmc* the signal is attributed to the equilibrium mixture of free and aggregated molecules distributed between the solution and the micelles, respectively. The *cmc* values determined by this method for the four *n*ACh·I studied in this work together with the values reported in the literature for the widely known alkyltrimethylammonium bromides (*n*ATMA·Br) are given in Table 1. Note that measuring *cmc* of *n*ACh·I in water required heating the samples above room temperature to reach the needed concentrations.

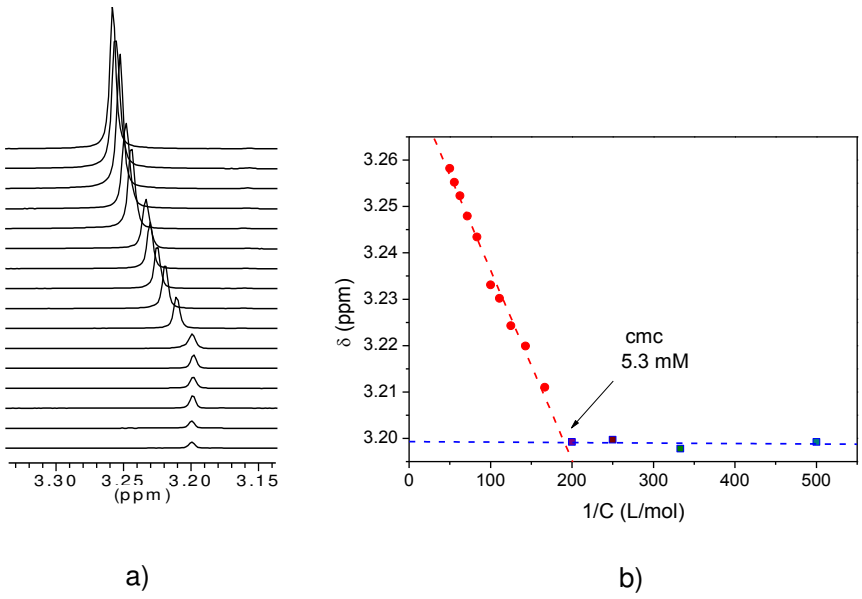

Figure 1. a) Evolution of the ^{1}H NMR methyl signal of 12ACh·I with concentration. b) Plot of the methyl chemical shift against concentration at 50 ºC with indication of the *cmc*.

Table 1. Values of *cmc* and Krafft temperatures of *n*ACh·I compared with *n*ATMA·Br.

	Critical micelle concentration (mM)				Krafft temperature (ºC)	
Surfactant	T (ºC)	cmc	solvent	method	visual	conductimetry
***n*ACh·I**						
12ACh·I	50	5.3	D_2O	NMR	38.5	37.9
12ACh·I	80	10.5	D_2O	NMR		
14ACh·I	60	1.9	D_2O	NMR	48.4	50.0
16ACh·I	80	1.0	D_2O	NMR	57.0	55.5
18ACh·I	95	1.2	D_2O	NMR	61.5	61.5
***n*ATMA·Br**						
12ATMA·Br	35	16.1[30]	D_2O	NMR	< 0[33]	<0[35]
14ATMA·Br	35	4.1[30]	D_2O	NMR	9.5-10.5[33]	13.2[36]
16ATMA·Br	25	0.9[31]	water	ultrasounds	26[34]	26[37]
18ATMA·Br	40	0.3[32]	water	conductimetry	35-36[33]	-

T_{Krafft} values determined by visual and conductimetric measurements are presented in Table 1. A satisfactory coincidence was found between the two methods. In all cases these temperatures are well above the room temperature and much higher than those reported for *n*ATMA·Br. As it could be anticipated the Krafft temperatures steadily increased with the number of methylenes of the alkyl chain.

1.3.2. Thermal decomposition

The TGA traces recorded from *n*ACh·I surfactants under an inert atmosphere are depicted in Figure 2, and the decomposition temperatures together with the weights remaining after heating at 600 ºC are listed in Table 2. Decomposition of *n*ACh·I was found to start around 200 ºC with onset temperatures increasing slightly with the length of the alkyl chain. TGA derivative curves (see SI) revealed that the decomposition process evolves trough a mechanism in two-steps that have their respective maximum temperature rates located within the 225-250 ºC and 320-325 ºC intervals. The sample weight loss after the first decomposition step increased steadily from 18% up to 56% with *n*, whereas no residue was left at the end of the heating treatment. Alkanoylcholines bearing long chains are less thermally stable than acetylcholine in about 30 ºC but compares well to the choline carboxylate soaps,[9] as well as to other cationic surfactants derived from alkylamines.[38]

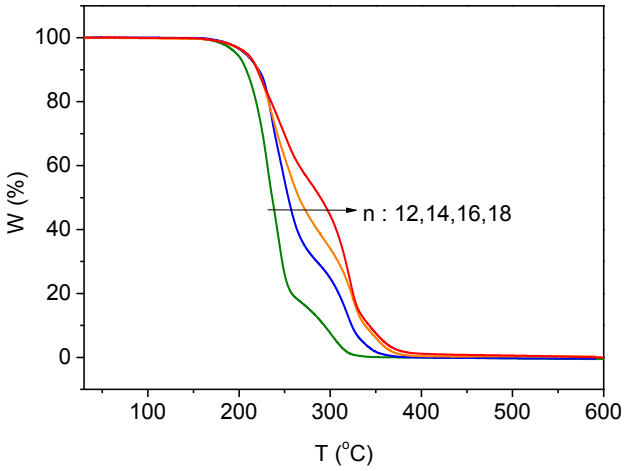

Figure 2. TGA traces of *n*ACh·I recorded under an inert atmosphere.

Table 2. Thermal properties of *n*ACh·I surfactants.

nACh·I	TGA[a]			DSC[b]					
				Transition temperatures (ºC) and Enthalpies in parenthesis (kJ·mol^{-1})					
				First Heating		Cooling		Second heating	
	$^{o}T_d$ (ºC)	$^{max}T_d$ (ºC)	W (%)	I_α/II	II/III	II/I_β	III/II	I_β/II	II/III
12ACh·I	197	231-243	18	83	169	41	165	52	168
		303	0	(25.9)	(14.2)	(-11.3)	(-13.8)	(10.9)	(13.8)
14ACh·I	207	236-247	30	93	164	47	161	59	162
		318	0	(33.4)	(14.6)	(-16.7)	(-13.0)	(15.5)	(13.8)
16ACh·I	209	233-254	37	99	163	59	160	70	161
		303	0	(41.4)	(14.6)	(-23.0)	(-13.8)	(22.1)	(14.2)
18ACh·I	209	225-247	56	104	161	70	157	80	160
		322	0	(50.2)	(15.0)	(-29.3)	(-14.6)	(24.7)	(14.6)
2ACh·I[c]	229	261	9	165		94		164	
		322	0	(32.6)		(-24.2)		(30.9)	

[a]Onset decomposition temperature at 5% weight lost ($^{o}T_d$), maximum rate decomposition temperature ($^{m}T_d$), and remaining weight (W) for each decomposition step.
[b]Transition temperatures and enthalpies recorded at the DSC run.
[c]Data for this compound refer to its meting/crystallization transition.

1.3.3. Differential scanning calorimetry

Since *n*ACh·I compounds start to decompose in the proximities of 200 ºC, the DSC study has been restricted to temperatures below this limit. An exploratory essay in which samples were heated up to 250 ºC did not show any sign of heat exchange in the 200-250 ºC range. DSC traces of successive heating-cooling cycles of *n*ACh·I along the 0-175 ºC range of temperatures are depicted in Figure 3, and temperatures and enthalpies recorded for the thermal transitions observed on first cycle traces are compared in Table 2. In the four cases, the first heating trace displays a group of two or three endothermic peaks within the 70-110 ºC interval, in addition to an isolate sharp peak located between 160 and 170 ºC. The multiple heat adsorption observed in the lower temperature range strongly suggests the presence of crystal polymorphs that could be simultaneously generated in the precipitation from solution step that is applied for purification in the synthesis stage. On the contrary, only two exothermic peaks are observed on the cooling traces of *n*ACh·I, which are respectively associated to the two endothermic peaks that are displayed on the second heating traces. These two exo/endo peak pairs are made to correspond to two reversible transitions taking place in *n*ACh·I along the examined temperature interval. Notice that the transition occurring in the low temperature region (below 110 ºC) implies a quite large supercooling (~40-50 ºC) and produces a material that shows at the second heating an endothermic peak at about 30 ºC lower than in the first heating. On the contrary, the high temperature transition is well reproduced in the second heating trace with both position and intensity of the endothermic peak essentially preserved at the initial values. Furthermore, this transition entails a very low supercooling indicating that a very effective nucleation must operate in the recovery of its lower temperature phase. These features strongly suggest that the low temperature exo/endo peaks must involve a crystal melting process whereas the heat exchange taking place at high temperature must arise from a transition implying two structurally close liquid-crystal phases. The DSC recorded from acetylcholine iodide (2ACh·I) (shown in the SI part) is of valuable help in this regard. The first heating trace of this compound consists of only one sharp endothermal peak at 165 ºC characteristic of melting that is well reproduced in the second heating trace; crystallization at cooling from the melt takes place at about 70 ºC supercooling. The melting peak observed for 2ACh·I is comparable in location to the high temperature transition endothermic peak observed for *n*ACh·I but it entails a much larger enthalpy and its recovery by cooling from the melt requires much larger supercooling. Such dissimilarities clearly indicate that the structural changes implied in each case must be different. Since no liquid-

crystal phase is conceivable for the relatively short 2ACh·I molecule, the endothermic peak observed for this compound doubtlessly arises from the melting of the crystal phase into an isotropic liquid phase. On the contrary, heating of *n*ACh·I in the proximities of 160-170 ºC would generate a partially ordered phase where the long amphiphilic molecules still maintain a considerable degree of side-by-side alignment.

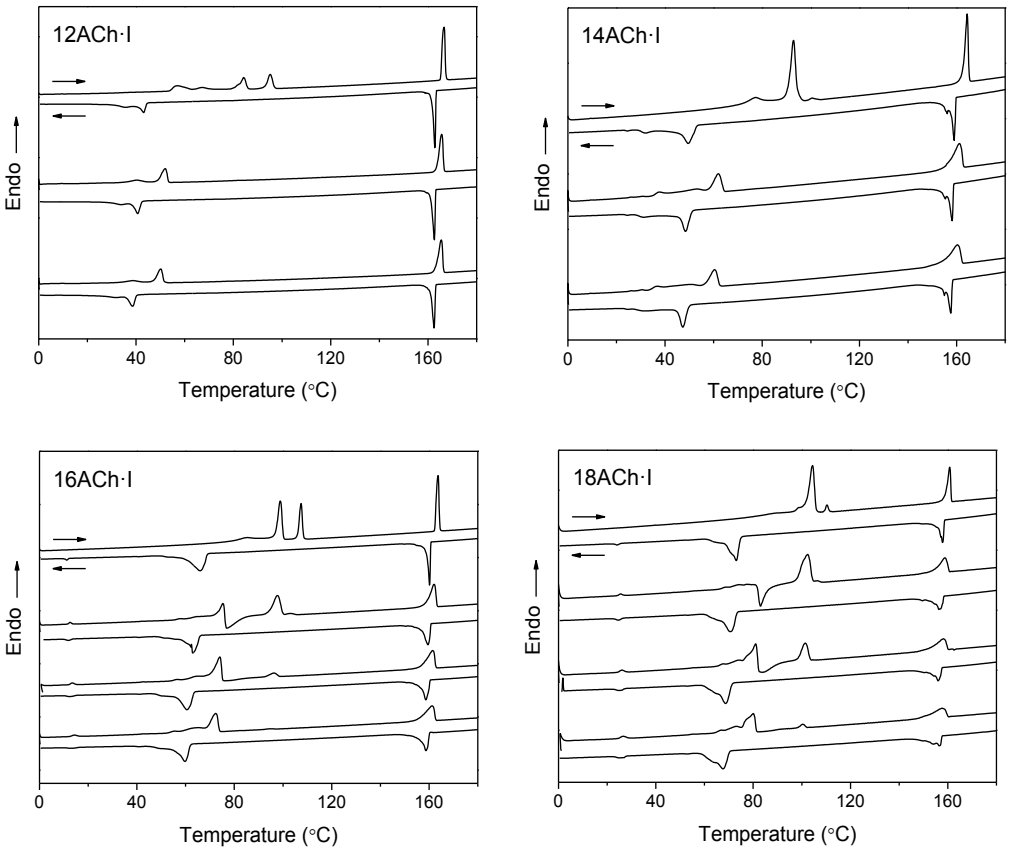

Figure 3. DSC traces of successive heating-cooling cycles (from top to bottom) of *n*ACh·I along the 0-175 ºC range of temperatures.

Coming back to the heat exchange taking place at temperatures below 120 ºC, it should be noticed that the behavior observed for both 18ACh·I and 16ACh·I at the second heating run was different from that displayed by their lower homologues. Both compounds underwent a complex heat exchange process that ended in a material showing an endothermic peak at a temperature similar to that observed for their respective pristine samples.

Such pattern is characteristic of a melting-recrystallization process involving a structural rearrangement from a less stable phase to a more stable one. This process however lost relevance with the number of applied heating-cooling cycles. In fact, the initial endothermic peak increased in intensity at the same time that the heat release decreased to fully disappear on the fourth heating trace. It should be stressed that this process was never observed neither for 14ACh·I·nor for 12ACh·I indicating their dependence on the alkyl chain length. The differences between higher (n = 18 and 16) and lower (n = 14 and 12) nACh·I compounds remained for samples that had been previously heated at temperatures below the temperature at which the second transition takes place (160-170 ºC). Furthermore, it was also found that the reverse behavior of 18ACh·I was dependent on the length of time that the sample was maintained under heating. DSC traces demonstrative of this behavior are provided in the ESI document.

At the light of DSC observations and disregarding at this moment the possible polymorphs present in the samples crystallized from solution, four phases may be identified for nACh·I: Two phases (Ph-Iα and Ph-Iβ with existence at low temperatures, one phase occurring at high temperatures (Ph-III), and one phase with a existence domain in the intermediate temperature region (Ph-II). Ph-Iα is assumed to be a well stable phase formed in the crystallization from solution whereas Ph-Iβ is a metastable phase that is generated by cooling the previously heated samples. Upon standing at room temperature for hours or by annealing, Ph-Iβ is converted in Ph-Iα. The interrelations among these phases are depicted in Scheme II and their structural details are discussed below.

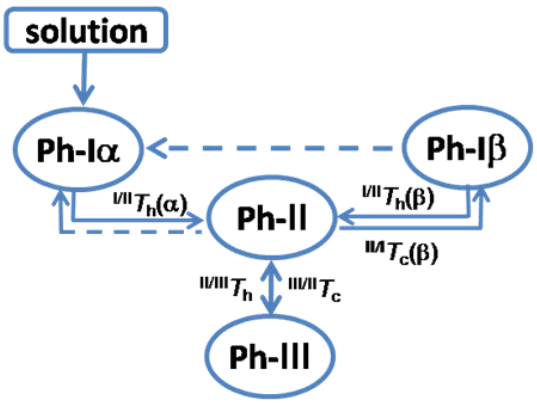

Scheme II. Interrelation between the nACh·I phases.

1.3.4. Thermal transitions

Several reversible thermal transitions have been characterized for nACh·I by DSC along the 0-200 ºC interval of temperatures. $^{I/II}T_h(\alpha)$ (measured at the first heating) and $^{I/II}T_h(\beta)$ (measured at the second heating) are the temperatures at which Ph-Iα and Ph-Iβ, respectively, are converted into Ph-II, and $^{II/III}T_h$ is the temperature of conversion of Ph-II into Ph-III. $^{II/I}T_c(\alpha)$ and $^{III/II}T_c$ are the temperatures measured on cooling for the Ph-II to Ph-Iβ and Ph-III to Ph-II transitions, respectively. The plot of transition temperatures against *n* is shown in Figure 4a revealing that a linear trend is followed for all nACh·I although noteworthy differences are observed among them. a) Transitions involving Ph-I and Ph-II take place at temperatures increasing with a similar slope but showing noticeable higher values for $^{I/II}T_h(\alpha)$. b) The supercooling ($^{I/II}T_h(\beta)$ - $^{II/I}T_c(\beta)$ associated to the lower temperature transition is noticeable (around 20 ºC) and essentially constant along the series. c) Both melting and crystallization involving Ph-II and Ph-III occur at temperatures slightly decreasing with n but that are practically coincident along the whole series. The supercooling required for reversing this transition is practically negligible.

The enthalpy and entropy values involved in the transitions are plotted against *n* in Figures 4b and 4c, respectively. The values associated to the low temperature transitions increase linearly with *n* as it should be expected provided that the alkanoyl chain is taking active part in the molecular rearrangement. Moreover the enthalpy associated to the conversion of Ph-Iα into Ph-II (first heating) takes values between 15 and 20 KJ·mol^{-1} higher than for Ph-Iβ, and its variation with *n* follows a slope of near 25% greater. This is a clear indication of that not only crystallinity of Ph-Iα is higher than of Ph-Iβ but also that the individual methylene contribution to the stability of Ph-I is greater in this phase, as it should be expected for a more efficiently packed crystal phase. With regards to the transition taking place at high temperature, both enthalpy and entropy appear to be practically independent of *n.* This result is fully consistent with the invariability found in both $^{II/III}T_h$ and $^{III/II}T_c$ along the series, and strongly suggests that the alkanoyl chain must not participate actively in the molecular rearrangement involved in this transition.

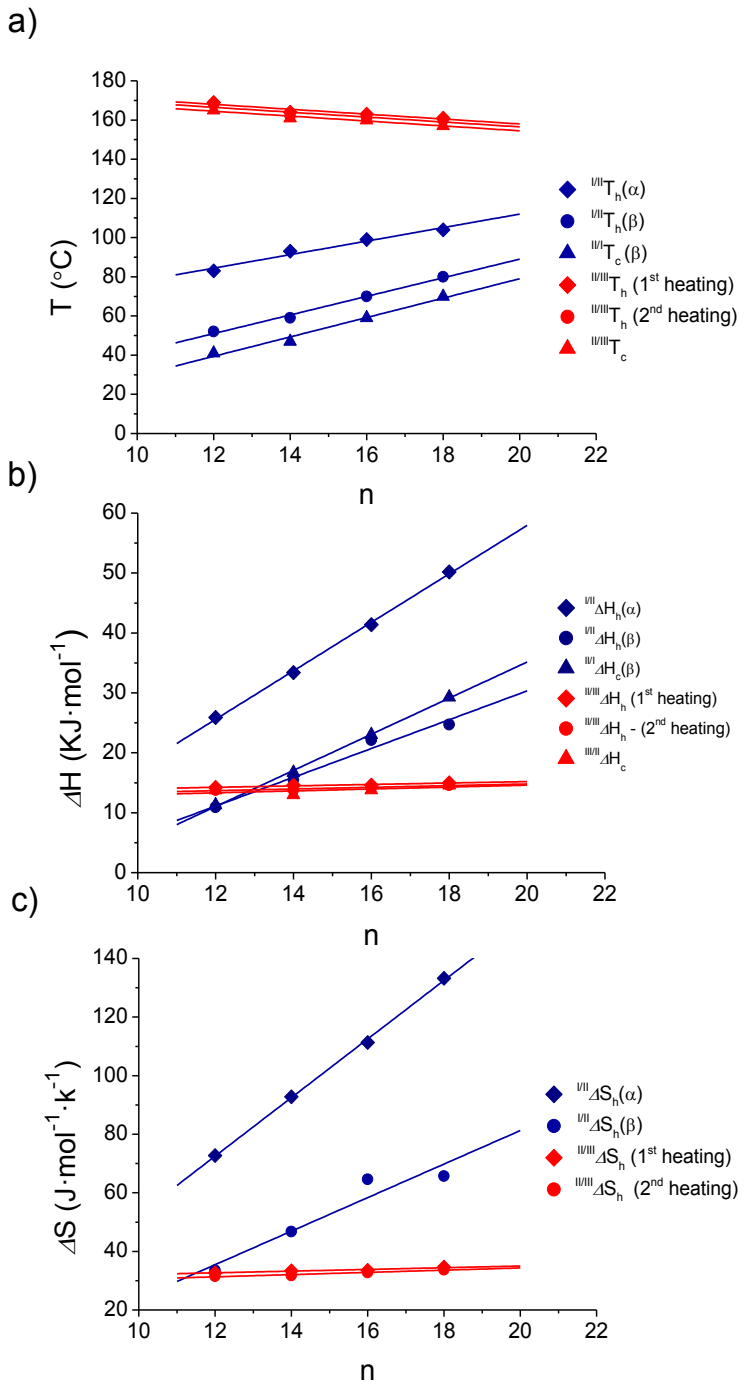

Figure 4. Phase transition temperatures a), enthalpies b), and entropies c) of *n*ACh·I compounds as a function of *n*. In b) the negative crystallization enthalpies are represented in positive values for a closer comparison with the melting enthalpies.

1.3.5. 18ACh·I: A single crystal study

*n*ACh·I were found to yield well shaped microcrystals upon casting from chloroform indicating that the phase Ph-Iα obtained by precipitation from this solvent at room temperature is highly crystalline. Illustrative pictures of the microcrystals made of 18ACh·I are included in the SI part. With the aim at elucidating in detail the structure present in this phase, a single crystal suitable for X-ray diffraction analysis (0.2 x 0.1 x 0.07 mm size and exempt of significant imperfections such as cracks or twinning) was grown using the vapor-diffusion method in absence of humidity. A picture of the crystal used for the analysis along with a full account of the crystallographic data collected and handled in this study is given in the SI section. The structure could be resolved with an *R* factor of 0.052. It was found that 18ACh·I crystallized in a triclinic lattice with space group *P*1 and unit cell dimensions *a* = 0.576 nm, *b* = 0.767 nm, *c* = 3.09 nm, α = 83.1º, β = 87.0º, γ = 89.3º, containing two molecules related by an inversion center. A representation of a portion of the crystal lattice including ten unit cells as viewed along the *b*-axis is depicted in Figure 5. In this crystal the stearoylcholine molecules are arranged in a bilayered structure with the polar trimethylammonium iodide head groups arranged along the *C*-plane and the ethyloxystearoyl tails protruding from this plane and following a bended trajectory caused by the kink introduced by the carboxylate unit. As a result the alkyl tails become tilted about 45º respect to the *c-axis* to fix an interlayer distance of ~3.1 nm without appreciable interdigitation. An ORTEP representation of the 18ACh·I molecule in the conformation adopted in the crystal together with a complete account of their atomic coordinates, bond distances and torsion angles are included in the SI part.

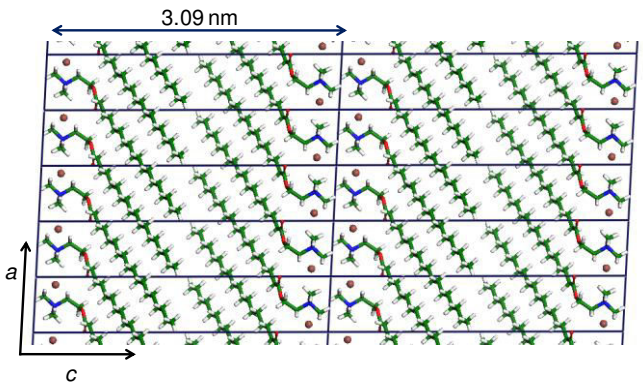

Figure 5. View of the 18ACh·I crystal (Ph Iα) projected along the *b*-axis. Ten unit cells are visualized.

Tarafdar et al.[24] have recently reported on the crystal structure of 18ACh·I. The structure found by these authors is also triclinic $P\bar{1}$ with unit cell dimensions a = 0.799 nm, b = 0.963 nm, c = 3. 5413 nm, α =86.40º, β = 84.79º, γ = 89.96° and contains 4 molecules. In this structure the alkyl chains are aligned practically parallel to the *c*-axis (tilt angle = 1.7 º) and they are deeply interdigitated. Obviously these authors are dealing with a crystal form of 18ACh·I different from that described above by us. It was noticed that one water molecule every two surfactant molecules was inserted in the crystal lattice described by these authors, which is consistent with the solvent they used for crystal growth (a mixture of chloroform, methanol and water). The presence of water in 18ACh·I could be reasonably invoked to explain the different lattice dimensions found in each case and the consequent difference in the arrangement adopted by the alkyl chains to fill the interlayer space in the two crystal forms. The critical dependence of the structural behavior of choline-based lipid bilayers on hydration has been accounted in the study of hydrated dihexadecyl phosphatidylcholine in a range of 5-70 wt% of water.[39-41] It was found there that the structure of this compound rearranged from a two-separated sheets bilayer to a deeply interdigitated bilayer as the content in water increased. Different factors including hydrogen bonding were claimed to be responsible for the described water-mediated transition. The amount of water involved in this study is much larger than that adsorbed in the 18ACh·I crystal described by Tarafdar et al.[24]. However the aqueous environment used by these authors for crystallization could favor initially a hydrated gel interdigitated structure that is retained after most of water is released to form the crystal.

1.3.6. Ph-Iα phase

The WAXS and SAXS profiles recorded from Ph-Iα of *n*ACh·I are compared in Figure 6 for the whole series, and the most characteristic spacings measured on such patterns are listed in Table 3. The samples subjected to this analysis were those coming from synthesis, *i.e.* generated by precipitation from chloroform by adding acetone, after being subjected to annealing in order to improve crystallinity; according to their melting temperatures they consist of Ph-Iα. The presence of a layered structure in these samples is ascertained by the strong reflection appearing in the SAXS region (Figure 6) at a spacing moving from 2.5 nm to 3.1 nm as the alkanoyl chain carbon number increases from 12 to 18. In the WAXS region, all the *n*ACh·I displayed similar patterns consisting of a fair number of sharp peaks concentrated in the 0.50-0.30 nm interval with the strongest one corresponding to the 0.455 nm

spacing. Most of the other peaks appearing at lower spacings can be grouped in three groups centered around 0.40, 0.36 and 0.30 nm. The similitude of the groups for the whole *n*ACh·I series is remarkable with main discrepancies concerning the reflections with $l \neq 0$ as it should be expected from differences in the alkanoyl chain length.

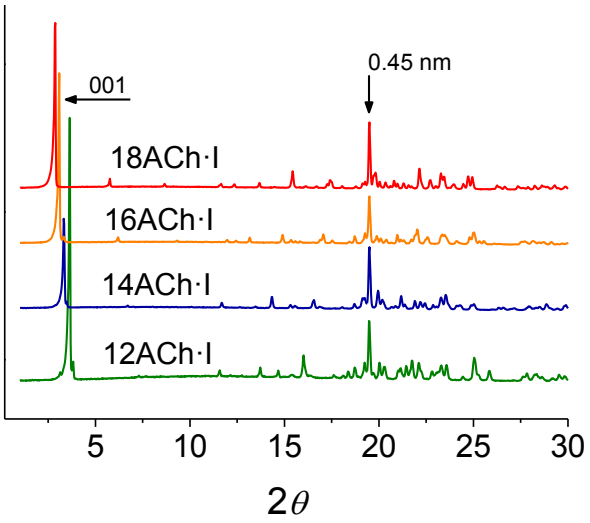

Figure 6. X-ray diffraction profiles of Ph-Iα phase of *n*ACh·I. The peak arising from the intesheet spacing (001) of the layered structure is displayed in the SAXS region ($2\theta < 5º$).The WAXS scattering ($2\theta > 15º$) contains the ~0.45 nm peak characteristic of this phase.

When the XRD pattern experimentally recorded from 18ACh·I powder was compared with the XRD pattern simulated for the crystal structure shown in Figure 5, an extremely close coincidence was found in both SAXS and WAXS regions (see SI), which confirmed that the structure determined for the monocrystal is that present in Ph-Iα. Furthermore, given the similar scattering displayed by the Ph-Iα phase in all the nACh·I, it can be reasonably assumed that same structure is shared by the whole series. Taking as reference the 18ACh·I crystal structure, similar lattices were built for the other members of the series (see SI part). The same crystallographic parameters but with the c-axis shortened according to the observed 001 spacing length were used for building, and the same molecular arrangement was maintained in all the cases.

Table 3. Temperature domains and XRD data for the *n*ACh·I phases.

n	Ph-Iα			Ph-Iβ			Ph-II			Ph-III		
	T (ºC)	SAXS (nm)	WAXS (nm)	T (ºC)	SAXS (nm)	WAXS (nm)	T (ºC)	SAXS (nm)	WAXS (nm)	T (ºC)	SAXS (nm)	WAXS (nm)
12	<83	2.5	0.30 0.36 **0.45**	<52	3.3	0.32 0.35 **0.40** 0.55	52-169	3.5	0.30 0.36 **0.40** 0.55	>169	3.1	-
14	<93	2.7	0.30 0.37 **0.45**	<59	3.6	0.32 0.35 **0.40** 0.55	59-162	3.8	0.30 0.36 **0.40** 0.55	>162	3.3	-
16	<99	2.9	0.30 0.37 **0.45**	<70	4.0	0.32 0.35 **0.40** 0.55	70-161	4.2	0.30 0.36 **0.40** 0.55	>161	3.7	-
18	<104	3.1	0.30 0.37 **0.45**	<103	4.2	0.32 0.35 **0.40** 0.55	103-160	4.5	0.30 0.36 **0.40** 0.55	>160	3.9	-

The strongest observed reflection in bold.

1.3.7. Ph-Iβ, Ph-II and Ph-III phases

Heating of Ph-Iα of *n*ACh·I at temperatures between 80 and 105 ºC led to Ph-II, and further heating of Ph-II above 160-170 ºC led to Ph-III. The exact temperatures at which the phase transitions take place for each surfactant are listed in Table 2. The structural modifications involved in these transitions were followed by X-ray diffraction in real time using synchrotron radiation with simultaneous recording of the scattering changes occurring in the small and wide angle regions. A list of the spacings observed for the whole series in the two regions with precise indication of the temperatures at which they appear is given in Table 3. For illustration the sets of SAXS plots registered from 16ACh·I at heating, cooling and reheating are depicted in Figure 7, and the whole collection of plots recorded from the other members of the series including also those obtained from 2ACh·I are provided in the SI part.

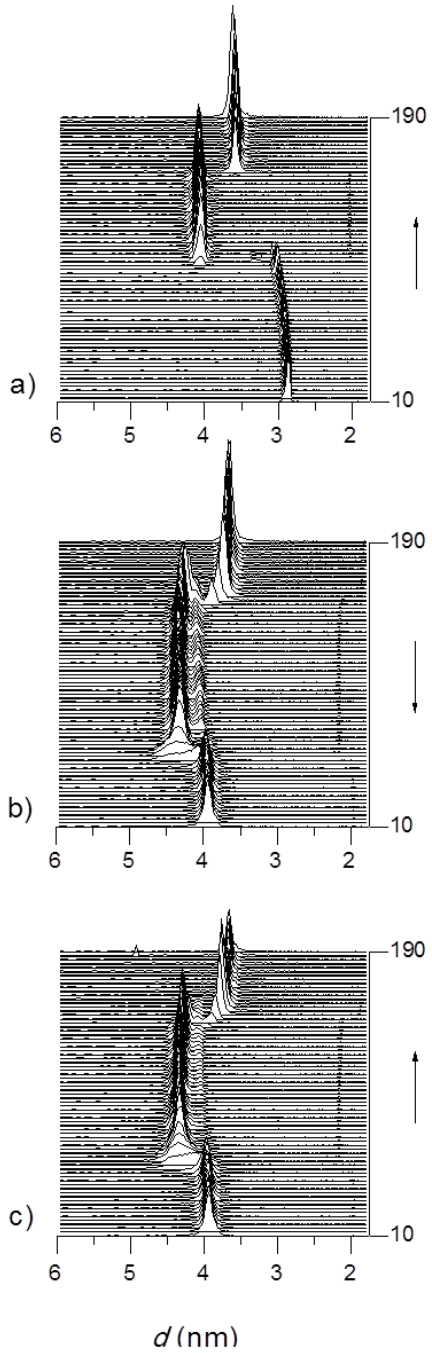

Figure 7. SAXS plots from 16ACh·I registered at heating from room temperature a), cooling b) and reheating c).

At first glance the two thermal transitions defining the existence domains of Ph-I, Ph-II and Ph-III phases are clearly denoted in the SAXS plots by jumps in the positions of their respective characteristic peaks. It is remarkable that whereas Ph-II and Ph-III are faithfully reproduced in second heating plots after cooling, the low-temperature peak (initially Ph-Iα) reappears in the second heating largely displaced towards higher spacings. Furthermore, the three peaks initially observed for 12ACh·I merged into one after cooling from the melt. These results are in concordance with the occurrence of two phases (Ph-Iα and Ph-Iβ) at low temperature, and prove the relative instability of Ph-Iβ respect to Ph-Iα. According to antecedents on other alkylammonium surfactants containing long alkyl chains, the long-spacings observed for *n*ACh·I should be associated to the interlayer distance *L* characteristic of the lamellar structure present in the crystal, semicrystalline or liquid crystalline phases eventually present in these systems.[25] In fact, no discrete SAXS at all was observed for 2ACh·I as it should be expected from the small acetyl group. The *L* values for the four phases that have been identified for *n*ACh·I are plotted against *n* in Figure 8. Remarkable features of this plot are the following: a) A linear trend is obtained for all the phases and extrapolation to *n*= 0 yields a similar value in the four cases. b) The straight lines resulting for Ph-Iβ, Ph-II and Ph-III are close to each other and have a very similar slope. On the contrary, much lower values of *L* are found for Ph-Iα and its increment with *n* occurs at a significant lower ratio.

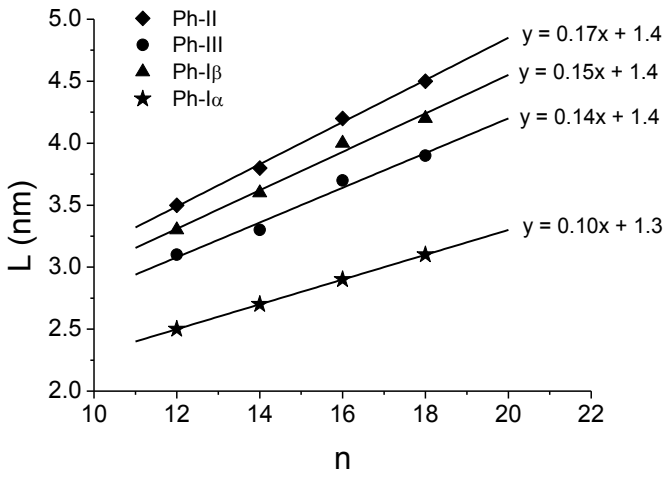

Figure 8. Lamellar interlayer spacing *L* of *n*ACh·I as a function of the number of carbon atoms in the alkanoyl chain.

A preliminary analysis of the SAXS data taking into account conformational considerations and assuming some approximations regarding molecular volumes allows outlining a first picture of the molecular arrangement present in each phase. First, the difference between the lamellar thickness and the *L*-intercept yields an estimation of the thickness (L_0) of the alkanoyl core in the structure; a comparison of this value with the length of the alkanoyl tail calculated for an *all-trans* conformation (*l*) gives indication of the extent of shortening undergone by the structure in terms of chain tilting, degree of interpenetration or *gauche* conformation present in each phase. The results of these calculations are compared in Table 4. The low (L-L_0)/*l* ratio (0.8) found for Ph-Iα is consistent with the tilting of the alkanoyl chains and in fully agreement with the crystal model resulting from the structural analysis of the monocrystal. The (L-L_0)/*l* ratio estimated for Ph-Iβ is between 1.25 and 1.30, which is noticeably higher than for Ph-Iα. Assuming that Ph-Iβ appears as a consequence of the normal orientation respect to the layer plane adopted by the alkanoyl chains upon heating while preserving their fully-extended conformation, the calculated (L-L_0)/*l* ratio for this phase is consistent with an interdigitated chain arrangement with around 75% of interpenetration. In Ph-II, the (L-L_0)/*l* ratio is essentially constant along the whole series with a value close to 1.4 according to an interpenetration of 60% provided that both orientation and conformation of the alkanoyl tail are the same as in Ph-Iβ. Regarding Ph-III, the (L-L_0)/*l* ratio takes values (~1.1) significantly lower than in Ph-II, and even lower than in Ph-Iβ, which reveals a maximum degree of interdigitation for this phase.

Table 4. Interlayer distance *(L*), choline iodide head size (L_0) and shrinkage ratio (L-L_0)/*l* in the *n*ACh·I phases.

n [a]	*l* [b]	Ph-Iα			Ph-Iβ			Ph-II			Ph-III		
		L	L_0	(L-L_0)/*l*	*L*	L_0	(L-L_0)/*l*	*L*	L_0	(L-L_0)/*l*	*L*	L_0	(L-L_0)/*l*
12	1.5	2.5	1.3	0.80	3.3	1.4	1.27	3.5	1.4	1.40	3.1	1.4	1.13
14	1.75	2.7	1.3	0.80	3.6	1.4	1.26	3.8	1.4	1.37	3.3	1.4	1.09
16	2.0	2.9	1.3	0.80	4.0	1.4	1.30	4.2	1.4	1.40	3.7	1.4	1.15
18	2.25	3.1	1.3	0.80	4.2	1.4	1.25	4.5	1.4	1.38	3.9	1.4	1.11

[a] Number of atoms in the alkanoyl tail.
[b] Length of the alkanoyl tail in *all-trans* conformation assuming a C-C bond length of 0.125 nm.

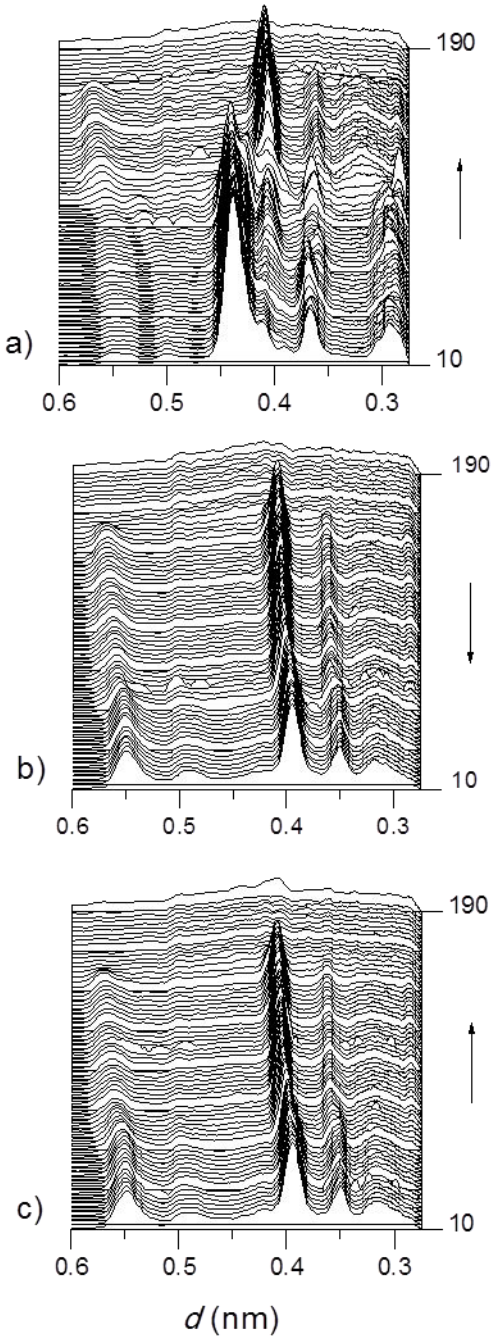

Figure 9. WAXS plots from 16ACh·I registered at heating from room temperature a), cooling b) and reheating c).

The real-time WAXS analysis of *n*ACh·I afforded invaluable information on the short distance rearrangements, *i.e.* those involving the head groups and alkanoyl tails side-by-side packing, that take place by effect of temperature. The three sets of WAXS profiles registered from 16ACh·I at heating, cooling and reheating are depicted in Figure 9 for illustration, and those recorded from the other members of the series including also those obtained from 2ACh·I, are provided in the SI section. The spacings of the characteristic peaks of the different phases occurring for *n*ACh·I are listed in Table 3. Inspection of Figure 9 brings to light the following relevant points: a) The initial profiles registered along the first heating run show the peaks characteristic of Ph-Iα in particular the prominent one at 0.45 nm. b) When temperature overpasses 100 ºC, the profiles become simpler and consist of one main peak located near to 0.40 nm accompanied by two other much weaker peaks at 0.36 and 0.30 nm; this is the pattern characteristic of Ph-II. c) At temperatures above 165 ºC, the scattering losses any vestige of discrete diffraction indicating that Ph-III is fully devoid of crystalline order. Crystallization from Ph-III invariably happens at cooling below 160 ºC with recovery of the WAXS pattern characteristic of Ph-II, which remains essentially unaltered along the whole cooling run finishing at 10 ºC. In fact, no appreciable differences between the WAXS patterns of Ph-II and Ph-Iβ were noticed indicating therefore that the arrangement in the crystalline part of the structure must be the same in the two phases. It seems that differences between Ph-Iβ and Ph-II exclusively concern the periodical repeat of the layered array; according to calculations, it must be the consequence of the different interdigitation degree attained by the alkanoyl tails in each one of these phases.

1.3.8. NMR study of Ph-Iα and Ph-II phases

Additional information of valuable help for the elucidation of the structural changes taking place in *n*ACh·I upon heating was afforded by solid-state ^{13}C CP-MAS NMR. Unfortunately the study of the high temperature interconversion of Ph-II and Ph-III was unfeasible due to limitations in the temperature level attainable by our equipment. The difficulty in the availability of the metastable Ph-Iβ phase in the amounts required for the analysis is an additional shortcoming of this study.

The transition involving Ph-Iα and Ph-II was examined for the whole *n*ACh·I series. Best results were obtained for 12ACh·I because the $^{I/II}T_h$ (α) of this surfactant is well below the maximum temperature allowed by the NMR probe head. All samples subjected to study were initially in Ph-Iα as ascertained by

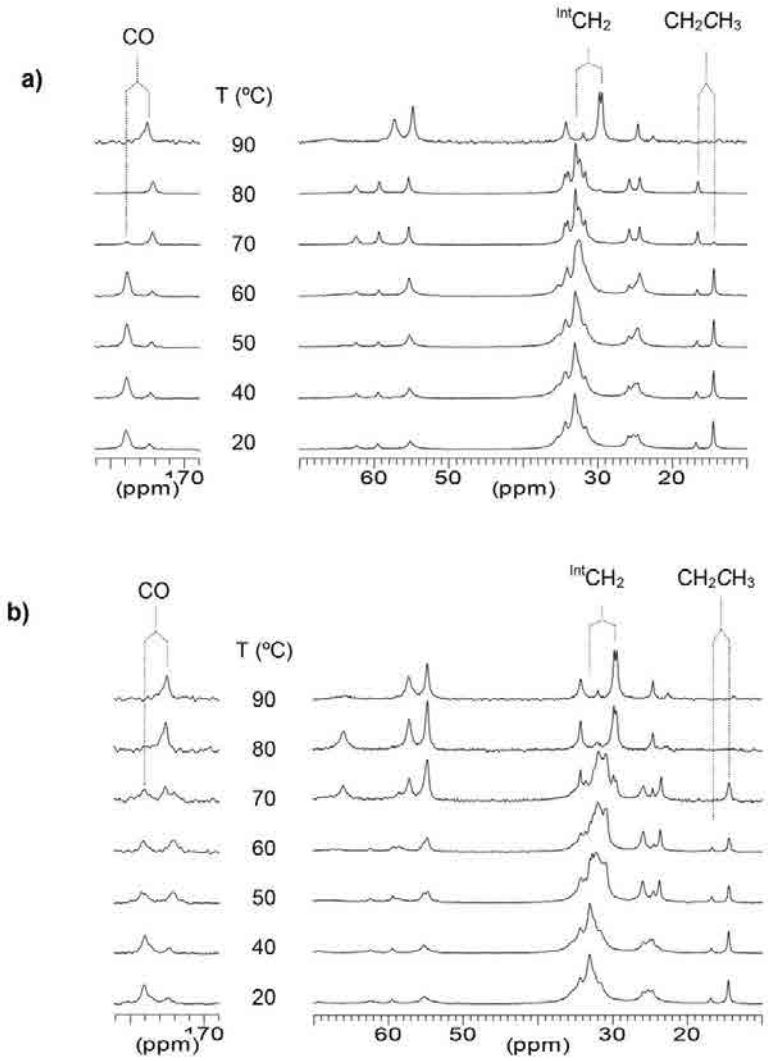

Figure 10. ^{13}C CP/MAS NMR spectra of 12ACh·I registered at the indicated temperatures. a) At heating and b) at cooling.

both DSC and WAXS. The spectra recorded from 12ACh·I when subjected to a heating-cooling cycle over the 20-90 ºC interval are reproduced in Figure 10 for illustration, and similar plots for the other members of the series are provided in the SI subdivision. The changes observed in the signals arising from internal methylene units contained in the alkanoyl chain, as well as those affecting to the carbonyl signal, indicate that the *all-trans* conformation initially

present (Ph-Iα) is partially lost when the compound is heated within the 80-90 ºC interval.[42] It is reasonable to interpret therefore that Ph-II consists of a "semicrystalline" phase in which the polar heads of the surfactant are crystallized whereas the alkanoyl tails are side-by-side aligned but without crystalline order. This picture of Ph-II is according to both SAXS and WAXS data and gives strong support to the interpretation of the Ph-Iα to Ph-II transition as a process entailing the melting of the alkanoyl chains accompanied by a slight rearrangement of the ionic pair head groups.

It is worth noting moreover that a change in the NMR signal was perceived in the 14-17 ppm before that Ph-Iα to Ph-II transition takes place. Specifically, the initial alkanoyl methyl signal at 14.5 ppm disappeared upon heating in the 60-70 ºC range, and a peak emerged at around 16.8 ppm instead, which also disappeared when temperature reached 80 ºC. Such changes are also related to variations in the polymethylene chain packing, and according to observations reported for *n*-alkanes, they must be ascribed to the occurrence of a crystal/crystal transition that is induced by thermal effects.[43]

1.3.9. Polarizing optical microscopy

The thermal transitions taking place in *n*ACh·I were examined by polarizing optical microscopy at both heating and cooling. A selection of the pictures taken from 16ACh·I is shown in Figure 11 and a complete assortment of images illustrating the texture changes occurring in the other members is afforded in the SI part. Samples for observation were prepared by casting from chloroform at room temperature so they were initially in Ph-Iα phase. The high crystallinity of Ph-Iα previously evidenced by both DSC and WAXS is reflected in the crystal-mosaic texture present in the first pictures taken at low temperatures; this well-defined geometrical morphology was lost after heating above 100 ºC and not recovered any more. The texture seen at 125 ºC corresponds to Ph-II which was observed to evolve with expansion of the material indicating that the Ph-Iα to Ph-II conversion takes place with a decrease in density in agreement with the increase in the interlayer spacing revealed by SAXS. A close inspection of this picture revealed the presence of the features characteristic of a smectic mesophase, which is in full agreement with SAXS results. Further heating at temperatures above ~165 ºC led to Ph-III which displayed a texture not very different from that of Ph-II. In fact, according to WAXS/SAXS data, Ph-II and Ph-III phases will share the same stratified pattern with alkanoyl chains in the molten state intercalated between the layers where the choline iodide counterparts are located. Differences

between the two phases concern the order degree of the ionic layer, which is crystallized in Phase II but disordered in Phase III, and the interdigitation degree, which is greater in Phase III. After cooling down to room temperature a strongly birefringent material devoid of any distinctive texture was generated; according to DSC and diffraction data it must correspond to Ph-Iβ, Ph-Iα of even a mixture of both.

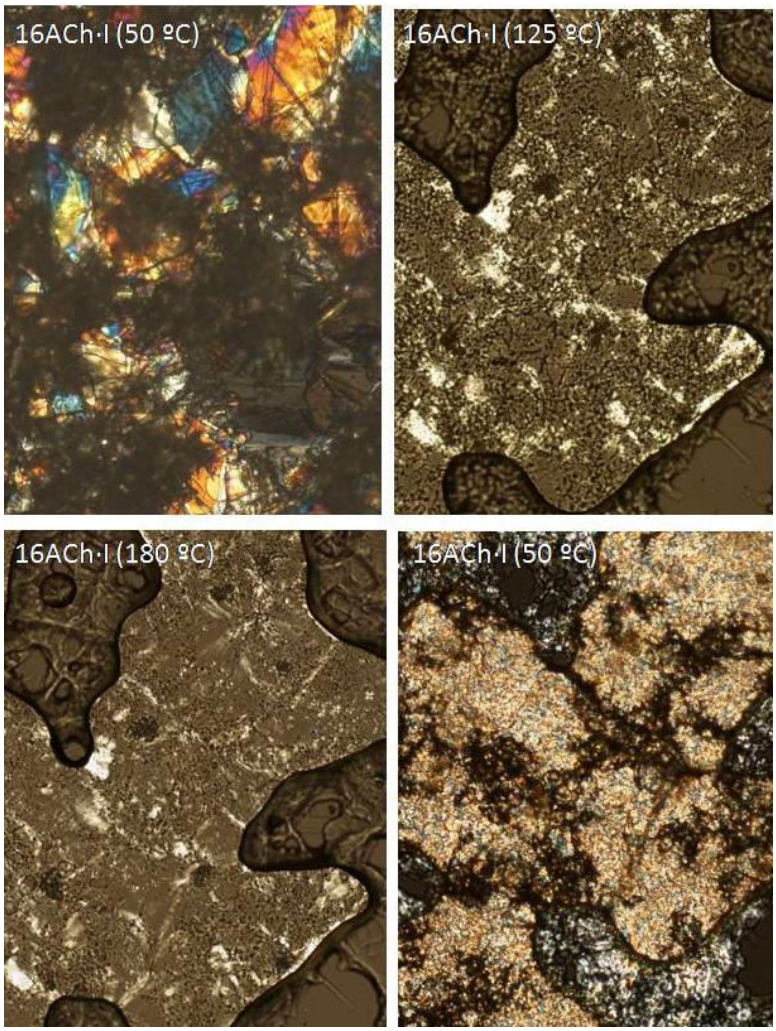

Figure 11. Micrographs recorded by POM from 16ACh·I. at the indicated temperatures (the bottom-right one at 50 ºC after cooling).

1.4. Conclusions

A homologous series of alkanoylcholine surfactants (*n*ACh·I) has been prepared from fatty acids with *n* = 12, 14, 16 and 18, and their thermal and structural properties studied as a function of temperature. These surfactants are particularly interesting because they are bio-based compounds displaying biodegradable and biocompatible properties, as well as for their suitability to prepare bio-based comb-like polymers by ionic coupling with naturally-occurring polyelectrolytes.

*n*ACh·I surfactants are soluble in warm water showing *cmc* within the 1 to 10 mM concentration range and Krafft temperatures between 30 and 60 ºC depending on *n*. In the condensed phases, *n*ACh·I invariably adopt a bilayered molecular arrangement in which ionic choline iodide heads and alkyl tails are alternating counterparts. Upon heating, a diversity of phases differing in order degree or/and mutual arrangement of layers are taken up according to temperature. At room temperature, a stable phase (Ph-Iα) made of triclinic microcrystals in $P\overline{1}$ space group prevails whereas at temperatures above 80-100 ºC (depending on *n*) a semicrystalline layered phase with the alkyl tails in the molten state but aligned and extensively interdigitated is formed (Ph-II). The semicrystalline Ph-II phase becomes fully melted above ~160 ºC with formation of a smectic-A mesophase (Ph-III); in this phase both choline iodide and alkyl tails are in a disordered state but the layered arrangement is still preserved with a higher degree of interpenetration of the alkanoyl chains (Figure 12). The structural changes taking place by heating effect are reversible. Nevertheless a metastable elusive phase (Ph-Iβ) appears when Ph-III is cooled to room temperature; the structure of Ph-Iβ is not well characterized but presumably it is similar to Ph-II but with a degree of side chain interpenetration comparable to Ph-III.

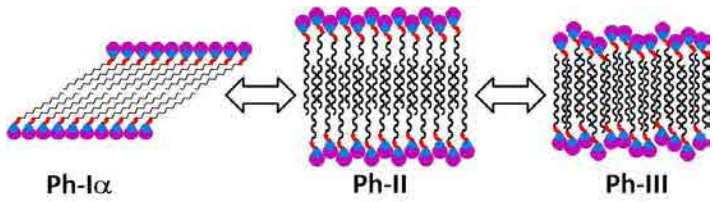

Figure 12. Raw scheme of crystalline, semicrystalline and liquid-crystal phases observed for *n*ACh·I.

1.5. References

1. Blusztajn, J. K.; Wurtman, R. J. Choline and cholinergic neurons. *Science* **1983**, *221*, 614-620.

2. Blusztajn, J. K. Choline, a vital amine. *Science* **1998**, *281*, 794-795.

3. Kortstee, G. J, The aerobic decomposition of choline by microorganisms. I. The ability of aerobic organisms, particularly coryneform bacteria, to utilize choline as the sole carbon and nitrogen source. *Arch. Mikrobiol*. **1970**, *71*, 235-244.

4. Gorke, J. T.; Srienc, F. Kazlauskas, R. Hydrolase-catalyzed biotransformations in deep eutectic solvents. *Chem Commun*. **2008**, 1235-1237.

5. Abbott, A. P.; Boothby, D.; Capper, G.; Davies, D. L.; Rasheed, R. K. Deep eutectic solvents formed between choline chloride and carboxylic acids: Versatile alternatives to ionic liquids. *J. Amer. Chem.* Soc. **2004**, *126*, 9142-9147.

6. Weaver, K. D; Kim, H. J.; Sun, J. Z.; MacFarlane, D. R.; Elliot, G. D. Cyto-toxicity and biocompatibility of a family of choline phosphate ionic liquids designed for pharmaceutical applications. *Green Chem*. **2010**, *12*, 507-513.

7. Klein, R.; Touraud, D.; Kunz, W. Choline carboxylate surfactants: biocompatible and highly soluble in water. *Green Chem.* **2008**, *10*, 433-435.

8. Klein, R.; Kellermeier, M.; Drechsler, M.; Touraud, D.; Kunz, W. Solubilisation of stearic acid by the organic base choline hydroxide. *Colloids Surf. A* 2009, **338**, 129-134.

9. Klein, R.; Dutton, H.; Diat, O.; Tiddy, G. J. T.; Kunz, W. Thermotropic phase behavior of choline soaps. *J. Phys. Chem B.* **2011**,*115*, 3838-3847.

10. Skoulios, A.; Luzzati, V. Structure of anhydrous sodium soaps at high temperatures. *Nature* **1959**, *183*, 1310-1312.

11. Binnemans, K. Ionic liquid crystals. *Chem. Rev*. **2005**, *105*, 4148-4204.

12. Ubbelohde, A. R.; Michels, H. J.; Duruz, J. J. Liquid crystals in molten salt systems. *Nature* **1970**, *228*, 50-52.

13. Shinoda, K.; Minegishi, Y.; Arai, H. Correlation between melting points of

alkanoic acids and Krafft points of their sodium salts. *J. Phys. Chem.* **1976**, *80*, 1987-1988.

14. Rengstl, D.; Diat, O.; Klein, R.; Kunz, W. Influence of chain length and double bond on the aqueous behavior of choline carboxylate soaps. *Langmuir* **2013**, *29*, 2506–2519.

15. Cho, K. S.; Proulx, P. Studies on the mechanism of hemolysis by acyl carnitines, lysolecithins and acyl cholines. *Biochim. Biophys. Acta* **1971**, *225*, 214-223.

16. Ahlström, B.; Chelminska-Bertilsson, M.; Thompson, R. A; Edebo, L. Long-chain alkanoylcholines, a new category of soft antimicrobial agents that are enzymatically degradable. *Antimicrob. Agents Chemother.* **1995**, *39*, 50–55.

17. Schneider, R.; Timms, A. R. Some aspects of the pharmacology of an ahomologous series of choline esters of fatty acids. *Br. J. Pharmacol.* **1957**, *12*, 30−38.

18. Carelli, V.; Liberatore, F.; Scipione, L.; Cardellini, M.; Rotiroti, D.; Rispoli, V. Choline derivative for the treatment of Alzheimer's disease. US Patent 0166721 A1, 2003.

19. Patel, H. Use of choline derivatives for memory, learning and cognition WO Patent 2005/018631 A1, 2005.

20. Alexander, J.; Fix, J. A. Enhancement of absorption of drugs from gastrointestinal tract using choline ester salts. US Patent 4822773, 1989.

21. Alexander, J.; Fix, J. A.; Repta, A. J. Choline esters as absorption-enhancing agents for drug delivery through mucous membranes of the nasal, buccal, sublingual and vaginal cavities. US Patent 4963556, 1990.

22. Klein, R.; Müller, E.; Kraus, B.; Brunner, G.; Estrine, B.; Touraud, D.; Heilmann, J.; Kellermeier, M.; Kunz, W. Biodegradability and cytotoxicity of choline soaps on human cell lines: effects of chain length and the cation. *RSC Adv.* **2013**, *3*, 23347-23354.

23. Watson, M. K.; Tezel, U.; Pavlostathis, S. G. 2012. Biotransformation of alkanoylcholines under methanogenic conditions. *Water Res.* **2012***, 46,* 2947-2956.

24. Tarafdar, P. K.; Reddy, S. T.; Swamy, M. J. Effect of Hofmeister series anions on the thermotropic phase behavior of bioactive O-acylcholines. *J. Phys. Chem. B* **2013**, *117*, 9900-9909.

25. Iwamoto, K.; Ohnuki, Y.; Sawada, K.; Seno, M. Solid-solid phase-transitions of long-chain normal alkyltrimethylammonium halides. *Mol. Cryst. Liq. Cryst.* **1981**, *73*, 95-103.

26. Malliaris, A.; Christias, C.; Margomenou-Leonidopoulou, G.; Paleos, C. M. Single chain quaternary ammonium-salts exhibiting thermotropic mesomorphism and organization in water. *Mol. Cryst. Liq. Cryst.* **1982**, *82*, 161-166.

27. Tolentino, A.; León, S.; Alla, A.; Martínez de Ilarduya, A.; Muñoz-Guerra, S. Comblike ionic complexes of poly(γ-glutamic acid) and alkanoylcholines derived from fatty acids. *Macromolecules* **2013**, *46*, 1607-1617.

28. Chachaty, C.; Ahlnäs, T.; Lindström, B.; Nery, N.; Tistchenko, A. M. NMR studies on micellar solutions of pyridinium octylhydrogen phosphate. *J. Colloid Interface Sci.* **1988**, *122*, 406-417.

29. Zhao, J.; Fung, B. M. NMR study of the transfromation of sodium dodecyl sulfate micelles. *Langmuir* **1993**, *9*, 1228-1231.

30. Lee, Y. S.; Woo, K. W. Micellization of aqueous cationic surfactant solutions at the micellar structure transition concentration – Based upon the concept of the pseudophase separation. *J. Colloid Interface Sci.* **1995**, *169*, 34-38.

31. Kudryashov, E.; Kapustina, T.; Morrissey, S.; Buckin, V.; Dawson, K. The compressibility of alkyltrimethylammonium bromide micelles. *J. Colloid Interface Sci.* **1998**, *203*, 59-68.

32. Barry, B. W.; Russell, G. F. J. Prediction of micellar molecular weights and thermodynamics of micellization of mixtures of alkyltrimethylammonium salts. *J. Colloid Interface Sci.* **1972**, *40*, 174-194.

33. Davey, T. W.; Ducker, W. A.; Hayman, A. R; Simpson, J. Krafft temperature depression in quaternary ammonium bromide surfactants. *Langmuir* **1998**, *14*, 3210-3213.

34. Kaneshina, S.; Matsuki, H.; Ichikawa, R.; Kuwahara, T. Thermotropic phase behavior of binary cationic surfactant mixtures in water, In *Studies in surface science and catalysis;* Iwasawa, Y.; Oyama, N.; Kunieda, H,. Eds.; Elsevier, 2001; Vol. 132, pp. 45-48.

35. Renoncourt, A. Ph.D dissertation, *University of Regensburg*, **2005**.

36. Sharma, K. S.; Patil, S. R.; Rakshit, A. K.; Glenn, K.; Doiron, M.; Palepu, R. M.; Hassan, P. A. Self-aggregation of a cationic-nonionic surfactant mixture in aqueous media: Tensiometric, conductometric, density, light scattering,

potentiometric, and fluorometric studies. *J. Phys. Chem. B* **2004**, *108*, 12804-12812.

37. Vautier-Giongo, C.; Bales, B. L. Estimate of the ionization degree of ionic micelles based on Krafft temperature measurements. *J. Phys. Chem. B* **2003**, *107*, 5398–5403.

38. Portilla-Arias, J. A.; García-Alvarez, M.; Martínez de Ilarduya, A.; Muñoz-Guerra, S. Thermal decomposition of microbial poly(γ-glutamic acid) and poly(γ-glutamate)s. *Polym. Degrad. Stab.* **2007**, *92*, 1916–1924.

39. Ruocco, M. J.; Siminovitch, D. J.; Griffin, R. G. Comparative-study of the gel phases of ether-linked and ester-linked phosphatidylcholines. *Biochemistry* **1985**, *24*, 2406-2411.

40. Kim, J. T., Mattai, J.; Shipley, G. G. Bilayer interactions of ether- and ester-linked phospholipids: dihexadecyl- and dipalmitoylphosphatidylcholines. *Biochemistry* **1987**, *26*, 6599–6603.

41. Haas, N. S.; Sripada, P. K.; Shipley, G. G. Effect of chain-linkage on the structure of phosphatidyl choline bilayers. Hydration studies of 1-hexadecyl 2-palmitoyl-sn-glycero-3-phosphocholine. *Biophys. J.* **1990**, *57*, 117-124.

42. Yamanobe, T.; Tsukahara, M.; Komoto, T.; Watanabe, J.; Ando, I.; Uematsu, I.; Deguchi, K.; Fujito, T.; Imanari, M. Conformation and dynamic aspects of poly(γ-*n*-octadecyl L-glutamate) in the solid state and liquid-crystalline state. *Macromolecules* **1988**, *21*, 48–50.

43. VanderHart, D. L. Influence of molecular packing on solid-state ^{13}C chemical shifts: The *n*-alkanes. *J. Magn. Reson.* **1981**, *44*, 117-125.

1.6. Supporting information

Supporting information part includes complementary data of *n*ACh·I: synthesis data; ^{1}H-NMR spectra; TGA derivatives traces; DSC traces; detailed description of single-crystal analysis methodology; polarizing optical microscope and SEM images of crystals and monocrystals; real time X-ray data (SAXS and WAXS); ^{13}C CP-MAS NMR spectraI; POM pictures.

SI Table 1. Synthesis data of alkanoylcholine iodides.

n	T_1 [a] (ºC)	T_2 [a] (ºC)	DMAE-*n*A	Yield (%)	Purity[b] (%)	*n*ACh·I
12	0	20	Clear oil (colorless)	25	99.5	White powder
14	0	20	Clear oil (colorless)	88	100	White powder
16	20	20	Clear oil (colorless)	97	100	White powder
18	20	40	Oily solid (brown)	94	100	White powder

T_1 and T_2: reaction temperatures used at the 1st step (esterification) and 2nd step (quaternization). [b]Estimated by ^{1}H NMR.

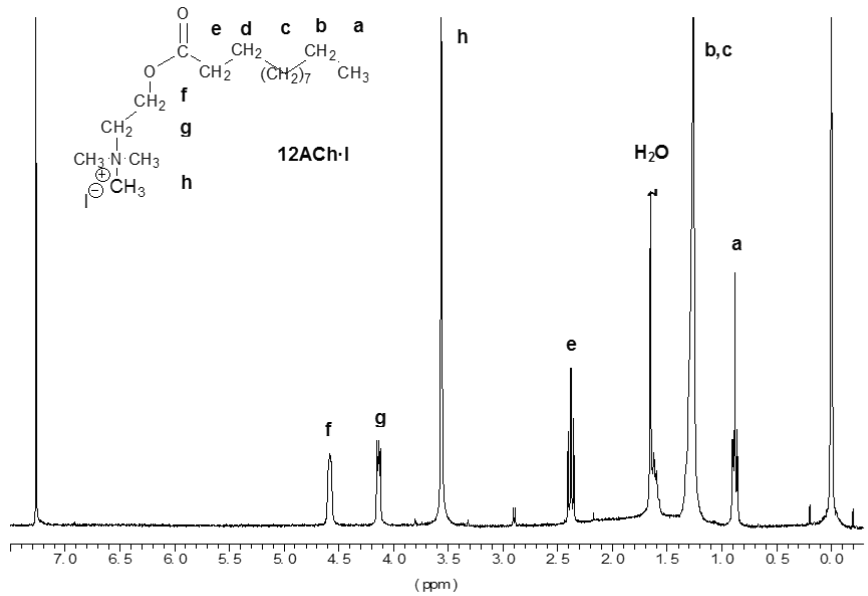

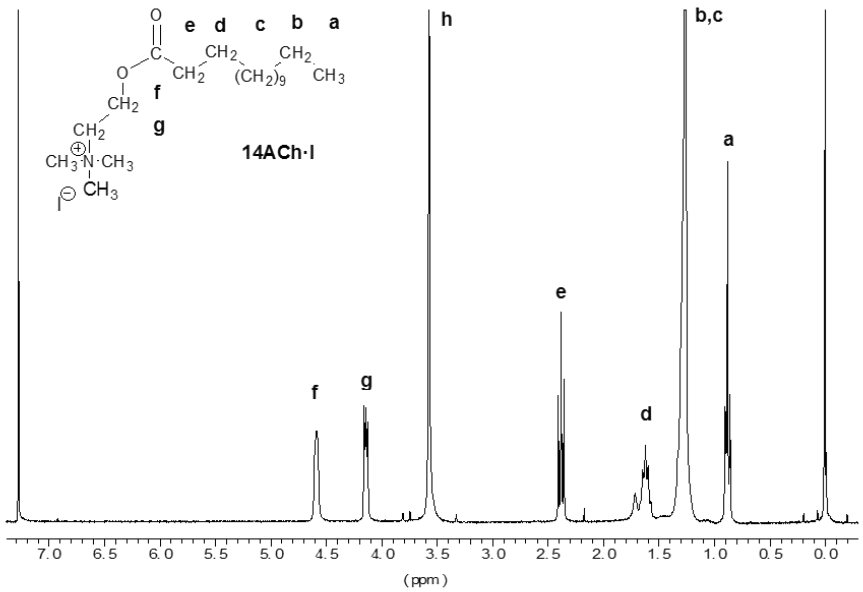
14ACh·I
h
b,c
a
e
f
g
d
7.0 6.5 6.0 5.5 5.0 4.5 4.0 3.5 3.0 2.5 2.0 1.5 1.0 0.5 0.0
(ppm)

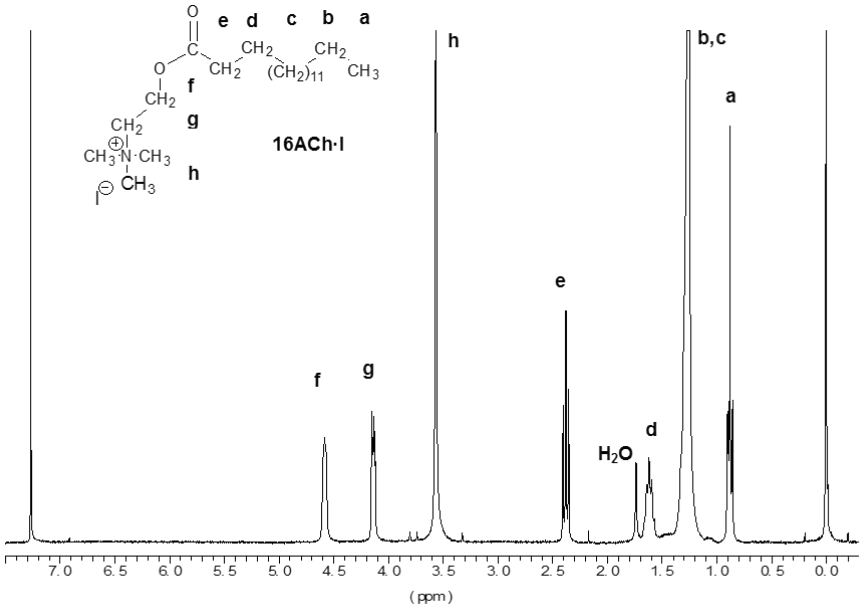
16ACh·I
h
b,c
a
e
f
g
H2O
d
7.0 6.5 6.0 5.5 5.0 4.5 4.0 3.5 3.0 2.5 2.0 1.5 1.0 0.5 0.0
(ppm)

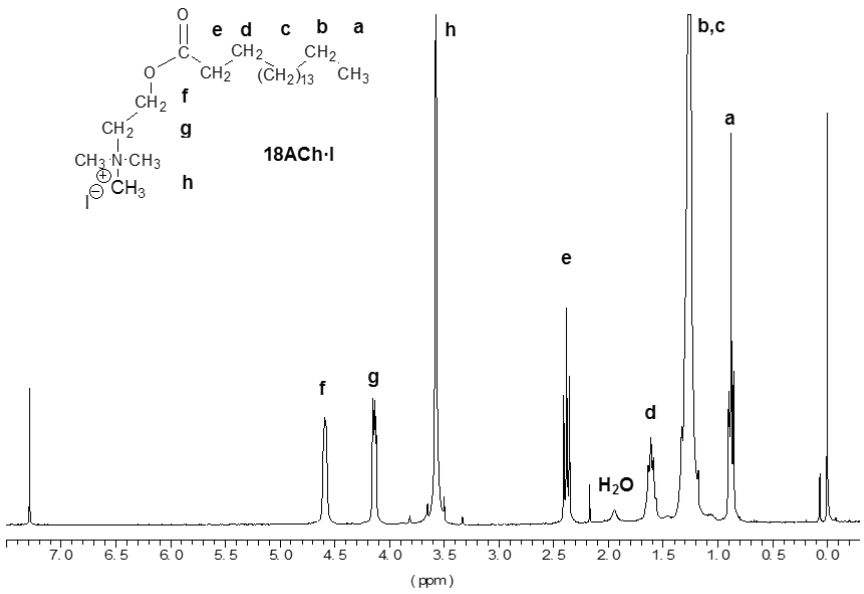

SI Figure 1. ^{1}H-NMR of *n*ACh·I series.

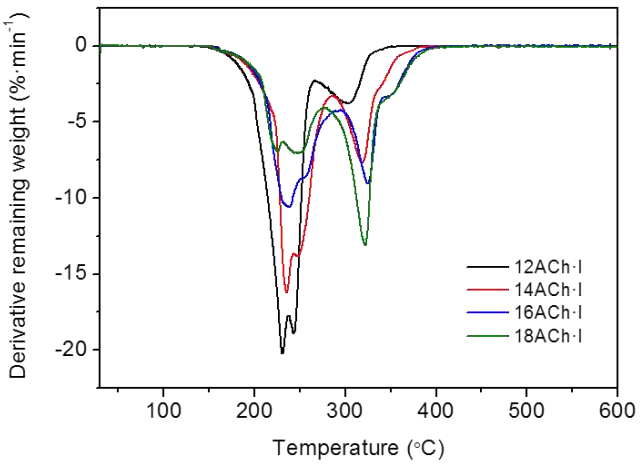

SI Figure 2. TGA derivatives of *n*ACh·I series.

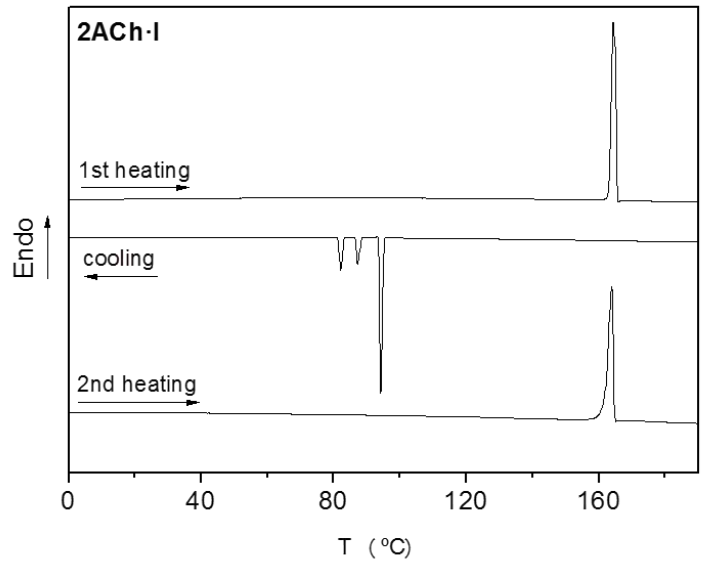

SI Figure 3. DSC traces of acetylcholine iodide.

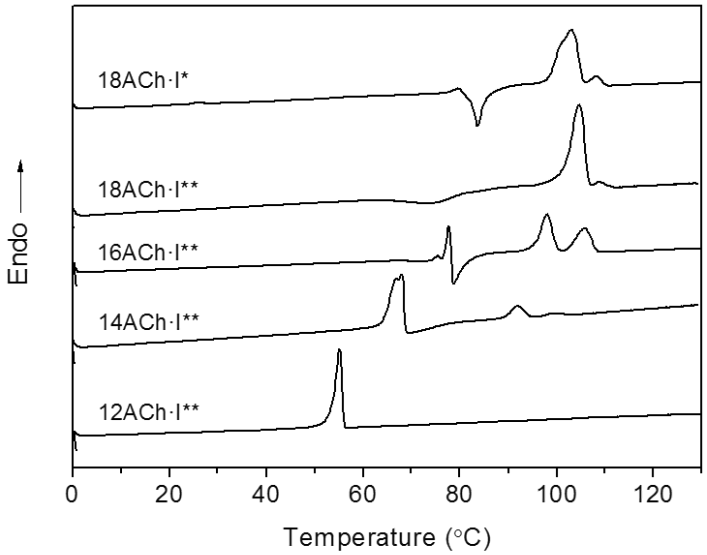

SI Figure 4. DSC reheating traces of *n*ACh·I previously heated at temperatures below T_2. (**) The Ph-Iβ is present in 12, 14 and 16ACh·I whereas 18ACh·I is in Ph-Iα form. (*) Trace of 18ACh·I from a sample heated below T2 for 2 h.

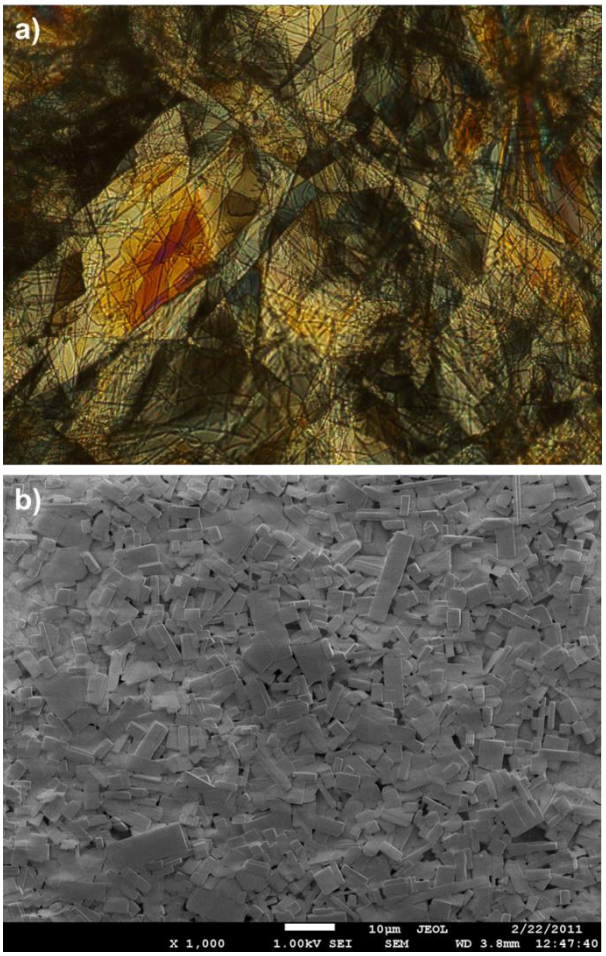

SI Figure 5. Film of *n*ACh·I prepared by casting from chloroform. a) Polarizing optical micrograph; b) SEM micrograph.

1.6.1. Methodology used for single-crystal analysis by X-ray diffraction.

A prismatic crystal (0.1 x 0.1x 0.2 mm) was selected and mounted on a MAR345 diffractometer with an image plate detector. Unit-cell parameters were determined from 1141 reflections ($3 < \theta < 31º$) and refined by least-squares method. Intensities were collected with graphite monochromatized Mo Kα radiation, using φ-scan-technique. 6616 reflections were measured in the range $1.33 \leq \theta \leq 32.32$, 4395 of which were non-equivalent by symmetry (Rint(on I) = 0.044). 3094 reflections were assumed as observed applying the

condition I > 2σ(I). Lorentz-polarization and absorption corrections were made.

The structure was solved by direct methods, using SHELXS computer program and refined by full-matrix least-squares method with SHELX97 computer program, using 6616 reflections, (very negative intensities were not considered). The function minimized was Σ w $||Fo|^2 - |Fc|^2|^2$, where w = $[\sigma^2(I) + (0.0262P)^2+1.8301P]^{-1}$, and P = $(|Fo|^2 + 2|Fc|^2)/3$, f, f' and f'' were taken from International Tables of X-Ray Crystallography. All H atoms were computed and refined, using a riding model, with an isotropic temperature factor equal to 1.2 times the equivalent temperature factor of the atom to which are linked. The final R(on F) factor was 0.052, wR(on $|F|^2$) = 0.098 and goodness of fit = 1.191 for all observed reflections. Number of refined parameters was 244. Max. shift/esd = 0.00, Mean shift/esd = 0.00. Max. and min. peaks in final difference synthesis was 0.358 and -0.439 $eÅ^{-3}$, respectively.

Regarding the crystal refinement parameter for the structural resolution, only reflections that have a value max of theta = 25° (ACTA 50) have been considered. Reflections between 25° and 32° have not been taken into account due to their poor quality. Lack of quality in reflections above 25 º is due to the fact that the crystal does not diffract very well and to the limitations in the kind of detector (image plate with spindle axis only) that was used. Further attempts of crystallization were done, but no single crystals of better quality could be obtained.

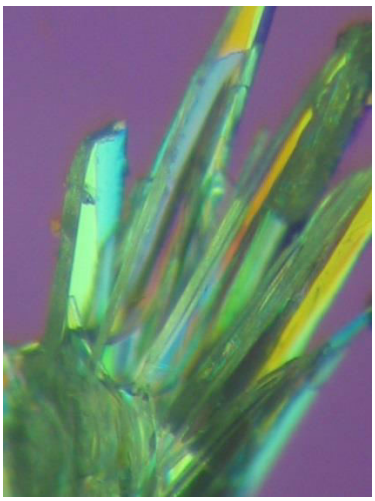

SI Figure 6. Optical microscope image from single-crystal of 18ACh·I obtained from vapor-diffusion technique**.**

SI Table 2. Crystal data and structure refinement of 18ACh·I

Empirical formula	$C_{23}\ H_{48}\ I\ N\ O_2$
Formula weight	497.52
Temperature	293(2) K
Wavelength	0.71073 Å
Crystal system, space group	Triclinic, $P\bar{1}$
Unit cell dimensions	a = 5.759(6) Å; α= 83.07(5)º
	b = 7.670(6) Å; β= 87.04(5)º
	c = 30.89(2) Å; γ= 89.32(5)º.
Volume	1353(2) $Å^3$
Z, Calculated density	2,1.221 Mg/m^3
Absorption coeficient	1.199 mm^{-1}
F(000)	524
Crystal size	0.2 x 0.1 x 0.07 mm
Theta range for data collection	1.33 to 32.32 º.
Limiting indices	-8<=h<=8, -11<=k<=11, -43<=l<=46
Reflections collected / unique	6616 / 4395 [R(int) = 0.0441]
Completeness to theta = 25.00	61.6 %
Absorption correction	Empirical
Max. and min. transmission	0.92 and 0.87
Refinement method	Full-matrix least-squares on F^2
Data / restraints / paràmetres	4395 / 0 / 244
Goodness-of-fit on F^2	1.191
Final R indices [I>2σ(I)]	R1 = 0.0524, wR2 = 0.0984
R indices (all data)	R1 = 0.0821, wR2 = 0.1167
Largest diff. peak and hole	0.358 and -0.439 e.$Å^{-3}$

Reference: In *International Tables of X-Ray Crystallography, Vol. IV*; Ibers J.A.; Hamilton W.C., Ed., Kynoch press: Birmingham, 1974; pp. 99-100 and 149.

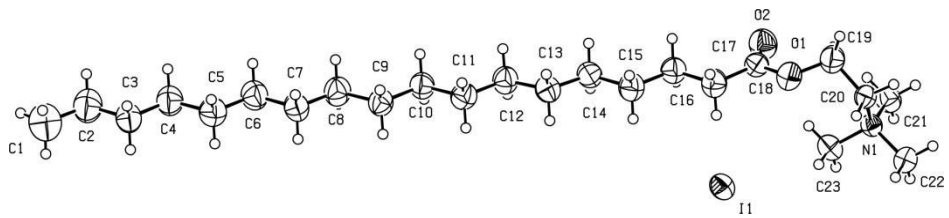

SI 27Figure 7. ORTEP representation of the 18ACh·I molecule conformation in the crystal obtained from vapor-diffusion technique**.**

SI Table 3. Atomic coordinates ($x10^4$) and equivalent isotropic displacement parameters ($Å^2 \cdot 10^3$) for 18ACh·I; U(eq) is defined as one third of the trace of the orthogonalized U_{ij} tensor.

Atom	Atomic coordenates ($x10^4$)			U (eq)
	x	y	z	
I (1)	8586 (1)	7143 (1)	669 (1)	62 (1)
O (1)	13855 (8)	10032 (6)	1632 (1)	65 (1)
O (2)	10090 (9)	10809 (7)	1732 (2)	81 (2)
N (1)	14657 (8)	12166 (6)	666 (1)	45 (1)
C (1)	-7817 (18)	-13183 (13)	4722 (3)	135 (4)
C (2)	-7729 (15)	-11224 (12)	4550 (3)	112 (3)
C (3)	-5389 (13)	-10592 (9)	4368 (2)	79 (2)
C (4)	-5409 (13)	-8641 (9)	4202 (2)	80 (2)
C (5)	-3028 (13)	-7923 (10)	4016 (2)	79 (2)
C (6)	-3021 (13)	-5977 (9)	3845 (2)	79 (2)
C (7)	-640 (12)	-5305 (9)	3659 (2)	71 (2)
C (8)	-663 (13)	-3388 (9)	3483 (2)	75 (2)
C (9)	1676 (11)	-2632 (9)	3292 (2)	66 (2)
C (10)	1642 (11)	-683 (8)	3119 (2)	64 (2)
C (11)	4039 (11)	-6 (9)	2950 (2)	67 (2)
C (12)	4032 (11)	1930 (8)	2774 (2)	68 (2)
C (13)	6433 (11)	2665 (8)	2611 (2)	65 (2)
C (14)	6418 (11)	4579 (8)	2418 (2)	64 (2)
C (15)	8799 (12)	5243 (9)	2232 (2)	71 (2)
C (16)	8892 (11)	7178 (8)	2066 (2)	63 (2)
C (17)	11281 (12)	7775 (9)	1884 (2)	70 (2)
C (18)	11582 (13)	9691 (9)	1751 (2)	55 (2)
C (19)	14471 (2)	11845 (9)	1510 (2)	69 (2)
C (20)	15952 (9)	11999 (8)	1085 (2)	48 (1)
C (21)	13196 (11)	13779 (8)	618 (2)	65 (2)
C (22)	16458 (10)	12305 (8)	289 (2)	59 (2)
C (23)	13156 (11)	10618 (8)	640 (2)	63 (2)

SI Table 4. Bond lengths [Å] and angles [º] for 18ACh·I

O(1)-C(18)	1.362(7)
C(21)-H(21A)	0.9600
C(21)-H(21B)	0.9600
C(21)-H(21C)	0.9600
C(22)-H(22A)	0.9600
C(22)-H(22B)	0.9600
C(22)-H(22C)	0.9600
C(23)-H(23A)	0.9600
C(23)-H(23B)	0.9600
C(23)-H(23C)	0.9600
C(18)-O(1)-C(19)	116.8(5)
C(21)-N(1)-C(23)	108.7(5)
C(21)-N(1)-C(22)	107.8(4)
C(23)-N(1)-C(22)	108.9(4)
C(21)-N(1)-C(20)	111.7(4)
C(23)-N(1)-C(20)	112.1(4)
C(22)-N(1)-C(20)	107.5(4)
C(2)-C(1)-H(1A)	109.5
C(2)-C(1)-H(1B)	109.5
H(1A)-C(1)-H(1B)	109.5
C(2)-C(1)-H(1C)	109.5
H(1A)-C(1)-H(1C)	109.5
H(1B)-C(1)-H(1C)	109.5
C(3)-C(2)-C(1)	114.4(8)
C(3)-C(2)-H(2A)	108.7
C(1)-C(2)-H(2A)	108.7
C(3)-C(2)-H(2B)	108.7
C(1)-C(2)-H(2B)	108.7
H(2A)-C(2)-H(2B)	107.6
C(2)-C(3)-C(4)	112.1(7)
C(2)-C(3)-H(3A)	109.2
C(4)-C(3)-H(3A)	109.2
C(2)-C(3)-H(3B)	109.2
C(4)-C(3)-H(3B)	109.2
H(3A)-C(3)-H(3B)	107.9
C(3)-C(4)-C(5)	114.0(6)
C(3)-C(4)-H(4A)	108.8
C(5)-C(4)-H(4A)	108.8
C(3)-C(4)-H(4B)	108.8
C(5)-C(4)-H(4B)	108.8
H(4A)-C(4)-H(4B)	107.7
C(6)-C(5)-C(4)	114.6(6)
C(6)-C(5)-H(5A)	108.6
C(4)-C(5)-H(5A)	108.6
C(6)-C(5)-H(5B)	108.6
C(4)-C(5)-H(5B)	108.6
H(5A)-C(5)-H(5B)	107.6
C(5)-C(6)-C(7)	113.5(6)
C(5)-C(6)-H(6A)	108.9
C(7)-C(6)-H(6A)	108.9
C(5)-C(6)-H(6B)	108.9
C(7)-C(6)-H(6B)	108.9
H(6A)-C(6)-H(6B)	107.7

C(8)-C(7)-C(6)	113.1(6)
C(8)-C(7)-H(7A)	109.0
C(6)-C(7)-H(7A)	109.0
C(8)-C(7)-H(7B)	109.0
C(6)-C(7)-H(7B)	109.0
H(7A)-C(7)-H(7B)	107.8
C(7)-C(8)-C(9)	115.6(6)
C(7)-C(8)-H(8A)	108.4
C(9)-C(8)-H(8A)	108.4
C(7)-C(8)-H(8B)	108.4
C(9)-C(8)-H(8B)	108.4
H(8A)-C(8)-H(8B)	107.4
C(10)-C(9)-C(8)	115.3(6)
C(10)-C(9)-H(9A)	108.5
O(1)-C(19)	1.440(7)
O(2)-C(18)	1.205(7)
N(1)-C(21)	1.485(8)
N(1)-C(23)	1.490(7)
N(1)-C(22)	1.515(7)
N(1)-C(20)	1.517(6)
C(1)-C(2)	1.532(12)
C(1)-H(1A)	0.9600
C(1)-H(1B)	0.9600
C(1)-H(1C)	0.9600
C(2)-C(3)	1.496(10)
C(2)-H(2A)	0.9700
C(2)-H(2B)	0.9700
C(3)-C(4)	1.522(9)
C(3)-H(3A)	0.9700
C(3)-H(3B)	0.9700
C(4)-C(5)	1.541(9)
C(4)-H(4A)	0.9700
C(4)-H(4B)	0.9700
C(5)-C(6)	1.522(9)
C(5)-H(5A)	0.9700
C(5)-H(5B)	0.9700
C(6)-C(7)	1.531(9)
C(6)-H(6A)	0.9700
C(6)-H(6B)	0.9700
C(7)-C(8)	1.505(9)
C(7)-H(7A)	0.9700
C(7)-H(7B)	0.9700
C(8)-C(9)	1.534(8)
C(8)-H(8A)	0.9700
C(8)-H(8B)	0.9700
C(9)-C(10)	1.526(8)
C(9)-H(9A)	0.9700
C(9)-H(9B)	0.9700
C(10)-C(11)	1.525(8)
C(10)-H(10A)	0.9700
C(10)-H(10B)	0.9700
C(11)-C(12)	1.518(9)
C(11)-H(11A)	0.9700
C(11)-H(11B)	0.9700
C(12)-C(13)	1.537(8)

C(12)-H(12A)	0.9700
C(12)-H(12B)	0.9700
C(13)-C(14)	1.516(8)
C(13)-H(13A)	0.9700
C(13)-H(13B)	0.9700
C(14)-C(15)	1.529(8)
C(14)-H(14A)	0.9700
C(14)-H(14B)	0.9700
C(15)-C(16)	1.511(9)
C(15)-H(15A)	0.9700
C(15)-H(15B)	0.9700
C(16)-C(17)	1.514(8)
C(16)-H(16A)	0.9700
C(16)-H(16B)	0.9700
C(17)-C(18)	1.487(9)
C(17)-H(17A)	0.9700
C(17)-H(17B)	0.9700
C(19)-C(20)	1.523(8)
C(19)-H(19A)	0.9700
C(19)-H(19B)	0.9700
C(20)-H(20A)	0.9700
C(20)-H(20B)	0.9700
C(8)-C(9)-H(9A)	108.5
C(10)-C(9)-H(9B)	108.5
C(8)-C(9)-H(9B)	108.5
H(9A)-C(9)-H(9B)	107.5
C(11)-C(10)-C(9)	112.4(6)
C(11)-C(10)-H(10A)	109.1
C(9)-C(10)-H(10A)	109.1
C(11)-C(10)-H(10B)	109.1
C(9)-C(10)-H(10B)	109.1
H(10A)-C(10)-H(10B)	107.8
C(12)-C(11)-C(10)	113.1(6)
C(12)-C(11)-H(11A)	109.0
C(10)-C(11)-H(11A)	109.0
C(12)-C(11)-H(11B)	109.0
C(10)-C(11)-H(11B)	109.0
H(11A)-C(11)-H(11B)	107.8
C(11)-C(12)-C(13)	114.4(6)
C(11)-C(12)-H(12A)	108.7
C(13)-C(12)-H(12A)	108.7
C(11)-C(12)-H(12B)	108.7
C(13)-C(12)-H(12B)	108.7
H(12A)-C(12)-H(12B)	107.6
C(14)-C(13)-C(12)	114.5(6)
C(14)-C(13)-H(13A)	108.6
C(12)-C(13)-H(13A)	108.6
C(14)-C(13)-H(13B)	108.6
C(12)-C(13)-H(13B)	108.6
H(13A)-C(13)-H(13B)	107.6
C(13)-C(14)-C(15)	113.4(6)
C(13)-C(14)-H(14A)	108.9
C(15)-C(14)-H(14A)	108.9
C(13)-C(14)-H(14B)	108.9
C(15)-C(14)-H(14B)	108.9

H(14A)-C(14)-H(14B)	107.7
C(16)-C(15)-C(14)	115.0(6)
C(16)-C(15)-H(15A)	108.5
C(14)-C(15)-H(15A)	108.5
C(16)-C(15)-H(15B)	108.5
C(14)-C(15)-H(15B)	108.5
H(15A)-C(15)-H(15B)	107.5
C(15)-C(16)-C(17)	113.1(6)
C(15)-C(16)-H(16A)	109.0
C(17)-C(16)-H(16A)	109.0
C(15)-C(16)-H(16B)	109.0
C(17)-C(16)-H(16B)	109.0
H(16A)-C(16)-H(16B)	107.8
C(18)-C(17)-C(16)	116.6(6)
C(18)-C(17)-H(17A)	108.1
C(16)-C(17)-H(17A)	108.1
C(18)-C(17)-H(17B)	108.1
C(16)-C(17)-H(17B)	108.1
H(17A)-C(17)-H(17B)	107.3
O(2)-C(18)-O(1)	123.1(6)
O(2)-C(18)-C(17)	127.4(6)
O(1)-C(18)-C(17)	109.5(6)
O(1)-C(19)-C(20)	108.8(5)
O(1)-C(19)-H(19A)	109.9
C(20)-C(19)-H(19A)	109.9
O(1)-C(19)-H(19B)	109.9
C(20)-C(19)-H(19B)	109.9
H(19A)-C(19)-H(19B)	108.3
N(1)-C(20)-C(19)	116.6(5)
N(1)-C(20)-H(20A)	108.1
C(19)-C(20)-H(20A)	108.1
N(1)-C(20)-H(20B)	108.1
C(19)-C(20)-H(20B)	108.1
H(20A)-C(20)-H(20B)	107.3
N(1)-C(21)-H(21A)	109.5
N(1)-C(21)-H(21B)	109.5
H(21A)-C(21)-H(21B)	109.5
N(1)-C(21)-H(21C)	109.5
H(21A)-C(21)-H(21C)	109.5
H(21B)-C(21)-H(21C)	109.5
N(1)-C(22)-H(22A)	109.5
N(1)-C(22)-H(22B)	109.5
H(22A)-C(22)-H(22B)	109.5
N(1)-C(22)-H(22C)	109.5
H(22A)-C(22)-H(22C)	109.5
H(22B)-C(22)-H(22C)	109.5
N(1)-C(23)-H(23A)	109.5
N(1)-C(23)-H(23B)	109.5
H(23A)-C(23)-H(23B)	109.5
N(1)-C(23)-H(23C)	109.5
H(23A)-C(23)-H(23C)	109.5
H(23B)-C(23)-H(23C)	109.5

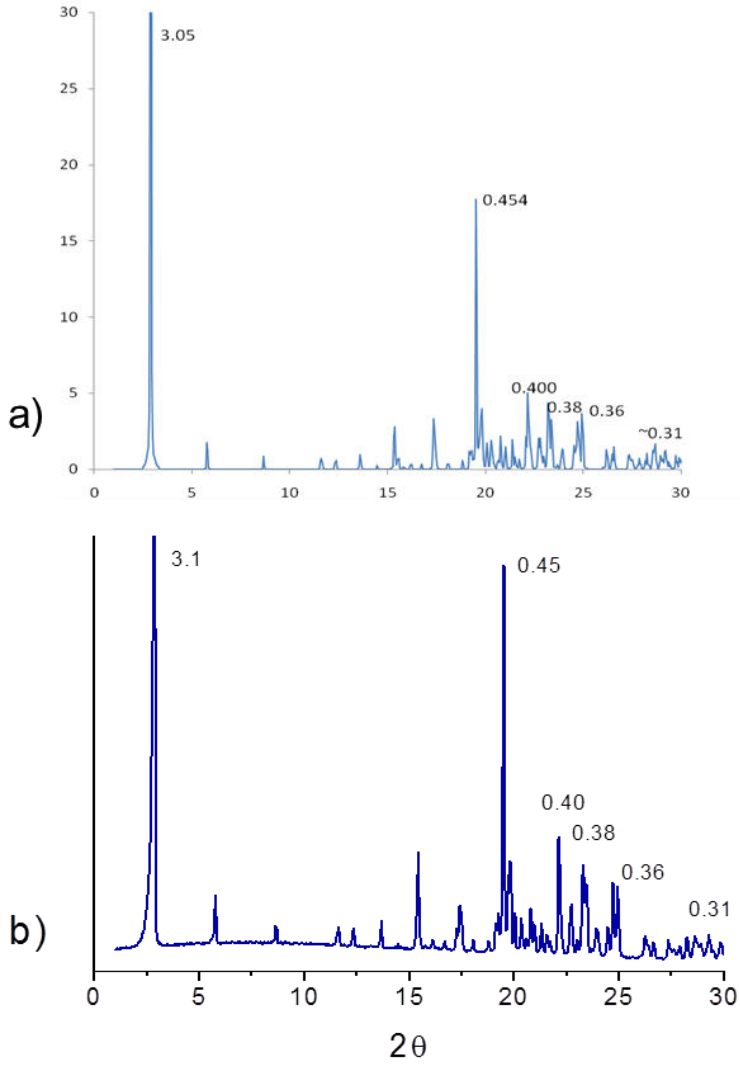

SI Figure 8. Compared X-ray diffraction profiles of Ph-Iα of 18ACh·I. a) Simulated for the crystal lattice determined from the monocrystal by direct method. b) Obtained from annealed powder sample.

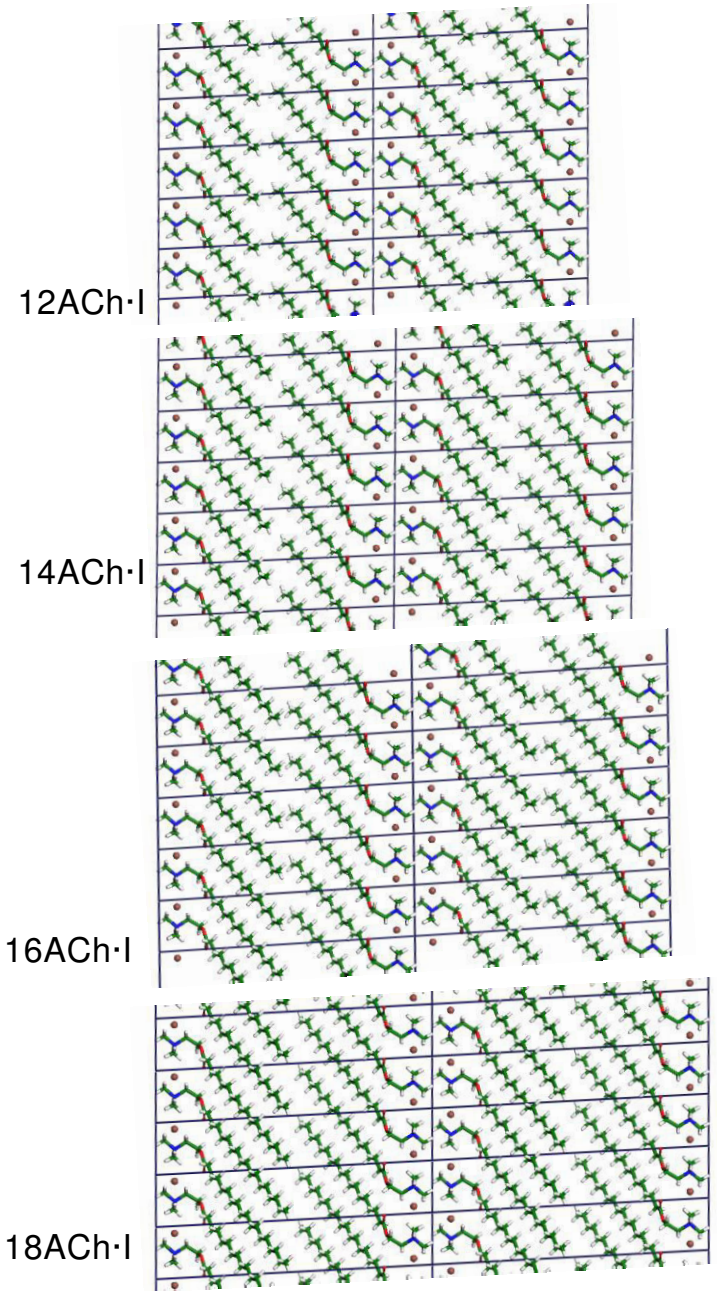

SI Figure 9. Crystal models of phase Ph-Iα of *n*ACh·I viewed along down *b*-axis. Ten unit cells are visualized for each compound.

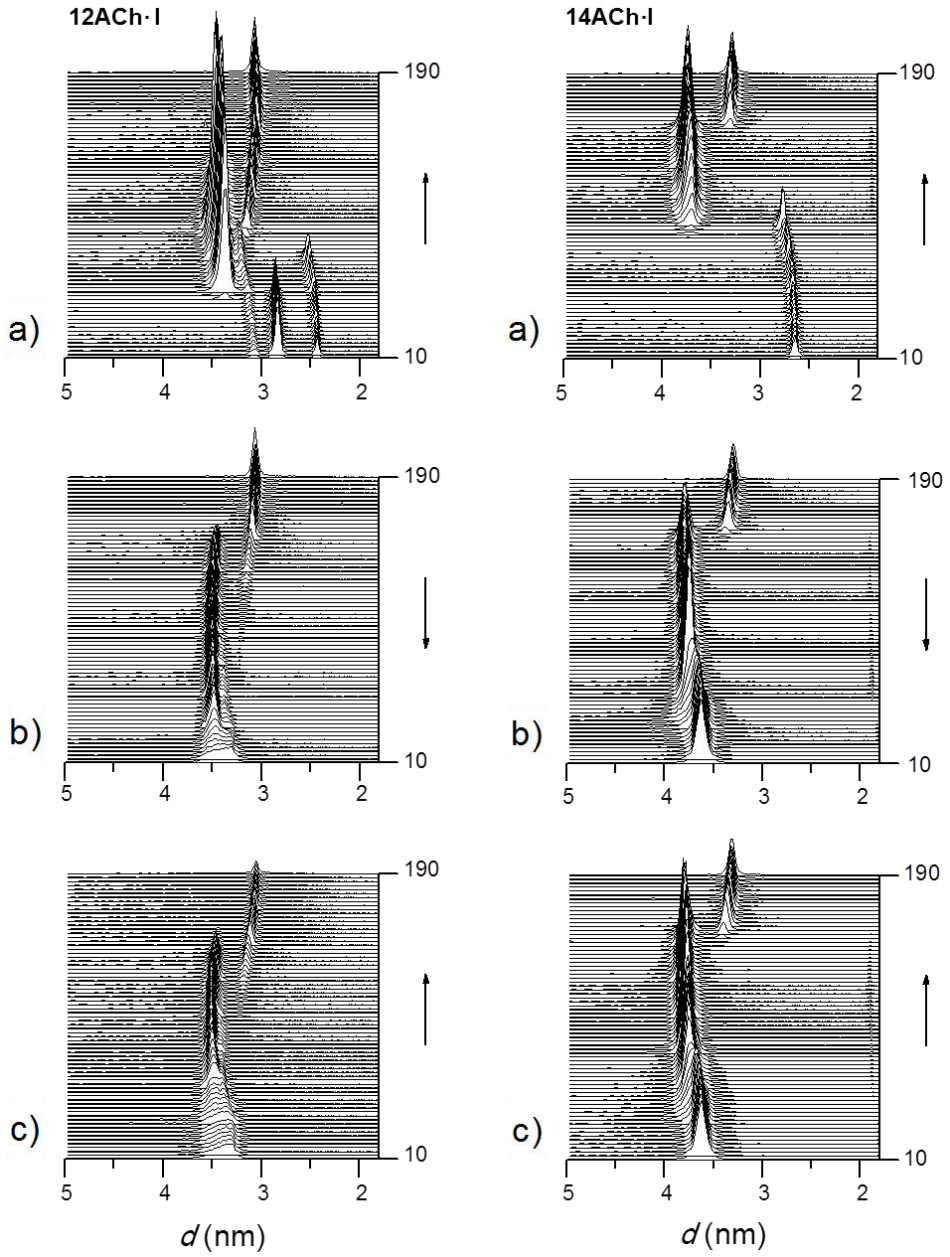
12ACh·I
14ACh·I
a)
b)
c)
190
10
5
4
3
2
d (nm)

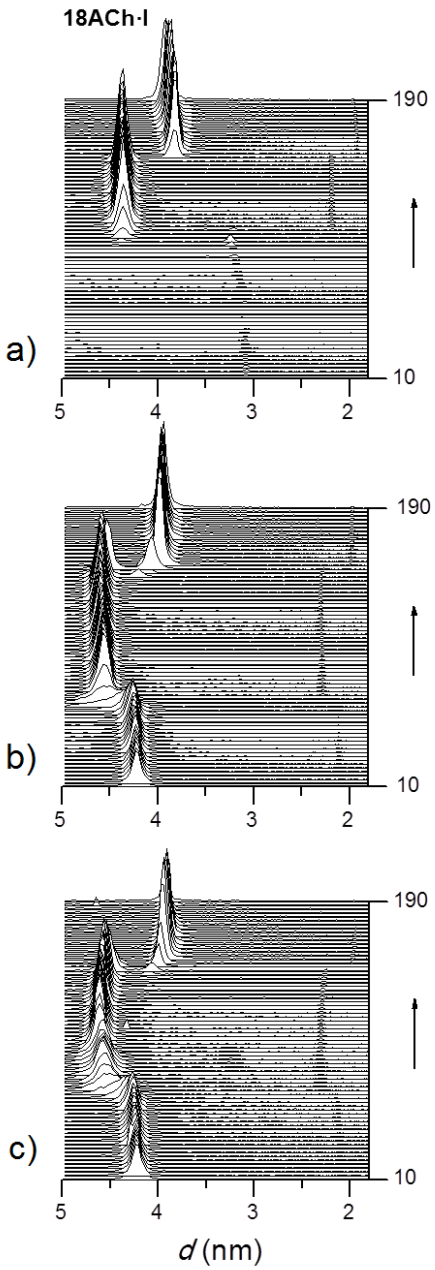
18ACh·I
a)
b)
c)
190
10
5
4
3
2
d (nm)

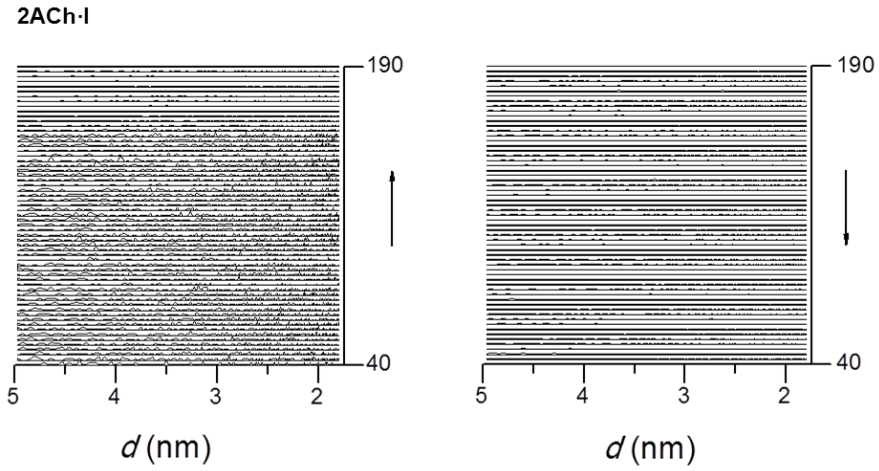

SI Figure 10. SAXS plots from 12, 14 and 18ACh·I and ·2ACh·I registered at heating from room temperature a), cooling b) and reheating c). No signs were observed in SAXS region for 2ACh·I.

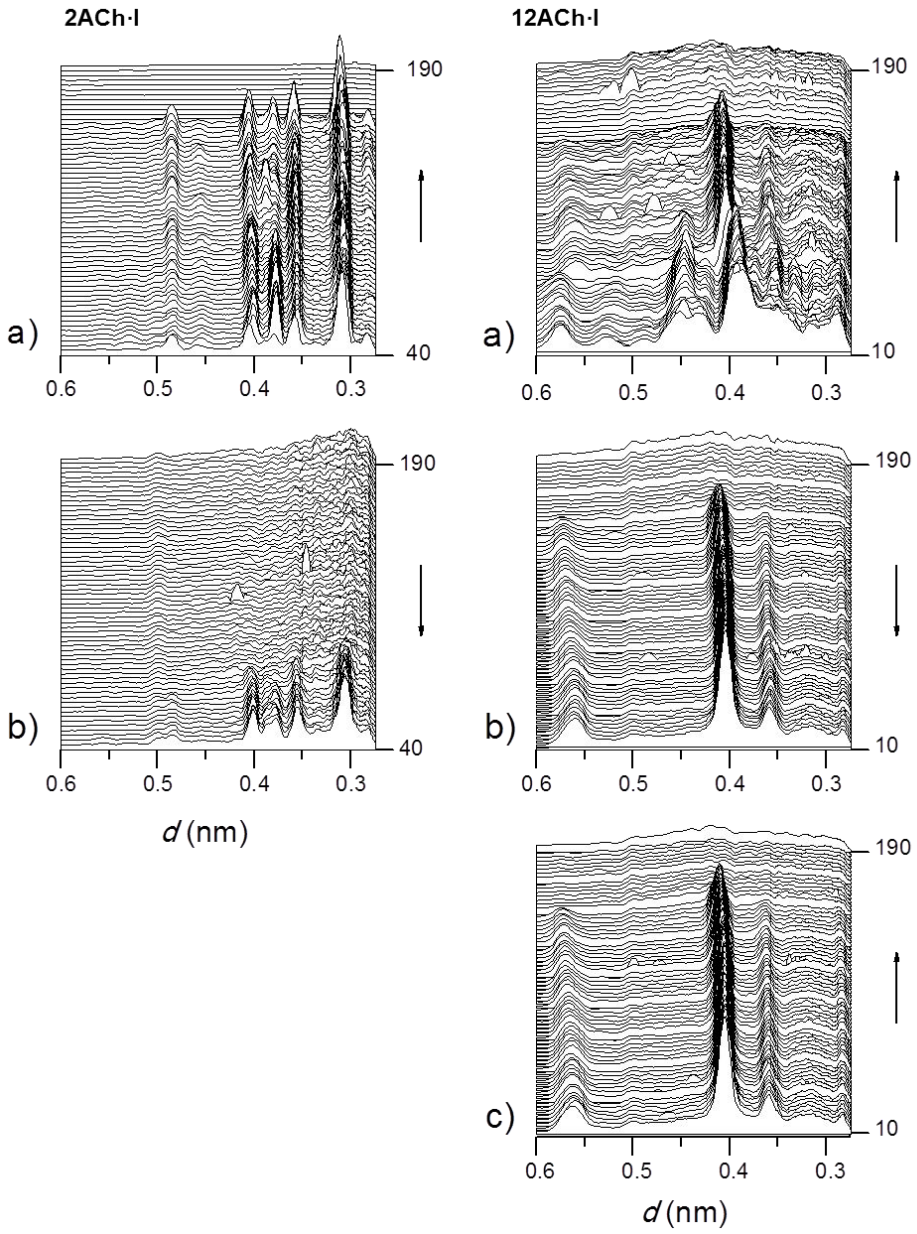
2ACh·I
12ACh·I
a)
b)
c)
190
40
10
0.6
0.5
0.4
0.3
d (nm)

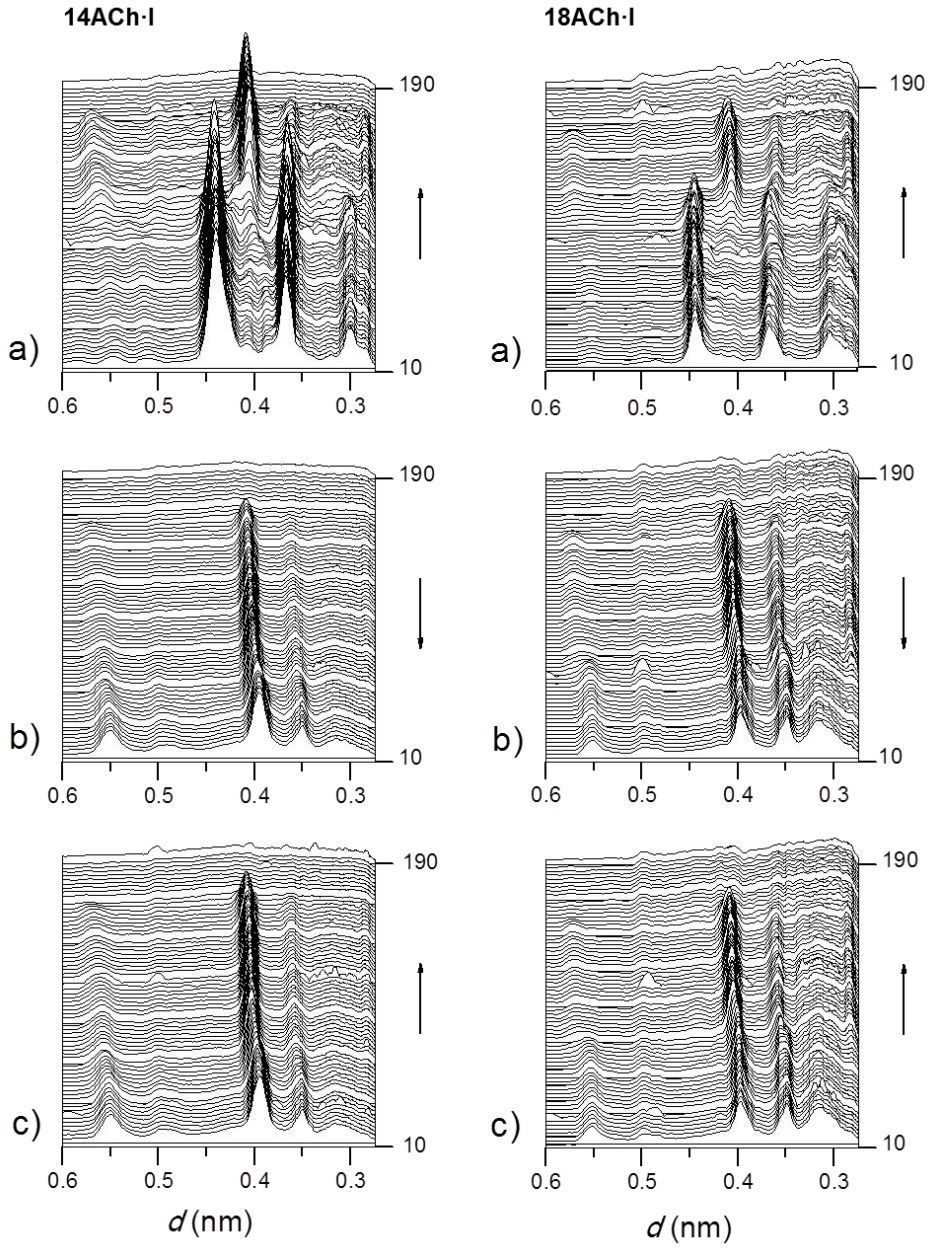

SI Figure 11. WAXS plots from 2, 12, 14 and 18ACh·I registered at heating from room temperature a), cooling b) and reheating c).

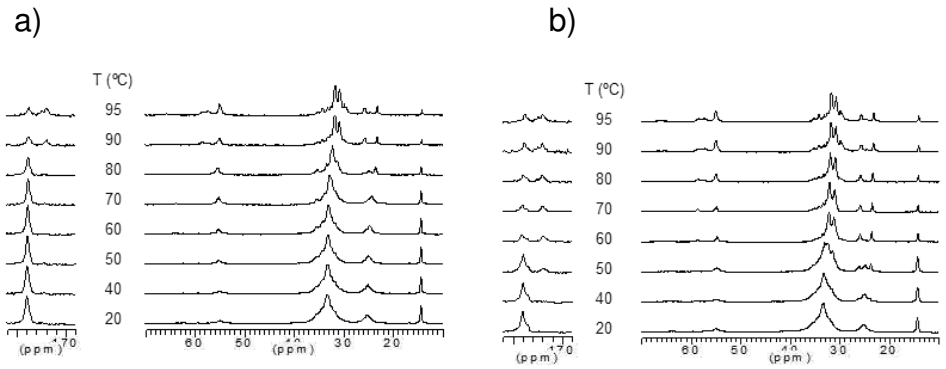

SI Figure 12. ^{13}C CP/MAS NMR spectra of 14ACh·I registered at the indicated temperatures. a) At heating and b) at cooling.

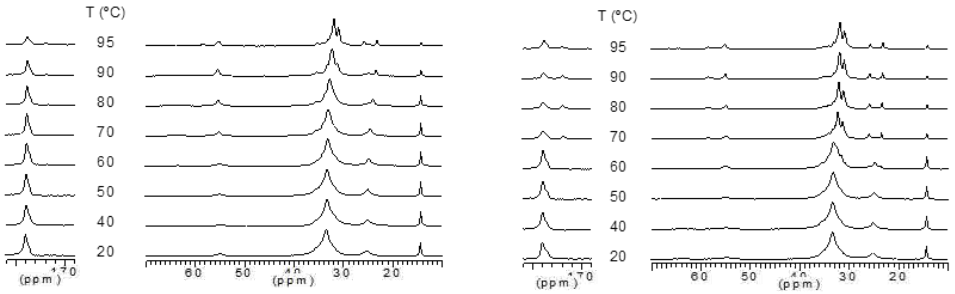

SI Figure 13. ^{13}C CP/MAS NMR spectra of 16ACh·I registered at the indicated temperatures. a) At heating and b) at cooling.

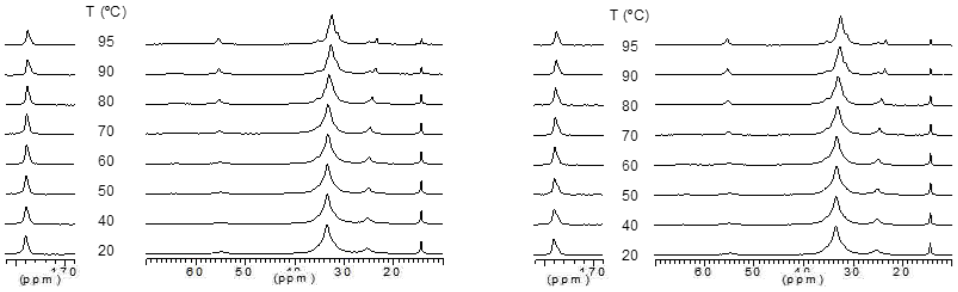

SI Figure 14. ^{13}C CP/MAS NMR spectra of 18ACh·I registered at the indicated temperatures. a) At heating and b) at cooling.

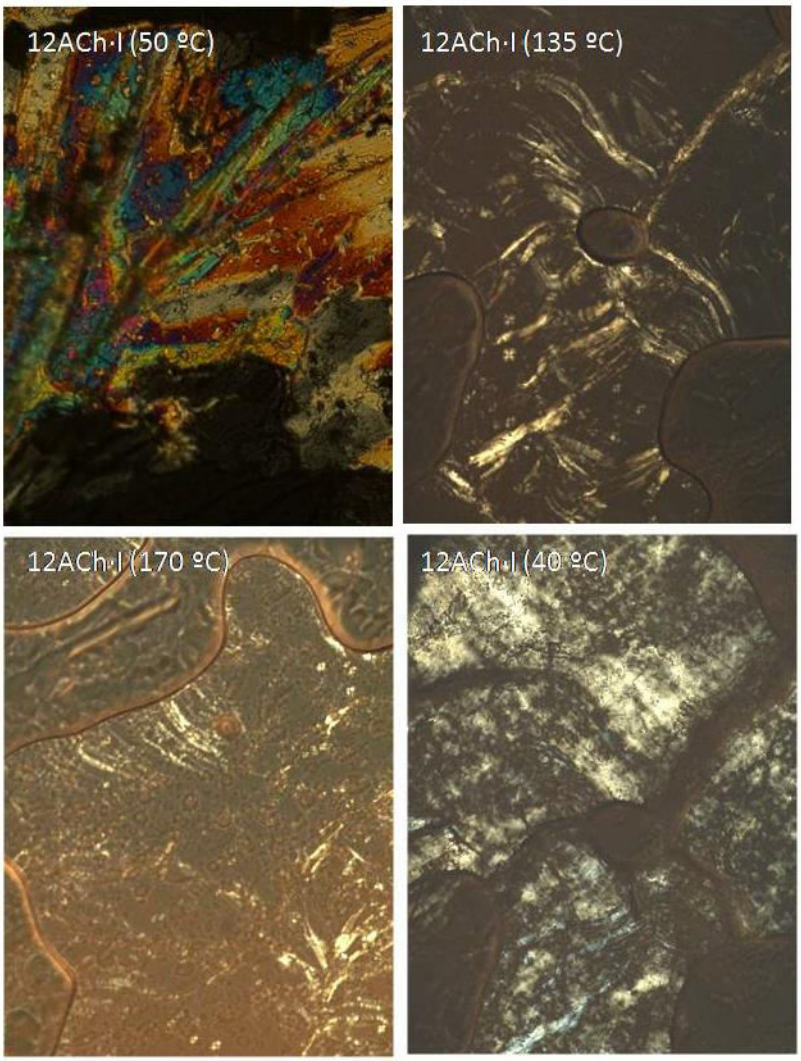

SI Figure 15. POM pictures of 12ACh·I at the indicated temperatures (the last one taken after cooling from high temperature).

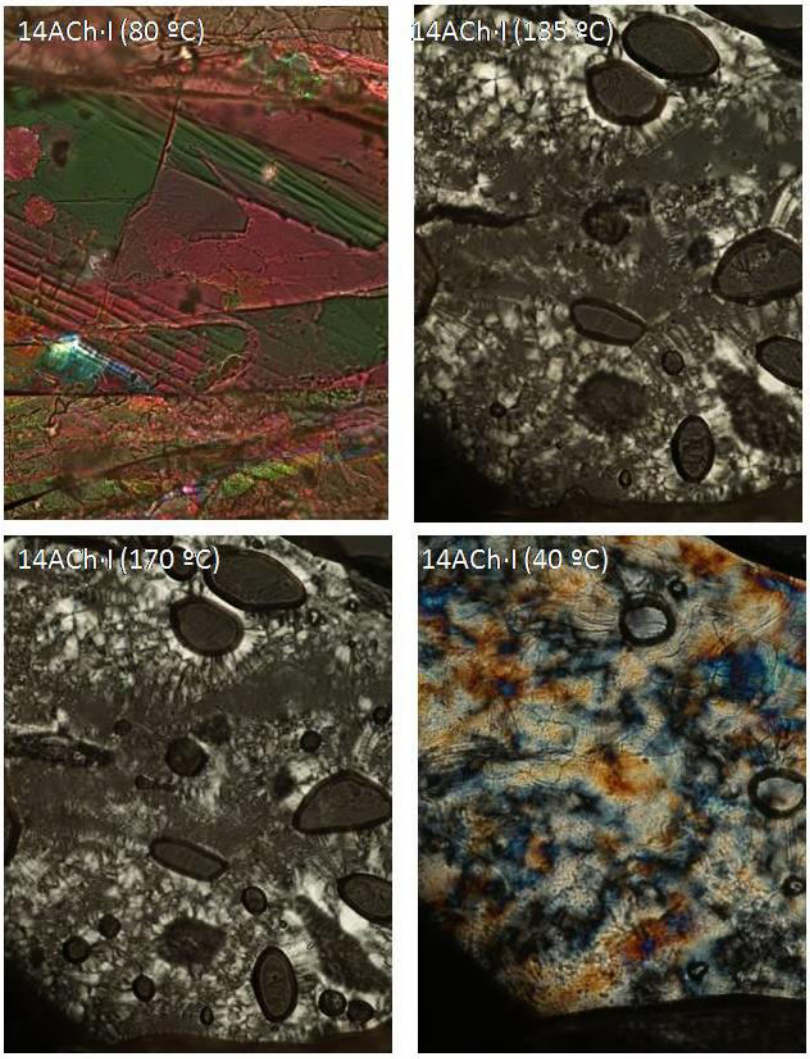

SI Figure 16. POM pictures of 14ACh·I at the indicated temperatures (the last one taken after cooling from high temperature).

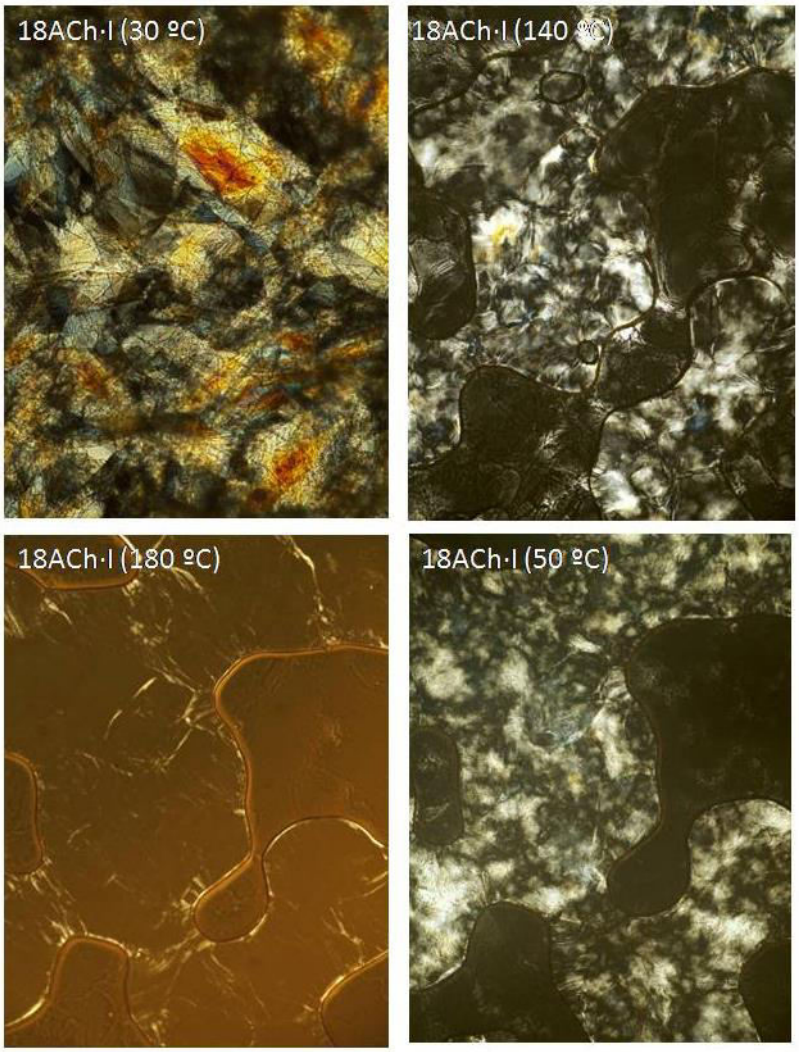

SI Figure 17. POM pictures of 18ACh·I at the indicated temperatures (the last one taken after cooling from high temperature).

2. Comb-like ionic complexes of poly(γ-glutamic acid) and alkanoylcholines derived from fatty acids

Summary: A series of ionic complexes with almost stoichiometric composition has been "synthesized" from bacterial poly(γ-glutamic acid) and alkanoylcholines derived from fatty acids with 12, 14, 16 and 18 carbon atoms. The complexes were stable up to temperatures close to 200 ºC and were non-water soluble but readily soluble in organic solvents. In the solid state they adopted the biphasic structure typical of comb-like systems with the polypeptide chains arranged in sheets and periodically separated by a paraffinic phase which was partially crystallized for C14, C16 and C18. The window width of the layered structure was estimated by SAXS to be within the 3.6-4.5 nm range, and WAXS showed that the alkyl tails were crystallized in a hexagonally packed lattice with a d_{100} spacing of 0.41 nm. These complexes displayed reversible melting of the paraffinic phase in the 40-65 ºC range at temperatures with values increasing with the length of the alkanoyl group. A slight expansion of the intersheet distance occurred at melting followed by contraction upon heating at higher temperatures but without significant alteration of the layered structure. The ^{13}C CP-MAS NMR analysis revealed the underlying polymethylene anti-to-gauche conformational conversion that takes place at the thermal transition. An energy-based simulation study of the crystallization process afforded a molecular picture of the complex and evidenced the favoring effect of the choline structure on the packing of the alkyl side chains.

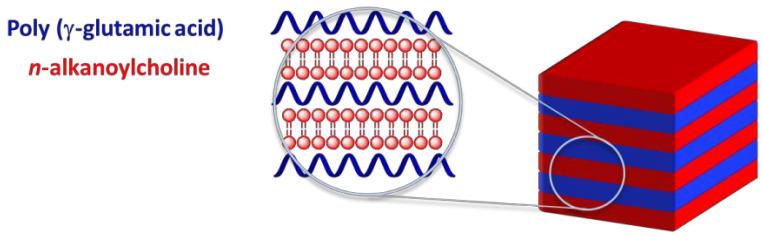

Publication derived from this work:

Tolentino, A.; León, S.; Alla, A.; Martínez de Ilarduya, A.; Muñoz-Guerra, S. Comblike ionic complexes of poly(γ-glutamic acid) and alkanoylcholines derived from fatty acids. *Macromolecules* **2013**, *46*, 1607-1617.

2.1. Introduction

Coupling of different building blocks by electrostatic interactions is a powerful tool to create new nanostructures with unconventional properties. As recently reviewed by Antonietti,[1] a wide diversity of combinations involving polyelectrolytes, surfactants, clusters, and extended rigid organic scaffolds are in principle possible by ionic coupling. Considering the simplicity of the "synthesis" and the wide range of materials and hybrids that may be generated with interesting and versatile functions, this new class of self-organizing compounds is opening its way in science and applications.

Oppositely charged polyelectrolytes spontaneously form complexes underlying strict stoichiometry but due to the double polymeric nature, reprocessing of such complexes via solution or the melt is usually unfeasible. On the contrary, coupling between a water-soluble polyelectrolyte and a counter charged surfactant usually results in a non-water soluble complex that may display reversible melting without decomposition of the supramolecular structure. Cast films of these complexes usually adopt a well ordered mesomorphous nanostructure whose appearance is mainly controlled by the topological matching between surfactant and polyelectrolyte.[2] A number of publications describing the formation of these complexes in water as a function of experimental parameters such as ionic strength, stoichiometry, and concentration have been reported.[3] The relevance of self-assembled polyelectrolyte-surfactant complexes in polymer science was reviewed in deep by Thunemann a decade ago.[4] These complexes distinguish because they combine the mechanical stability characteristic of synthetic polymers with the ability of surfactants to form highly ordered mesophases.

A particular class of polyelectrolyte-surfactant complexes is that consisting of a polypeptide coupled with a surfactant bearing a long linear alkyl chain. These complexes have a comb-like architecture and in the solid state they display a biphasic structure due to the incompatibility of the polypeptidic and the paraffinic counterparts at the nanoscale level. Pioneering works carried out by Ponomarenko et al.[5,6] on poly(α,L-glutamate)/alkyltrimethylammonium complexes for alkyl lengths of C12, C16 and C18, showed the occurrence of a structure made of alternating layers of α-helical polypeptide and almost fully extended alkyl side chains, the which are normally oriented respect to the α-helix and able to crystallize in the case of C18. Analogous complexes of poly(α,L-lysine)/dodecylsulfate also showed the lamellar organization but here the polypeptide adopted a mixture of α-helix and β-sheet conformations.[7] More recently, Kodona et al.[8] have reported on complexes of both poly(α,L-

aspartic) and poly(α,L-glutamic) with cationic surfactants C14TAB and C16TAB which were able to take up either a lamellar structure or a hexagonal packing of micellar aggregates depending on pH. These authors also showed that the α-helix of poly(α,L-glutamic acid) in these complexes gradually transformed into a mixture containing increased amounts of the 3_{10} helix as the temperature increased from 10 up to 70 ºC.[9]

In the last decade the ionic complexes of naturally-occurring poly(γ-glutamic acid) (PGGA) have attracted great attention.[10] This γ-polypeptide is a widely known biodegradable and biocompatible biopolymer that is produced by a group of bacteria of the genus Bacillus. PGGA is particularly interesting as a potential platform for the synthesis of copolymers and conjugates of application in biomedicine.[11-13] The complexes of PGGA with cationic polyelectrolytes such as chitosan[14] or poly(ε,L-lysine)[15] have been proved to be exceptional for the preparation of internally structured nanoparticles exploitable as vectorized drugs and genes delivery systems. Stoichiometric complexes (*n*ATMA·PGGA) of anionically charged PGGA and alkyltrimethylammoniumcations bearing long alkyl chains with even numbers of carbons (*n* from 12 to 22), were reported by us some years ago.[16] All these complexes share the biphasic layered structure that is schematized in Figure 1. This structure consists of sheets made of aligned PGGA helical chains that are regularly separated by a paraffinic phase in which the alkyl chains become partially crystallized for high values of *n*. Films of *n*ATMA·PGGA with this structure may be prepared by casting and they have been investigated as prospective delivery systems for drugs;[17] the layered arrangement present in these complexes was found to be determinant for lodging and releasing of the host compound.

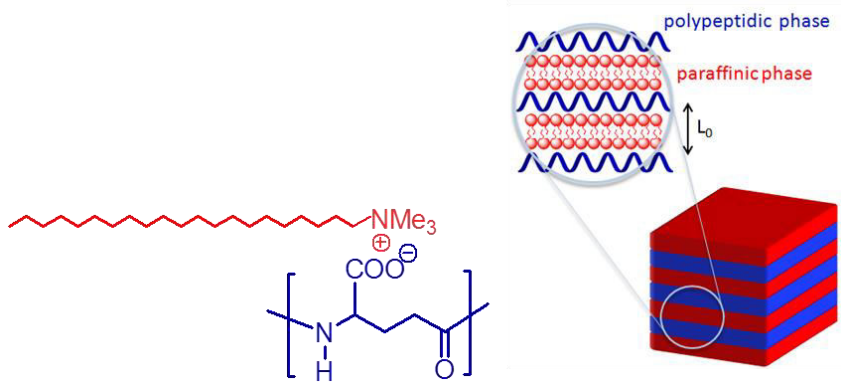

Figure 1. Simplified scheme of the biphasic layered structure adopted by comb-like ionic complexes of PGGA.

As a step ahead in the progress of comb-like ionic polypeptidic systems, we have now focused our efforts on the study of complexes made from PGGA and alkanoylcholines derived from fatty acids, called henceforth *n*ACh·PGGA with n standing for the number of carbons in the alkanoyl group. To our knowledge, *n*ACh·PGGA complexes constitute the first comb-like ionic system entirely made of bio-based components that is reported. The choice of the system was motivated by both structural and functional reasons: a) Although it can be reasonably anticipated that the *n*ACh·PGGA complexes will adopt a lamellar structure similar to the *n*ATMA·PGGA complexes, the presence of the relatively flexible ethylenoxycarbonyl group moving away the alkyl chain from the ammonium ion, is expected to have relevant consequences on the crystallization of the paraffinic phase with subsequent differences in the thermal properties of the complexes. b) Alkanoylcholines have been proved to be hydrolyzed by butyrylcholine esterase,[18] which is present in human serum and mucosal, producing common components of human metabolism. Furthermore, these compounds are antimicrobial agents and have proven to display therapeutic activity in the treatment of the Alzheimer disease[19] and certain gastrointestinal disorders.[20] These characteristics together with the well proven biodegradability and biocompatibility of PGGA endow *n*ACh·PGGA complexes with the basic biochemical features required to be valid candidates for building bioactive biomaterials usable in temporal applications.

2.2. Experimental part

2.2.1. Materials

The sodium salt of poly(γ-glutamic) acid (Na·PGGA) sample used in this work was kindly supplied by Dr. Kubota of Meiji.Co.(Japan). It is of biosynthetic origin, has a D/L enantiomeric ratio of 59/41 and a molecular weight of ~300,000 Da. Lauroyl (98%), miristoyl (97%), palmitoyl (97%) and stearoyl (90%) chlorides, N,N-dimethylamino-2-ethanol (98%) and methyl iodide (99%) used for the synthesis of choline surfactants, were supplied from Sigma-Aldrich and used as received.

2.2.2. Complexes of poly(γ-glutamic acid) with alkanoylcholines (*n*ACh·PGGA)

Firstly the choline iodide esters (*n*ACh·I) were prepared. For that the corresponding fatty acid chloride dissolved in chloroform was added drop-wise to a solution of N,N-dimethylamino-2-ethanol in the same solvent at a temperature between 0 and 20 ºC, and after neutralization with aqueous $NaHCO_3$, the organic phase was separated and added with a molar excess methyl iodide. Upon standing overnight the alkanoylcholine iodide was obtained in good yield as a white precipitate that could be easily separated.

The complexes were then prepared following the methodology initially reported by Ponomarenko et al.[6] for poly(α-glutamate) complexes and later applied by us with some minor modifications to the preparation of complexes of poly(γ-glutamic acid) and alkyltrimethylammonium surfactants.[16] In brief, an aqueous solution of the *n*ACh·I surfactant in a concentration range between 0.007M and 0.01 M was added drop-wise to a solution of Na·PGGA (0.01 M) in water under stirring at temperatures between 40 and 80 ºC depending on n. The complex precipitated upon standing for a few hours as a white fine powder that was isolated by centrifugation, washed several times in water and dried under vacuum.

2.2.3. Methods

Calorimetric measurements were performed with a Perkin-Elmer Pyris1 DSC instrument provided with an Intracooler device and calibrated with indium and zinc. Sample weights of about 2-5 mg were examined within a temperature range of -30 to +120 ºC at heating and cooling rates of 10 ºC·min^{-1} under a nitrogen atmosphere. Thermogravimetric analyses were performed at a heating rate of 10 ºC·min-1 from 30 to 600 ºC under an inert atmosphere on a Perkin-Elmer TGA6 thermobalance. X-ray diffraction studies were carried out using synchrotron X-ray radiation in both WAXS and SAXS modes at the A2 beamline of DORIS III light source at DESY in Hamburg. Variable temperature experiments were performed at heating and cooling rates of 5 ºC·min^{-1}. The energy employed corresponded to a 0.15 nm wavelength, and spectra were calibrated with PET and rat tail tendon for WAXS and SAXS, respectively. ^{1}H- and ^{13}C-NMR spectra were recorded on a Bruker AMX-300 NMR instrument operating at 300.1 and 75.5 MHz, respectively. The samples were dissolved in chloroform or methanol, and TMS or sodium 3-(trimethylsilyl)-propanesulphonate were used as internal references. 128 FIDs for ^{1}H-NMR

spectra were recorded with 2.3 μs (30º) pulse width, 3.4 s acquisition time, 20 s relaxation delay, and 4.9 KHz spectral width. For ^{13}C-NMR spectra, 1000 to 10,000 FIDs were recorded using pulse and spectral widths of 4.3 μs (90º) and 18 KHz, respectively. Solid-state ^{13}C CP-MAS NMR spectra were recorded at 75.5 MHz in the temperature range 25 to 70 ºC. A Bruker AMX-300 NMR instrument equipped with a CP-MAS accessory and a variable-temperature unit was used with the sample held a minimum of 10 min at each temperature previous to spectral acquisition. A sample of 200 mg weight was spun at 4.1-4.2 kHz in a cylindrical ceramic rotor. All the spectra were acquired with contact and repetition times of 2 ms and 5 s, respectively, and about 2048 transients were accumulated. The spectral width was 31.2 kHz, and the number of data points was 4K. Chemical shifts were externally calibrated against the carbonyl peak of glycine appearing at 176 ppm relative to TMS. For transmission electron microscope (TEM) studies, samples were embedded in epoxy resin, sectioned with a Leica EM UC7 cryo-ultramicrotome and gold sections were stained with uranyl acetate and observed on a Zeiss 922 Omega instrument. This study was carried out in the Macromolecular Chemistry II group of Bayreuth University (Germany).

2.2.4. Modeling and simulation

All the simulations have been carried using the TINKER package[21-23] and the MM3 force-field[24] was used for all the systems under study. Since the main focus is on the crystallization of the surfactant moieties and it is known that it occurs with hardly detectable changes in the structure of the polypeptidic sheets, the atomic positions of the PGGA chains have been kept fixed during the simulations. To model the 18ATMA·PGGA and 18ACh·PGGA complexes, a periodic box ($a \times b \times c$) containing 6 chains, each one comprised of 17 repeat units, has been considered; in such box, polymer chains are oriented along the *c*-axis direction and arranged in sheets normal to the *b*-axis direction, i.e., the PGGA chains are side-by-side aligned along the *a*-axis. Box dimensions have been chosen to be in agreement with the experimental values found by SAXS for the separation between sheets and the *c* dimension was made to correspond to the 17/5 helical period. The *a* value was inferred making use of the experimentally estimated densities which were 1.1 and 1.09 mL^{-1} for 18ATMA·PGGA and 18ACh·PGGA, respectively. Thus the following box dimensions were fixed as 7.18 nm × 3.80 nm × 2.56 nm for 18ATMA·PGGA and 7.18 nm × 4.10 nm × 2.56 nm for 18ACh·PGGA.

2.3. Results and discussion

2.3.1. Synthesis of *n*ACh·PGGA complexes

The synthesis of the choline based ammonium surfactants was a task exempted of significant difficulty. All the *n*ACh·I compounds were obtained in good yields as powdered solids displaying melting temperatures above 80 ºC. The chemical constitution and purity of all these compounds were assessed by NMR. A brief account of the basic thermal properties of *n*ACh·I is provided in the Supporting Information (SI) material associated to this chapter.

Table 1. Synthesis data of *n*ACh·PGGA ionic complexes.

*n*ACh·PGGA	T^a(ºC)	Yield (%)	*n*ACh:PGGA[b]
12ACh·PGGA	40	72	1.03:1
14ACh·PGGA	40	82	1.02:1
16ACh·PGGA	60	87	1.05:1
18ACh·PGGA	80	85	1.16:1
18*c*ACh·PGGA	40	80	1.15:1

[a]Mixing temperature
[b]Alkoylcholine to PGGA ratio determined ^{1}H NMR.

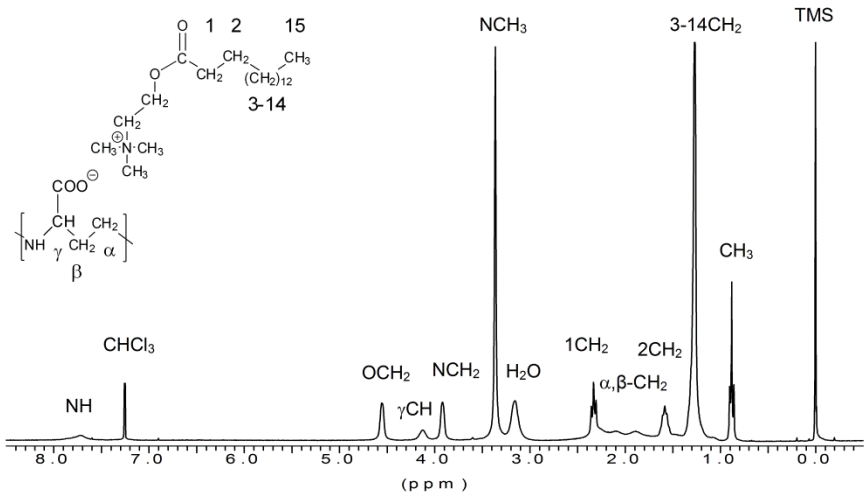

Figure 2. ^{1}H NMR spectrum of 16ACh·PGGA with indication of peak assignments.

The *n*ACh·PGGA complexes were readily obtained by precipitation upon mixing the aqueous solutions of the two components. In order to minimize the excess of surfactant in the complexes, the mixing temperature had to be carefully selected. As it is shown in Table 1, the complexes were obtained in yields around 80% and with nearly stoichiometric compositions. The ACh to PGGA ratio present in the complexes was accurately determined by ^{1}H-NMR making use of the ratios of α-CH2 (PGGA) to *N*-CH2 (*n*ACh) signal areas observed in these spectra. For illustration, the ^{1}H-NMR spectrum of 16ACh·PGGA with full assignment of peaks is depicted in Figure 2 and the spectra of the whole set of complexes are compared in the associated SI material. The *n*ACh·PGGA complexes were non-soluble in water but readily soluble in organic solvents such as chloroform, methanol or hexafluoroisopropanol. Although markedly hygroscopic they could be handled at ease and appeared fairly stable when stored in desiccators for long periods of time.

2.3.2. Thermal properties

The thermal behavior of *n*ACh·PGGA complexes was examined by TGA and DSC and the data afforded by these analyses are collected in Table 2. The TGA traces recorded from the whole set of complexes are compared in Figure 3a and their derivative curves showing the maximum decomposition rate peaks are depicted in Figure 3b. All complexes lost between 5 and 8% of water upon heating at temperatures around 100 ºC which can be taken as an approximate indication of their moisture content. Thermal decomposition started at temperatures within the 190-220 ºC range with values increasing with the value of n. The decomposition process was found to occur in two well differentiated stages with maximum decomposition rates at temperatures located in the 245-280 ºC and 320-340 ºC ranges, respectively, with values within each interval steadily increasing without exception with the length of the alkanoyl side chain. Most of weight loss took place in the low temperature stage (>80%) whereas only about 10% was lost in the second stage.

A combined TGA/NMR study of the thermal decomposition of complexes made of alkyltrimethylammonium surfactants and PGGA has been recently reported.[25] These complexes also decompose in two stages taking place at similar temperatures and involving weight losses similar to those observed for the choline complexes. Cyclodepolymerization of the main chain together with decomposition of the ionic complex were the processes found to occur in the

Table 2. Thermal parameters of *n*ACh·PGGA ionic complexes.

*n*ACh·PGGA	TGA			DSC							
				1st Heating			2nd Heating			Cooling	
	$^{o}T_d$[a] (ºC)	T_d[b] (ºC)	W[c] (%)	$^{1}T_m$ (ºC)	$^{1}\Delta H_m$ (Kcal·mol^{-1})	$^{1}n_c$[d]	$^{2}T_m$ (ºC)	$^{2}\Delta H_m$ (Kcal·mol^{-1})	$^{2}n_c$[d]	T_c (ºC)	ΔH_c (Kcal·mol^{-1})
12ACh·PGGA	189	247/323	14/6	--	--	--	--	--	--	--	--
14ACh·PGGA	191	268/322	12/3	43	3.8	4.9	5	1.0	1.2	1	0.8
16ACh·PGGA	207	275/329	13/3	53	4.9	6.3	29	2.6	3.1	24	2.8
18ACh·PGGA	221	281/340	16/4	64	6.9	8.9	49	4.4	5.2	41	4.6
18*c*ACh·PGGA	189	280/342	18/4	--	-	--	--	--	--	--	--

[a]Onset decomposition temperature calculated by the tangent method.
[b]Maximum rate decomposition temperatures for the two stages.
[c]Remaining weight at the end of each step.
[d]Number of crystallized methylenes in the paraffinic phase.

first stage whereas partial decomposition of the quaternary alkyltrimethylammonium hydroxide produced in the first stage took place inthe second stage with generation of alkyl and alkylenamines. Given the close similitude of these complexes in both chemical structure and TGA behavior with the *n*ACh·PGGA here studied, a similar mechanism can be reasonably assumed to occur in the thermal decomposition of the two families.

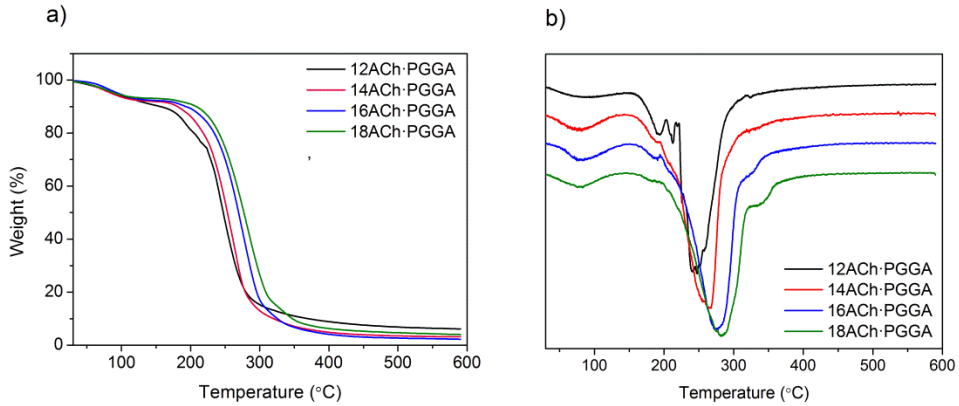

Figure 3. Compared TGA traces of *n*ACh·PGGA series a), and their derivative curves b).

The DSC analysis of the *n*ACh·PGGA complexes made of saturated fatty acids revealed that they are semicrystalline for n values of 14, 16 and 18. In fact, the heating DSC traces recorded from pristine samples of these complexes displayed characteristic melting peaks at temperatures of 43, 53 and 64 ºC, respectively (Figure 4a). By analogy with other comb-like systems consisting of a polypeptidic main chain with attached alkyl side chains,[16] such peaks are interpreted as arising from the melting of the polymethylene segments that crystallized in a separate paraffinic phase. Both melting temperature and enthalpy increased with the length of the alkanoyl group as it could be expected given the dependence of crystal size and perfection on the length of the crystallizing segment. Conversely, no endothermic peak was detected in the DSC trace of 12ACh·PGGA; apparently, the polymethylene segment in this complex is not long enough to form stable crystallites.

All the crystalline *n*ACh·PGGA complexes were able to recrystallize after melting. For illustration, the first and second heating DSC scans registered from a film of 18ACh·PGGA that was initially obtained by casting from chloroform are shown in Figure 4b. Most of the molten material crystallized at small supercooling (less than 10 ºC) whereas a minor amount did it at much

lower temperature. The position and shape of the endothermic peak appearing in the second heating trace are very similar to those of the melting peak observed at the first heating although the enthalpy diminished appreciably. Much the same behavior was displayed by powdered samples coming from precipitation when they were examined by DSC although in these cases the recrystallized material melted at significant lower temperature than the original one. Crystallization and melting data of the three complexes are compared in Table 2 indicating that only 60% of the initially crystallized material could be recovered in the best case.

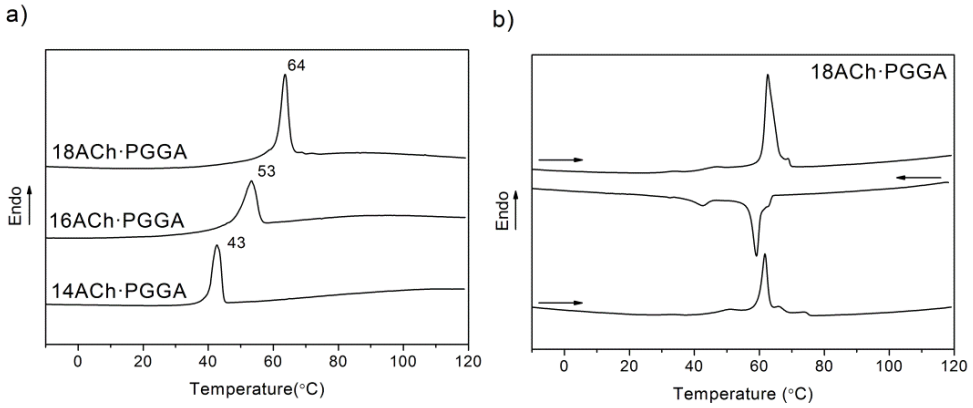

Figure 4. a) First heating traces of *n*ACh·PGGA for n = 14, 16 and 18. b) DSC heating and cooling traces of a film of 18ACh·PGGA.

The melting enthalpy of *n*ACh·PGGA complexes measured by DSC may be used to estimate the fraction of methylene units participating in the crystalline part of the paraffinic phase provided that data for various alkyl chain lengths are available.[26] An almost linear correlation of enthalpy against alkyl chain length is usually found across short ranges of n values according to the equation $\Delta H_m=\Delta H_{end}+nk$, where ΔH_{end} and k are constants reflecting the contribution made to the heat of fusion by the chain ends and by each added methylene unit, respectively. When ΔHm obtained for the *n*ACh·PGGA complexes were plotted against n, a nearly straight line with a slope of 0.8 kcal·mol^{-1}·CH2^{-1} was found for both first and second heating traces (Figure 5).

Such value of k corresponds to a pseudohexagonal arrangement of polymethylene chains rather than to the rhombic or triclinic phases described for polyethylene, which is about 1 Kcal·mol^{-1}. The result is in accordance with other closely related comb-like systems like poly(α-alkyl γ-glutamate)s[27] and

ionic complexes made of tetralkylammonium surfactants and poly(γ-glutamic acid).[16] Furthermore, the number of crystallized methylenes (n_c) for each complex may be determined by subtracting to n the minimum number of methylenes required for crystallization, which is estimated by making $\Delta H_m = 0$ in the ΔH_m vs n plot.

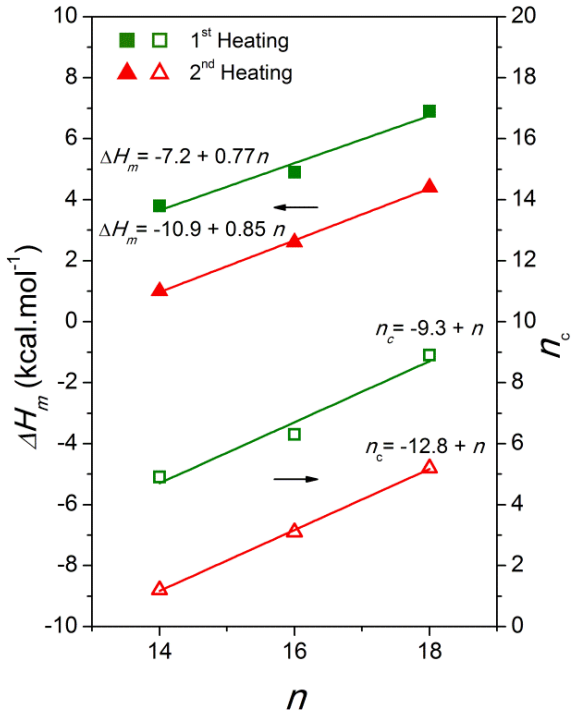

Figure 5. Melting enthalpy, ΔHm (left) and number of crystallized methylenes (nc) against the number of carbons contained in the alkanoyl side group of *n*ACh·PGGA.

The resulting values for pristine complexes samples and for those crystallized from the melt are compared in Table 2. Noticeable points regarding the n_c values are the following:

a) Values obtained for samples crystallized from the melt are considerable smaller than for pristine samples but they show a similar linear trend with a comparable slope; this indicates that although a less order was attained in the paraffinic phase after melting, the same packing pattern was taken up by the polymethylene chains in both cases.

b) Compared to nc values reported for PGGA complexes with alkyltrimethylammoniumcations (0, 2 and 4 for n = 14, 16, 18),[16] a higher number of methylene units were able to crystallize in the case of choline based complexes. Apparently, it is the relatively high flexible ethylenoxycarbonyl group that provides the polymethylene chain with greater mobility and makes easier its crystallizability. The modeling study described below gives support to this interpretation.

2.3.3. Self-assembled nanostructure of *n*ACh·PGGA complexes

The SAXS and WAXS profiles recorded from *n*ACh·PGGA complexes are depicted in Figure 6 and data obtained therefrom are listed in Table 3. All SAXS profiles displayed a sharp peak located within the 3-5 nm interval with a spacing that increased steadily with the number of carbons in the alkanoyl side chain except in the case of 12ACh·PGGA. According to well established antecedents on related comb-like complexes, the observed spacing is associated to the periodical distance L_0 of a layered structure made of alternating paraffinic and polypeptidic phases. Whereas this peak is unique for n = 16 and 18, a second broader peak with a slightly larger spacing is observed for n =14. The presence of this second peak implies the occurrence of a second periodicity in the structure that could be associated to that fraction of material in which the paraffinic phase is fully disordered. The WAXS profiles of complexes for n = 14, 16 and 18 displayed a sharp peak characteristic of crystalline scattering with a spacing of 0.41-0.42 nm. This spacing arises from the 100 interplanar distance of the hexagonal lattice in which the polymethylene side segments are crystallized. The absence of this sharp peak and the presence instead of a broad one in the 12ACh·PGGA indicates that, according to DSC data, the alkyl chains remains completely uncrystallized in this complex. The incapacity of the dodecanoyl group to crystallize would explain the deviation in the L_0 value observed for this complex; a different mesophase probably consisting of a spherical micellar structure could be adopted in such case but this issue has not been further investigated in this work.

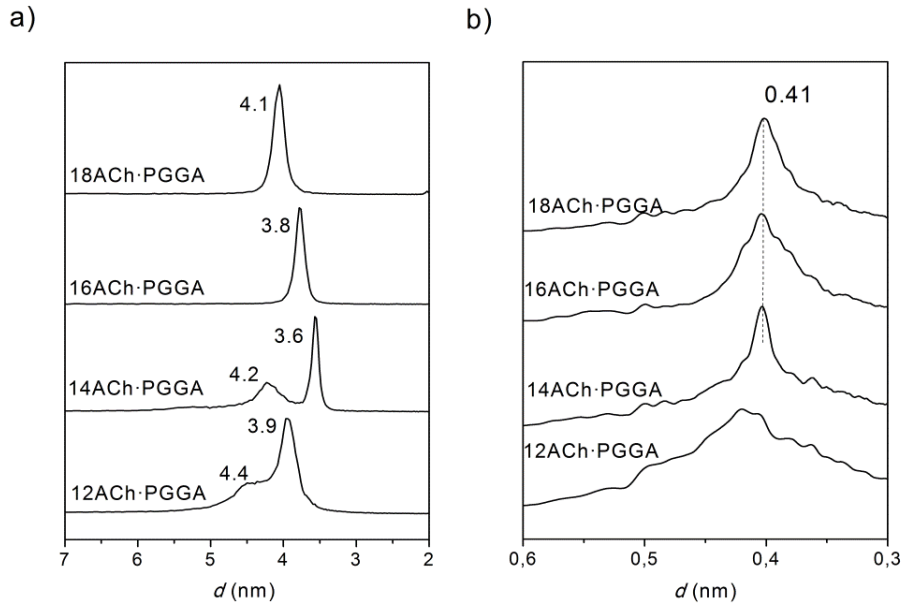

Figure 6. SAXS a) and WAXS b) profiles of *n*ACh·PGGA complexes series at 10 ºC.

Table 3. X-Ray diffraction data of *n*ACh·PGGAcomplexes.[a]

*n*ACh·PGGA	SAXS				WAXS		
	$L_0^{10\ ºC}$	L_0^{Tm}	$L_0^{120\ ºC}$	$L_0^{10\ ºC}$	$d_{100}^{10ºC}$	d_{100}^{Tm}	$d_{100}^{10ºC}$
12ACh·PGGA	3.9 4.4	--	3.7	3.6 4.0	0.44	0.44	0.44
14ACh·PGGA	3.6 4.2	3.9 4.1	3.5	3.6	0.41	0.45	0.41
16ACh·PGGA	3.8	4.0 4.4	3.7	3.8	0.41	0.45	0.41
18ACh·PGGA	4.1	4.3	4.1	4.1	0.41	0.45	0.41

[a] L_0 (lamellar space) and d_{100} (interplanar space) measured at 10 ºC (at both heating and cooling), at the melting temperature and at 120 ºC.

The lamellar structure inferred from DSC and XRD data was visualized by TEM. Micrographs taken at room temperature from a18ACh·PGGA film obtained by casting before and after heating to 120 ºC are shown in Figure 7. The periodical structure adopted by the complex was faintly detected in the initial film but it became much more clearly evidenced after thermal treatment;

not only the periodicity appeared sharper defined but the layered texture spread over the whole visualized area. It is apparent that the thermal treatment not only improved the lamellar order of the structure but also induced an orientation rearrangement of the layers with subsequent increasing in the size of the monocrystalline domains. Nevertheless the measured spacing periodicity is in both cases about 4 nm in agreement with the L_0 spacing afforded by SAXS. It should be noticed that differences in the L_0 spacing that could be eventually caused by thermal treatment are expected to be too small as to be able of being detected by this technique.

A simultaneous SAXS/WAXS analysis of complexes subjected at variable temperature over the 10-120 ºC range was carried out in real time using synchrotron radiation. Data obtained from this study supported the conclusions derived from the previous DSC study, and also afforded new insights on the melting-crystallization process taking place in the biphasic layered structure of the complexes upon heating and cooling across the transition temperature. The evolution of the SAXS and WAXS profiles of 18ACh·PGGA complex along the heating-cooling cycle is displayed in Figure 8, and all the other similar plots recorded for the whole set of complexes studied in this work are provided in the SI part at the end of this chapter. Variations in both long and short spacings measured along these experiments are listed in Table 3.

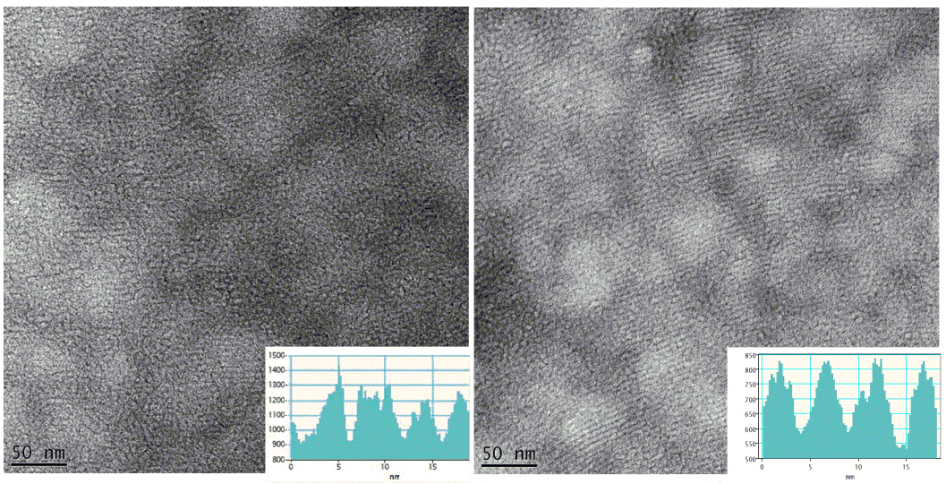

Figure 7. TEM images of a 18ACh·PGGA film obtained by casting. a) As prepared, and b) after heating to 120 ºC and cooling to room temperature at 10 ºC·min-1. Insets: Optical density profiles showing the structural periodicity present in each case.

The SAXS plots shown in Figure 8a evidence vividly the occurrence of a well-defined periodicity whose spacing increased upon heating at 60-65 ºC to keep them essentially unaltered up to temperatures above 100 ºC. At cooling the process was reverted displaying contraction of the structure at 40-50 ºC so that the initially observed spacing was finally reached. WAXS plots displayed in Figure 8b show the disappearance of the 0.41nm peak at melting at the same time that a broad scattering centered on 0.45 nm emerged. This change is indicative of the melting of the paraffinic hexagonal lattice into a partially disordered structure in which chains become separated by an average distance of 0.45 nm. The whole sequence of observations is interpreted as the manifestation of a reversible melting-crystallization process that concerns exclusively to the paraffinic phase and that only entails slight displacements of the polypeptidic sheets.

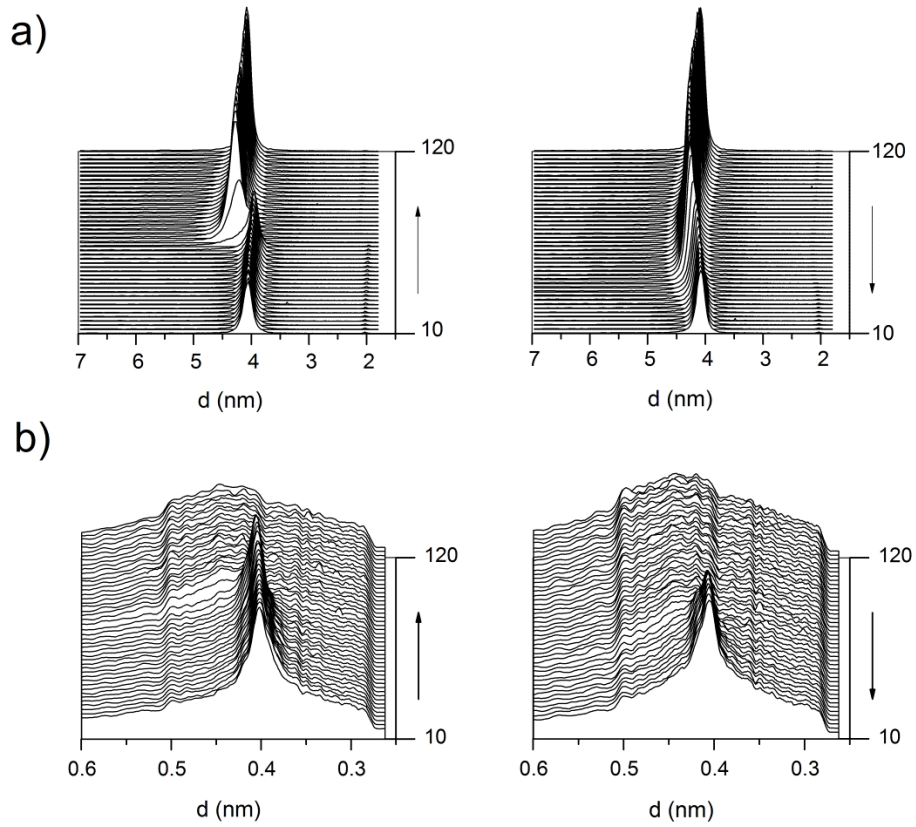

Figure 8. Evolution of SAXS a) and WAXS b) profiles of 18ACh·PGGA with temperature at heating and cooling.

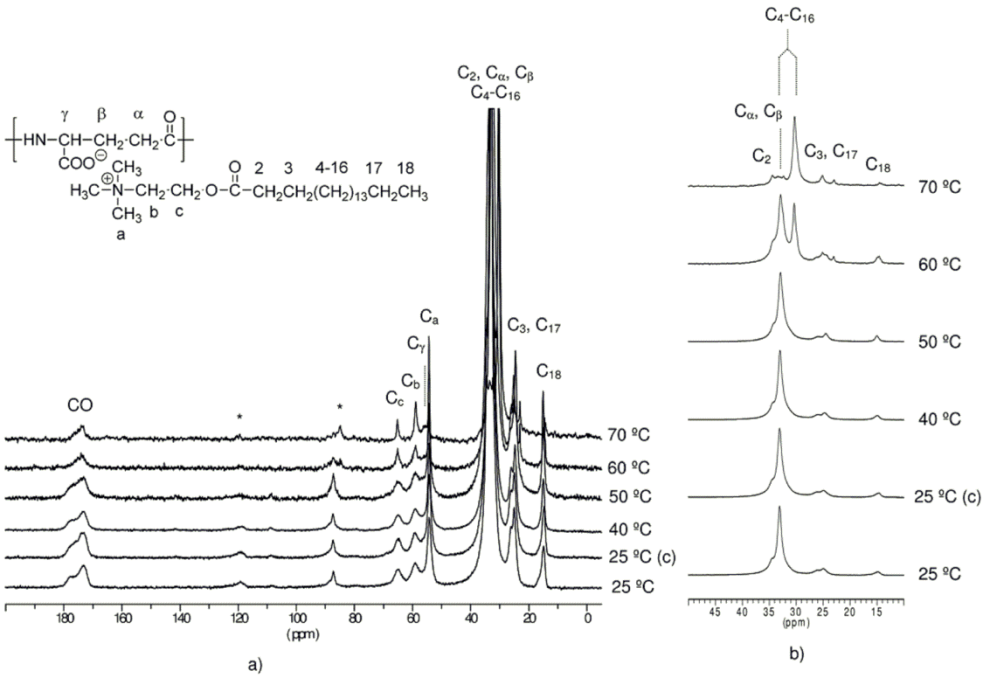

Figure 9. ^{13}C CP/MAS NMR spectra of 18ACh·PGGA at variable temperature. a) Whole spectral region. b) Inner methylenes region showing peak splitting and merging as a function of temperature.

A remarkable fact is the increasing intensity and sharpness exhibited by the peak seen in the SAXS profiles when the complex is heated above the melting temperature, which is indicative of the improved ordering attained in the layer structure; it could be inferred from this fact that melting of the paraffinic phase allows for a more precise regular assembling of the polypeptidic layers. It is known that melting of the alkyl side chains in comb-like systems usually occurs without losing the positions they had in the crystallized phase but implying only a slight conformational anti-to-gauche change;[28] such unusual behavior would be due to the spatial constraint imposed by the confining polypeptidic sheets and would explain the L_0increasing observed at melting and the ready reversibility exhibited by the melting-crystallization process. In order to corroborate that this mechanism is also operating in the *n*ACh·PGGA complexes, a solid-state ^{13}C CP/MAS NMR analysis was carried out at variable temperature. Figure 9 shows the evolution of the spectrum of 18ACh·PGGA along heating from 25 to 80 ºC and after cooling to the initial temperature. In these spectra the main chain carbon signals are partially overlapping with those arising from side chain ones (Figure 9a). Nevertheless the signals due to the inner side chain methylenes

(C4-C16) at 25 ºC appear differentiated enough as to be useful for the conformational analysis of the polymethylene segment (Figure 9b). At 25 ºC, this signal appeared at 33.1 ppm, which is indicative that the methylenes are arranged in all-anti conformation according to what should be expected from a crystallized state.[26] When the sample was heated at 60 ºC a new peak emerged at 30.4 ppm. This peak was associated to a fraction of methylenes involved in an anti-to-gauche fast equilibrium. At 70 ºC the 33.1 ppm peak vanished and only the high field peak was present indicating that all themethylenes in the side chains were in an interconversional state. In agreement with DSC data such conformational changes are concomitants to the melting of the alkyl side chains that happens at the surroundings of 60 ºC. The reversibility of the melting-crystallization process was assessed at cooling; in fact the spectrum recorded at 25 ºC (spectrum c in Figure 9b) was almost identical to that obtained from the untreated sample.

2.3.4. Modeling of 18ATMA·PGGA and 18ACh·PGGA complexes

A comparative modeling study of 18ATMA·PGGA and 18ACh·PGGA complexes has been performed by means of molecular dynamics simulations. The objective is to simulate the crystallization of the surfactant moiety in order to assess the differences in the degree of order attained by the paraffinic phase in each type of complexes such as they were evidenced by DSC and SAXS/WAXS.

In order to get a reasonable description of the structure of the systems under study, the following approach has been adopted. First, an initial geometry was generated with all the side chains in the complex in a fully crystallized state and oriented normally to the polypeptidic sheets. Next, the geometry was subjected to molecular dynamics at a high temperature (1000 K) to allow the side chains to relax, while the polypeptide chains were kept fixed in their initial positions. Afterwards, the temperature was decreased to 298 K, and the geometry was minimized before running a long molecular dynamics trajectory of 12,000 ps with polymer main chains also kept fixed.

2.3.5. Helical conformation for PGGA chains

The two helical models, a left-handed 17/5 helix and a right-handed 5/2 helix, proposed in previous works for benzyl[29] and alkyl[30] esters of poly(γ-glutamic acid) respectively, have been initially considered to describe the geometry of

the PGGA main chain in the complexes. A third helical model consisting of a 37/10 helix was also proposed but it has been discarded in this study because its extremely close conformational similitude with the 17/5 helix. The geometry optimization of the two considered models when used for representing the PGGA chain ionically coupled to the ammonium surfactant revealed only small conformational deviations with changes in torsional angles less than 15% (see SI). Therefore both helices appeared in principle suitable for building the complex model. Preliminary calculations using a small box showed however that the 17/5 helix was clearly more stable than the 5/2 helix for both *n*ACh·PGGA and *n*ATMA·PGGA complexes, and consequently only the former was finally considered for carrying out complexes modeling and calculations.

2.3.6. Alignment and conformation of the side chains

First of all, the arrangement of the long tails attached to the ammonium moieties in the intersheet space was evaluated in terms of the intermolecular radial distribution (defined as the probability to find a pair of carbon atoms at a given distance from the confining sheets). The radial distribution function obtained for the 18ACh·PGGA complex showed sharp peaks indicative of a partially crystallized arrangement of the polymethylene segments. A similar multi-peak function resulted for the 18ATMA·PGGA complex, although in this case peaks appeared much broader than for the 18ACh·PGGA complex and they tended to merge as the distance from the sheet increased. These results indicate that the polymethylene segments of the side chains are partially crystallized in the two complexes but in a considerable higher degree in the case of the choline containing complex. The comparative representation of the two functions is provided in the SI part at the end of this chapter. The molecular order attained in the intersheet space can be also evaluated in terms of the density profile of the different groups (ammonium, methylene and methyl) present in the side chains as a function of their distance to the sheets. As it is depicted in Figure 10, although the methylene groups show a very structured distribution along the intersheet distance in both complexes, a more clearly pronounced layering is observed for 18ACh·PGGA, in agreement with the higher degree of crystallinity experimentally found for this system. This feature is also reflected in the profiles of the methyl end groups; although in both cases, they tend to concentrate laterally in accordance with a more or less extended conformation for the side chains, such a trend is much more apparent in the case of the choline based complex.

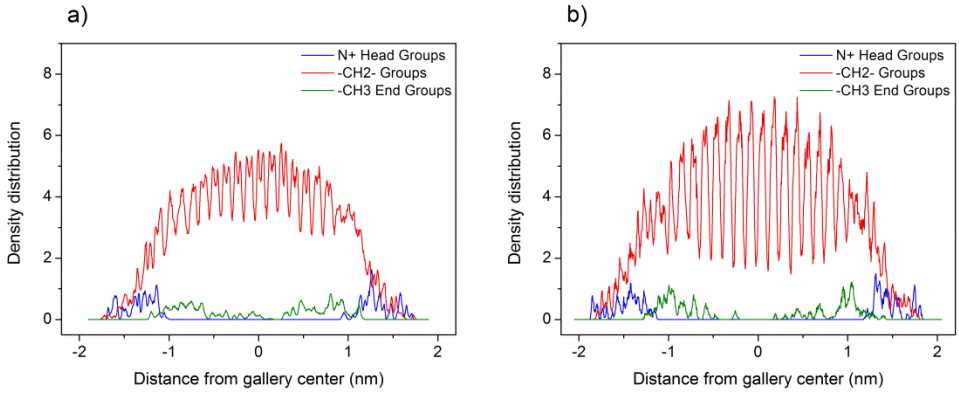

Figure.10. Density profile of ammonium (blue), methylene (red) and methyl groups (green) as a function of the distance from the inter-sheet distance center for the 18ATMA·PGGA (left) and 18ACh·PGGA (right) complexes.

A more precise detailed description of the arrangement of the side chains in the intersheet space of the complexes was provided by the conformational analysis in terms of the frequency in which the staggered anti arrangement appears in the polymethylene segment. More specifically, the fraction of bonds in *anti* conformation has been evaluated and compared for the dihedral angles along the long side chains in both 18ACh·PGGA and 18ATMA·PGGA complexes. For the 18ACh·PGGA complex, a remarkable fraction of the side chains presents a nearly all-anti conformation (close to 90% for bonds 11 to 18), while for the 18ATMA·PGGA complex both the total fraction of bonds in *anti* conformation and the length of the all-anti segment were significantly smaller (close to 90% for bonds 11 to 13). It is also worth noting that the ethylene unit joining the ammonium and carboxylate groups in the choline unit appeared almost entirely in gauche conformation; it is reasonable to infer therefore that it is the ethylenoxycarbonyl group that allows a high mobility of the alkyl tail and facilitates it to attain the extended conformation required for close packing and crystallization.

The alignment of the side chains in the intersheet space was quantified by analyzing the tilt angle distribution as well as the orientation order parameter for the vector Z connecting two alternating atoms in the side chain. The tilt angle θ is defined as the angle between the Z vector and the normal to the PGGA sheets,[31-33] and the orientation parameter, as described by Leach,[34] is defined by the expression,

$$S_{zz} = \frac{1}{2}\left\langle 3\cos^2\theta - 1 \right\rangle$$

which may take values from 1 to 0 for the Z orientation going from perpendicular to the sheets to a random distribution; the value of -0.5 would correspond to Z oriented parallel to the sheet surface. The plots of tilt angle and orientation parameter against the position of the carbon atoms along the side chain are shown in Figure 11 where the carbon numbering is that indicated in Scheme I. The tilt angle distribution shows the same trends as the anti conformation indicating that this arrangement is associated with the perpendicular orientation of the polymethylene segment to the PGGA sheets. The distribution function obtained for the order parameter confirms this picture; in fact, parameter values near to 1 were obtained for the 9-to-18 polymethylene segment in the case of 18ACh·PGGA complex and for the 11-to-14 in 18ATMA·PGGA whereas they approach to zero in both cases as the atoms are located closer to the sheet.

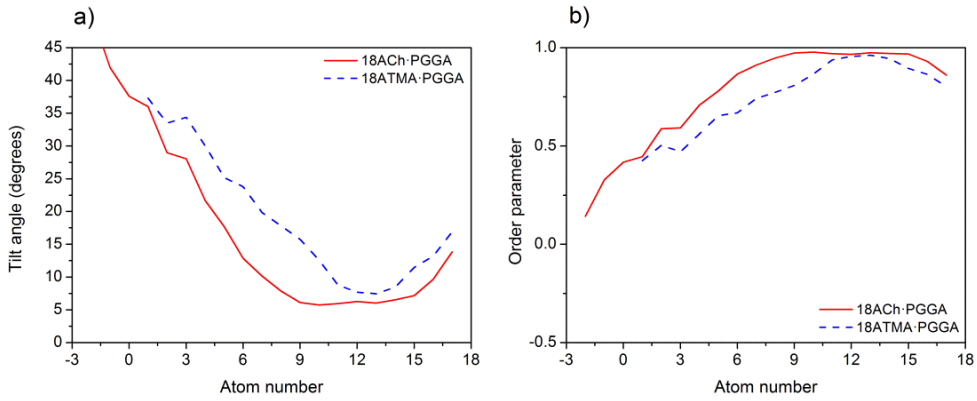

Figure 11. Tilt angle (left) and order parameter distribution (right) of alkyl side chains as a function of bond angle number for 18Ach·PGGA (red solid line) and 18ATMA·PGGA (blue dashed line) complexes. Each i-th tilt angle is computed between the (i-1)th and the (i+1)th CH2 unit according to the numbering indicated in Scheme I.

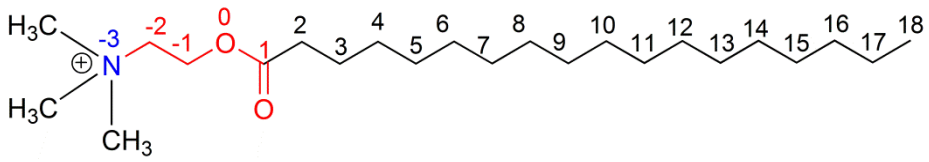

Scheme I. Depiction of the numbering of atoms in the side chains used to compute the tilt angle and order parameter distributions in the 18ACh·PGGA and 18ATMA·PGGA complexes. In red, atoms of the ethylenoxycarbonyl group of choline.

The structures resulting after crystallization of the side chains of the 18ACh·PGGA and 18ATMA·PGGA complexes are compared in Figure 12. Both models are projected along the c-axis so that the ab plane of the structure is laying normal to the view. The PGGA chains in 17/5 helical conformation were aligned side-by-side along the a-axis and arranged in antiparallel to generate the polypeptidic sheet. In both complexes the long alkyl chains protrude from the sheet with an almost perpendicular orientation to become interdigitated with those belonging to the neighboring sheet. The projected chain-to-chain distance is about 0.4 nm corresponding to the 100 interplanar distance of the pseudohexagonalpolymethylene lattice and indicating that this lattice is oriented with the plane 110 normal to the c-axis of the structure. A close comparative inspection of the two models revealed that a higher order is achieved by the paraffinic phase of the 18ACh·PGGA complex which is evidenced by the better alignment that the methylene units attain when viewed along down the c-axis. Furthermore, the randomized interphase jointing the alkyl tails to the polypeptide helices extents broader for the 18ACh·PGGA complex due to the presence of the additional ethylenoxycarbonyl unit that remains uncrystallized. Although these models are able to differentiate the crystallinity degree that is achieved by the two complexes, they fail in giving a precise picture of the distribution of the crystallized domains throughout the structure. Nevertheless the higher melting temperature displayed by *n*ACh·PGGA respect to the *n*ATMA·PGGA (about 15 ºC for n = 18) strongly suggests that a higher number of methylene units are crystallized along the b-axis rather than along the a-axis in the first case, as it was rightly revealed by the tilt angle and the order parameters functions discussed above.

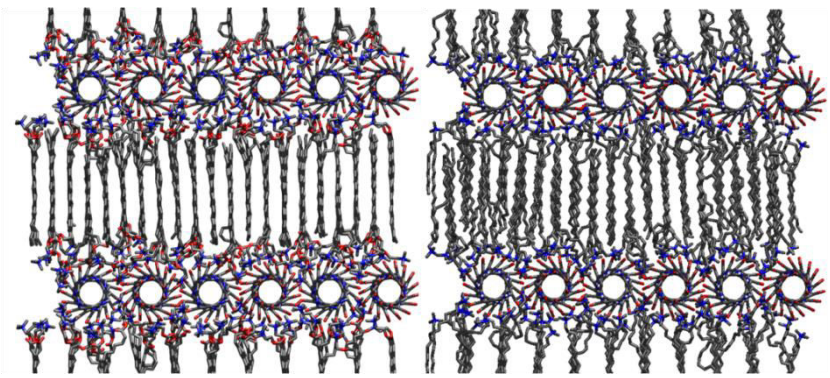

Figure 12. Schematic view of the antiparallel model of 18ACh·PGGA (left) and 18ATMA·PGGA (right) complexes projected along the c-axis. Hydrogens are not represented.

2.4. Conclusions

Almost stoichiometric ionic complexes of poly(γ-glutamic acid) and choline surfactants bearing long fatty alkanoyl chains have been prepared and characterized. The complexes are stable up to temperatures close to 200 ºC and soluble in organic solvents. In the solid state they adopt an extremely well-defined structure made of alternating polypeptidic and paraffinic layers with the choline unit interlocking the two phases. The complexes containing miristoyl (C14), palmitoyl (C16) and stearoyl (C18) groups display melting-crystallization of the alkyl tails within the 40-70 ºC range with slight changes in the overall arrangement of the layered structure; a rapid fully-reversible anti-to-gauche interconversion of the polymethylene segments is the only apparent change taking place at the thermal transition. The order degree achieved by the paraffinic phase in these complexes is considerably higher than that observed for previously reported complexes made of tetralkylammonium surfactants, which is due to the enhancing effect that the choline structure exerts on the mobility of the alkyl chains.

To our knowledge it is the first time that a polyelectrolyte/surfactant comb-like complex entirely made of bio-based components is reported. The extremely easy preparation of the complexes combined with their unique bio-characteristics and their amphiphilic nanostructure make these compounds outstanding candidates for building bioactive materials of potential utility in diverse biomedical applications.

2.5. References

1. Faul, C. F. J.; Antonietti, M. Ionic Self-Assembly: Facile synthesis of supramolecular materials. *Adv. Mater.* **2003**, *15*, 673–683.

2. Antonietti, M.; Conrad, J.; Thünemann, A. Polyelectrolyte-surfactant complexes: A new type of solid, mesomorphous material. *Macromolecules* **1994**, *27*, 6007–6011.

3. Hayakawa, K.; Santerre, J. P.; Kwak, J. C. T. Study of surfactant poly-electrolyte interactions – Binding of dodecyltrimethylammonium and tetradecyltrimethylammonium bromide by some carboxylic poly-electrolytes. *Macromolecules* **1983**, *16*, 1642-1645.

4. Thünemann, A. F. Polyelectrolyte – surfactant complexes (synthesis, structure and materials aspects). *Progr. Polym. Sci.* **2002**, *27*, 1473–1572.

5. Ponomarenko, E. A.; Waddon, A. J.; Bakeev, K. N.; Tirrell, D. A.; Macknight, W. J. Self-assembled complexes of synthetic polypeptides and oppositely charged low molecular weight surfactants. Solid-state properties. *Macromolecules* **1996**, *29*, 4340-4345.

6. Ponomarenko, E. A.; Waddon, A. J.; Tirrell, D. A.; Macknight, W. J. Structure and properties of stoichiometric complexes formed by sodium poly (α,L-glutamate) and oppositely charged surfactants. *Langmuir* **1996**, *12*, 2169–2172.

7. Ponomarenko, E. A.; Tirrell, D. A.; Macknight, W. J. Stoichiometric complexes of synthetic polypeptides and oppositely charged surfactants in organic solvents and in the solid state. *Macromolecules* **1996**, *29*, 8751–8758.

8. Kodona, E. K.; Alexopoulos, C.; Panou, E.; Pomonis, P. J. Self-organized meso- and hybridic phases of poly(aspartic acid) and poly(glutamic amino acid) with cationic surfactants (C(*n*)TAB, n= 14, 16) and a silica source (TEOS). *Chem. Mater.* **2007**, *19*, 1853-1861.

9. Kodona, E. K.; Alexopoulos, C.; Panou-Pomonis, E.; Pomonis, P. J. Chirality and helix stability of polyglutamic acid enantiomers. *J. Colloid Interface Sci.* **2008**, *319*, 72-80.

10. Muñoz-Guerra, S.; García-Alvarez, M.; Portilla-Arias, J. A. Chemical modification of microbial poly(γ-glutamic acid): Progress and perspectives. *J. Renew. Mater.* **2013**, *1*, 42–60.

11. Richard, A.; Margaritis, A. Poly(glutamic acid) for biomedical applications. *Crit. Rev. Biotechnol.* **2001**, *21*, 219–232.

12. Sung, M.-H.; Park, C.; Kim, C.-J.; Poo, H.; Soda, K.; Ashiuchi, M. Natural and edible biopolymer poly-gamma-glutamic acid: synthesis, production, and applications. *Chem. Rec.* **2005**, *5*, 352–366.

13. Buescher, J. M.; Margaritis, A. Microbial biosynthesis of polyglutamic acid biopolymer and applications in the biopharmaceutical, biomedical and food industries. *Crit. Rev. Biotechnol*. **2007**, *27*, 1–19.

14. (a) Mi, F. L.; Wu, Y.Y.; Lin, Y. H.; Sonaje, K.; Ho, Y. C.; Chen, C. T.; Juang, J. H.; Sung, H. W. Oral delivery of peptide drugs using nanoparticles self-assembled by poly(γ-glutamic acid) and a chitosan derivative functionalized by trimethylation. *Bioconjug. Chem.* **2008**, *19*, 1248-1255. (b) Peng, S. F.; Yang, M. J.; Su, C. J.; Chen, H. L.; Lee, P. W.; Wei, M. C.; Sung, H. W. Effects of incorporation of poly(γ-glutamic acid) in chitosan/DNA complex nanoparticles on cellular uptake and transfection efficiency. *Biomaterials* **2009**, *30*, 1797-1808. (c) Sonaje, K.; Chen, Y. J.; Chen, H. L.; Wey, S. P.; Juang, J. H.; Nguyen, H. N.; Hsu, C.W.; Lin, K. J.; Sung, H. W. Enteric-coated capsules filled with freeze-dried chitosan/poly(γ-glutamic acid) nanoparticles for oral insulin delivery. *Biomaterials* **2010***, 31*, 3384-3394. (d) Tang, D. W.; Yu, S. H.; Ho, Y. C.; Mi, F. L.; Kuo, P. L.; Sung, H. W. Heparinized chitosan/poly(γ-glutamic acid) nanoparticles for multifunctional delivery of fibroblast growth factor and heparin. *Biomaterials* **2010**, *31*, 9320-9332. (e) Peng, S. F.; Tseng, M. T.; Ho, Y. C.; Wei, M. C.; Liao, Z. X.; Sung, H. W. Mechanisms of cellular uptake and intracellular trafficking with chitosan/DNA/poly(γ-glutamic acid) complexes as a gene delivery vector. *Biomaterials* **2011**, *32*, 239-248.

15. Akagi, T.; Watanabe, K.; Kim, H.; Akashi, M. Stabilization of polyion complex nanoparticles composed of poly(amino acid) using hydrophobic interactions. *Langmuir* **2010**, *26*, 2406-2413.

16. (a) Pérez-Camero, G.; García-Alvarez, M., Martínez De Ilarduya, A.; Fernández, C., Campos, L., Muñoz-Guerra, S. Comblike complexes of bacterial poly(γ,D-glutamic acid) and cationic surfactants. *Biomacromolecules*. **2004**, *5*, 144–152. (b) García-Alvarez, M.; Alvarez, J.; Alla, A.; Martínez de Ilarduya, A.; Muñoz-Guerra, S. Comb-like ionic complexes of cationic surfactants with bacterial poly(γ-glutamic acid) of racemic composition. *Macromol. Biosci.* **2005**, *5*, 30–38.

17. Portilla-Arias, J. A; García-Alvarez, M.; Martínez de Ilarduya, A.; Muñoz-Guerra, S. Ionic complexes of biosynthetic poly(malic acid) and poly(glutamic acid) as prospective drug-delivery systems. *Macromol. Biosci*. **2007**, *7*, 897–906.

18. (a) Chelminska-Bertilsson, M.; Allenmark, S. Butyrylcholinesterase activity towards long-chain alkanoylcholines- Kinetics and mechanism. *Biochim. Biophys. Acta.* **1993**, *1202*, 56-60. (b) Ahlström, B.; Chelminska-Bertilsson, M.; Thompson, R. A; Edebo, L. Long-chain alkanoylcholines, a new category of soft antimicrobial agents that are enzymatically degradable. *Antimicrob. Agents Chemother.* **1995**, *39*, 50–55.

19. (a) Carelli, V.; Liberatore, F.; Scipione, L.; Cardellini, M.; Rotiroti, D.; Rispoli, V. Choline derivative for the treatment of Alzheimer's disease. US Patent 0166721 A1, 2003. (b) Patel, H. Use of choline derivatives for memory, learning and cognition. US Patent 018631 A1, 2005.

20. (a) Alexander, J.; Fix, J. A. Enhancement of absorption of drugs from gastrointestinal tract using choline ester salts US Patent 4822773, 1989. (b) Alexander, J.; Fix, J. A.; Repta, A. J. Choline esters as absorption-enhancing agents for drug delivery through mucous membranes of the nasal, buccal, sublingual and vaginal cavities US Patent 4963556, 1990.

21. Ponder, J. W.; Richards, F. M. An efficient Newton-like method for molecular mechanics energy minimization of large molecules. *J. Comp. Chem.* **1987**, *8*, 1016-1024.

22. Kundrot, C. E.; Ponder, J. W.; Richards, F. M. Algorithms for calculations excluded volume and its derivatives as a function of molecular-conformation and their use in energy minimization. *J. Comp. Chem.* **1991**, *12*, 402-409.

23. Dudek, M. J.; Ponder, J. W. Accurate modeling of the intramolecular electrostatic energy of proteins. *J. Comp. Chem.* **1995**, *16*, 791-816.

24. Allinger, N. L.; Yuh, Y. H.; Lii, J. H.. Molecular mechanics. The MM3 force-field for hydrocarbons .1. *J. Amer. Chem. Soc.* **1989**, *111*, 8551-8566.

25. Portilla-Arias, J. A.; García-Alvarez, M.; Martínez de Ilarduya, A.; Muñoz-Guerra, S. Thermal decomposition of microbial poly (γ-glutamic acid) and poly γ-glutamate)s. *Polym. Degrad. Stab.* **2007**, *92*, 1916–1924.

26. Jordan, E. F.; Feldeisen, D. W. Side-chain crystallinity. 1. Heats of fusion and melting transitions on selected homopolymers having long side chains. *J. Polym. Sci. A Polym. Chem.* **1971**, *9*, 1835.

27. Morillo, M.; Martinez de Ilarduya, A.; Alla, A.; Muñoz-Guerra, S. Comblike alkyl esters of biosynthetic poly (γ-glutamic acid). 2. Supramolecular structure and thermal transitions. *Macromolecules* **2003**, *36*, 7567–7576.

28. Mathias, L. J. Variable temperature solid-state nuclear magnetic-resonance of side-chain crystalline comb polymers. *Polym. Comm.* **1988**, *29*, 352-354.

29. Melis, J.; Zanuy, D.; Aleman, C.; García-Álvarez, M.; Muñoz-Guerra, S. On the crystal structure of poly(α-benzyl-γ-D,L-glutamate)s. Macromolecules **2002**, *35*, 8774-8780.

30. Curcó, D.; Zanuy, D.; Alemán, C.; Rude, E.; Muñoz-Guerra, S. Comblike poly(α-alkyl γ-glutamate)s: Computer simulation studies of an intermediate termal phase. *Biomacromolecules* **2003**, *4*, 87-95.

31. Zeng, Q. H.; Yu, A. B.; Lu, G.Q.; Standish, R. K. Molecular dynamics simulation of the structural and dynamic properties of dioctadecyldimethyl ammoniums in organoclays. *J. Phys. Chem. B* **2004**, *108*, 10025-10033.

32. Adolf, D. B.; Tildesley, D. J.; Pinches, M. R. S.; Kingdon, J. B.; Madden, T. Molecular-dynamics simulations of dioctadecyldimethylammonium chloride monolayers. *Langmuir* **1995**, *11*, 237-246.

33. Smith, P.; Lynden-Bell, R. M.; Earnshaw, J. C.; Smith, W. The surface-ordered phase of liquid heptadecane: a simulation study. *Mol. Phys.* **1999**, *96*, 249-257.

34. Leach, A. R. In *Molecular modeling: principles and applications*, 1st Edition; Addison-Wesley Longman Ltd: London, 1996.

2.6. Supporting information

SI Table 1. Synthesis data of alkoylcholine iodides.

*n*ACh·I	Yield (%)	T_m[a] (ºC)	T_d[b] (ºC)
12ACh·I	Powder (white)	83/169	197
14ACh·I	Powder (white)	93/164	207
16ACh·I	Crystalline powder (white)	99/163	209
18ACh·I	Crystalline powder (white)	104/161	209

[a] T_m, Melting temperature obtained from DSC from pristine samples.
[b] T_d, Onset decomposition temperature determined from TGA traces by the tangent method.

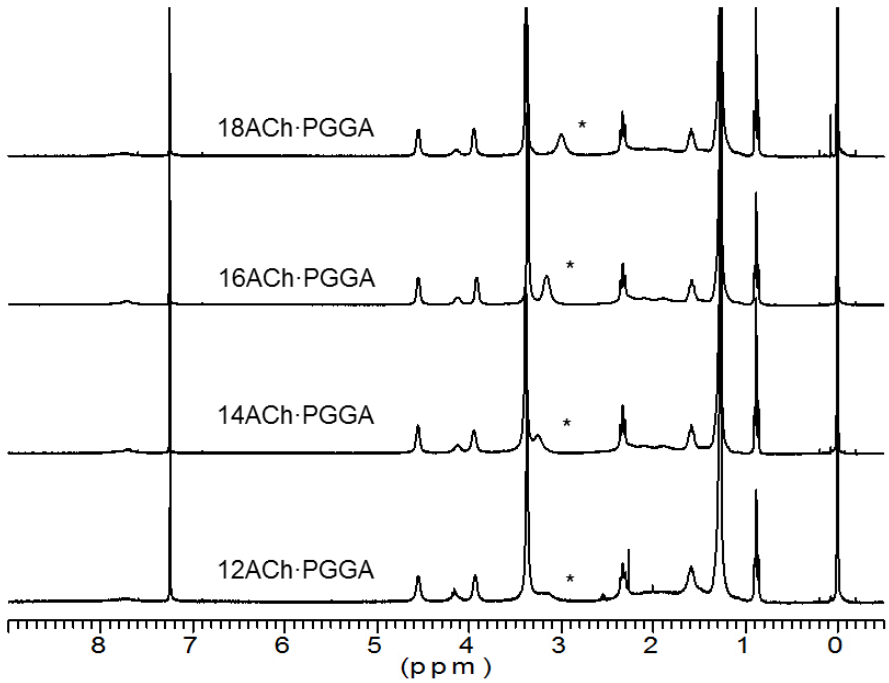

SI Figure 1. Compared ^{1}H NMR spectra of *n*ACh·PGGA in CDCl3. (*) Peak of residual water.

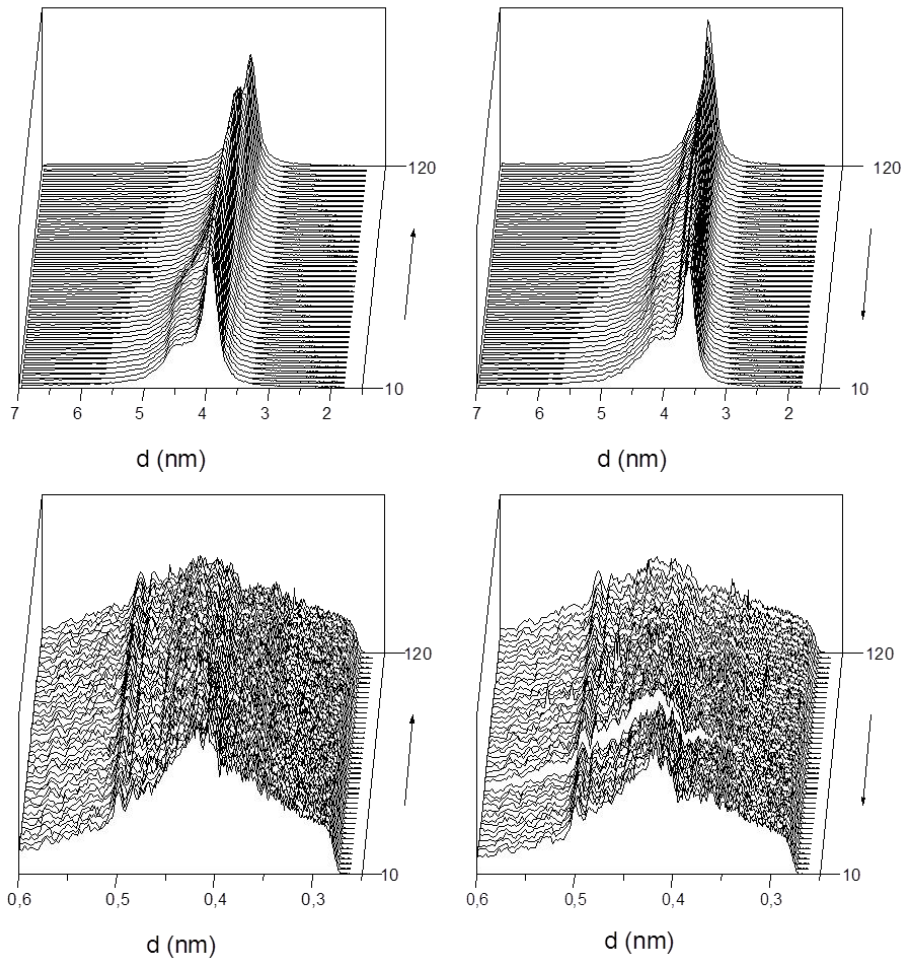

SI Figure 2. SAXS (top) and WAXS (bottom) profiles of 12ACh·PGGA at heating and cooling.

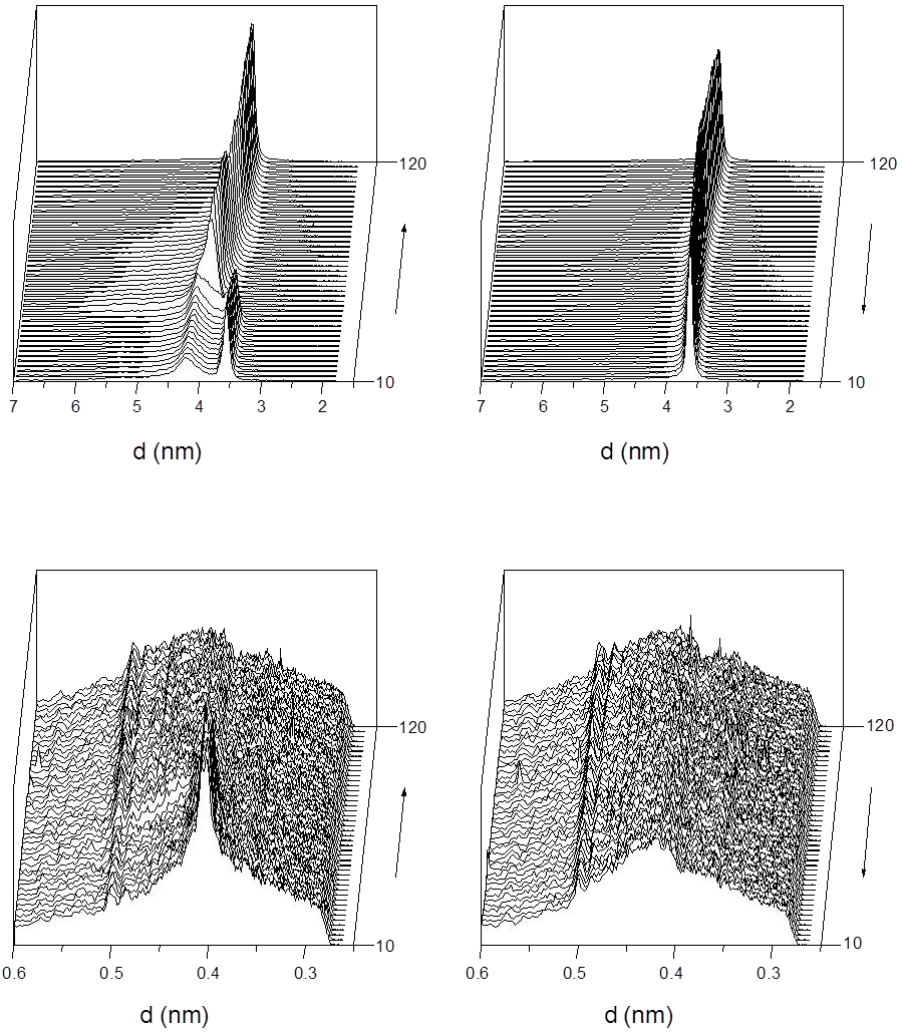

SI Figure 3. SAXS (top) and WAXS (bottom) profiles of 14ACh·PGGA at heating and cooling.

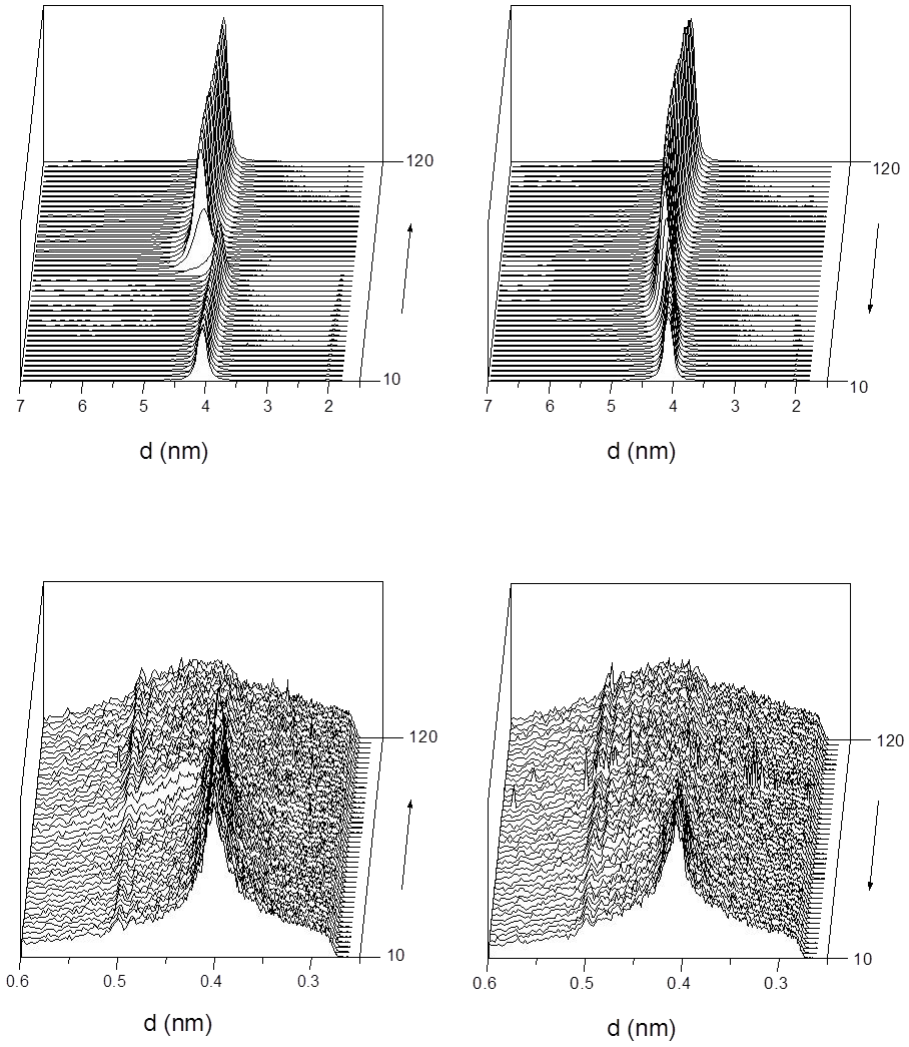

SI Figure 4. SAXS (top) and WAXS (bottom) profiles of 18ACh·PGGA at heating and cooling.

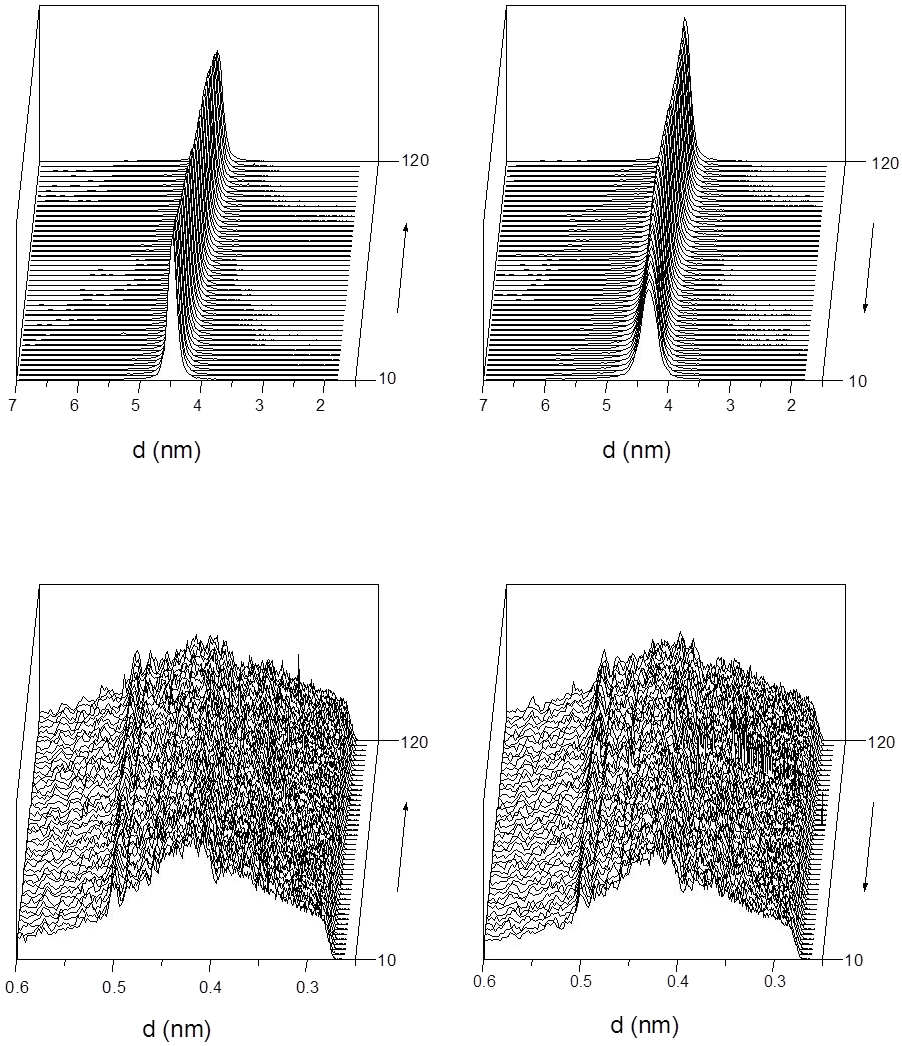

SI Figure 5. SAXS (top) and WAXS (bottom) profiles of 18cACh·PGGA at heating and cooling.

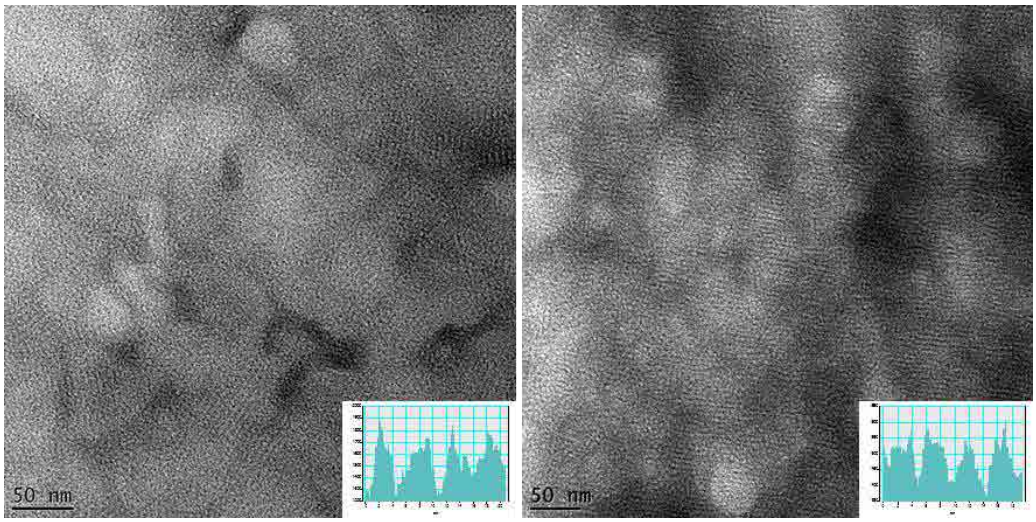

SI Figure 6. TEM images of 14ACh·PGGA a) and 16ACh·PGGA b) films obtained by casting. Insets: Optical density profiles showing the structural periodicity observed in each case.

SI Table 2. Conformational angles and parameters for the helical conformations considered in this work. Comparison of starting values with those obtained after geometry optimization.

	5/2		17/5	
	Starting	Optimized	Starting	Optimized
φ	-137.9	-132.7	70.9	58.0
ξ_1	53.0	60.6	52.8	56.4
ξ_2	75.6	64.8	-171.0	-173.6
ψ	-143.8	-147.0	159.9	167.8
Rise per residue	2.02	2.02	1.50	1.48

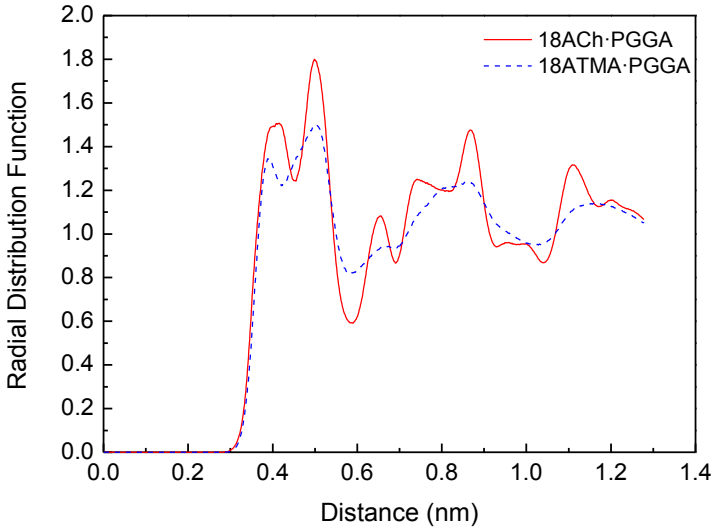

SI Figure 7. Comparison of the intermolecular radial distribution function for the methylene and methyl groups of the side-chains as a function of the distance for 18ACh·PGGA (red solid line) and 18ATMA·PGGA (blue dashed line) complexes from molecular dynamics simulations at room temperature (298 K).

3. Complexes of polyglutamic acid and long-chain alkanoylcholines: Nanoparticle formation and drug release

Summary: Ionic complexes of microbial poly(γ-glutamic acid) and alkanoylcholines are fully bio-based comb-like systems able to self-organize in an ordered amphiphilic structure made of hydrophobic and hydrophilic alternating layers. Incubation of complexes films under physiological conditions for one month promoted the dissociation of the complex and the hydrolysis of the choline ester without almost degradation of polyglutamic acid. Complex decomposition rates were depending on the alkanoyl chain length and complex stoichiometry as well. Nanoparticles with 50-100 nm diameters were successfully prepared from the stearoylcholine complex with a surfactant to polymer ratio of 0.75 and loaded with theophylline, carbamazepine or doxorubicin drugs. The releasing of the drugs from nanoparticles took place upon incubation at very different rates depending on the drug. Theophylline and carbamazepine were released in hours whereas doxorubicin was very slowly delivered along months. The observed differences were related to the different interaction mechanism operating between the drug and the complex.

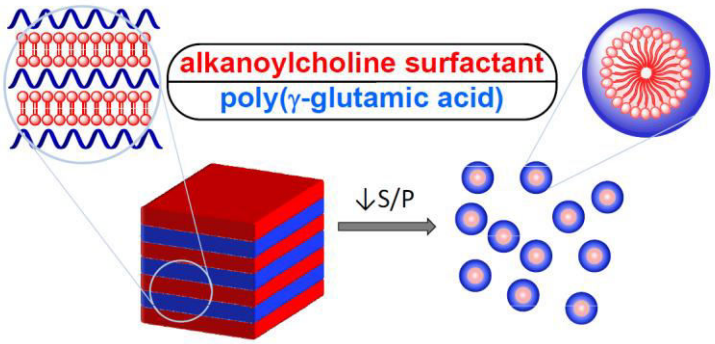

Publication derived from this work:

Tolentino, A.; Alla, A.; Martínez de Ilarduya, A.; Muñoz-Guerra, S. Complexes of polyglutamic acid and long-chain alkanoylcholines: nanoparticle formation and drug release. *Int. J. Biol Macromol.* **2014** (Accepted).

3.1. Introduction

The mutual interaction between blocks of different nature within a grafted polymer or copolymer usually affords a wide variety of morphologies with a diversity of properties and applications. Ionic complexes made of oppositely charged polyelectrolytes and surfactants constitute a versatile system whose molecular arrangement may be controlled by adjusting variables such as stoichiometry, ionic strength or temperature.[1,2] These comb-like complexes display a synergic combination of the tendency of the surfactant to form ordered mesophases and the mechanical resistance and processing capacity afforded by the polymer counterpart.[3] In the last decade, self-assembled polymer complexes and their architectures have been object of several reviews,[2,4,5] in which the relative easiness in obtaining them was remarked. The interest for polyelectrolyte-surfactant complexes as biomaterials, specifically for application as drug delivery systems, has largely increased in these last years.[5,6]

Polymer nanoparticles are outstanding systems for targeting delivery of drugs, genes or proteins, at either cell or organ level.[5,7] For such purpose, size at the nanometric scale is a required parameter to provide stability in body fluids and permeation through cell membranes.[8] Drug delivery devices made of amphiphilic systems are particularly suitable for selective entrapping of drugs and for their controlled releasing according to desired specifications.[9] Complexes made of relatively hydrophilic polymers and surfactants bearing long alkyl chains are very convenient for building amphiphilic nanoparticles with a well-defined structure provided that molecular parameters and preparation conditions are properly adjusted. Dissociation of the complex by water may be an additional advantage afforded by these systems since the releasing profile can be adjusted not only by controlling the diffusion of the drug through the matrix but also by regulating the complex decomposition rate.

Poly(γ-glutamic acid), PGGA, is a naturally occurring polypeptide that is commercially produced by microbiological methods.[10] The well-known biodegradability and non-toxicity displayed by this biopolymer are the main factors promoting its study as a forthcoming biomaterial, in particular for drug delivery systems.[9,11] The direct ionic coupling of Doxorubicin with PGGA in the presence of alkylammonium cations has been recently reported as a convenient method for an efficient encapsulation of the drug.[12] Nevertheless, the high solubility of PGGA in water is a limitation for many applications that can be eluded by chemical modification.[13] Esterification and amidation of the carboxyl side group of PGGA are known to lead to water non-soluble

derivatives suitable for the preparation of protein or drug carriers to be used as delivery systems.[14-16] Ionic coupling of PGGA with cationic alkyltrimethylammonium surfactants with long alkyl chains (*n*ATMA·PGGA) affords a second option to prepare non-soluble water PGGA.[17] These complexes are known to self-assemble in water to adopt an amphiphilic layered structure with sheets of polypeptidic α-helixes alternating with the paraffinic phase made of alkyl chains. Films of *n*ATMA·PGGA complexes obtained by casting have been studied as drug delivery systems using erythromycin.[18] It was revealed in these studies that the drug was hosted in the hydrophobic subphase of the complex, and that its release rate was dependent on the alkyl side chain length. The detergent activity of quaternary alkylammonium compounds against cellular membranes of living organisms including human cells, is however a severe shortcoming of *n*ATMA·PGGA system for their application as biomaterial.[19]

Recently, we have published on the preparation and structural characterization of totally bio-based ionic complexes made of polyglutamic acid and alkanoylcholines derived from fatty acids,[20] namely *n*ACh·PGGA with carbon numbers *n* of 12, 14, 16 and 18. These complexes are chemically close to *n*ATMA·PGGA and adopt the same biphasic layered structure but they distinguish in their fully bio-based origin. The proven biocompatibility of alkanoylcholine, which is hydrolysable by butyrylcholine esterase and other enzymes,[21,22] makes these compounds excellent candidates as prospective drug delivery devices. Moreover, the established therapeutic effect of alkanoylcholines in the treatment of different diseases such as gastrointestinal[23] or cognitive disorders, *e.g.* Alzheimer disease;[24,25] offers an added value to their complexes. The present work was undertaken with the final purpose of evaluating the capacity of *n*ACh·PGGA complexes to form nanoparticles and their suitability as drug delivery systems. First the vulnerability of the complexes to the action of water has been appraised and then, the encapsulation and releasing of three model drugs, theophylline (THEO), carbamazepine (CBZ), and doxorubicin (DOX), largely differing in their molecular structures, have been comparatively examined.

3.2. Experimental part

3.2.1. Materials

The complexes (12ACh·PGGA and 18ACh·PGGA) used in this work were prepared from poly(γ-DL-glutamic acid) (PGGA) of biosynthetic origin (Meiji Co, Japan) and the alkanoylcholine iodides (12ACh·I and 18ACh·I), as described in detail elsewhere.[20] Alkanoylcholine iodides were synthesized from 2-(dimethylamino)-ethanol and lauric or stearic acids as previously reported (Chapter III.1).[26] The drugs used in this study were theophylline from Sigma-Aldrich, and carbamazepine and doxorubicin from AK Scientific, Inc.

3.2.2. Hydrolytic degradation study

0.8 cm diameter discs of *n*ACh·PGGA complexes were cut from films previously prepared by casting from chloroform and dried for 48 h under vacuum. For the degradation study, the discs were placed into vials containing 10 mL of phosphate buffer at pH 7.4, sealed to avoid partial evaporation of fluids, and stored in a heated chamber at 37 ºC. The evolution of the changes taking place upon incubation was followed by weighting of the remaining disk, and ^{1}H-NMR spectroscopy and gel permeation chromatography (GPC) analysis of both the residue and the products released to the aqueous medium.

3.2.3. Nanoparticles and drug encapsulation and delivery

Nanoparticles made of 18ACh·PGGA complex with a surfactant/polymer (S/P) ratio of 0.75 were prepared by the ionotropic gelation technique. A 2 mM aqueous solution of 18ACh·I at 70 ºC was added dropwise to a 5 mM aqueous solution of Na·PGGA at 70 ºC over a period of 1 min at 70 ºC. The suspension was left under stirring for 4 h at 70 ºC and dialyzed against water for 2 h at 70 ºC and for 48 h at room temperature. Nanoparticles were recovered by centrifugation at 10,000 rpm.

For the preparation of films of 12ACh·PGGA or 18ACh·PGGA complexes with entrapped Theo or CBZ, 10% (w/w) of the corresponding drug were added to a chloroform/methanol solution of the complex and the solution left to

evaporate. For encapsulation of drugs in nanoparticles, these were prepared as described above but adding to the aqueous solution of PGGA the corresponding drug at the selected (w/w) proportions: THEO (10%), CBZ (10%) and DOX (18%). Theo and CBZ were encapsulated in complexes with an S/P ratio of 0.75, whereas a ratio of 0.40 was employed for the encapsulation of DOX. The drug content was checked by UV spectrophotometry for CBZ and THEO, and by ^{1}H-NMR for DOX.

For drug delivery evaluation, 10 mg sample of either drug loaded powdered film or nanoparticles were dispersed in 1mL of phosphate buffer at pH 7.4, the dispersion placed inside a cellulose membrane tube of 8,000-10,000 MWCO and dipped under stirring in 10 mL of buffered aqueous solution at 37 ºC. Unloaded complex was used as blank. Drug releasing was monitored by UV-spectroscopy with previous calibration made with THEO (270 nm), CBZ (285 nm) and DOX (480 nm).

3.2.4. Methods

^{1}H-NMR spectra were recorded on a Bruker AMX-300 NMR instrument operating at 300.1 MHz with samples dissolved in deuterated chloroform, deuterated methanol and deuterated water, using TMS and the sodium salt of 3-(trimethylsilyl)-propanesulfonic acid (TMSP) as internal references. Sixty-four scans were acquired with 32K data points as well as relaxation delays of 1s. Gel permeation chromatography was performed at 35 ºC using a Waters equipment provided with a refraction index detector with a flow rate of 0.5 mL min^{-1}. *n*ACh·PGGA complexes were chromatographed using 0.05 M sodium trifluoroacetate-hexafluoroisopropanol (Na·TFA-HFIP) and chromatograms were calibrated against poly(methyl methacrylate) (PMMA) monodisperse standards. Scanning electron microscopy (SEM) was used to examine the morphology and size of films and nanoparticles. Gold coating was accomplished by using a Balzers SDC-004 Sputter Coater. The SEM microphotographs were taken with a field-emission JEOL JSM-7001F instrument (JEOL, Japan) from uncoated samples.

3.3. Results and discussion

3.3.1. Hydrolytic degradation study

The resistance to water of choline derivative complexes was evaluated under physiological conditions, *i.e.* in PBS, pH=7.4, 37 ºC. The complexes selected out for this study were stoichiometric 12ACh·PGGA and 18ACh·PGGA as well as 18ACh·PGGA(0.5). This selection allows to examine comparatively the susceptibility of the complexes to the water action regarding the influence of the alkanoyl side chain as far as both crystallinity and surfactant/polyacid (S/P) coupling ratio are concerned.

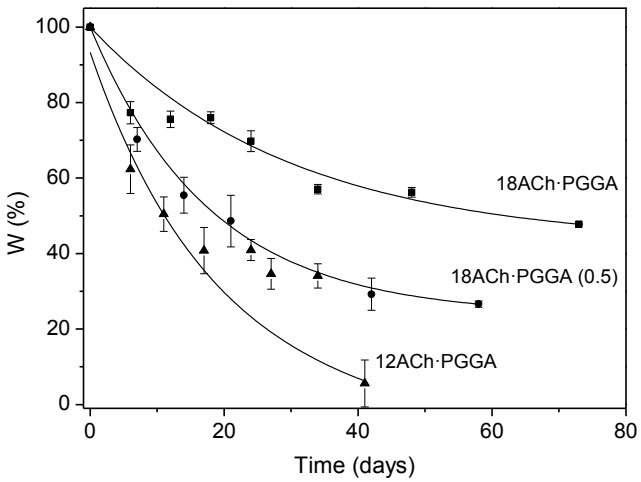

Figure 1. Remaining weight of *n*ACh·PGGA discs incubated under physiological conditions.

It was noticed by visual inspection that upon incubation, 12ACh·PGGA discs disintegrated and the aqueous media became turbid whereas 18ACh·PGGA discs were apparently unaltered and the media remained transparent. In the graph of Figure 1 the remaining weight of the incubated discs are plotted against incubation time for the three selected complexes. A notably loss of weight happens in the three cases with relative rates according to what should be expected. 12ACh·PGGA appears to be most sensitive to the water attack because it is made of shorter chains that are not crystallized.[20] On the contrary stoichiometric 18ACh·PGGA is observed to lose weight at the minimum rate due to the shielding effect provided by the long hydrophobic

octadecanoyl chains. The behaviour displayed by 18ACh·PGGA(0.5) is intermediate revealing the compromise between the two effects. It should be remarked that the weight loss rate of these complexes is significantly lower than for PGGA, for which a loss of 60% in 2 days was reported upon incubation under the same conditions.[27] Obviously, it is the hydrophobicity provided by the presence of the alkanoyl chains the responsible for such a dramatic difference; in fact the behaviour of *n*ACh·PGGA is comparable to that reported for *n*ATMA·PGGA where a similar hydrophobicity is operating. [18]

The GPC analysis of remaining discs after 40 days of incubation revealed that the initial molecular weight of the complexes had decreased less than 20%. The GPC results obtained from the analysis of the products released to the incubation media were not very different with a maximum decrease in molecular weight of 30% of the original value (Table 1). These data strongly suggest that the weight loss observed for the discs must be consequence of a dissolution process probably favoured by previous complex dissociation.

Table 1. *n*ACh·PGGA complexes upon incubation in PBS for 40 days at 37 ºC

*n*ACh·PGGA		Remaining weight (%)	Molecular weight ($g \cdot mol^{-1}$)		
Complex	S/P		initial	disc	medium
12ACh·PGGA	1	5	47000	38000	33000
18ACh·PGGA	1	30	38000	32000	28000
18ACh·PGGA	0.5	60	36000	34000	27000

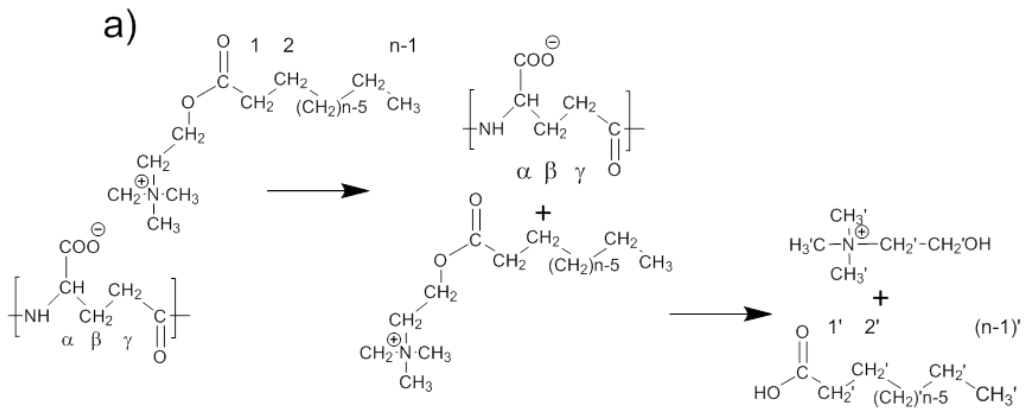

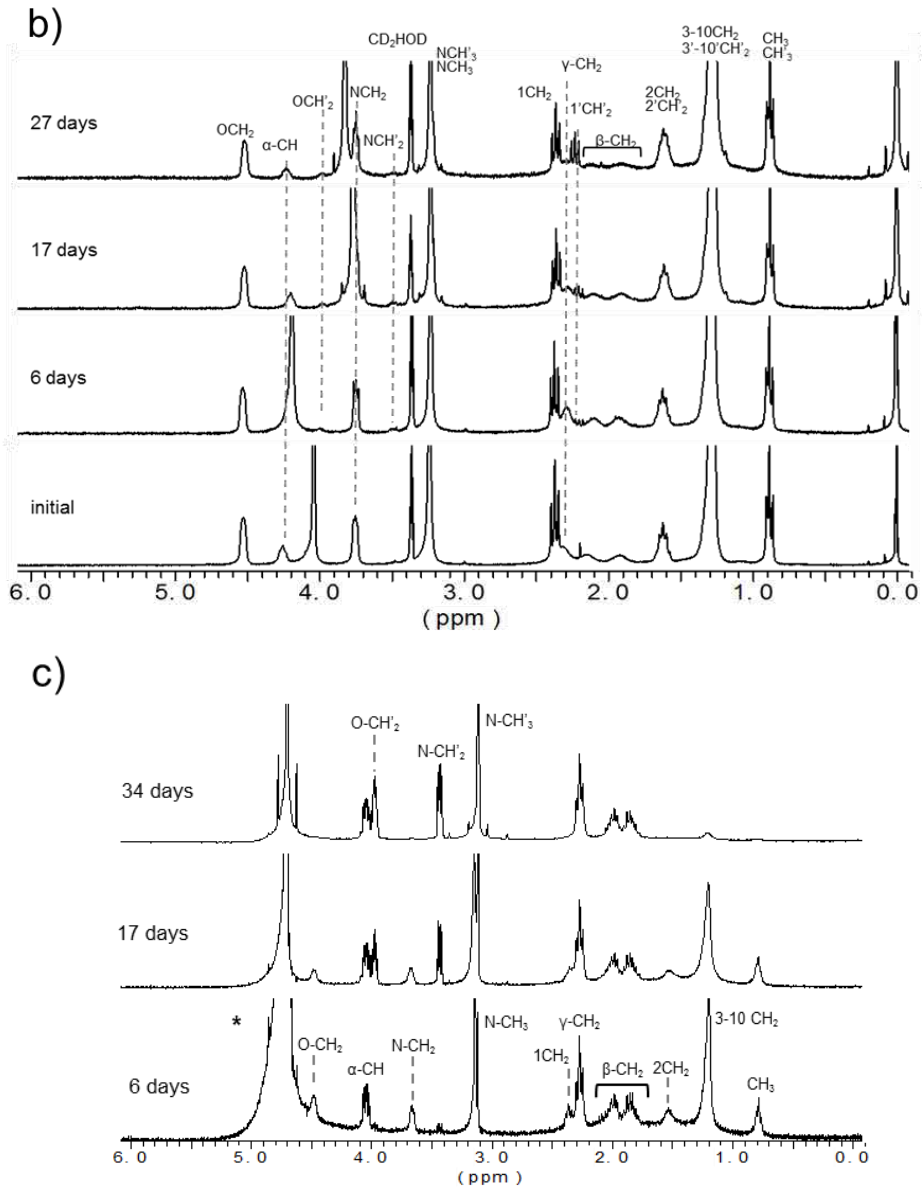

Figure 2. Decomposition of 12ACh·PGGA upon incubation in PBS at 37 ºC. a) Decomposition mechanism. b) ^{1}H-NMR spectra of residual sample. c) ^{1}H-NMR spectra of products released to the incubation medium.

^{1}H-NMR spectra recorded from the residual disc and from the released products to the aqueous medium for incubated 12ACh·PGGA complex along time are compared in Figure 2. The ^{1}H-NMR spectra of residual discs correspond essentially to *n*ACh·PGGA complexes accompanied by a series of

small signals attributable to a minor presence of 2-hydroxyethyl-trimethylammonium. The presence of lauric acid in the residue was detected by the signal 1'CH_2' appearing at 2.20 ppm and ingreasing with incubation time. On the other hand, spectra from water soluble products revealed initially the predominant presence of the alkanoyl cholinium and PGGA salts in the medium, and its progressive hydrolysis to cholinium and lauric acid. A progressive disappearance of the signals arising from the fatty acid is observed with time, which is explained by the limited solubility of this compound in the aqueous medium. Given the complex dissociation that is shown to occur upon incubation, the influence of solubility of the alkanoylcholine salts should be considered as an additional factor in determining the decomposition of the complexes. Lauroylcholine salt is soluble in water at 40 ºC whereas, stearoylcholine needs temperatures around 80ºC to be dissolved (Chapter III.1).[26] Such differences are of help in explaining the different weight loss rate observed among the complexes. The ^{1}H-NMR spectra recorded for incubated 18ACh·PGGA are afforded in the SI.

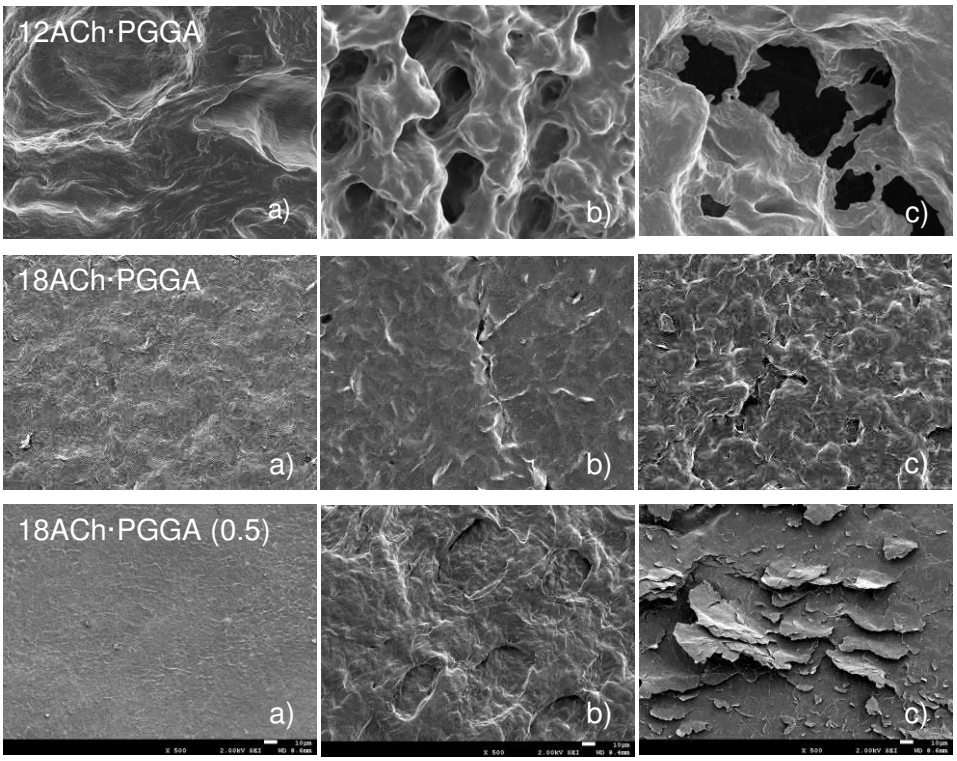

Figure 3. SEM micrographs of complexes after incubation in PBS at 37 ºC for the indicated periods of times. 12ACh·PGGA: initial, 6 and 17 days; 18ACh·PGGA: initial, 12 and 34 days; 18ACh·PGGA (0.5): initial, 7 h and 58 days.

The morphological changes taking place in the discs upon incubation were followed by SEM (Figure 3). According to what is observed by weighting, 12ACh·PGGA discs showed a higher disintegration degree of the material when comparing to the 18ACh·PGGA complex. These noticeable differences in erosion are in agreement with the consistency displayed by the complex when incubated in PBS which were discussed above. Besides this, all the complexes of PGGA with choline esters displayed homogeneous erosion with a deep alteration of the material according to the occurrence of a bulk mechanism.

3.3.2. Nanoparticles of *n*ACh·PGGA

Different techniques involving dialysis-precipitation,[28] miniemulsion[29] and ionotropic gelation[30] were tested with the purpose of obtaining nanoparticles of 18ACh·PGGA complexes with S/P ratios of 0.25; 0.33; 0.50; 0.66; 0.75 and 1. Dialysis and miniemulsion led to film formation or particle aggregation in all cases (see SI). On the other hand, isolated nanoparticles could be obtained by applying the ionotropic gelation method to non-stoichiometric complexes. Furthermore since this technique avoids the use of organic solvents, which were necessary by both dialysis-precipitation and miniemulsion processes, it stands out as a sustainable method for processing bio-based materials such as *n*ACh·PGGA. Figure 4 shows SEM images of dispersions of complexes varying in the S/P ratio revealing that formation of particles is favoured by high S/P values. In fact, a particulated film was formed for 0.25 (Figure 4a), aggregates of irregular size were produced at 0.50 ratio (Figure 4b), and rather homogeneous and well dispersed particles could be finally obtained for a 0.75 ratio (Figure 4c). Above this optimum value, *i.e.* when composition becomes close to stoichiometry, precipitation of the complex occurred.

Further efforts were dedicated to optimise nanoparticle formation from 18ACh·PGGA (0.75) complex. According to Israelachvili et al,[31] the S/P ratio is the main factor at determining the variation in morphology of surfactant-polyelectrolyte complexes, which changes from a continuous lamellar phase to individualized spherical particles as the relative amount of surfactant decreases. In addition to the S/P ratio, other variables[5,32,33] such as ionic bond density, solvent, or applied shearing contribute to determine the morphology of the precipitated material. It was found that application of high shear forces during the self-assembly of the complex by means of an ultrasound tip allowed the homogenization and reduction of particle diameter from ~0.5 µm, which was the diameter obtained under stirring, down to 50-100 nm (see SI

part). It is worthy to remark how the combination of the counterion ratio and shear force allows to improve nanoparticle formation provided that solution concentration and solvent have been adequately selected. The optimized parameters for obtaining the nanoparticles of 18ACh·PGGA complex used in this study are gathered in Table 2.

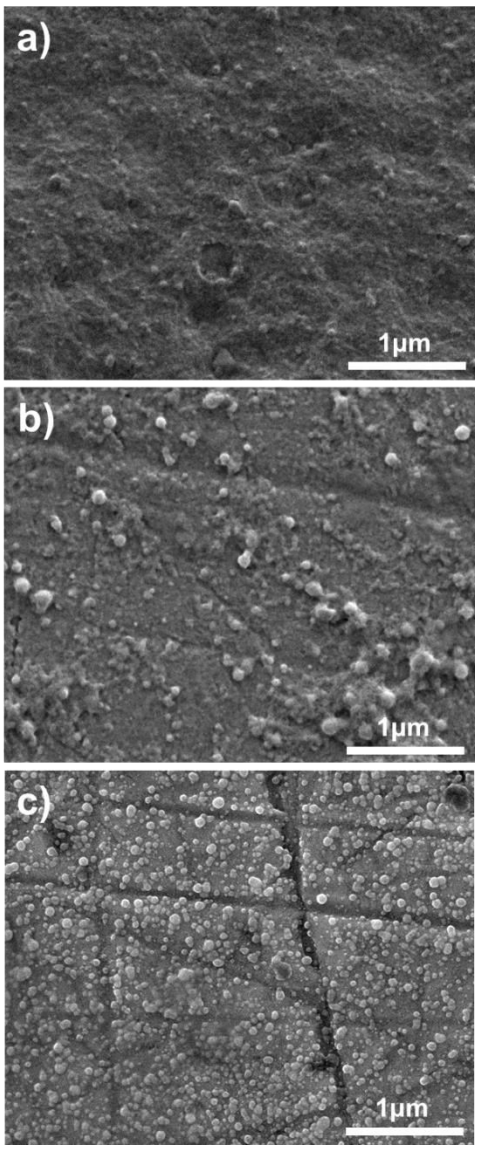

Figure 4. Dispersions of 18ACh·PGGA complexes obtained by ionotropic gelation method with S/P ratio of 0.25 (a); 0.50 (b) and 0.75 (c).

Table 2. Optimized parameters for nanoparticle formation by ionotropic gelation method.

Parameters	18ACh·PGGA
Na·PGGA[a]	5 mM
18ACh·I[a]	2 mM
Shear force	Ultrasound tip
S/P[b]	0.75
Particle size	50-100 nm

[a] Concentration in aqueous solution (mM); [b] Surfactant/polymer molar ratio

3.3.3. Encapsulation and release of drugs

The feasibility of these complexes for their use as drug delivery systems was tested by encapsulation and in-vitro release of three model drugs: carbamazepine (CBZ), theophylline (THEO) and doxorubicin (DOX). For THEO and CBZ, films of ionic complexes of 12ACh·PGGA and 18ACh·PGGA with S/P values of 1 and 0.5, respectively, containing 10% of drug were prepared by casting from solution. Dox loaded films could not be prepared due to the insolubility in organic solvents of the ionic complex that this drug form with *n*ACh·PGGA. In addition nanospheres of non-stoichiometric 18ACh·PGGA containing each of the three drugs were prepared by using the in-situ self-assembly technique. Nanoparticles were prepared from an initial concentration of drug to complex of 10% (w/w) to achieve an effective load of 3 and 0.5% for CBZ and THEO respectively. In the case of DOX, the initial concentration was 18% (w/w), whereas the effective content of drug was around 30%. (see SI) These large differences observed in drug charging efficiency is very likely due to the different interaction of drugs with the matrix. DOX contains a protonable amine that can be coupled to free carboxylate groups of the polyglutamic chain. On the contrary, the interaction of THEO and CBZ with the matrix would be exclusively controlled by weak hydrophobic or van der Waals forces.

The morphology of the drug-loaded nanoparticles was checked by SEM (Figure 5). It was observed that while unloaded nanoparticles showed a broad distribution of sizes usually ranging from 25 to 100 nm, the loaded nanoparticles displayed a significantly narrower distribution of diameters which were close to 100 nm for CBZ and DOX, and in the short 25-50 nm range in the case of THEO.

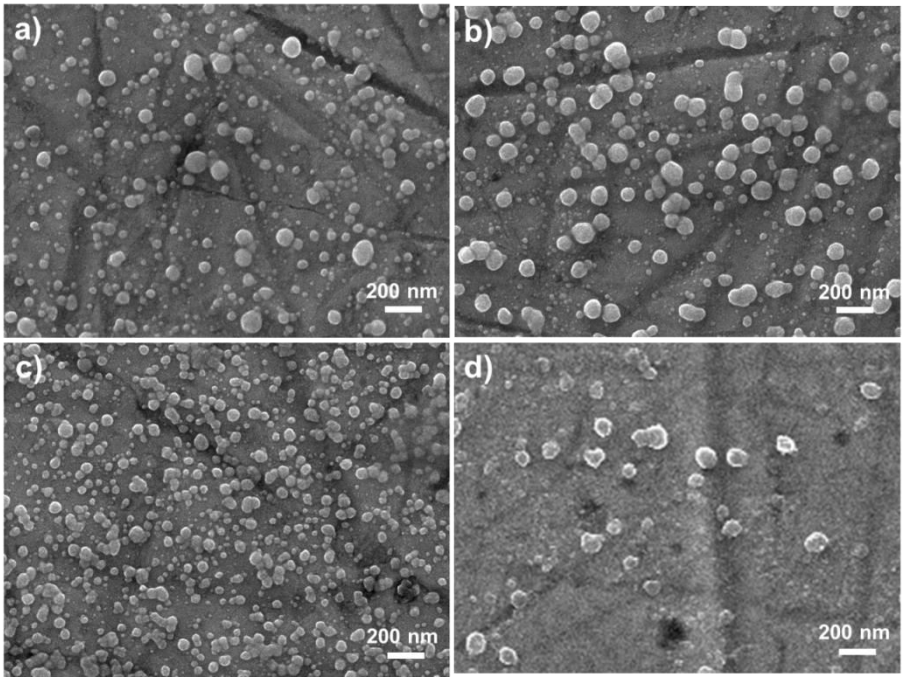

Figure 5. SEM micrographs of 18ACh·PGGA (0.75) complex nanoparticles without drug load a) and loaded with CBZ 3% b), THEO 0.5% c), and DOX 30% d).

Drug release tests were performed by incubation of films and nanoparticles under physiological conditions and following the drug delivery by UV spectroscopy. Since *n*ACh·PGGA and their degradation products are sensitive to UV, unloaded films and NP were used for calibration. Compared releasing profiles of the loaded nanoparticles are represented in Figure 6 for the three drugs. The release of THEO was very fast and completed in around 30 hours whereas CBZ was delivered at a significantly slower rate needing about six days to be completely discharged. In both cases however most of the drug was released in a few hours following a similar slope. On the contrary, the release of DOX occurred according to a completely different profile; it not only exhibited a much slower delivery rate (only 10% of the drug was discharged after one month) but it proceeded in a steadily manner without any boosting at the initial incubation stage. The different behaviour displayed by the three drugs may be rationalized taking into account the complex-drug interactions present in each case. Since the amine group of DOX can be protonated in aqueous solution, ionic complexation with the carboxylate free groups in the polyanion is feasible; the release of the drug will be governed therefore by the dissociation rate of such complex in water.

On the contrary, the interactions between the polymeric matrix and THEO and CBZ are of hydrophobic nature and therefore their release will be determined by diffusion. The slight differences observed in the releasing profiles of the two drugs might be attributed to their differences in hydrophobicity; the more hydrophilic THEO would interact preferentially with the PGGA hydrophilic shell of the nanoparticle whereas the more hydrophobic CBZ must be more internally lodged due to its higher affinity for the hydrophobic alkanoyl chains. In both cases however the drug must be located not far from the surface since most of it is released at very short incubation times.

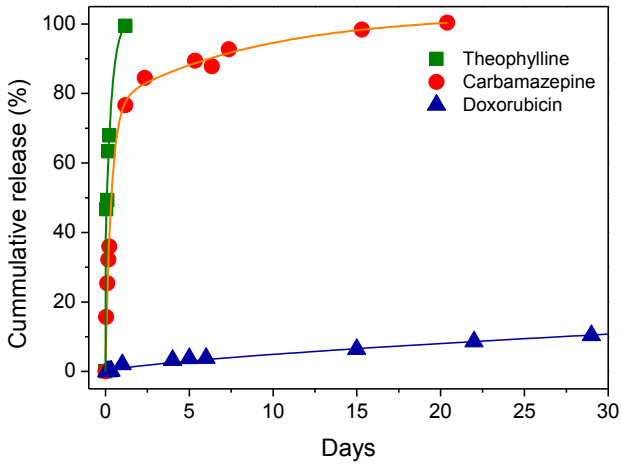

Figure 6. Drug release from nanoparticles of 18ACh·PGGA (0.75) complex at pH 7 and 37 ºC

The drug release observed for nanoparticles was compared with that displayed by films prepared by casting for both THEO and CBZ (see SI). No significant differences were appreciated for CBZ whereas in the case of THEO the discharge of the drug was even faster in the films than in the nanoparticles, which must be attributed to the different preparation conditions used in each case; the relatively stronger interaction of THEO with the complex taking place in the nanoparticles may be due to the high hydrophilic surface that is developed by the ionotropic gellation method. On the other hand, it is worthy to note that differences in the release rate of both THEO and CBZ were unnoticeable among the three complexes. It seems that neither alkyl chain length nor the grafting degree of the complex exerts any effect on drug release, which is in agreement with the picture of a superficial attachment of the drug rather than an entrapment in the inner part of film.

3.4. Conclusions

To our knowledge, this work is pioneer in exploring fully bio-based ionic complexes as prospective drug delivery systems. The main conclusions drawn from this study are the following.

a) *n*ACh·PGGA ionic complexes were proven to be sensitive to water attack under simulated physiological conditions needing long periods of time to decompose. Decomposition took place by complex dissociation and subsequent hydrolysis of the alkanoylcholine moiety into the cholinium salt and the corresponding fatty acid whereas the polyacid main chain remained almost unaltered.

b) Nanoparticles of 50-100 nm diameter were successfully prepared from non-stoichiometric *n*ACh·PGGA complexes with an S/P ratio of 0.75 by means of the ionotropic gelation method and applying ultrasonic forces.

c) Neutral drugs THEO and CBZ were entrapped in the *n*ACh·PGGA nanoparticles with low efficiency with most of the drug being superficially attached. Drug release from the loaded nanoparticles happened at very high rates so all THEO and near 80% of CBZ became fully discharged in hours.

d) Nanoparticles of *n*ACh·PGGA (0.75) loaded with 30% of DOX could be obtained. The release of DOX from this system proceeded at a rate comparable to that observed for the decomposition of the complex with less than 10% of the drug discharged after one month of incubation. Ionic coupling of DOX with the carboxylic groups remaining free in the complex is the reason for the distinguishing behaviour exhibited by this drug.

The reported results have proven the capacity of non-stoichiometric *n*ACh·PGGA complexes to become self-assembled in well-defined nanoparticles as well as the suitability of these nanoparticles to encapsulate cationic charged drugs with high efficiency and to deliver the drug at very slow releasing rates. The biocompatible nature of both the complex and its decomposition products ensure the viability of these compounds for drug store and delivery and place them in a privileged position in the development of DDS systems.

3.5. References

1. (a) Hayakawa, K. Kwak, J. C. T. Study of surfactant-polyelectrolyte interactions. 2. Effect of multivalent counterions on the binding of dodecyltrimethylammonium ions by sodium dextran sulfate and sodium poly (styrene sulfonate) in aqueous solution. *J. Phys. Chem.* **1983***, 87*, 506-509. (b) Hayakawa, K.; Santerre, J. P.; Kwak, J. C. T. Study of surfactant poly-electrolyte interactions – Binding of dodecyltrimethylammonium and tetradecyltrimethylammonium bromide by some carboxylic poly-electrolytes. *Macromolecules* **1983**, *16*, 1642-1645. c) Malovikova, A.; Hayakawa, K.; Kwak, J. C. T. Surfactant-polyelectrolyte interactions. 4. Surfactant chain length dependence of the binding of alkylpyridinium cations to dextran sulfate. *J. Phys. Chem.* **1984***, 88*, 1930-1933.

2. Kötz, J.; Kosmella, S.; Beitz, T. Self-assembled polyelectrolyte systems. *Progr. Polym. Sci.* **2001**, *26*, 1199–1232.

3. Thünemann, A. F. Polyelectrolyte – surfactant complexes (synthesis, structure and materials aspects). *Progr. Polym. Sci.* **2002**, *27*, 1473–1572.

4. Faul, C. F. J.; Antonietti, M. Ionic Self-assembly: Facile synthesis of supramolecular materials. *Adv. Mater.* **2003**, *15*, 673–683.

5. Thünemann, A. F.; Müller, M.; Dautzenberg, H.; Löwen, J. J. H. Polyelectrolyte complexes. *Adv. Polym. Sci.* **2004**, *166*, 113–171.

6. Elsabee, M.Z.; Morsi R.E.; Al-Sabagh, A. M. Surface active properties of chitosan and its derivatives, *Colloids Surf. B* **2009**, *74*, 1-16.

7. Singh, S. Nanomedicine-nanoscale drugs and delivery systems. *J. Nanosci. Nanotechnol.* **2010**, *10,* 7906-7918.

8. Jani, P.; Halberg, G. W.; Langridge, J.; Florence, A. T. Nanoparticle uptake by the rat gastrointestinal mucosa: quantitation and particle size dependency. *J. Pharm. Pharmacol.* **1990***, 42*, 821-826.

9. Akagi, T.; Baba, M.; Akashi, M. Preparation of nanoparticles by the self-organization of polymers consisting of hydrophobic and hydrophilic segments: Potential applications. *Polymer* **2007**, *48*, 6729–6747.

10. Shih, I. L.; Van, Y. T. The production of poly(γ-glutamic acid) from microorganisms and its various applications. *Bioresource Technol.* **2001**, *79*, 207–225.

11. Bajaj, I.; Singhal, R. Poly (glutamic acid) – An emerging biopolymer of commercial interest. *Bioresource Technol.* **2011**, *102*, 5551–5561.

12. Manocha, B.; Margaritis, A. Controlled release of doxorubicin from doxorubicin/γ-polyglutamic acid ionic complex, *J. Nanomater.* **2010**, *9*, DOI:10.1155/2010/780171.

13. Muñoz-Guerra, S.; García-Alvarez, M.; Portilla-Arias, J. A. Chemical modification of microbial poly(γ-glutamic acid): Progress and perspectives. *J. Renew. Mater.* **2013**, *1*, 42–60.

14. Portilla-Arias, J. A.; Camargo, B.; García-Álvarez, M.; Martínez de Ilarduya, A.; Muñoz-Guerra, S. Nanopartilces made of microbila poly(γ-glutamate)s for encapsulation and delivery of drugs and proteins, *J. Biomater. Sci. Polym. Ed.* **2009**, *20*, 1065-1079.

15. Tachibana, Y.; Kurisawa, M.; Uyama, H.; Kobayashi, S. Thermo-and pH-responsive biodegradable poly (α-N-substituted γ-glutamine)s. *Biomacromolecules* **2003**, *4*, 1132-1134.

16. Akagi, T.; Kaneko, T.; Kida, T.; Akashi, M. Preparation and characterization of biodegradable nanoparticles based on poly(γ-glutamic acid) with L-phenylalanine as a protein carrier. *J. Control. Release.* **2005**, *108*, 226–236.

17. (a) Pérez-Camero, G.; García-Alvarez, M., Martínez De Ilarduya, A.; Fernández, C., Campos, L., Muñoz-Guerra, S. Comblike complexes of bacterial poly(γ,D-glutamic acid) and cationic surfactants. *Biomacromolecules*. **2004**, *5*, 144–152. (b) García-Alvarez, M.; Alvarez, J.; Alla, A.; Martínez de Ilarduya, A.; Muñoz-Guerra, S. Comb-like ionic complexes of cationic surfactants with bacterial poly(γ-glutamic acid) of racemic composition. *Macromol. Biosci.* **2005**, *5*, 30–38.

18. Portilla-Arias, J. A; García-Alvarez, M.; de Ilarduya, A. M.; Muñoz-Guerra, S. Ionic complexes of biosynthetic poly(malic acid) and poly(glutamic acid) as prospective drug-delivery systems. *Macromol. Biosci.* **2007**, *7*, 897–906.

19. Tischer, M.; Pradel, G.; Ohlsen, K.; Holzgrabe, U. Quaternary ammonium salts and their antimicrobial potential: targets or nonspecific interactions? *ChemMedChem* **2012**, *7*, 22–31.

20. Tolentino, A., León, S., Alla, A., Martínez de Ilarduya, A., Muñoz-Guerra, S. Comblike ionic complexes of poly (γ-glutamic acid) and alkanoylcholines derived from fatty acids. *Macromolecules*, **2013**, *46,* 1607-1617.

21. Chelminska-Bertilsson, M.; Allenmark, S.; Edebo, L. Butyrylcholinesterase activity towards long-chain alkanoylcholilnes – Kinetics and mechanism. *Biochim. Biophys. Acta* **1993**, *1202*, 56-60.

22. Ahlström, B.; Chelminska-Bertilsson, M.; Thompson, R. A; Edebo, L. Long-chain alkanoylcholines, a new category of soft antimicrobial agents that are enzymatically degradable. *Antimicrob. Agents Chemother.* **1995**, *39*, 50–55.

23. (a) Alexander, J.; Fix, J. A. Enhancement of absortion of drugs from gastrointestinal tract using choline ester salts. US Patent 4822773, 1989. (b) Alexander, J.; Fix, J. A.; Repta, A. J. Choline esters as absorption-enhancing agents for drug delivery through mucous membranes of the nasal, buccal, sublingual and vaginal cavities. US Patent 4963556, 1990.

24. Carelli, V.; Liberatore, F.; Scipione, L.; Cardellini, M.; Rotiroti, D.; Rispoli, V. Choline derivative for the treatment of Alzheimer's disease. US Patent 0166721 A1, 2003.

25. Patel, H. Use of choline derivatives for memory, learning and cognition. US Patent 018631 A1, 2005.

26. Tolentino, A.; Alla, A.; Martínez de Ilarduya, A.; Font-Bardia, M.; Leon, S.; Muñoz-Guerra, S. Thermal behavior of long-chain alkanoylcholine soaps. *RSC Adv.* **2014**, *4*, 10738-10750.

27. Akagi, T.; Higashi, M.; Kaneko, T.; Kida, T.; Akashi, M. In vitro enzymatic degradation of nanoparticles prepared from hydrophobically-modified poly(gamma-glutamic acid*). Macromol. Biosci.* **2005,** *5*, 598-602.

28. Manocha, B.; Margaritis, A. Production and characterization of gamma-polyglutamic acid nanoparticles for controlled anticancer drug release. *Crit. Rev. Biotechnol.* **2008**, *28*, 83–99.

29. Anton, N.; Benoit, J.P.; Saulnier, P. Design and production of nanoparticles formulated from nano-emulsion templates- A review. *J. Control. Release* **2008**, *128*, 185-199.

30. Patil, J. S.; Kamalapur, M. V; Marapur, S. C.; Kadam, D. V Ionotropic gelation and polyelectrolyte complexation: The novel techniques to design hydrogel, particulate sustained, modulated drug delivery system: A Review. *Dig. J. Nanomater. Bios.* **2010**, *5*, 241–248.

31. Israelachvili, J. N.; Mitchell, D. J.; Ninham, B. W. Theory of self-assembly of hydrocarbon amphiphiles into micelles and bilayers. *J. Chem. Soc. - Faraday Transaction II* **1976**, *72*, 1525-1568.

32. Hansson, P. Surfactant self-assembly in oppositely charged polymer networks. Theory. *J. Phys. Chem. B* **2009**, *113*, 12903–15.

33. Wang, Y. L.; Kimura, K.; Dubin, P. L.; Jaeger, W. Polyelectrolyte-micelle coacervation: Effects of micelle surface charge density, polymer molecular weight, and polymer/surfactant ratio. *Macromolecules* **2000**, *33*, 3324-3331.

3.6. Supporting information

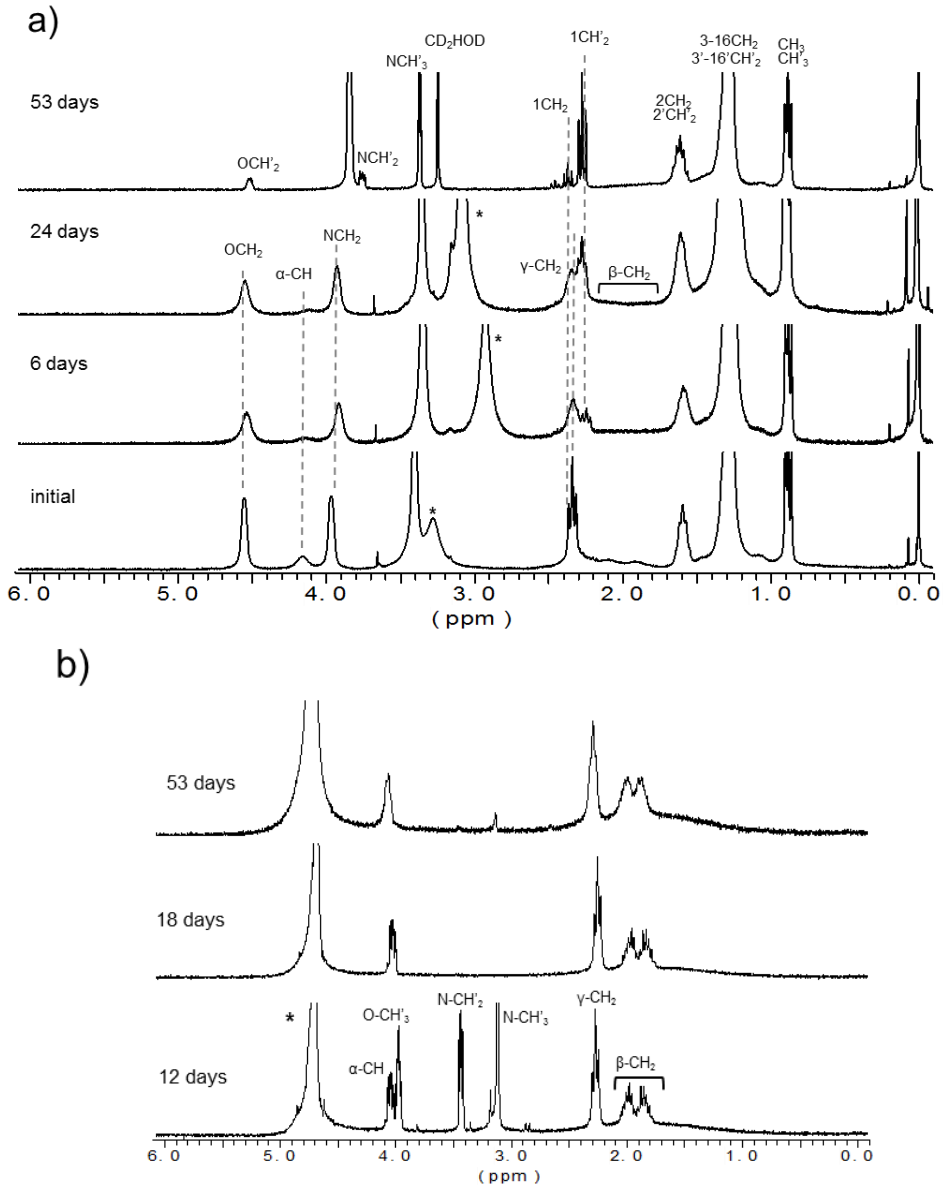

SI Figure 1. Decomposition of 18ACh·PGGA upon incubation in PBS at 37 ºC. a) ^{1}H-NMR spectra of residual sample. c) ^{1}H-NMR spectra of products released to the incubation medium.

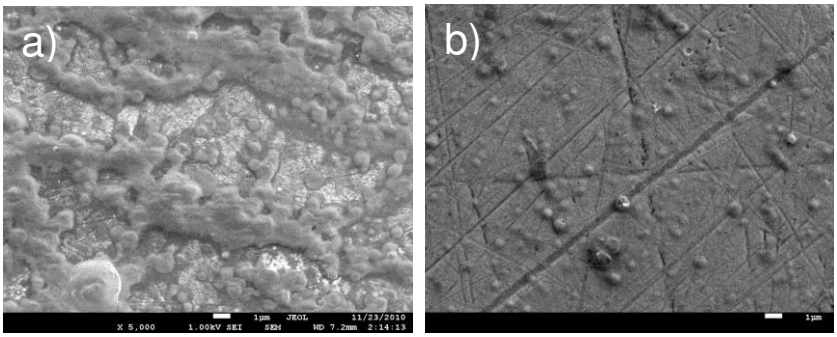

SI Figure 2. SEM micrographs of 18ACh·PGGA dispersions obtained by dialysis-precipitation method with S/P ratio= 1 (a) and miniemulsion method with S/P= 0.75.

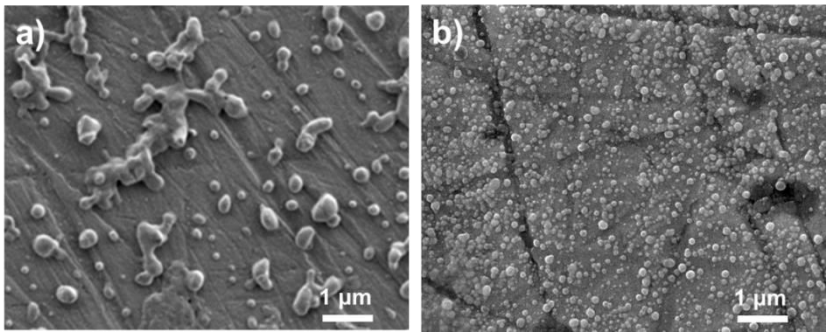

SI Figure 3. Dispersions of 18ACh·PGGA with S/P= 0.75 obtained without (a) and with application (b) of high shearing.

SI Table 1. Initial and effective load of drugs in nanoparticles

Loaded systems	Initial concentration[a]					Effective concentration[b]				
	Drug		18ACh·PGGA Complex		S/P	Drug		18ACh·PGGA Complex		S/P
	W%[c]	M%[d]	W%[c]	M%[d]		W%[c]	M%[d]	W%[c]	M%[d]	
18NP-CBZ	10	16	90	84	0.75	3	5	97	95	0.75
18NP-Theo	10	20	90	80	0.75	0.5	1.1	99.5	98.9	0.75
18NP-Dox	18	10	82	90	0.40	30	19	70	81	0.70

Initial concentrations a) in the preparation of encapsulation and final concentrations b) of recovered encapsulated nanoparticles, in weight c) and molar d) proportions.

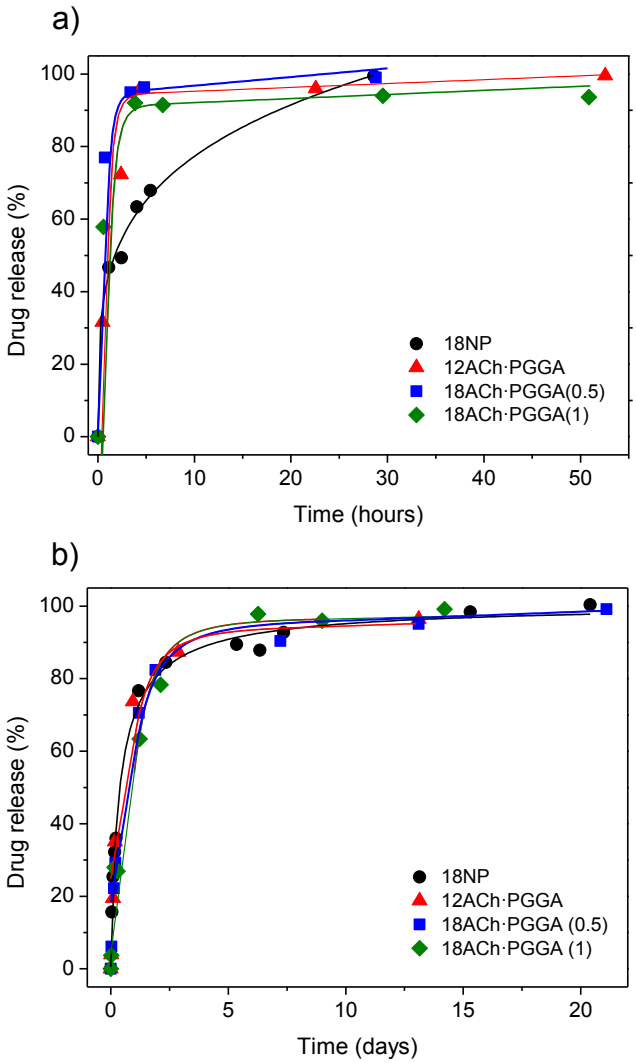

SI Figure 4. Drug release of theophylline a) and carbamazepine b) from nanoparticles and powdered films of *n*ACh·PGGA ionic complexes at pH 7 and 37 ºC.

Chapter IV: Poly(γ-glutamic acid)/nanoclay layered composites

As it is stated and described in previous chapters, ionic complexes of alkyl trimethylammonium-polyglutamic acid, *n*ATMA·PGGA show a defined biphasic layered structure. Helical polyglutamic backbones are distributed in parallel with a constant interlayer distance, whereas the alkyl side chains of surfactants are crystallized perpendicularly to the main chain. The fact that this layered morphology remains unaltered upon heating and melting of polymethilenic chains, make these complexes interesting materials for thermal response applications. Nevertheless, despite their good processability; the mechanical properties displayed by *n*ATMA·PGGA complexes are relatively poor when compared to commodities, as many other biopolymers, hindering their use in a wide number of applications.

The addition of clays as reinforcement into polymeric matrices in one of the strategies employed to afford better physical properties for those materials. The key to afford the best results is related to the dispersion of the clay in the matrix. Layered silicates, such as montmorillonite, formed by platelets with one of the dimensions in nanometric scale, contain a huge specific area, making these clays suitable for such purpose. The good compatibility of two phases, polymeric organic matrix and dispersed inorganic clay, is given by the combination of two factors. On the one hand, clay platelets must be well separated and dispersed showing no aggregation along the whole matrix. In addition, the affinity of the clay to the polymer must be strong enough to avoid phase separation or reaggregation of silicates. For this reason, in order to increase their hydrophobicity, modification of the clays, which are highly hydrophilic, by organic ions is a common method to get compatible and well-dispersed systems. The replacement of sodium cations of interlayer gap by larger organic ions allows not only a better compatibility with the polymer, but also an increase in platelets interdistance, giving rise to a better dispersion.

In the present case, montmorillonites whose sodium interlayer cations have been exchanged by alkylammonium ions, i.e. commercial Cloisite 30B, seem to be a good option for the obtaining of compatibilized *n*ATMA·PGGA nanocomposites. Alkylammonium cations would act as a double compatibilizer agent, for both inorganic clay and PGGA. Moreover, the

layered nature of the clay and the ionic complex could give rise to a nanocomposite with better physical properties, remaining this specific morphology for the use as a new hybrid material with improved performance.

As follows, the study of the obtaining of *n*ATMA·PGGA·x%CL nanocomposites of *n*ATMA·PGGA ionic complexes with different grades of Cloisite 30B is detailed. In addition, the effect of the clay content in thermal and mechanical properties has been analyzed. And, finally, a deep study of the conformation and structure of the new hybrid materials has been carried out.

1. Nanocomposites of comb-like ionic complexes of bacterial poly(glutamic acid) with nanoclays

Summary: Nanocomposites made from stoichiometric complexes of bacterial polyglutamic acid with alkyltrimethyl ammonium surfactants and Cloisite 30B were prepared for a wide range of compositions spanning from 3 to 90% of inorganic contents. The TGA analysis ascertained the compositions of the nanocomposites and revealed that their thermal decomposition proceeded through a mechanism similar to that of the complexes. Their structure and nanomorphology were examined by DSC, XRD and TEM which evidenced an exfoliated structure for low contents in cloisite (less than 10%). Nanocomposites with high cloisite compositions consisted of mixtures of isolated clay lamellae with stacks of intercalated polyacid-cloisite layers heterogeneously dispersed in a disordered complex matrix. Both thermal and mechanical properties of the surfactant complexes changed steadily with the increasing amount of added nanoclay. An exceptional mechanical tensile behavior was however observed for the composite containing 3% of cloisite, which was associated to the occurrence of a fully exfoliated structure.

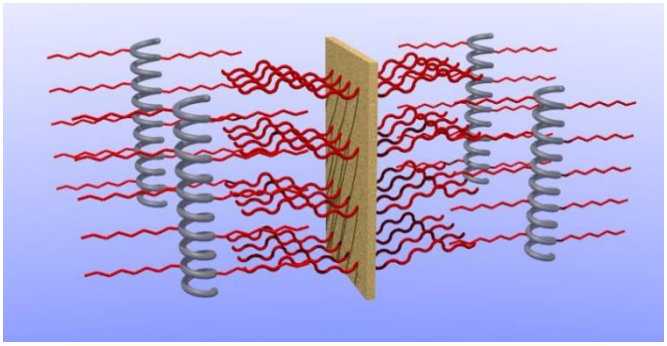

Publication derived from this work:

Tolentino, A.; Alla, A.; Muñoz-Guerra, S. Nanocomposites of comb-like ionic complexes of bacterial poly(glutamic acid) with nanoclays. *Eur. Polym. J.* **2012**, *48*, 1838–1845.

1.1. Introduction

Poly(γ-glutamic acid) (PGGA or γ-PGA) is an emerging biopolymer of commercial interest which is produced by several species of the genus Bacillus. It is water-soluble, biodegradable and edible, and has multiple potential applications in the food, biomedical, healthcare and water-treatment fields.[1,2] With the purpose of extending its use to applications requiring non-water solubility or higher hydrophobicity, PGGA has been subjected to diverse chemical modifications as esterification,[3-6] amidation,[7,8] and others[9,10]. A more recent approach towards the production of water-resistant PGGA derivatives consisted of coupling the naturally-occurring polyacid with quaternary ammonium surfactants to render stoichiometric ionic complexes. In these complexes the polypeptide chain tends to adopt an α-like helix conformation and the ammonium group of the surfactant interacts simultaneously with one amide and two carboxylate groups of PGGA to form a fairly strong link.[11] The complexes appear to be well stable; the helical arrangement ensures a homogeneous distribution of the surfactant molecules around the polypeptide chain and the ionic coupling minimizes the repulsive effect between equally charged ions.

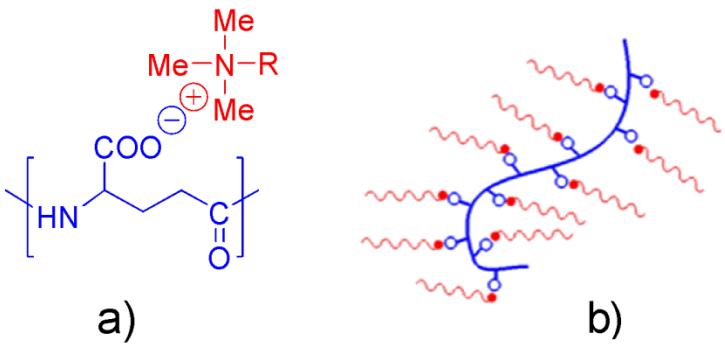

Scheme 1. a) Chemical structure of the ionic complex of PGGA with alkyltrimethylammonium surfactants; b) Comb-like complex shape in solution with surfactant side chains (in red) tethered on the polypeptide main chain (in blue).

By using long linear alkyltrimethylammonium surfactants, comb-like complexes *n*ATMA·PGGA (n being the number of carbons of the surfactant alkyl chain with even values from 12 to 22) with structure and properties similar to poly(α-alkyl-γ-glutamate)s were obtained.[12-14] These comb-like complexes (Scheme 1) are soluble in organic solvents such as chloroform and methanol but not in water, and they are stable to heat up to temperatures above 200 ºC. In the solid state, *n*ATMA·PGGA with n ≥ 16 are arranged in a

biphasic layered structure with the polypeptide chains aligned in sheets and the surfactant alkyl tails crystallized in a hexagonal or pseudo-hexagonal lattice. This layered structure is characterized by an interlayer repeating distance that increases with the length of the alkyl side chain from ~3.5 to ~4.5 nm. The paraffinic phase of the structure melts upon heating at temperatures between 30 and 70 ºC without significant alteration of the bidimensional arrangement. Films prepared from these complexes by casting in chloroform are transparent and display a fair consistency, but their mechanical modules are far from satisfactory and their toughness is low due to their incapacity for flowing.

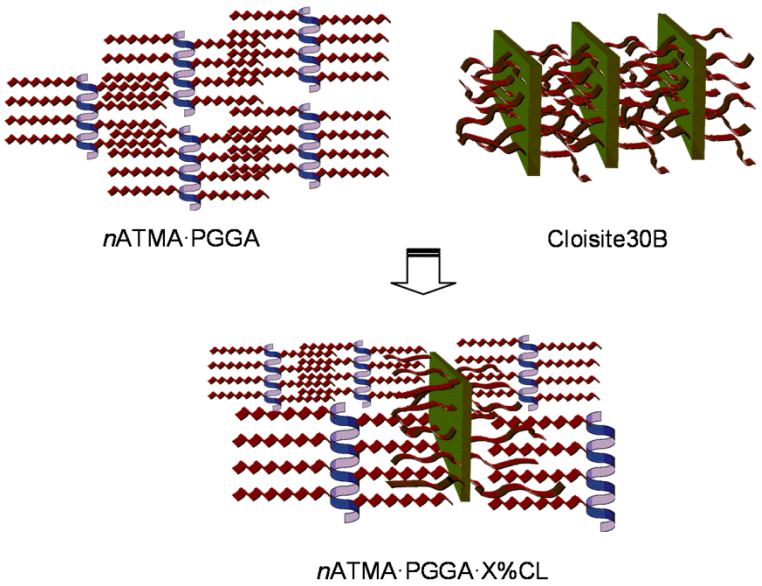

Scheme 2. Intercalation of PGGA and Cloisite 30B layers with partial interdigitation of their respective ionically coupled long alkylammonium side chains.

Addition of small amounts of nanoclays to polymer matrices is a fashionable way of doing to improve physical properties of polymeric materials.[15] The key for the effectiveness of this technique is to reach a good dispersion of the nanoclay into the polymer, a fact that becomes largely determined by the compatibility of the two components. Modification of either the polymer or the clay to enhance their reciprocal affinity is a quite common strategy that produces successful results in many cases. Ion-exchange of pristine montmorillonites with quaternary alkylammoniun salts leads to organophilic clays that are much more convenient for the intercalation of relatively hydrophobic polymers. In this work we wish to present the results obtained in the preparation of three-components nanocomposites made from PGGA and

Cloisite 30B using alkylammonium compounds as compatibilizer agents, the which will be called *n*ATMA·PGGA·X%CL where X represents the percentage of inorganics in the composite. The interest of this study relies on the particular features displayed by the implicated systems that are a priori favourable for the generation of homogeneous mixtures. a) Both PGGA in the complexes and silicate in Cloisite 30B have as counterions alkyammoniun surfactants bearing long polymethylene chains, which will be able to act as compatibilizers between the clay and the polypeptide. b) The same arrangement at the nanometric scale is shared by the complexes and Cloisite 30B which will facilitate the intercalation of the two structures without needing to abandon the layered arrangement (Scheme 2). Our results will indicate however that these expectations are only partially fulfilled.

1.2. Experimental Part

1.2.1. Materials

The sodium salt of poly(D,L-γ-glutamic acid) (Na·PGGA) with a D:L enantiomeric ratio of 59:41 and a weight-average molecular weight of about 300,000 g·mol^{-1} used in this work was kindly supplied by Dr. Kubota of Meiji Co. (Japan). Linear alkyltrimethylammonium cationic surfactants of general formula RMe_3NBr were purchased from Sigma (octadecyl, R= $-C_{18}H_{37}$) or synthesized by us (eicosyl, R= $-C_{20}H_{41}$ and docosyl, R= $-C_{22}H_{45}$) according to a procedure described in the literature.[16] The nanoclay Cloisite 30B (CL), an organically modified montmorillonita with n-alkyl-di(2-hydroxiethyl)-methylammonium (n being a mixture of 14,16 and 18) as counterion, was supplied by SCP from Rockwood Aditives.

1.2.2. *n*ATMA·PGGA ionic complexes

Complexes of poly(D,L-γ-glutamic acid) with ammonium surfactants were prepared following the methodology initially reported by Ponomarenko et al.[17] for poly(α-glutamate) complexes and later applied by us with some minor modifications to the preparation of these complexes.[12,13] In brief, an aqueous solution of the *n*ATMA·Br surfactant was added dropwise to a solution of Na·PGGA in water under stirring at temperatures of 40, 50 or 60 ºC for n= 18, 20 and 22 respectively. The complex precipitated upon standing for a few

hours as a white fine powder that was isolated by centrifugation, washed several times in water and dried under vacuum.

1.2.3. *n*ATMA·PGGA·X%CL nanocomposites

Composites of *n*ATMA·PGGA complexes with Cloisite 30B were prepared applying the following procedure: The amount of Cloisite 30B corresponding to the composition of the composite to be prepared was dispersed in chloroform (1 $g \cdot L^{-1}$) under stirring for 30 min and the dispersion was then sonicated for one hour in a Rosset cell at 0 ºC using a Bandelin HD 2200 Sonoplus ultrasonic homogenizer equipped with 2 mm diameter MS72 tip. The sonicated dispersion was then added to a 0.002M *n*ATMA·PGGA chloroform solution under stirring and the mixture was stirred for 20 h at room temperature. The mixture was then concentrated in vacuo and cast onto a Petri dish allowing a slow evaporation of the solvent. The cast films were dried under vacuum for several days. 18ATMA·PGGA·X%CL and 22ATMA·PGGA·X%CL composites for X = 3, 10, 20, 30, 50, 70 and 90 in addition to the 20ATMA·PGGA·3%CL composite were prepared by such procedure.

1.2.4. Methods

Calorimetric measurements were performed with a Perkin-Elmer Pyris1 DSC instrument provided with an Intracooler device and they were calibrated with indium and zinc. Sample weights of about 2-4 mg were used in a temperature range from -30 to 120 ºC at heating and cooling rates of 10 $ºC \cdot min^{-1}$ under a nitrogen atmosphere. Thermogravimetric analyses were performed at a heating rate of 10 $ºC \cdot min^{-1}$ from 30 to 800 ºC under an inert atmosphere using a Perkin-Elmer TGA6 thermobalance. X-ray diffraction studies were carried out using synchrotron X-ray radiation (WAXS and SAXS). These experiments were performed at A2 Hasylab beam line of DESY in Hamburg (Germany) and at BM16 beam line of ESRF in Grenoble (France). In both cases the energy employed corresponded to a 0.15 nm wavelength. The dispersion grade of Cloisite 30B in composites and mixtures was appraised by surface reflection X-ray diffraction in a PANalytical X'Pert PRO MPD Alpha1 diffractometer using Cu Kα (λ=0.1542 nm) radiation in the Bragg-Brentano geometry. Films properties were evaluated by tensile assays. For these assays, cast films with ~100 μm thickness were cutting in 3 mm-width strips, while the distance between the tensile marks was 10 mm. The Young's modulus, elongation at break, and tensile strength were measured at a

stretching rate of 30 mm·min^{-1} on a Zwick 2.5/TN1S testing machine coupled with a compressor Dalbe DR 150. For TEM observations samples were sectioned with a Leica EM FC7 cryo-ultramicrotome and gold sections were stained with uranyl acetate and observed on a Zeiss 922 Omega electron microscope. This study was carried out in the Macromolecular Chemistry II group of Bayreuth University (Germany).

1.3. Results and discussion

The composites to be studied in this work were prepared by mixing the three components according to the following sequence: Firstly the stoichiometric ionic complexes *n*ATMA·PGGA were created by adding drop wise the aqueous solution of the ammonium surfactant bromide to the aqueous solution of PGGA in the salt form. The precipitated complex was then recovered by filtration and characterized by NMR (SI). All the complexes were approximately stoichiometric with a slight excess of the surfactant component that increased with the length of the alkyl side chain. A finely divided dispersion of Cloisite 30B in chloroform was then obtained by vigorous stirring of the mixture followed by severe sonication until no microaggregates were perceived under the optical microscope. This dispersion was then added to a chloroform solution of the complex and the mixture left under stirring until no sedimentation was observed to take place after ceasing the agitation. The products resulting by casting the fine chloroform dispersion were collected as transparent or translucent films. Composites prepared in this way included complexes bearing alkyl side chains with 18, 20 and 22 carbon atoms and for a wide range of contents in Cloisite 30B going from 3 to 90% of inorganics.

1.3.1. Thermal and mechanical behavior

In first place the composites were analyzed by TGA. The weight loss vs temperature traces for the 18ATMA PGGA·X%CL series are comparatively depicted in Figure 1a and those obtained for the other composites are provided in the SI material. The profiles displayed for the whole series, including those recorded from both the 18ATMA·PGGA complex (0%) and Cloisite 30B (100%), are very similar in shape and show several well separated decomposition stages. The thermal decomposition of *n*ATMA·PGGA complexes has been studied previously in some detail and found to happen through a complex process involving at least three decomposition stages.[18] The first decomposition step of *n*ATMA·PGGA was reported to take place in the 250-290 ºC interval and to involve both

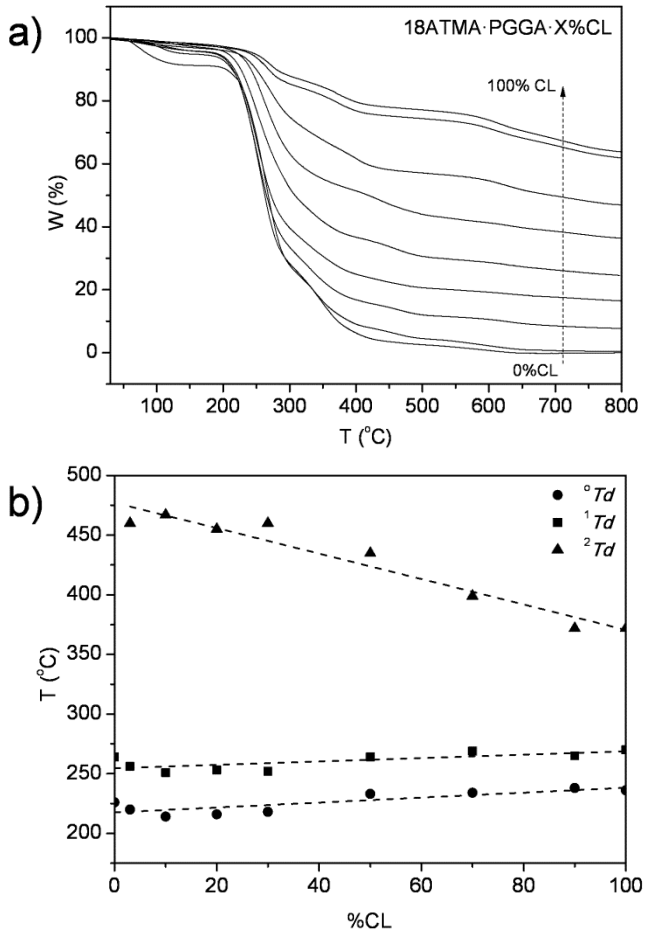

Figure 1 a) TGA traces of the 18ATMA·PGGA·X%CL series recorded under inert atmosphere. b) Evolution of onset and intermediate decomposition temperatures of 18ATMA·PGGA·X%CL with the Cloisite 30B content.

decomposition of the ionic complex promoted by the adsorbed water and cyclodepolymerisation of the PGGA main chain with releasing of pyroglutamic acid. Decomposition of the alkyltrimethyl ammonium compounds generated in the first step and the cracking of the resulting nitrogenated products was found to take place in a wide range of temperatures that goes up to 370 ºC and proceeds along more than one decomposition stage. It seems that 18ATMA·PGGA·X%CL composites thermally degrade following such decomposition pattern regardless their composition. Even Cloisite 30B seems to decompose in the same manner, in this case obviously without generation of pyroglutamic acid. The onset together with the maximum decomposition rate temperatures characterizing the first and second decomposition steps for the 18ATMA PGGA·X%CL series are plotted in Figure 1b as a function of the

clay content. Both ${}^{o}T_d$ and ${}^{1}T_d$ moderately increased with the content in Cloisite 30B whereas ${}^{2}T_d$ markedly decreased. In the three cases decomposition temperatures oscillate between those of the complex and Cloisite 30B indicating that the observed trends are the simple result of the additive mutual influence of the two components.

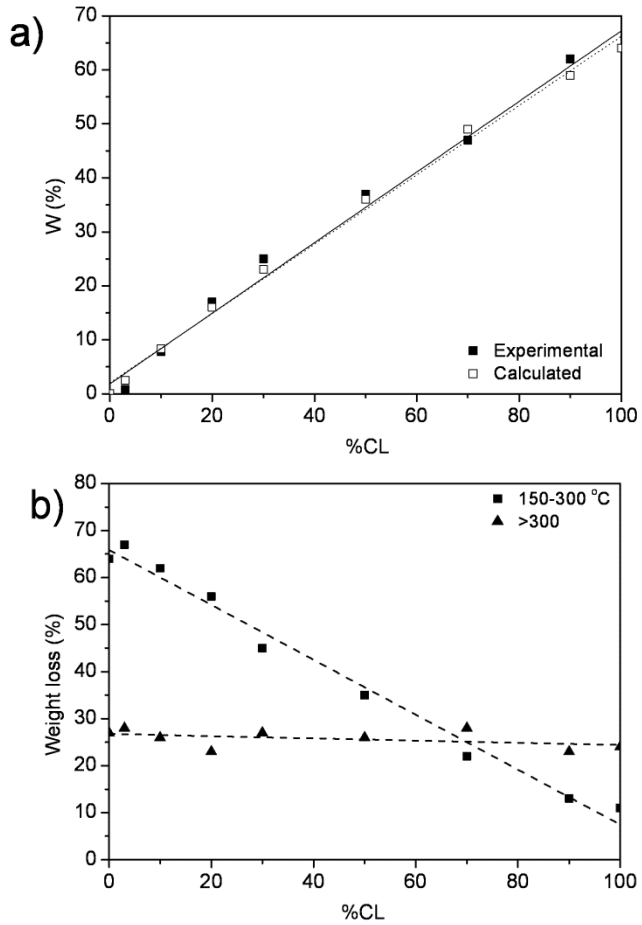

Figure 2. a) Remaining weight after heating at 800 ºC compared to the calculated inorganic content. b) Weight loss observed for the two indicated heating intervals.

Regarding weight loss, it is apparent that the amount of volatile material that is released along the decomposition process varies according to composition. In fact, the remaining residue after heating at 800 ºC increases steadily with the inorganic content, as logically expected; as it is shown in Figure 2a, an excellent correlation was found between the observed values and those

calculated for the composites according to the amount of Cloisite 30B added to prepare them, which definitely ascertains their compositions. The weight loss observed for the first decomposition step and for decomposition at temperatures higher than 300 ºC as a function of the clay content is plotted in Figure 2b. As it is seen most of the lost material is released in the first step taking place between 150 ºC and 300 ºC, and this amount decreased according to the content in Cloisite 30B. Conversely, the weight loss observed at temperatures higher than 300 ºC is much less sensitive to composition so it remains practically constant along the whole series. These results are consistent with the above indicated decomposition mechanism; the weight loss observed at low temperatures reflects mainly the decomposition of the complex with releasing of pyroglutamic acid whereas degradation of the alkyltrimethylammoniun counterparts and volatilization of the corresponding generated amines take place in both complex and Cloisite 30B at heating above 300 ºC.

DSC of *n*ATMA·PGGA complexes with n = 18, 20 and 22 display an unique melting peak at temperatures close to 50, 60 and 70 ºC, respectively, which is known to arise from the fusion of the alkyl side chains.[13] This pattern is more or less changed in the *n*ATMA PGGA·X%CL nanocomposites depending on the content in Cloisite 30B. The first and second heating DSC traces of 18ATMA·PGGA complex, the physical mixture of the complex containing 3% of Cloisite 30B and the composite 18ATMA PGGA·3%CL are compared in Figure 3 (left). What it is remarkable is the peak multiplicity that is observed for the nanocomposite compared to the single peak observed for both the complex and the physical mixture. Furthermore, the melting peak appearing in the second heating of the physical mixture is broadened and clearly displaced to lower temperature whereas recrystallized 18ATMA PGGA·3%CL shows a melting peak that retains its initial shape and position.

The heating traces of the other composites Figure 3 (right) also display peak multiplicity in number and with intensity that is strongly depending on composition; initially, multiplicity is apparent and even increases, but above 50 % of clay, peaks broaden and merge finally in a unique endothermic signal that spreads over a wide temperature range. Similar results were obtained for the 22ATMA PGGA·%XCL series and the whole account of melting temperatures and enthalpies provided by DSC is supplied in the SI file. Enthalpy data for the two series are comparatively analyzed in Figure 4. As expected, the total melting enthalpy for the different compositions regularly diminished as the content in inorganic material increased. On the contrary, the contribution of the secondary peaks to the total melting enthalpy increased proportionally to the content in Cloisite 30B indicating that the occurrence of such peaks is favored by the presence of the nanoclay. These observations

could be explained by considering the occurrence of diverse populations of *n*ATMA·PGGA crystallites differing in size and melting therefore at different temperatures. Differences in size would be the consequence of the mutual intercalation of the complex with the clay, which would happen in more or less extent depending on composition. It is worthy to note that secondary peaks appeared frequently at temperatures higher than the initial one revealing the beneficial influence of the clay on crystallite size, most probably due to its nucleating effect.

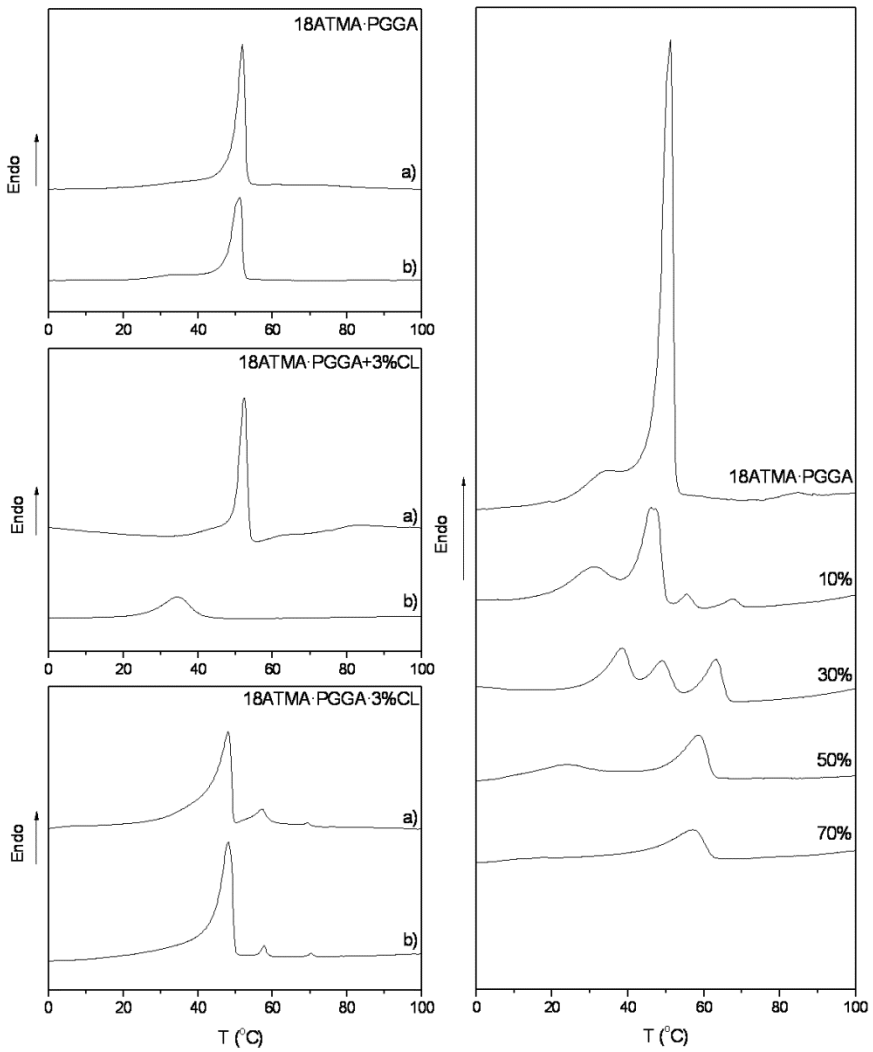

Figure 3. Left: First heating (a) and second heating (b) DSC traces of 18ATMA·PGGA complex, the physical mixture of the complex with 3% of Cloisite 30B, and 18ATMA·PGGA·3%CL composite. Right: Second heating traces of 18ATMA·PGGA·X%CL composites with the indicated contents in Cloisite 30B.

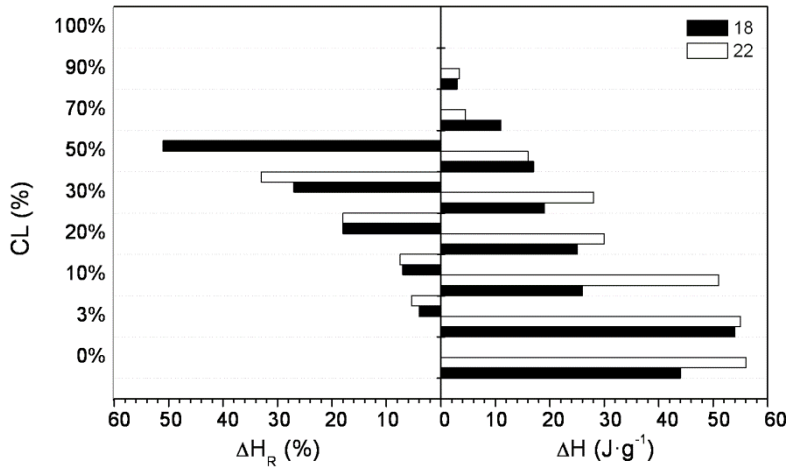

Figure 4. Enthalpy of secondary melting peaks of the *n*ATMA·PGGA·X%CL composite series for n= 18 and 22. Right: Absolute enthalpy values; Left: Percentage of the total melting enthalpy.

The effect of composition on the stress-strain behaviour of the 22ATMA·PGGA·X%CL nanocomposites is shown in Figure 5 and numerical values of the most significant parameters are given in Table 1. The tensile behaviour displayed by 22ATMA·PGGA complex is typical of a brittle weak material with an elastic modulus of around 102 MPa and practically unable to flow. Upon addition of Cloisite 30B, the modulus increased almost steadily to reach a value of about eightfold the original one, which evidenced the strong positive influence of the nanoclay on the stiffness of the material. On the contrary, the effect of composition on elongation was tricky. In overall it was found that increasing contents in Cloisite 30B slightly diminished the ductility of the original complex as it is known to happen frequently in nanoclay-based polymer composite systems.[15] Nevertheless, an exceptional stretching behaviour was exhibited by the composite containing 3% of Cloisite 30B, which was able to be lenghtened near 60% before failure. According to previous reported observations for polymer composites reinforced with nanoclays[19-21] and nanospheres[22] and on the basis of our own results described below, a plausible explanation for such a particular mechanical response would rely on the homogeneous dispersion that is attained in the nanocomposite at that specific level of cloisite content.

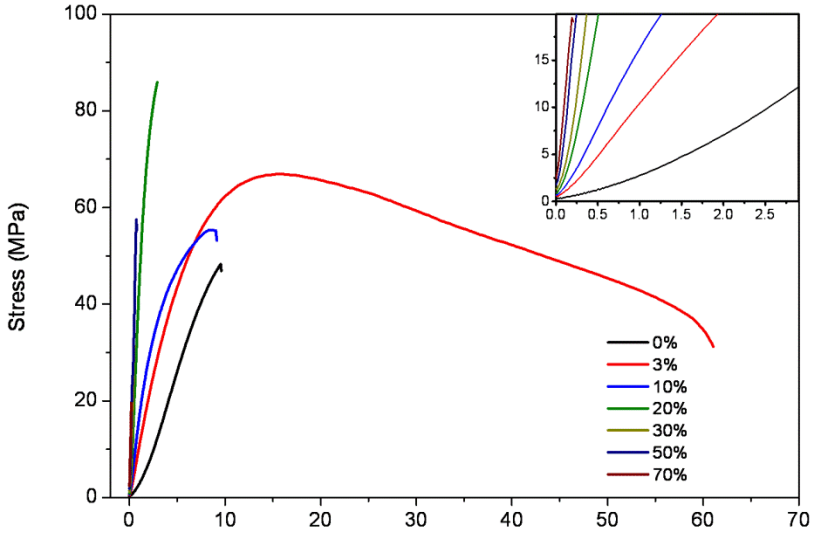

Figure 5. Stress-strain traces of the 22ATMA·PGGA·X%CL series. Inset: Region of low deformation (less than 3%) showing the steady increasing of the elastic modulus with the content in cloisite.

Table 1. Stress-strain properties of 22ATMA·PGGA·X%CL.

X (%)	E (MPa)	σ_{max} (MPa)	ε_b (%)
0	111	5.5	11
3	126	7.5	59
10	194	6.7	9.7
20	546	4.8	1.8
30	687	2.9	1.5
50	875	4.9	1.1
70	839	2.7	0.37

E: Young Modulus, σ_{max}: Maximum tensile stress, ε_b: Strain at break.

1.3.2. Structure and morphology

The X-ray diffraction properties of *n*ATMA·PGGA complexes is well documented.[12-14] The layered structure of these complexes is reflected in the SAXS region as a strong sharp peak in the ~3-4 nm interval (with a weak second order peak at ~1.5-2 nm) arising from the interlamelar spacing, and in

the WAXS region, as a relatively weak peak at 0.41-0.42 nm arising from the hexagonal lattice in which the alkyl side chains are crystallized. In Figure 6 the overall XRD profile of the 18ATMA PGGA complex and the 18ATMA PGGA·3%CL composite are compared.

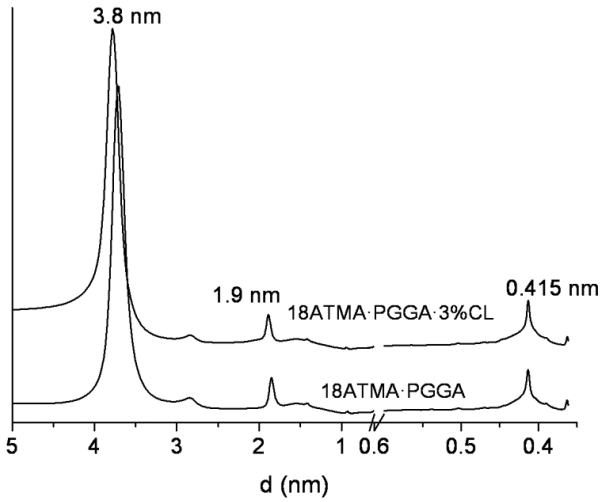

Figure 6. Overall XRD profiles of the complex 18ATMA·PGGA and of the hybrid nanocomposite containing 3% of cloisite.

Both profiles are essentially identical indicating that the structure of the complex is fully retained in the presence of the nanoclay with 3% of cloisite. Furthermore no peak at ~1.8 nm, which could be expected to arise from Cloisite 30B, is detected in the composite profile. In principle the absence of such peak could be taken as indicative that the nanoclay is fully exfoliated. However, since the amount of Cloisite 30B in this composite is small, its detectabilty is uncertain and the conclusion drawn therefrom questionable. In order to support more firmly such indication, the XRD scattering patterns produced by the *n*ATMA PGGA complex, the physical mixture containing 3% of Cloisite 30B and the *n*ATMA PGGA·3%CL composite in the $3º < 2\theta < 10º$ region (which is the region where the characteristic peak of the layered structure of Cloisite 30B should appear), were recorded for the two composites series with n equal to 20 and 22, and these profiles are comparatively depicted in Figure 7. The presence of the layered structure of the nanoclay is clearly detected in the physical mixture as a prominent shoulder (~1.8 nm) of the second order peak of the complex whereas no sign of such reflection is perceived in the profiles of the composites.

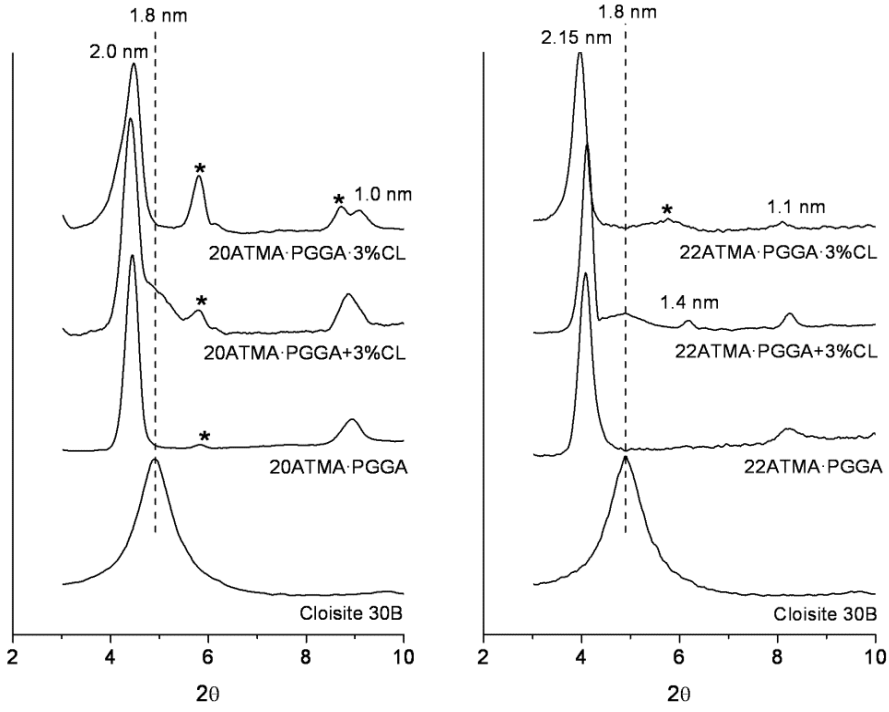

Figure 7. a) Compared XRD profiles for the 20ATMA·PGGA (left) and 22ATMA·PGGA (right) systems and Cloisite 30B in the scattering region around the cloisite main diffraction peak. The strong peak appearing at ~ 2 nm is the second order of the main peak arising from the layer periodicity of the complex. (*) Peak arising from the excess of 20ATMA·Br and 22ATMA·Br that is present in small amounts in some preparations.

The SAXS profiles of the whole series of 18ATMA PGGA·X%CL nanocomposites are shown in Figure 8. The sharp peak arising from the nanostructure of the complex is clearly observed for composites with contents in Cloisite 30B up to 30% whereas for higher compositions the scattering becomes diffuse and located above the ~4 nm spacing. This diffuse scattering is also present in the 18ATMA PGGA·30%CL as a prominent shoulder of the main scattering peak coming from the nanocomplex, and it is still perceived in composites with 10 and 20 % of cloisite as a very weak shoulder. On the other hand, the WAXS region of these composites shows the sharp peak at 0.42 nm characteristic of the crystallized paraffinic phase, which remains almost unaltered up to contents of 30% in cloisite to disappear for higher compositions.

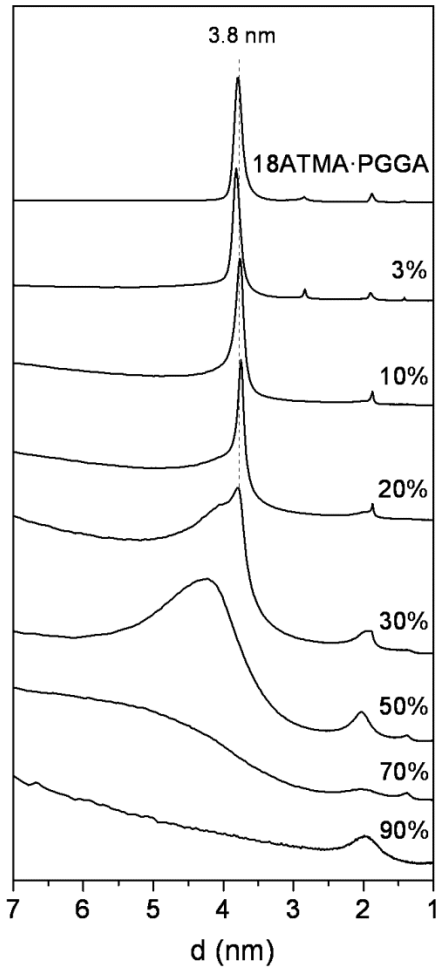

Figure 8. Compared SAXS profiles for the 18ATMA·PGGA·X%CL nanocomposite series showing the evolution of the long spacing of the structure as a function of composition.

A preliminary TEM analysis of the composites provided unambiguous evidence on the nanomorphology of the dispersions that are created when Cloisite 30B is introduced into the matrix of the *n*ATMA·PGGA complex at different concentrations. Representative micrographs from crio sections of the 18ATMA PGGA·X%CL nanocomposites are depicted in Figure 9. The picture of the composite containing 3% of Cloisite 30B (Figure 9a) shows the layered structure of the complex as a regular bidimensional pattern with a repeating spacing of about 3.8 nm. In this case the individual cloisite sheets are hardly seen probably due to the masking effect of the prominent structure of the complex. The structure of the complex is much fainter in the picture taken

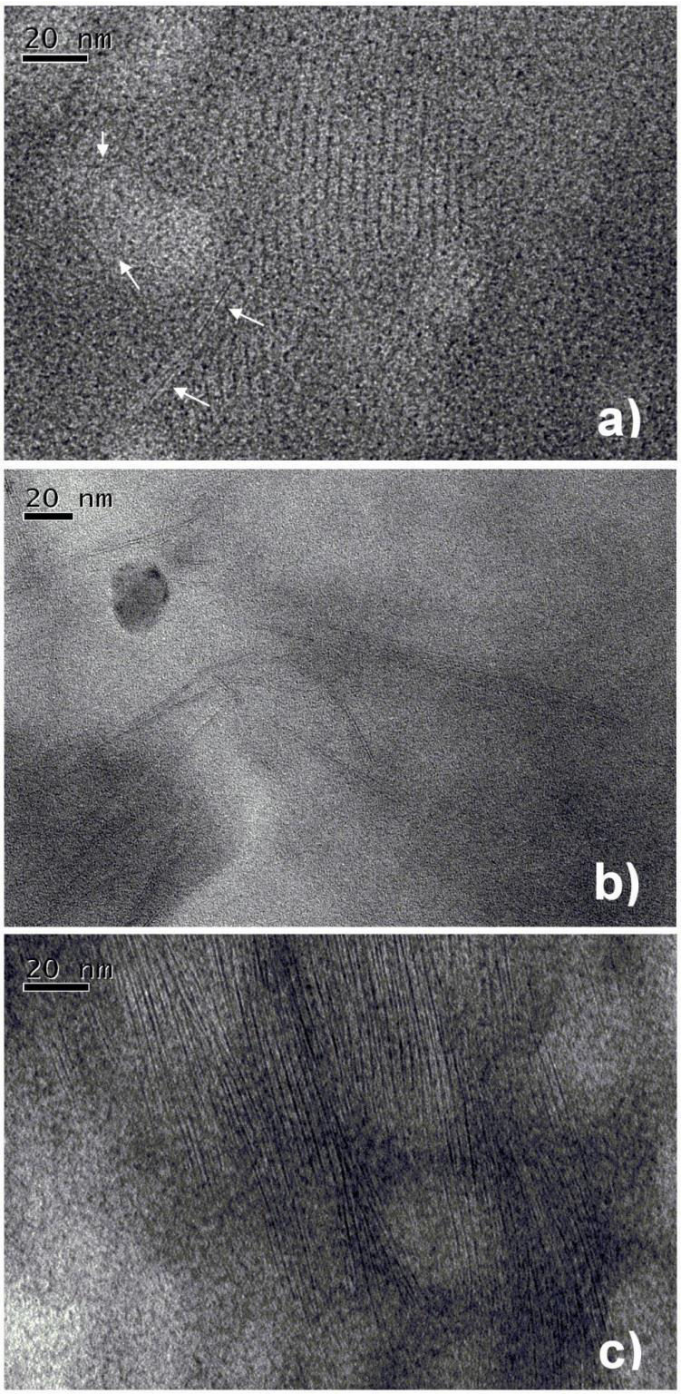

Figure 9. TEM micrographs of 18ATMA·PGGA·X%CL composites containing 3% (a), 30% (b) and 50% (c) of Cloisite 30B. Arrows in (a) point to some distinguishable isolated cloisite lamellae.

from the composite with 30% of Cloisite 30B (Figure 9b) allowing to see the isolated lamellae with a thickness of about 1.0-1.5 nm. Finally, the structure of the complex becomes completely absent in the picture taken from 18ATMA PGGA·50%CL composite (Figure 9c). The distinguishing feature of this composite is the frequent presence of bundles of Cloisite 30B lamellae with a rather variable repeating spacing that oscillates around 4.5 nm. The information provided by these images is in agreement with the XRD results described above. In the light of the collected information it can be concluded that Cloisite 30B form nanocomposites with an exfoliated structure at low contents of inorganics. For large incorporated amounts of clay, extensive intercalation of the polyacid in the cloisite gallery takes place favoured by the compatibilizing effect of the alkylammonium chains. Nevertheless, the intercalated nanoclay stacks remain separated from the rest of the complex generating a somewhat discontinuous structure. The occurrence of such heterogeneities is invoked to be the responsible for the decay in ductility that is observed in the composites containing large amounts of Cloisite 30B.

1.4. Conclusions

Three-components nanocomposites were prepared by mixing Cloisite 30B with the comb-like stoichiometric complexes made of PGGA and alkyltrimethylammonium surfactants with 18, 20 and 22 carbon atoms in the alkyl side chain. These nanocomposites decomposed upon heating above 200 ºC with depolymerisation of PGGA and destruction of the complex followed by degradation of the generated alkylamines. The nanometric layered structure characteristic of the complex was retained in the composites with low contents in cloisite whereas the order in the organic matrix faded away when the amount of nanoclay attained 30%. According to DSC, XRD and TEM results, the arrangement of cloisite in the composite largely depended on composition; it evolved from a homogeneous dispersion of exfoliated lamellae in the ordered complex polypeptidic matrix to a greatly heterogeneous state profuse in intercalated PGGA tactoids. The elastic modulus of the material increased steadily with the content in inorganics from 0.1 MPa up to 0.8 MPa whereas both the elongation to break and the maximum stress decreased. The nancomposite containing 3% of nanoclay distinguished by displaying an exceptional ductility, which is interpreted to be due to the homogeneous dispersion of the clay in the complex that is attained for such composition.

1.5. References

1. Gross R, A. Bacterial γ-poly(glutamic acid). In: *Biopolymers from Renewable Resources*, Kaplan, D. L. Ed.; Springer: Berlin, 1998: pp 195.

2. Bajaj, I.; Singhal, R. Poly (glutamic acid) – An emerging biopolymer of commercial interest. *Bioresource Technol.* **2011**, *102*, 5551–5561.

3. Kubota, H., Nambu, Y.; Endo, T. Convenient and quantitative esterification of poly(gamma-glutamic acid) produced by microorganism. *J. Polym. Sci. A Polym. Chem*. **1993**, *31*, 2877-2878.

4. Gross, R. A.; McCarthy, S. P.; Shah, D. T. Gamma-poly(glutamic) acid esters. US Patent 5378807, 1995.

5. Melis, J.; Morillo, M.; Martínez de Ilarduya, A.; Muñoz-Guerra, S. Poly (α-alkyl γ-glutamate) s of microbial origin : I. Ester derivatization of poly (γ-glutamic acid) and thermal degradation. *Polymer* **2001**, *42*, 9319–9327.

6. Morillo, M.; Martinez de Ilarduya, A.; Alla, A.; Muñoz-Guerra, S. Comblike alkyl esters of biosynthetic poly (γ-glutamic acid). 2. Supramolecular structure and thermal transitions. *Macromolecules* **2003**, *36*, 7567–7576.

7. Kunioka, M. Biosynthesis and chemical reactions of poly(amino acid)s from microorganisms. *Appl. Microbiol. Biotechnol.* **1997**, *47*, 469–475.

8. Akagi, T.; Kaneko, T.; Kida, T.; Akashi, M. Preparation and characterization of biodegradable nanoparticles based on poly(γ-glutamic acid) with L-phenylalanine as a protein carrier. *J. Control. Release.* **2005**, *108*, 226–236.

9. Murakami, S.; Endo, T. Preparation and properties of biodegradable poly(γ-glutamic acid) gels (I). Crosslinking reactions by diepoxides. *Kenkyu-Hokoku*. **2001**, *7*, 72-75.

10. Tsubokawa, N.; Inagaki, M.; Endo, T. Graft polymerization of methyl methacrylate initiated by pendant azo groups introduced onto γ-poly(glutamic acid). *J. Polym. Sci. A Polym. Chem.* **1993**, *31*, 563-568.

11. Zanuy, D.; Alemán, C. Molecular dynamics study of complexes of poly (glutamate) and dodecyltrimethylammonium. *Biomacromolecules* **2007**, *8*, 663–671.

12. Pérez-Camero, G.; García-Alvarez, M., Martínez De Ilarduya, A.; Fernández, C., Campos, L., Muñoz-Guerra, S. Comblike complexes of bacterial poly(γ,D-glutamic acid) and cationic surfactants. *Biomacromolecules*. **2004**, *5*, 144–152.

13. García-Alvarez, M.; Alvarez, J.; Alla, A.; Martínez de Ilarduya, A.; Herranz, C.; Muñoz-Guerra, S. Comb-like ionic complexes of cationic surfactants with bacterial poly(γ-glutamic acid) of racemic composition. *Macromol. Biosci.* **2005**, *5*, 30–38.

14. Tolentino, A.; Martínez de Ilarduya, A.; Alla, A.; Muñoz-Guerra, S. Ionic complexes of polyacids and cationic surfactants. *Macromol. Symp.* **2010**, *296*, 265–271.

15. Tjong, S. C. Structural and mechanical properties of polymer nanocomposites. *Mater. Sci. Eng. R* **2006**, *53*, 73–197.

16. Hendrix, W. T.; von Rosenberg, J. L. The mechanism of the rearrangement of the hydrocobalt carbonyl catalyzed isomerization of 3-phenylpropene. *J. Am. Chem. Soc.* **1976**, *98*, 4850–4852.

17. Ponomarenko, E. A.; Waddon, A. J.; Tirrell, D. A.; Macknight, W. J. Structure and properties of stoichiometric complexes formed by sodium poly (α,L-glutamate) and oppositely charged surfactants. *Langmuir* **1996**, *12*, 2169–2172.

18. Portilla-Arias, J. A.; García-Alvarez, M.; Martínez de Ilarduya, A.; Muñoz-Guerra, S. Thermal decomposition of microbial poly (γ-glutamic acid) and poly (γ-glutamate)s. *Polym. Degrad. Stab.* **2007**, *92*, 1916–1924.

19. Song, M.; Hourston, D. J.; Yao, K. J.; Tay, J. K. H.; Ansarifar, M. A. High performance nanocomposites of polyurethane elastomer and organically modified layered silicate. *J. Appl. Phycol.* **2003**, *90*, 11–13.

20. Lebaron, P. C.; Pinnavaia, T. J. Clay nanolayer reinforcement of a silicone elastomer. *Chem. Mater.* **2001**, *13*, 3760–3765.

21. Tien, Y. I.; Wei, K. H. High-tensile-property layered silicates/polyurethane nanocomposites by using reactive silicates as pseudo chain extenders. *Macromolecules* **2001**, *34*, 9045–9052.

22. Xie, X.-L.; Li, R. K.-Y.; Liu, Q.-X.; Mai, Y.-W. Structure-property relationships of in-situ PMMA modified nano-sized antimony trioxide filled poly(vinyl chloride) nanocomposites. *Polymer* **2004**, *45*, 2793–2802.

1.6. Supporting information

SI Table 1. DSC data of *n*ATMA·PGGA-X%CL composite series.

Complex	1st heating			2nd heating			cooling	
	T_m^1	ΔH_m^1 TOT.	ΔH_m^1 REL.	T_m^2	ΔH_m^2 TOT.	ΔH_m^2 REL.	T_c	ΔH_c TOT.
	(ºC)	($J \cdot g^{-1}$)	(%)	(º C)	($J \cdot g^{-1}$)	(%)	(ºC)	($J \cdot g^{-1}$)
18 series								
18ATMA ·PGGA	**52**	56	--	**51**	44	--	46	41
3%CL	**48**, 57, 69	58	10	**48**, 58, 70	54	4.0	44, 55	48
10%CL	**49**, 54, 67	55	3.1	**46**, 56, 67	26	7.0	25, 41	30
20%CL	**43**, 48, 52, 64	44	6.5	26, **43**, 52, 64	25	18	23, 37, 48	20
30%CL	**41**, 50, 63	34	14	39, 49, **63**	19	27	34, 47	19
50%CL	**53**, 60	28	19	24, **59**	17	51	18, 44	17
70%CL	**58**	9	--	**57**	11	--	47	7
90%CL	**44**	2	--	**43**	3	--	40	3
22 series								
22ATMA ·PGGA	**69**	63	--	**72**	56	--	66	56
3%CL	**66**, 72, 80	74	3.5	**69**, 78, 83	55	5.4	66	57
10%CL	53, **64**, 69, 77, 90	75	5.6	**66**, 80	51	7.5	50, 60	51
20%CL	**61**, 68, 77	58	7.6	55, **79**	30	18	45, 56, 64	36
30%CL	**61**, 76	51	15.4	58, **76**	28	33	40, 62	28
50%CL	58, **69**	33	42.4	**66**	16	--	53	12
70%CL	**52**	1.7	--	**36**	4.5	--	30	2.9
90%CL	--	--	--	**35**	3.4	--	43	3.1

Tm (**main peak**, secondary peaks): melting temperature at first (1) and second (2) heating. *Tc:* crystallization temperature. ΔHm_{TOT}: total melting enthalpy. ΔHm_{REL}: relative melting enthalpy of secondary peaks. ΔHc: crystallization enthalpy.

SI Table 2. Thermal data of *n*ATMA·PGGA complexes, physical mixture and composites from TGA.

Compounds	Thermogravimetric data		
	$^{o}T_d$ [a] (ºC)	$^{m}T_d$ [b] (ºC)	W [c] (%)
18ATMA·PGGA	204	**247**/344	**24**/0
18ATMA·PGGA + 3%CL	206	**245**/344	**28**/0.8
18ATMA·PGGA·3%CL	205	**243**/321	**25**/2.7
20ATMA·PGGA	204	**250**/323	**21**/0.7
20ATMA·PGGA + 3%CL	202	**250**/354	**30**/0.4
20ATMA·PGGA·3%CL	203	**249**/341	**34**/4.2
22ATMA·PGGA	204	**262**/384	**32**/0.7
22ATMA·PGGA + 3%CL	204	**271**/381	**39**/2.5
22ATMA·PGGA·3%CL	205	**266**/351	**31**/3.2

(a) Onset decomposition temperature. (b) Derived temperature maximum peaks correspond to degradation **main** and secondary step. (c) Remaining weight after each degradation step.

SI Table 3. Thermal data of composites 18ATMA·PGGA·X%CL from TGA.

Composites	Thermogravimetric data		
	$^{o}T_d$ [a] (ºC)	$^{m}T_d$ [b] (ºC)	W [c] (%)
18ATMA·PGGA	213	**264**/349	**24**/0
3%CL	209	**256**/336/460	**27**/8/0.8
10%CL	204	**251**/330/467	**31**/16/7.8
20%CL	203	**253**/354/455	**38**/25/17
30%CL	208	**252**/340/460	**47**/38/25
50%CL	219	**264**/435	**53**/37
70%CL	226	**276**/431	**69**/53
90%CL	220	**265**/372/610	**84**/75/62
Cloisite30B film	222	**270**/372/617	**87**/78/64

(a) Onset decomposition temperature. (b) Derived temperature maximum peaks correspond to degradation **main** and secondary steps. (c) Remaining weight after each degradation step; final value at 800 ºC.

SI Table 4. Thermal data of composites 22ATMA·PGGA·X%CL30B from TGA.

Composites	Thermogravimetric data		
	$^{o}T_d$ [a] (ºC)	$^{m}T_d$ [b] (ºC)	W [c] (%)
22ATMA·PGGA	206	85/**243-293**/384	92/**25**/0.4
3%CL	206	80/**244-283**/362	92/**28**/3.1
10%CL	207	72**/288**/334/451	92/**31**/19/13
20%CL	203	73/**283**/358/456	94/**40**/26/19
30%CL	204	76/**273**/355/439	94/**47**/33/25
50%CL	215	95/**278**/404	97/**60**/45
70%CL	230	97/**282**/405	98/**73**/57
90%CL	220	56/**275**/401/591	98/**83**/69/65
Cloisite30B film	222	60/**270**/372/617	99/**87**/78/64

(a) Tangential onset decomposition temperature. (b) Derivated temperature maximum peaks correspond to degradation **main** and secondary steps. (c) Remaining weight after each degradation step; final value at 650 ºC.

SI Table 5. Tensile mechanical properties of 22ATMA·PGGA·X%CLO30B series.

Compound	Young Modulus E (MPa)	Maximun Elongation (%)	Maximum Stress (MPa)
22ATMA·PGGA	111	10.8	5.5
3%CL	126	59	7.5
10%CL	194	9.7	6.7
20%CL	546	1.8	4.8
30%CL	687	1.5	2.9
50%CL	875	1.1	4.9
70%CL	839	0.37	2.7

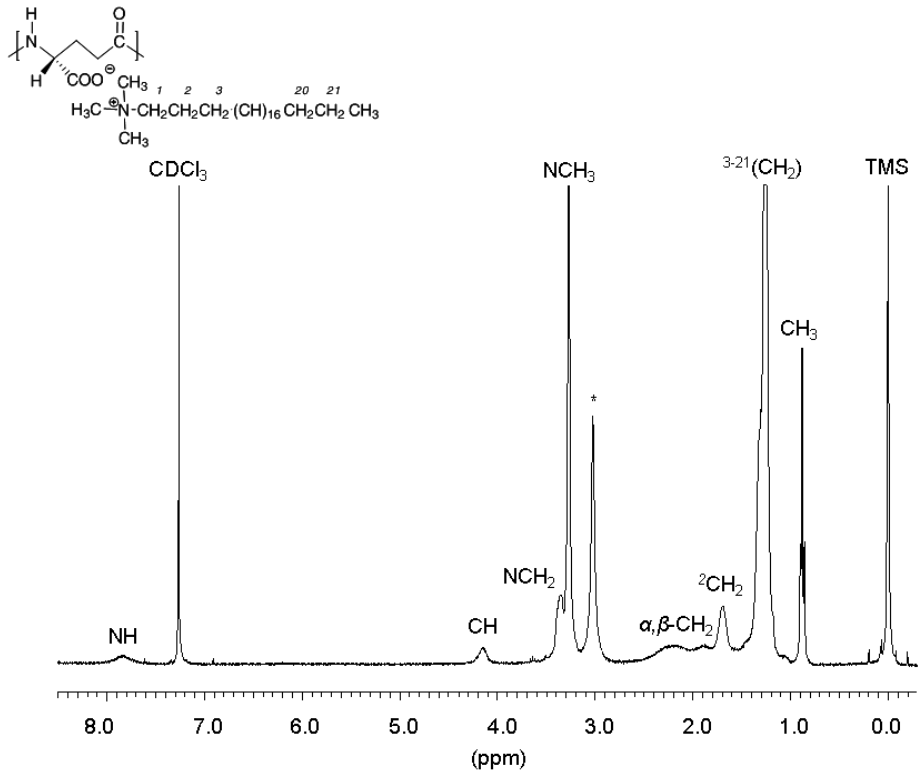

SI Figure 1. ^{1}H NMR spectra of 22ATMA·PGGA complex in $CDCl_3$ recorded at 25 ºC. (*) peak of water.

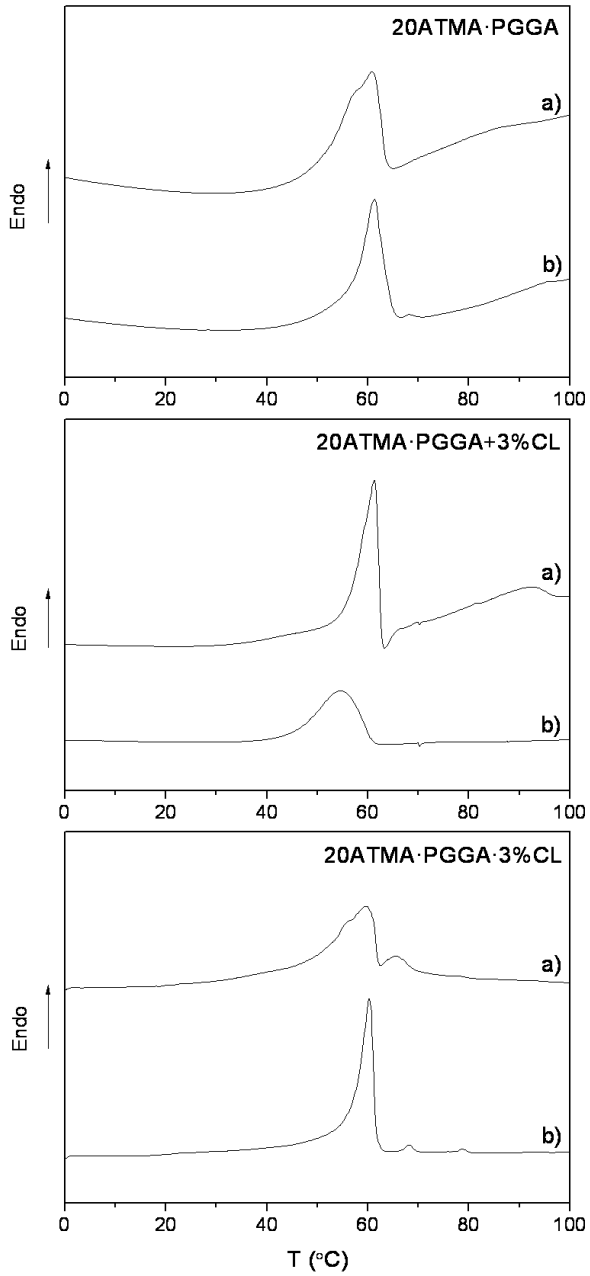

SI Figure 2. First heating (a) and second heating (b) DSC traces of 20ATMA·PGGA complex, physical mixture of the complex with 3% CL, and 20ATMA·PGGA·3%CL composite.

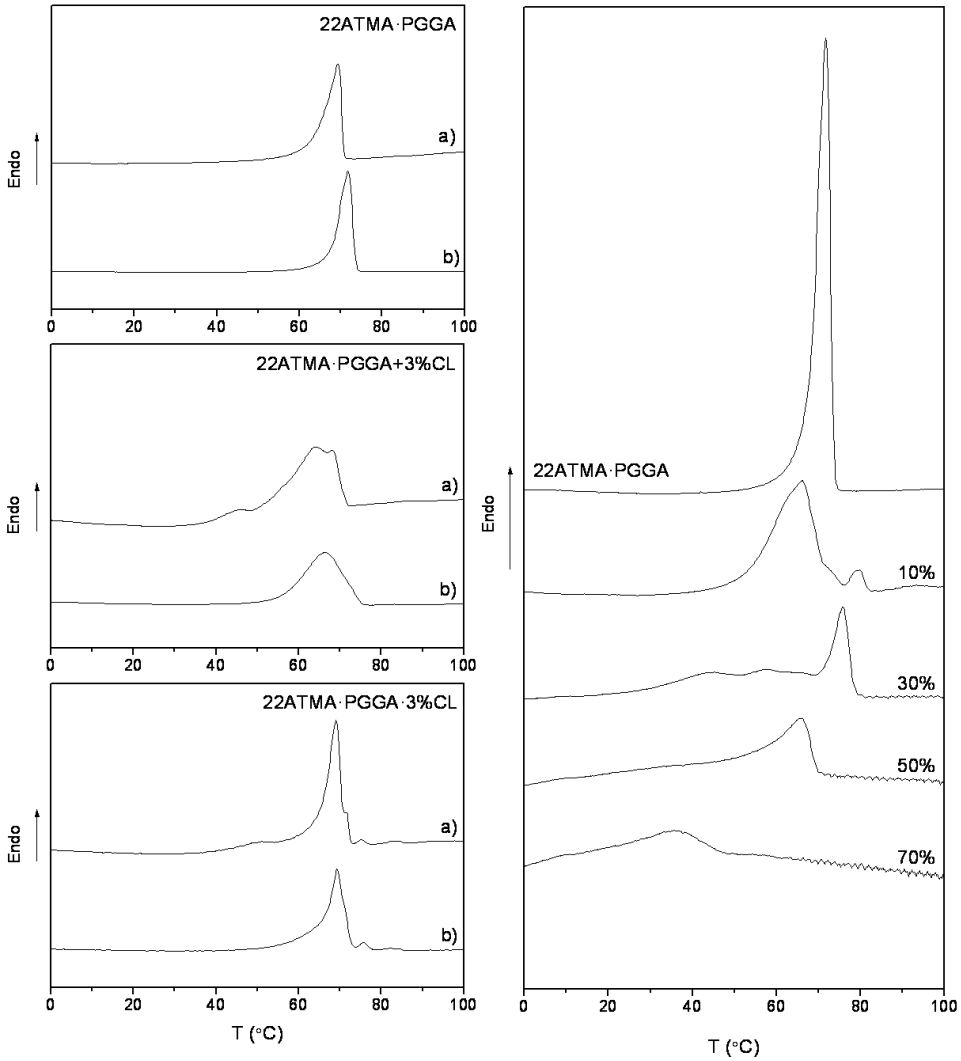

SI Figure 3. Left: First heating (a) and second heating (b) DSC traces of 22ATMA·PGGA complex, physical mixture of the complex with 3% CL, and 22ATMA·PGGA·3%CL composite. Right: Second heating traces of 22ATMA·PGGA·X%CL composites with the indicated contents in CLO30B.

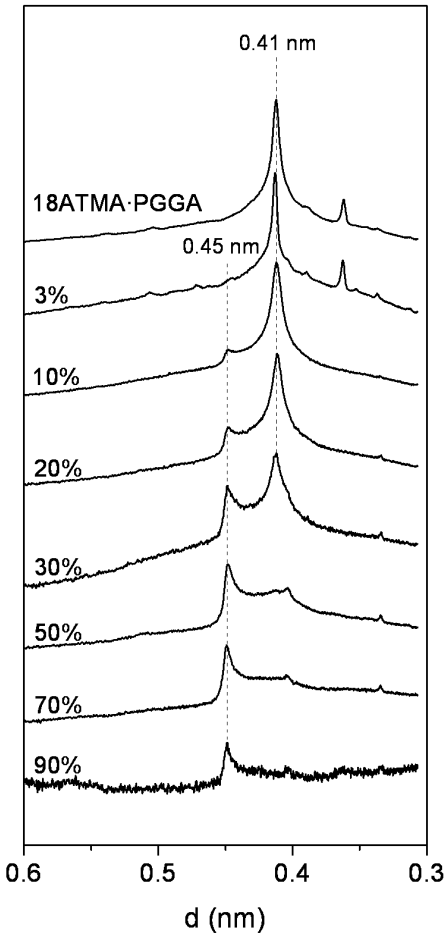

SI Figure 4. Compared WAXS profiles for the 18ATMA·PGGA·X%CL composite series showing the evolution of the long spacing of the structure as a function of composition.

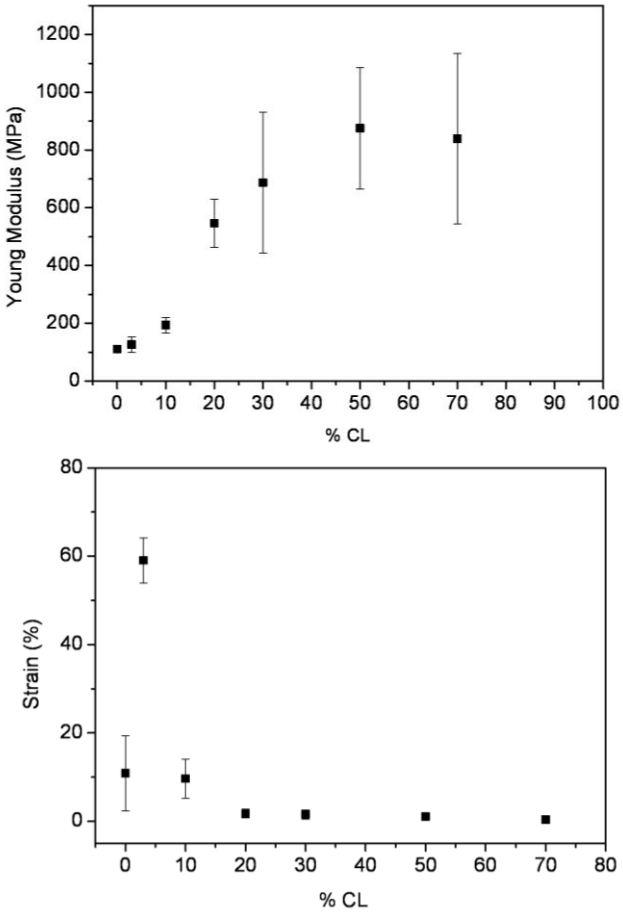

SI Figure 5. Young modulus (top) and strain (bottom) of 22ATMA·PGGA-x%CL composites series obtained from tensile tests.

2. The structure of poly(γ-glutamic acid)/nanoclay hybrids compatibilized by alkylammonium surfactants

Summary: Stoichiometric ionic complexes of bacterial poly(γ-glutamic acid) with the cationic N-octadecyl and N-docosyl-N,N,N-trimethylammonium surfactants were mixed with alkylammonium modified bentonite (Cloisite 30B) to generate hybrid compounds covering a wide range of clay/polymer compositions. The structure of these compounds was examined by XRD and cryoTEM, which indicated extensive penetration of the biopolymer into the nanoclay galleries with widening or even destruction of the layered arrangement of the complex and the clay. Simultaneous SAXS/WAXS analysis in real time showed that hybrids with moderate inorganic contents displayed melting/crystallization upon heating/cooling within the 40-60 ºC interval with concomitant expansion/contraction of the intersheet spacing. 13C CP-MAS NMR revealed that an anti-to-gauche conformational interconversion of the alkyl chains was involved in the melting/crystallization process. The results provided by energy-based dynamical simulations proved the feasibility of the polyacid and the nanoclay to be homogenized in the hybrid due to the compatibilizing effect of the surfactant.

Publication derived from this work:

Tolentino, A.; León, S.; Alla, A.; Martínez de Ilarduya, A.; Muñoz-Guerra, S. The structure of poly(γ-glutamic acid)/nanoclay hybrids compatibilized by alkylammonium surfactants. *Eur. Polym. J.* **2013**, *49*, 2596-2609.

2.1. Introduction

Poly(γ-glutamic acid) (PGGA) is a water-soluble, biodegradable and edible biopolymer with multiple potential applications in the food, biomedical, healthcare and water-treatment fields.[1-3] PGGA has been subjected to diverse chemical covalent modifications on the carboxylic side group in order to expand its use in frontier applications such as active packaging or biomaterials.[4] The effects pursued with such modifications are to diminish the affinity of PGGA for water,[5-7] to improve its physical properties[8-10] or to make it suitable for building drug delivery systems.[11-14] Another convenient method to modify PGGA is by complexation with quaternary ammonium compounds. Thus, coupling of PGGA with cationic polyelectrolytes such as chitosan[15-17] or poly(ε-lysine) leads to the formation of stable complexes with outstanding potential in biomedicine. Additionally, coupling with cationic tetraalkylammonium surfactants at nearly stoichiometric ratios constitutes also a very appealing approach to render non-water-soluble PGGA modifications.[19,20] Such complexes are easily prepared and comfortably handled, and they are fairly stable to heat. In these compounds (Scheme 1), the PGGA adopts an α-like helix conformation and the surfactant molecules are distributed around the polypeptide chain with the ammonium and carboxylate groups mutually interacting, so the intramolecular repulsive charge effects are minimized and the system becomes well stabilized.[21,22]

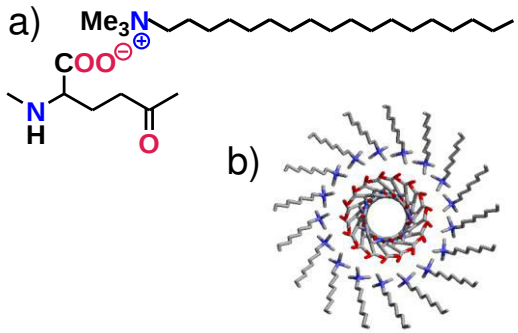

Scheme 1. Chemical structure of the ionic complex of PGGA /octadecyltrimethylammonium surfactant (a) and the axial projection of its helical conformation.

Comb-like complexes made of PGGA coupled with alkyltrimethylammonium surfactants (*n*ATMA·PGGA, n being the number of carbons of the alkyl group with even values from 12 to 22) were synthesized for the first time more than ten years ago.[23] These *n*ATMA·PGGA complexes are remarkable from a

structural point of view because in the solid state they tend to self-assemble in a biphasic arrangement made of alternating paraffinic and polypeptidic layers. For *n*ATMA·PGGA with n ≥ 18, the long alkyl tails filling the paraffinic phase are crystallized in a pseudohexagonal lattice adopting an almost extended conformation and oriented more or less perpendicular to the polypeptide helical chains. The most relevant features of the comb-like *n*ATMA·PGGA complexes with n = 18, 20 and 22 are compared in Table 1. These all three complexes display by DSC a well-defined endothermic peak characteristic of melting that moves from ~50 to ~70 ºC as the length of the alkyl chain increases. Their SAXS profiles are distinguished by an intense sharp reflection arising from the periodical spacing of the layered structure with values of 3.8, 4.0 and 4.2 nm for n being 18, 20 and 22, respectively. In turn their WAXS patterns show a unique signal at 0.42 nm coming from the 100 interplanar distance of the hexagonal lattice in which the alkyl side chains are crystallized. The DSC traces and XRD profiles of these complexes are provided in the Supporting Information chapter (SI).

Addition of small amounts of nanoclays to polymer matrices may render composites with enhanced physical properties, the success of the method being largely determined by the compatibility of the two components.[24] Even when the polymers are hydrophilic, their intimate mixing with the nanoclay is highly challenging because the kinetics and topologic difficulty of the polymer chain to penetrate into the silicate galleries. Ionic polypeptides have been directly mixed with unmodified oppositely charged nanoclays to get benefit from the counter-charge interaction for attaining extensive exfoliation. Thus sodium montmorillonites-based nanocomposites of poly(L-lysine), either neat[25,26] or mixed with poly(α-glutamic acid),[27,28] have been investigated and found to display intimate specific polymer-clay interactions for a wide range of compositions. On the other hand, PGGA has been mixed with magnesium/aluminium layered double hydroxides using the anion exchange method; in this case the silicate layered structure was preserved and the only changes concerning dehydration and consequent contraction of the interlayer distances were observed.[29,30] Pomonis et al.[31] have reported on structured hybrids made of poly(amino acid)-cationic surfactant complexes on which a silicate shell was attached to render mesoporous silicate materials.

Table 1. Characteristic data of *n*ATMA·PGGA complexes.

	Composition		TGA[a]		DSC[b]				XRD[c]			TEM[d]
					1st Heating		2nd Heating		SAXS		WAXS	
	ATMA:PGGA (mol:mol)	ρ (g·mL^{-1})	$^{o}T_d$ (ºC)	$^{max}T_d$ (ºC)	T_m (ºC)	ΔH_m (kcal·mol^{-1})	T_m (ºC)	ΔH_m (kcal·mol^{-1})	L_0^1 (nm)	L_0^2 (nm)	d_{100} (nm)	L_0 (nm)
18ATMA·PGGA	1.0:1	1.06	213	264	48	3.6	50	3.8	3.8	1.9	0.42	3.8
20ATMA·PGGA	1.2:1	1.01	211	250	55	5.6	58	5.4	4.0	2.0	0.42	4.0
22ATMA·PGGA	1.3:1	1.02	206	243	72	6.9	68	5.7	4.2	2.1	0.42	4.4

[a] Onset and maximum rate decomposition temperatures recorded by TGA. [b] Melting temperatures and enthalpies measured by DSC. [c] X-Ray diffraction data registered in the small angle and wide angle regions. [d] Periodical spacing measured on TEM micrographs of uranyl acetate stained cryosections.

Modification of montmorillonites with alkylammoniun ions is a method frequently used to facilitate the intercalation of the highly polar silicate structures with relatively hydrophobic polymers.[24] Recently we have published on the preparation and preliminary characterization of three-component nanocomposites made from *n*ATMA·PGGA complexes and Cloisite30B (Chapter IV.1).[32] These composites were coded *n*ATMA·PGGA·X%CL where X represents the percentage of inorganics in the mixture. In that work the basic features of these composites regarding composition as well as their thermal and mechanical properties were examined. It was then found that the texture of such composites was more or less homogeneous depending on composition, and that their properties changed almost steadily with increasing amounts of the added nanoclay. Now we wish to report in detail on the structure of these composites and on the effects that temperature exerts on the mutual arrangement of the complex and clay moieties in the layered hybrid assemblies. This study has been performed using basically a combination of X-ray diffraction and electron microscopy techniques, and it has been substantiated with energy-based modeling and simulation.

2.2. Experimental part

2.2.1. Materials

The sodium salt of poly(D,L-γ-glutamic acid) (Na·PGGA) with a D:L enantiomeric ratio of 59:41 and a weight-average molecular weight of about 300,000 g·mol-1 used in this work was kindly supplied by Dr. Kubota of Meiji Co. (Japan). Linear alkyltrimethylammonium cationic surfactants of general formula RMe_3NBr were purchased from Sigma (octadecyl, R= $-C_{18}H_{37}$) or synthesized by us (docosyl, R= $-C_{22}H_{45}$) according to a procedure described in the literature.[33] The nanoclay Cloisite30B (CL), a montmorillonite modified with n-alkyl(alkylenyl)-di(2-hydroxyethyl) methylammonium with n being a mixture of 14,16 and 18, was supplied by Rockwood Aditives Limited (UK).

2.2.2. *n*ATMA·PGGA ionic complexes and *n*ATMA·PGGA·X%CL. composites.

Complexes of poly(D,L-γ-glutamic acid) with ammonium surfactants were prepared following the methodology initially reported by Ponomarenko et al.[34] for the synthesis of poly(α-glutamate) complexes and later applied by us with

some minor modifications in several occasions.[19,20] In brief, an aqueous solution of the *n*ATMA·Br surfactant was added drop-wise to a solution of Na·PGGA in water under stirring at temperatures of 40 or 60 ºC for n= 18 and 22, respectively. The complex precipitated upon standing for a few hours as a white fine powder that was then isolated by centrifugation, washed several times with water, and dried under vacuum.

Composites of *n*ATMA·PGGA complexes with CL were prepared as previously described by us (Chapter IV.1).[32] In brief, the clay was finely dispersed in chloroform at a concentration of 1 g·L-1, and the suspension was then added to a solution of *n*ATMA·PGGA in chloroform at room temperature, and gently stirred until no sedimentation was detected upon standing. Evaporation under vacuum followed by casting of the concentrated suspension rendered consistent films of 18ATMA·PGGA·X%CL and 22ATMA·PGGA·X%CL composites for X = 3, 10, 20, 30, 50, 70 and 90. The appearance of these films was more or less translucent depending on clay content (see illustrative pictures in the SI chapter).

2.2.3. Methods.

Calorimetric measurements were performed with a Perkin-Elmer Pyris1 DSC instrument provided with an Intracooler device, and thermograms were calibrated with indium and zinc. Sample weights of about 2-4 mg were used in a temperature range from -30 to 120 ºC at heating and cooling rates of 10 ºC·min-1 under a nitrogen atmosphere. X-ray diffraction (XRD) studies were carried out using synchrotron X-ray radiation at wide and small angles (WAXS and SAXS) simultaneously. These experiments were performed at A2 Hasylab beam line of DESY in Hamburg (Germany) and at BM16 beam line of ESRF in Grenoble (France). In both cases the energy employed corresponded to a 0.15 nm wavelength. The transmission electron microscopy (TEM) study was carried out in the Macromolecular Chemistry II group of Bayreuth University (Germany) using a Zeiss 922 Omega electron microscope. For observation, samples were sectioned with a Leica EM FC7 cryo-ultramicrotome and gold sections were stained with uranyl acetate. Scanning electron microscopy (SEM) images were taken with a field emission JEOL JSM-7001F instrument. The samples were coated with Pt/Pd with a thickness about 1 nm using a Cressington Sputter Coater 208 HR equipment.

2.2.4. Modeling and simulation

Molecular dynamics simulations have been performed on models representing the two counterparts of the nanocomposite, namely the 18ATMA·PGGA complex and the Cloisite30B clay, and also the intercalation nanocomposite containing equal amounts of them. All the simulations were carried using the TINKER package.[35,36] The MM3 force-field[37,38] was used for all the organic components, while special parameters were applied to the atoms of the clay. Due to the complexity of the systems under study, and since the main focus is on the behavior of the surfactant molecules, the atomic positions of both PGGA helices and clay sheets were kept fixed during the simulations.

The most stable 17/5 helical conformation of PGGA[39] has been used in this work for modeling the 18ATMA·PGGA complex, and since no significant differences were found between the models built with chains in parallel or antiparallel, only the parallel arrangement has been taken into account. A periodic box containing 6 chains in parallel arrangement and dimensions 6a x b x c, each chain containing 17 repeat units, has been considered. According to experimental data on separation between sheets (b = 3.8 nm) and density (1.05 g·mL-1), and the axial periodicity of 2.57 nm given for the 17/5 helix, the interhelix distance along the sheet should be approximately 1.18 nm. However, in order to build a simulation box with the same dimension than that used for Cloisite30B along the sheet direction, the dimensions of the whole simulation supercell were fixed as X = 7.19 nm, Y = 3.80 nm, Z = 2.56 nm, which would correspond to a density of 1.02 g mL-1.

The organically modified clay Cloisite 30B has been modeled by a periodic infinite montmorillonite sheet with the modifying molecules placed in the intersheet space. The modifier is a methyl dihydroxyethyl ammonium tallow made of 62% of C18 (mixture of alkyl and alkylene groups), 30% of C16 and 8% of C14). The atom positions in the clay sheets were taken from the structure reported in the literature and the aluminum to magnesium substitutions were incorporated in 2/3 of the unit cells at random positions, according with the clay cationic exchange capacity (CEC of 0.9 meq·g-1) reported by the supplier. The dimensions fixed for the whole simulation supercell were X = 7.18 nm, Y = 1.85 nm, Z = 2.56 nm which corresponds to 8b x c x 5a, where a = 0.51 nm, b = 0.90 nm and c = 18.5 nm comprising therefore 40 unit cells with 27 aluminum to magnesium substitutions. The dimensions of this supercell are consistent with those taken for the box chosen for the 18ATMA·PGGA complex, and has the sheets arranged normal to the same direction (Y-direction).

Finally an idealized intercalated system consisting of alternating parallel sheets of 18ATMA·PGGA and Cloisite was built for modelling the 18ATMA·PGGA·50%CL nanocomposite. Specifically, the periodic supercell comprised 6 PGGA helices with 17 repeat units and a sheet of 6 x 5 of CL unit cells, and both cells were mutually oriented along the Y-axis. According with SAXS observations, several values in the 4.0 and 4.5 nm range were initially considered for the intersheet distance. Since the obtained results were essentially similar, only those obtained for an intersheet distance of 4.0 nm will be presented. Thus, the simulation supercell finally adopted for the intercalation nanocomposite was X = 7.18 nm, Y = 8.0 nm, Z = 2.56 nm.

In order to get a reasonable description of the structure of the systems under study, the following approach was adopted. For the 18ATMA·PGGA complex and the 18ATMA·PGGA·50%CL nanocomposite, an initial geometry was generated with all the side alkyl chains between the polypeptidic or/and silicate sheets arranged in an extended conformation. Next, the geometries were subjected to a molecular dynamics at a high temperature (1000 K) to allow the alkyl tails to relax, while the polymer main chains and clay atoms were kept fixed at their initial positions. Afterwards, the temperature was decreased to 298 K and the geometry minimized before running a long molecular dynamics trajectory of 1500 ps, with polymer main chains and clay atoms hold fixed as before. The same procedure was applied to the Cloisite model, starting from an intersheet initial value of 3.6 nm in order to provide space for the extended alkyl chains. This intersheet distance was progressively reduced in short molecular dynamics simulations, allowing the modifying molecules to relax until the experimental value (1.85 nm) was finally achieved. As with the other models, the clay atoms were kept fixed during the simulations.

2.3. Results and discussion

*n*ATMA·PGGA·X%CL composites made of *n*ATMA·PGGA complexes for n = 18 and 22, and Cloisite with inorganics to complex ratios ranging from 3 to 90% were generated by applying a straightforward methodology designed to ensure an intimate mixing of the components. Their compositions and relevant properties are given in Table 2.

In contrast to *n*ATMA·PGGA complexes, the DSC traces of the composites showed multiple melting of the paraffinic phase with peaks varying in number and intensity according to composition. These peaks broadened with increasing contents in Cloisite to finally merge into one wide plateau. As

expected the melting enthalpy steadily diminished as the content in inorganic material increased. Such behavior is interpreted as due to the melting of the different size crystallized domains that are generated in the intercalation of the complex with the clay and subsequent nucleation.[40] Regarding the mechanical behavior the elastic modulus and strength of the composites increased steadily with increasing contents in Cloisite whereas the elongation to break diminished in an unevenly manner. *n*ATMA·PGGA·3%CL composite was unique in deviating from the general trend most likely due to the complete exfoliation attained for such composition; this composite displays a melting enthalpy slightly larger than the complex and an elongation at break of around ten times larger than for any other composition (Chapter IV.1).[32]

Table 2. Data of *n*ATMA·PGGA·X%CL nanocomposites.

%[a]		DSC[d]				E^e (MPa)
I	C	1st heating		2nd heating		
		T_m (ºC)	ΔH_m (cal·g^{-1})	T_m (ºC)	ΔH_m (cal·g^{-1})	
			***n* = 18**			
0	100	52	13.4	51	10.5	30
3	96	48,57,69	13.9	48,58,70	12.9	40
10	87	49,54,67	13.1	46,56,67	6.2	115
20	75	43,48,52,64	10.5	26,43,52,64	6.0	150
30	64	41,50,63	8.1	39,49,63	4.5	230
50	43	53,60	6.7	24,59	4.1	-
70	24	58	2.2	57	2.6	-
90	8	44	0.5	43	0.7	-
			***n* = 22**			
0	100	69	15.0	72	13.4	110
3	96	66,72,80	17.7	69,78,83	13.1	125
10	87	53,64,69,77,90	17.9	66,80	12.2	190
20	75	62,68,77	13.9	54,79	7.2	550
30	64	61,76	12.2	58,76	6.7	690
50	43	58,69	7.9	66	3.8	875
70	24	52	0.4	36	1.1	840
90	8	-	-.	35	0.8	-

[a]Composite composition expressed in % of inorganics (I) and complex content (C).
[b]Melting temperature and enthalpy (global value for all peaks) measured by DSC at heating from pristine samples and from samples cooled after heating at 120 ºC.
[c]Elastic modulus measured in tensile essays.

2.3.1. Structural analysis of composites.

First the nanomorphology of the *n*ATMA·PGGA complexes was examined by TEM. For such purpose, thin films of the complexes were prepared by casting from chloroform and subjected to cryo-sectioning. TEM observation of the uranyl acetate stained cryo-sections afforded for the first time direct evidence on the layered arrangement adopted by the complexes. As it is shown in Figure 1 the paraffinic and polypeptidic layers are revealed as alternating light and dark parallel stripes according to the affinity of the phase for the stain. Comparison of the micrographs taken from complexes with n = 18 and 22 shows clearly how the interlayer distance increases with n taking values that correlates well with those measured by SAXS. Furthermore the level of regularity observed in these micrographs is fully consistent with the relative degree of crystallinity estimated for each complex.

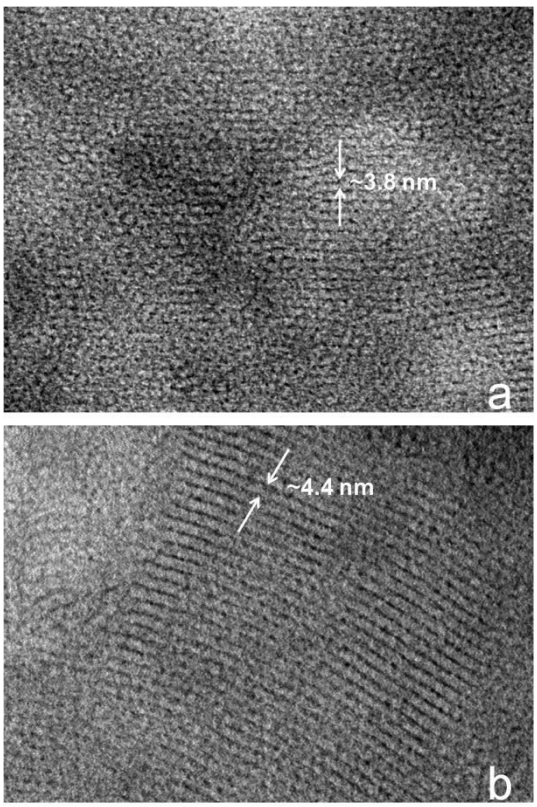

Figure 1. TEM micrographs of the *n*ATMA·PGGA complexes. a) n = 18; b) n = 22.

The SAXS and WAXS profiles registered from the whole series of 18ATMA•PGGA•X%CL including the complex itself are compared in Figure 2.

The sharp peak at 3.8 nm, which is characteristic of the layered structure of the 18ATMA•PGGA complex,[19,20] was found to be also present in composites with contents in Cloisite up to 30% (Figure 2a). For higher compositions the 3.8 nm peak vanished and a new scattering embracing spacings above 4 nm came out. This signal broadened progressively as the content in Cloisite increased to finally disappear when the composition in inorganics reached 90%. It should be noticed that this broad signal was visible in the 18ATMA•PGGA•30%CL as a prominent shoulder of the 3.8 nm peak, and even perceivable in composites with low contents in Cloisite. The WAXS profiles (Figure 2b) show the gradual disappearance of the sharp peak at 0.41 nm characteristic of the crystallized paraffinic phase of the complex as the content in Cloisite increases; the profile evolution observed in WAXS is parallel to that observed in SAXS indicating that the structural changes taking place at the two levels must occur simultaneously.

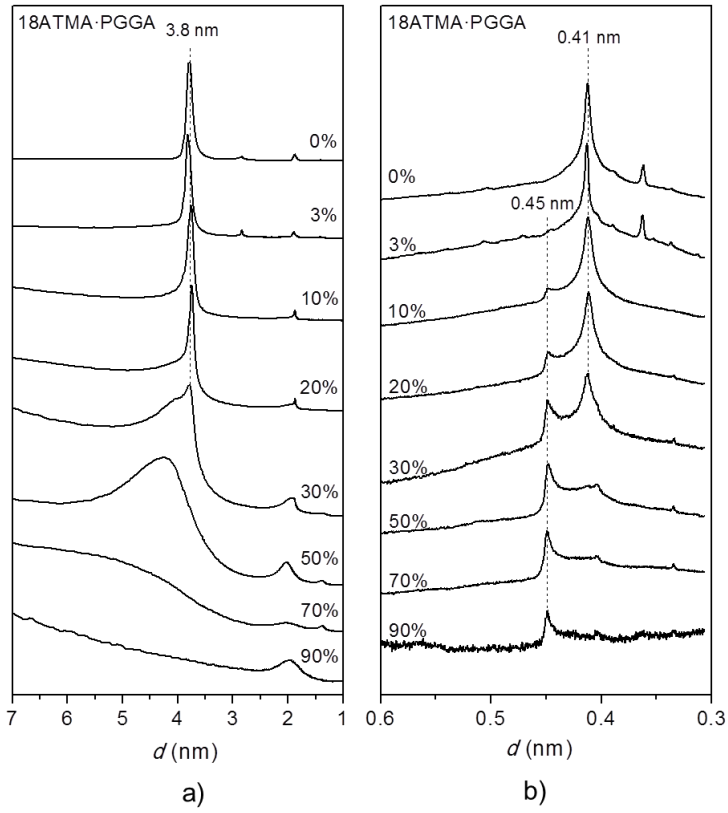

Figure 2. Compared SAXS (a) and WAXS (b) profiles for the 18ATMA·PGGA·X%CL series showing the evolution of the long spacing of the layered biphasic structure and the scattering associated to the paraffinic phase, respectively, with increasing content in Cloisite.

The XRD results are coherent with DSC data and indicate that an extensive intercalation of Cloisite and the 18ATMA·PGGA complex must have happened in the composite, which is responsible for both the expansion of the intersheet distance and the disordering of the paraffinic phase observed for high inorganic contents. The occurrence of extensive intercalation should be confirmed by the disappearance of the ~1.8 nm peak characteristic of Cloisite30B. Unfortunately, this cannot be tested for 18ATMA·PGGA·X%CL since the second order of the basic intersheet spacing L_0 of this complex appears at ~1.9 nm masking the scattering that could arise from the nanoclay. This is not the case for 22ATMA·PGGA·X%CL whose L_0 spacing second order appears at ~2.1 nm. The evolution of the scattering produced by 22ATMA·PGGA·X%CL within the 1.5-5º Bragg angle region with increasing contents in Cloisite is shown in Figure 3. In this comparative plot it is clearly seen that the characteristic 1.8 nm peak of Cloisite30B is absent in the nanocomposites for all compositions, and that the L0 second order of the complex moves to higher spacings and broadens with increasing clay contents. These observations proved that the original layered structures present in both complex and Cloisite were significantly modified by mutual interaction with generation of other layered arrangements with enlarged intersheet spacings.

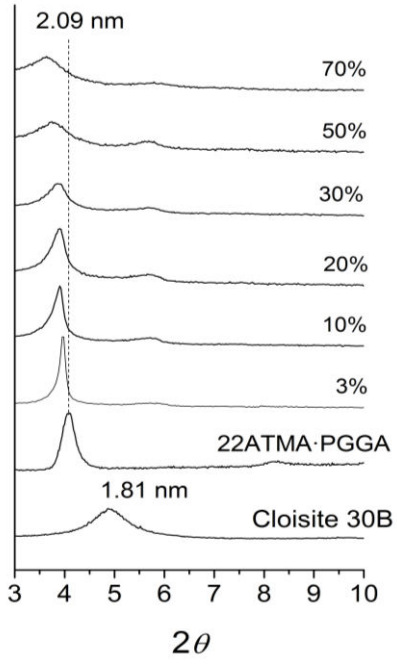

Figure 3. Compared XRD profiles for 22ATMA·PGGA complex, Cloisite30B, and 22ATMA·PGGA·X%CL composites series in the 1.5-5º Bragg angle region.

The SEM analysis of cryo-fractured surfaces of the nanocomposites revealed noteworthy changes in the micromorphology of the complex matrix upon incorporation of the Cloisite. A sequence of SEM micrographs recorded from the 18ATMA·PGGA complex and its composites with increasing clay contents is shown in Figure 4. The texture appears uniform in all cases without apparent distinction between phases. Furthermore the rather sticky appearance displayed by the complex evolves progressively to a sharply leaf-like morphology typical of nanoclays as the content in Cloisite increases; at 90% concentration the texture becomes highly porous and largely exfoliated. These observations bring out the occurrence of a system that exhibits the morphology characteristic of the major component without perceivable segregation of the minor one, at least at the micrometer level at which the analysis was performed.[41]

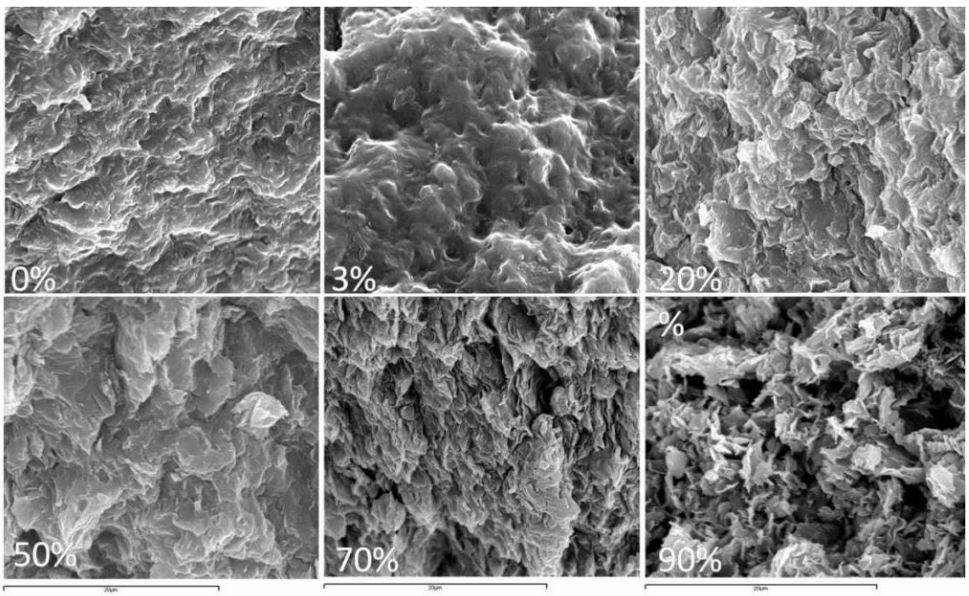

Figure 4. SEM micrographs of cryo-fractured surfaces of 18ATMA·PGGA and 18ATMA·PGGA·X%CL films with the indicated compositions.

The TEM analysis of the composites a unambiguous evidence on the type of dispersions that was created when Cloisite30B was introduced into the matrix of the *n*ATMA·PGGA complex at different concentrations. Micrographs from composites containing low amounts of clay showed the complex banded unaltered, which is interpreted due to the masking effect of the deeply stained polypeptidic phase on the Cloisite sheets. Representative pictures taken from

cryo-sections of the 22ATMA·PGGA·X%CL nanocomposites with contents of 30 and 50% of Cloisite are depicted in Figure 5. In both pictures a texture consisting of more or less parallel straight dark lines of constant thickness that delineate an interline space of variable width and slighter stained, is filling part of the viewed area. Such texture is interpreted as arising from an intercalated structure made of clay and polypeptidic layers alternating with a paraffinic phase made of surfactant with the long alkyl tails in a more or less crystallized state. The interline distance oscillates between 3.5 and 5 nm with higher values being much more frequent in the case of 22ATMA·PGGA·50%CL. It is worthy noticeable that the area surrounding the layered region exhibits a disordered appearance although some reminiscences of the grainy layered structure characteristic of the complex are still detectable.

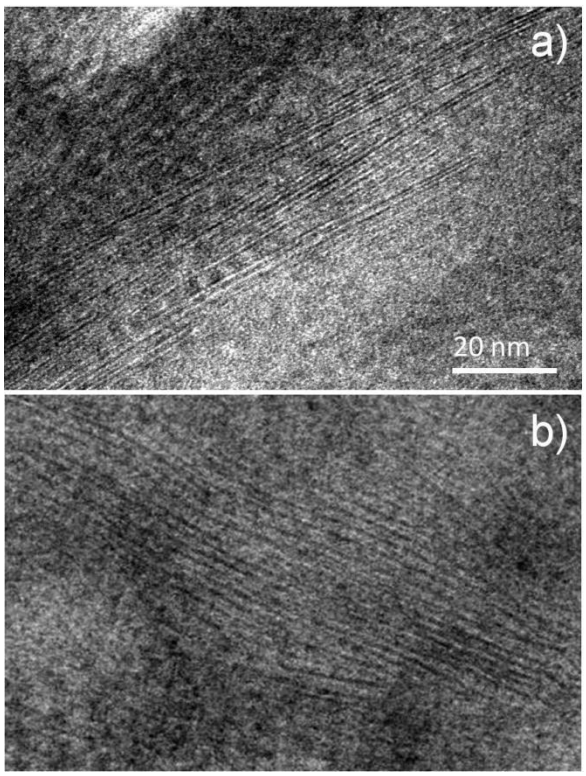

Figure 5. TEM micrographs of 22ATMA·PGGA·X%CL composites with 30% (a) and 50% (b) of inorganic content.

The micrograph shown in Figure 6 was taken from the 22ATMA·PGGA·70%CL. It displays a large view of the composite with plenty of Cloisite sheets spread over the whole area and arranged in a variety of

recognizable patterns.[41]. Closed aggregates of sheets with an average intersheet spacing oscillating between 2 and 5 nm (inset a), bundles of Cloisite sheets separated by distances of 10 nm or even more (inset b), and individual sheets without apparent interrelation (inset c), are seen on this impressive image. The SAXS profile recorded from this composite consisted of a broad scattering signal embracing a range of spacings going from 4 nm up to above 10 nm, which is consistent with the intersheet spacing populations identified by TEM.

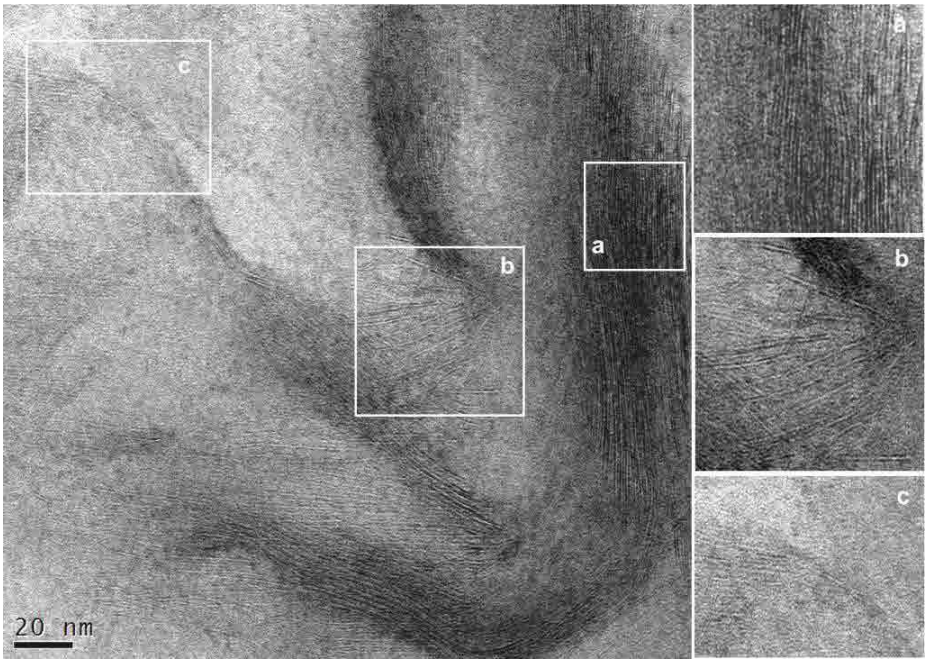

Figure 6. TEM image of 22ATMA·PGGA·70%CL with Cloisite distributed as aggregated (a), intercalated (b) and exfoliated (c) structures.

The information provided by XRD and TEM allows to conclude that PGGA was able to penetrate the galleries of Cloisite forming a hybrid layered arrangement that retains the basic features of the original nanostructure characteristics of both the complex and the nanoclay. For compositions with minor amounts of Cloisite, all the incorporated clay became exfoliated and the silicate sheets were homogeneously dispersed in the complex phase. When large amounts of Cloisite were added, the silicate in the composite was also intimately mixed with PGGA but unevenly distributed in the form of individual lamellae and stacks with varying intercalation degrees; in addition some compact bundles of clay platelets appear clearly segregated from the complex containing phase.

2.3.2. Thermal effects.

Melting/crystallization of the paraffinic phase are well characterized transitions that take place reversibly in comb-like *n*ATMA·PGGA complexes when they are heated at rather mild temperatures (<100 ºC).[23] Similar processes are observed in *n*ATMA·PGGA·X%CL for those compositions at which the alkyl side chains are able to crystallize. The real time XRD analysis using synchrotron radiation and registering SAXS and WAXS in parallel was used to follow in detail the structural changes involved in these processes, and data obtained from such experiments are collected in Table 3.

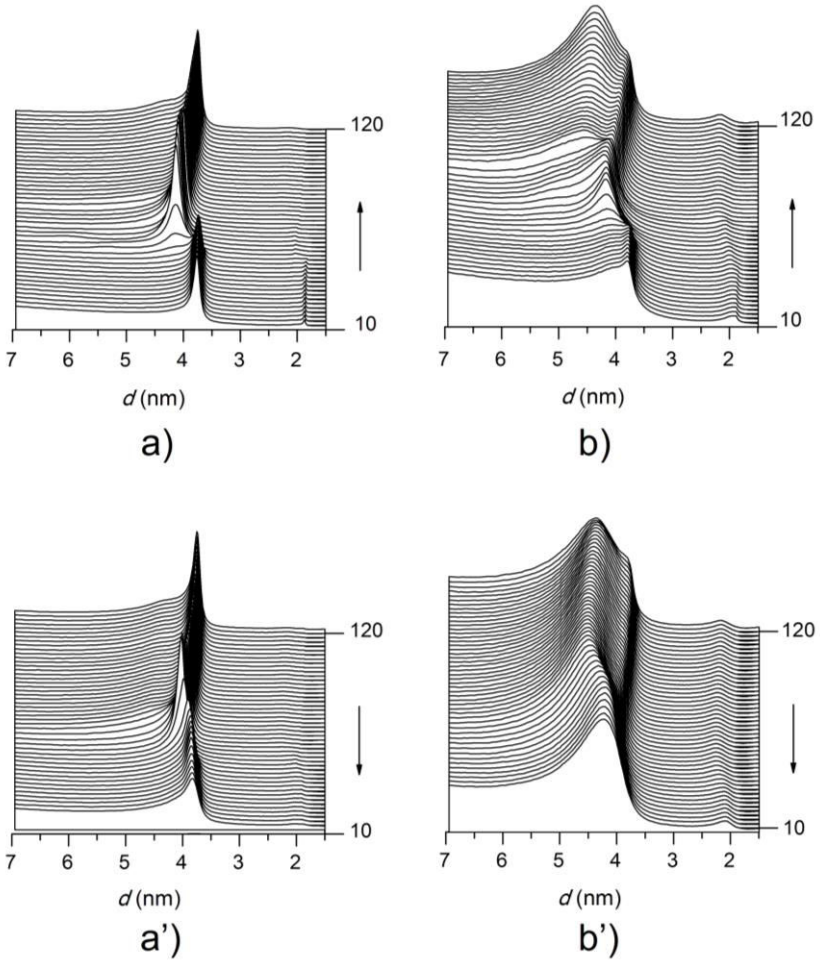

Figure 7. Time resolved SAXS profiles recording at heating and cooling from 18ATMA·PGGA·10%CL (a, a') and 18ATMA·PGGA·30%CL (b, b') nanocomposites.

Table 3. SAXS and WAXS diffraction spacing data (in nm) of *n*ATMA·PGGA·X%CL.

*n*ATMA·PGGA X%CL	SAXS[a]			WAXS[b]		
	$L_0^{10ºC}$	$L_0^{120ºC}$	$L_0^{10ºC}$	$d^{10ºC}$	$d^{120ºC}$	$d^{10ºC}$
			***n* = 18**			
0%	3.8	3.7	3.7	0.41	0.46	0.41
3%	3.8	3.7	3.7	0.41	0.46	0.41
		4.4	4.3			
10%	3.8	3.8	3.8	0.41	0.40	0.41
		4.3		0.45	0.45	0.45
20%	3.8	3.8	3.9	0.41	0.40	0.41
		4.3	4.2	0.45	0.45	0.45
30%	3.8	3.8	4.2	0.41	0.40	0.40
	4.1	4.4		0.45	0.45	0.45
50%	4.2	4.3	4.1	0.40	0.40	0.40
				0.41	0.45	0.42
				0.45		0.45
70%	--	--	--	0.40	0.40	0.40
				0.45	0.45	0.42
						0.45
90%	--	--	--	0.40	0.40	0.40
				0.45	0.45	0.45
			n = 22			
0%	4.2	4.0	3.9	0.41	0.46	0.41
3%	4.3	4.0	4.0	0.41	0.46	0.41
		4.5	4.5			
10%	4.4	4.2	4.2	0.41	0.44	0.41
		4.8	4.6	0.44	0.46	0.44
20%	4.4	4.1	4.1	0.41	0.41	0.41
		4.6	4.5	0.44	0.44	0.44
					0.46	
30%	4.4	4.6	4.1	0.41	0.41	0.41
			4.5	0.44	0.44	0.44
					0.46	
50%	4.6	4.5	4.5	0.41	0.41	0.41
				0.44	0.44	0.44
70%	--	4.5	4.6	0.44	0.40	0.41
					0.45	0.44
90%	--	--	--	0.40	0.40	0.40
				0.44	0.45	0.44
Cloisite30B	--	--	--	0.40	0.40	0.40
				0.45	0.45	0.45

[a]Lamellar spacings (L_0) of the layered structure.
[b]interplanar distances in the paraffinic phase.

The SAXS profiles of 18ATMA·PGGA·X%CL composites with several representative compositions recorded at 10 ºC, 120 ºC, and 10 ºC after cooling, are compared in Figure 8. Apparently the L_0 peak remained almost intact along the heating/cooling process in composites with low clay contents whereas in those with 30% of Cloisite or more, it moved towards higher spacing values and broadened, which means that the intersheet distances have been made larger and more disperse. The TEM analysis corroborated that the changes observed by SAXS at variable temperature correspond to the rearrangement taking place in the layered structure by heating effect.

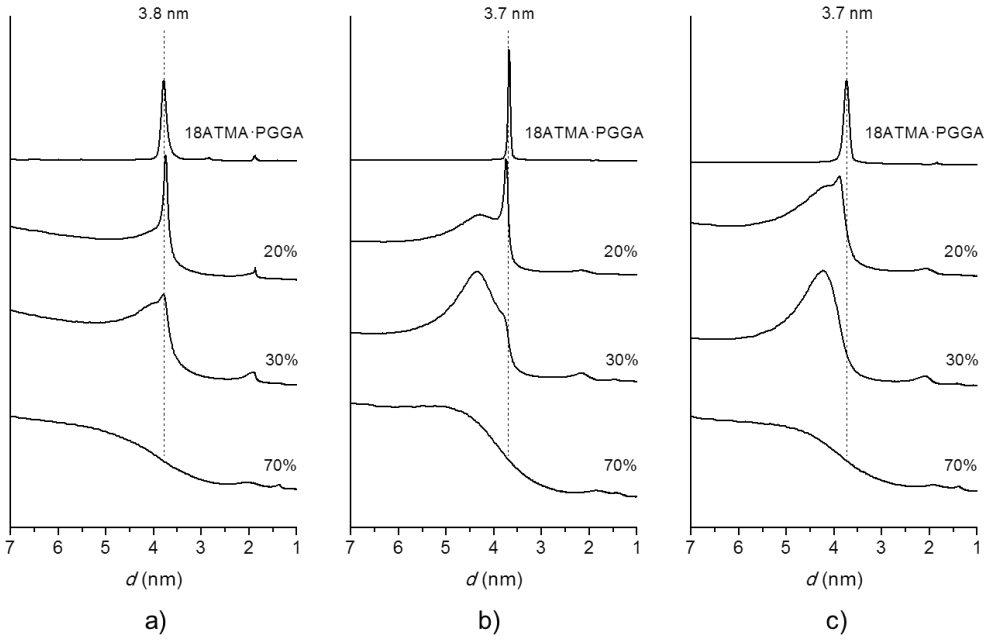

Figure 8. Compared SAXS profiles for 18ATMA·PGGA complex and composites at 10 ºC (a), 120 ºC (b), and 10 ºC after cooling (c).

The micrographs shown in Figure 9 compare the lamellar nanomorphology present in the 22ATMA·PGGA·50%CL composite before and after the heating treatment. Apparently, the interlayer spacing of the layered structure increased with heating and appears more disperse in lengths, which is fully consistent with the changes observed by SAXS. Similar observations were made from other composites with different compositions; SAXS profiles and micrographs illustrating additional examples are provided in the SM file. These results are demonstrative of the homogenizing effect that temperature exerts on the composite nanostructure, i.e. the interpenetration of clay and

PGGA sheets in composites is favoured by heating provided that high amounts of inorganic material are present.

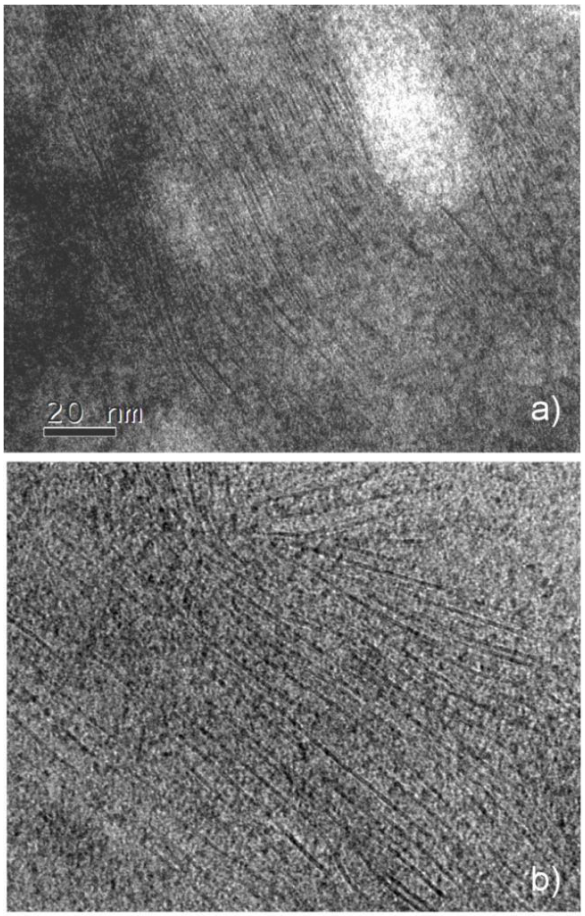

Figure 9. Effect of heating on the lamellar nanomorphology of 22ATMA·PGGA·50%CL. a) Original sample; b) Sample heated at 120 ºC for a few minutes. The two images displayed at the same magnification.

The analysis by WAXS in real time at variable temperature revealed what happened in the paraffinic phase of the composites upon heating. The 0.41-0.42 nm peak characteristic of the crystallized paraffinic phase of the complex was also present in the composites with an intensity that decreases with increasing content in Cloisite to almost disappear for compositions higher than 70%. This peak vanished upon heating at temperatures around melting and a new broad signal at ~0.45 nm emerged and partially overlapped with the peak arising from the Cloisite structure. The evolution of the WAXS profiles of 18ATMA·PGGA·10%CL and 18ATMA·PGGA·30%CL registered at

heating/cooling is shown in Figure 10 for illustration, and the collection of profiles registered for other compositions are provided in the SM file. The fact common to all the series is that the original peak at 0.41-0.42 nm was recovered after cooling but with broader width and diminished intensity, a behavior that was found to be more pronounced as the content in Cloisite increased.

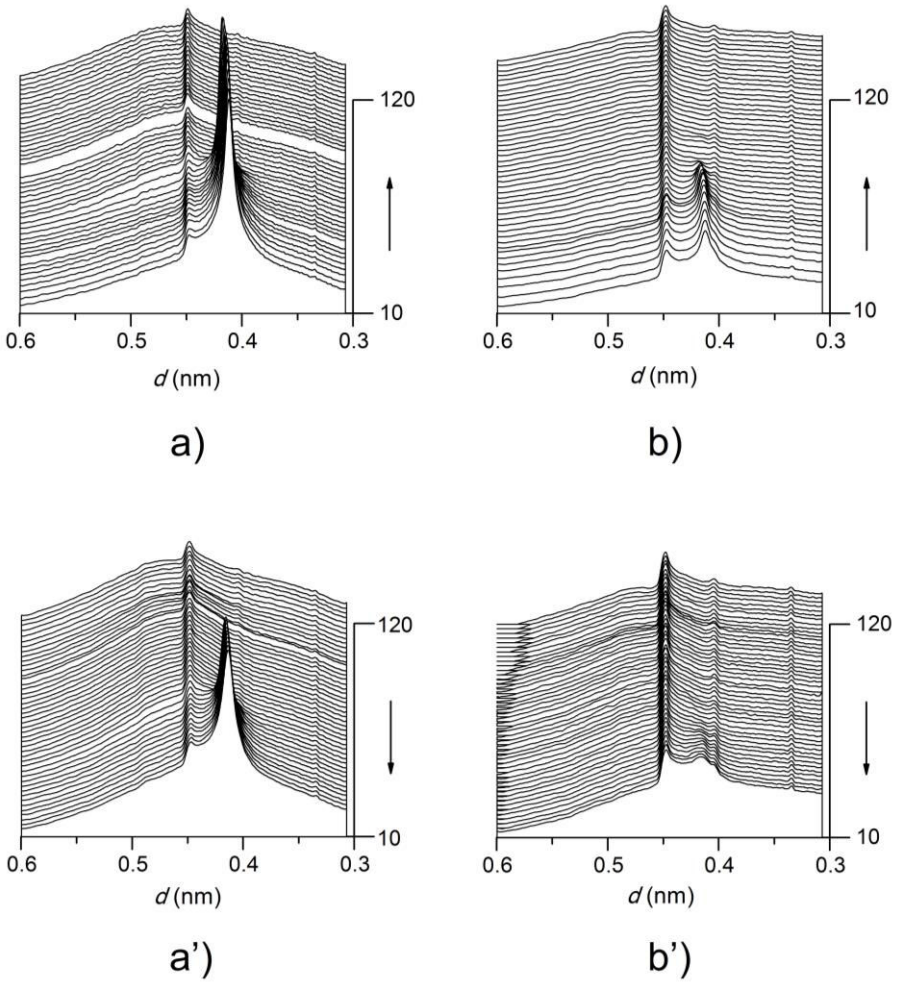

Figure 10. Time resolved WAXS profiles recording at heating and cooling from 18ATMA·PGGA·10%CL (a, a') and 18ATMA·PGGA·30%CL (b, b') nanocomposites.

The 13C CP-MAS NMR analysis unrevealed that the melting/crystallization process taking place at heating/cooling involved an anti to gauche conformational conversion of the inner methylenes of the alkyl side chain of the complex.[13,42,43] The evolution of the signal arising from the methylene

carbons of the octadecyl side chain in the 18ATMA·PGGA·X%CL is depicted in Figure 11. For the complex and the composite containing 10% of Cloisite, the methylene signal consisted of a single peak attributable to the carbon resonance of methylenes in anti-arrangement whereas a double-peak signal was present in the spectrum of the 50%CL composite. These two peaks are made to correspond to an ordered all-anti (downfield) of methylenes and to a disordered mixture of anti/gauche (upfield) conformations in which the hydrocarbon side chains of the complex and Cloisite are respectively arranged. After heating at 80 ºC, which is well above the melting temperature of the complex, a single signal corresponding to the mixture of anti/gauche conformations in fast exchange was observed.

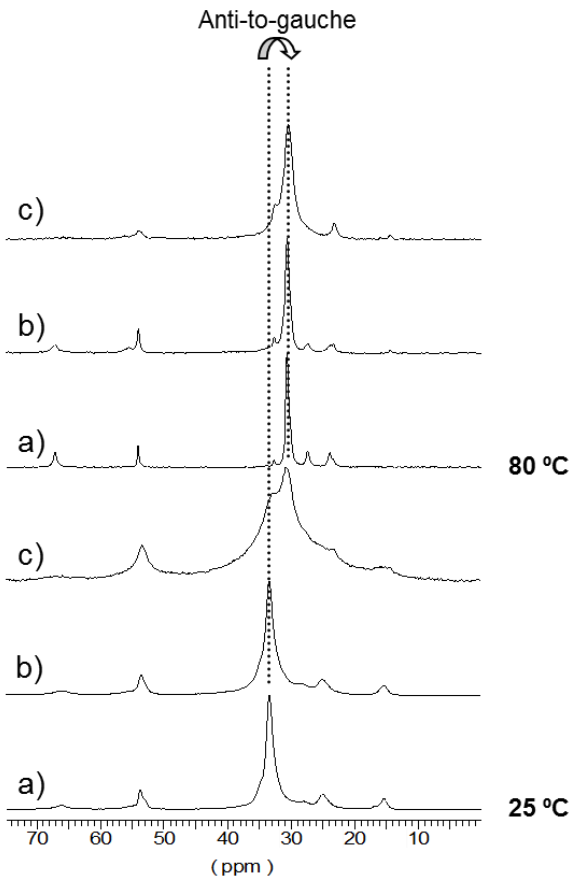

Figure 11. Evolution of the 13C CP-MAS NMR spectrum of 18ATMA·PGGA·X%CL composites at 25 and 80 ºC revealing the anti-to-gauche transition taking place in the polymethylene segment. a) 18ATMA·PGGA; b) 18ATMA·PGGA·10%CL; c) 18ATMA·PGGA·50%CL.

2.3.3. Modeling the 18ATMA·PGGA·50%CL nanocomposite

To investigate the interaction between PGGA and the clay mediated by the presence of the tetralkylammoniun surfactant, a model for the intercalated 18ATMA·PGGA·50%CL nanocomposite has been simulated and energetically compared with each of their components.

First of all, the intermolecular radial distribution function has been analyzed for the alkyl segments in the surfactant and modifier molecules for the systems under study (Figure 12). This function represents the probability for a pair of given particles being at a given distance between them; for a crystal, it consists of a fair number of very sharp peaks while a small number of broad peaks will be produced by an amorphous fluid. For the 18ATMA·PGGA complex, the radial distribution function shows several narrow and well localized peaks, indicating a partially crystallized arrangement of the polymethylene segments. The same result was attained for both parallel and antiparallel arrangement of the helices within the sheets. For Cloisite30B, the profile shows a wide peak around a distance of 0.5 nm, similarly to what is observed for the intermolecular pair distribution function for methylene groups of liquid C18 alkane. The two shoulders at ~0.4 and ~0.6 nm indicate however that somewhat degree of organization is present, probably due to the confined nature of the system between the silicate sheets. For the nanocomposite, the radial distribution function is intermediate between those of the complex and the modified clay with two peaks at about ~0.55 nm and ~1 nm. Compared to the 18ATMA·PGGA complex, the polymethylene segments in the composite are completely melted but the presence of the peak at ~1 nm indicates that certain slight ordering extends to distances greater than in Cloisite30B.

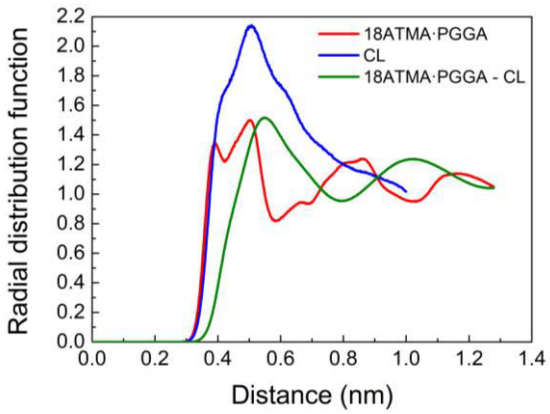

Figure 12. Radial distribution in the intersheet space of the carbon atoms contained in the alky side chain of C18 of 18ATMA·PGGA complex, Cloisite30B) and the 18ATMA·PGGA·50%CL nanocomposite.

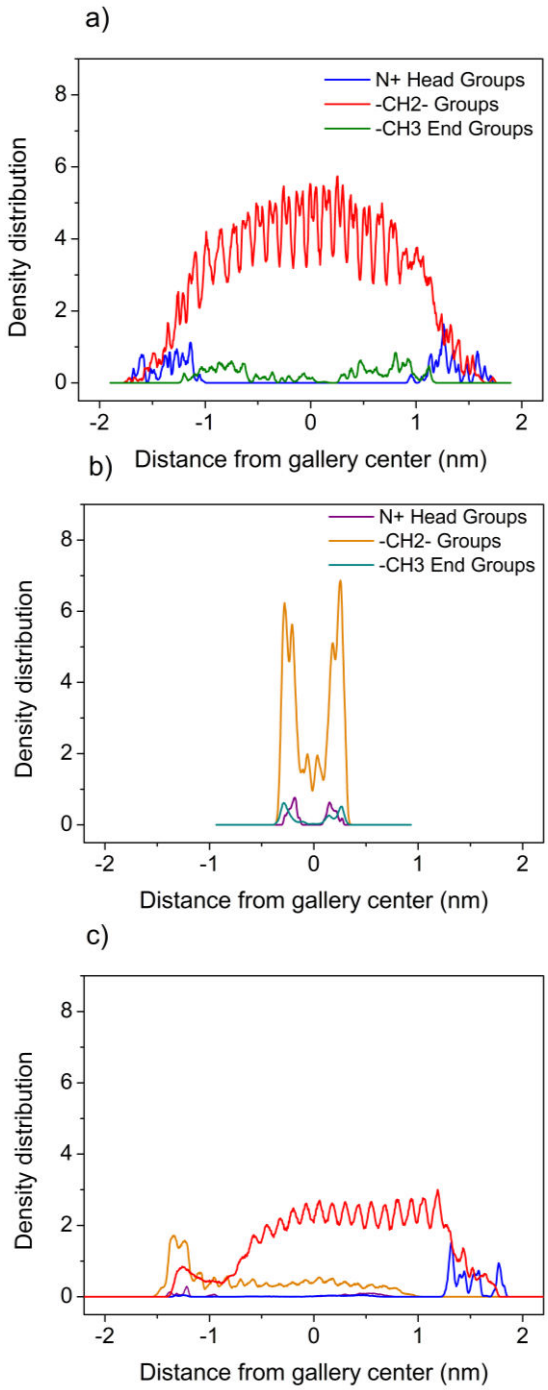

Figure 13. Depth profile distribution in the intersheet space of the carbon atoms contained in the alky side chain of C18 of a) 18ATMA·PGGA complex, b) Cloisite30B, and c) 18ATMA·PGGA·50%CL nanocomposite.

The arrangement of the alkyl segments in the intersheet space can also be evaluated in terms of the atoms depth profile, i.e. the atom number density as a function of the distance from the gallery centre (Figure 13). For the 18ATMA·PGGA complexes, the depth profiles show that the surfactant molecules adopt an almost completely extended conformation with the ammonium head groups localized around the helices and the methyl end groups close to the neighboring sheet. The position of both head and end groups is not unique because these groups are unevenly distributed around the helices according to its symmetry. A strong layering is observed for the methylene groups, which is more pronounced around the centre of the gallery, indicating that crystallinity increases with the distance from the sheets. For CLO30B, the density profile can be compared to those observed for other organically modified montmorillonites.[39,40] Both ammonium head groups and methyl end groups are strongly localized close to the clay surfaces and the methylene groups are arranged mainly in four layers, with the two closer to clay surface being better defined. This suggests that the modifying molecules adopt an arrangement preferentially parallel to the sheets.

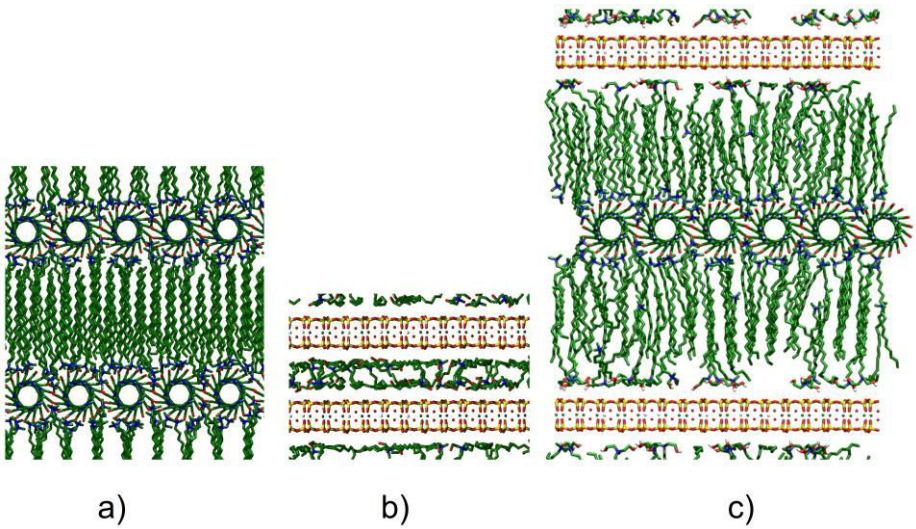

Figure 14. Molecular models of the 18ATMA·PGGA complex (a), Cloisite30B (b), and the 18ATMA·PGGA·50%CL hybrid. The models are viewed as projected along down the c-axis of the structure which corresponds to the PGGA helix axis and clay sheets seen on-edge.

All the trends displayed in the distribution functions become reflected in the molecular models depicted in Figure 14, which correspond to snapshots obtained during the molecular dynamics simulations for the three systems. The model generated for the 18ATMA·PGGA shows the side chain in a nearly

full extended conformation with a high degree of ordering fully consistent with both the radial and the depth profile distribution functions represented in Figures 12 and 13. On the contrary, the hydrocarbon tails in Cloisite30B appear disordered and arranged mostly parallel to the clay surfaces to be able to be accommodated into the relatively short intersheet space of 1.85 nm experimentally determined for this organoclay. Regarding the 18ATMA·PGGA·50%CL hybrid, the model displays low degree of ordering for the alkyl chains indicating that the crystalline structure of the paraffinic phase characteristic of the complex is lost. What it is really interesting in this model is the arrangement adopted by the hydrocarbon tails of the Cloisite30B modifying molecules; at difference with happens in the isolate clay, they are protruding from the silicate sheets to become interdigitated with the alkyl side chains of 18ATMA·PGGA in a significant extension. This affinity will be in great part the responsible for the large degree of intercalation observed for the 18ATMA·PGGA·X%CL nanocomposites.

2.4. Conclusions

The structure of the three-component hybrids made of PGGA, Cloisite30B and alkyltrimethylammonium surfactant has been examined and the effect of heating on the mixing of components was evaluated. The main conclusions drawn from this study are the following: a) At low concentrations in Cloisite, the clay became uniformly dispersed in the complex as single entities; in these conditions the complex retained its original layered structure with the helical polyglutamic chains arranged in sheets and the attached alkyl chains oriented more or less perpendicularly to the sheet plane. b) For high concentrations in Cloisite, the clay and the complex are interacting at different degrees with the result of a heterogeneous mixture at the nanoscale level in which independent clay platelets coexist with bundles of intercalated clay and complex sheets; in addition, either compact Cloisite aggregates or uniform complex domains were also present according to which component was predominant in the mixture. c) After heating up to temperatures of 120 ºC the composites not only retained the layered structure but they attained a remarkable increasing in the intercalation of clay and PGGA sheets. This result indicates that the mixing process is kinetically controlled and that a fully intercalated structured could be achieved by application of the appropriate heating treatment. d) The compatibilizing effect of the alkylammonium surfactant on the mixing of the PGGA and the silicate evidenced by experiments was further supported by energy-based modeling and simulation results.

The alternating polypeptide-silicate structure adopted by these compounds is conceptually very interesting since it is reminiscent of some naturally-occurring materials like nacre, that distinguish by their exceptional physical properties.

2.5. References

1. Sung, M.-H.; Park, C.; Kim, C.-J.; Poo, H.; Soda, K.; Ashiuchi, M. Natural and edible biopolymer poly-gamma-glutamic acid: synthesis, production, and applications. *Chem. Rec.* **2005**, *5*, 352–366.

2. Buescher, J. M.; Margaritis, A. Microbial biosynthesis of polyglutamic acid biopolymer and applications in the biopharmaceutical, biomedical and food industries. *Crit. Rev. Biotechnol*. **2007**, *27*, 1–19.

3. Bajaj, I.; Singhal, R. Poly (glutamic acid) – An emerging biopolymer of commercial interest. *Bioresource Technol.* **2011**, *102*, 5551–5561.

4. Muñoz-Guerra, S.; García-Alvarez, M.; Portilla-Arias, J. A. Chemical modification of microbial poly(γ-glutamic acid): Progress and persectives. *J. Renew. Mater.* **2013**, *1*, 42–60.

5. Shah, D. T.; McCarthy, S. P.; Gross, R. A. New polymers derived from gamma-poly(glutamic acid). *Abs. Pap. Amer. Chem. Soc*. **1992**, *204*, 249.

6. Kubota, H., Nambu, Y.; Endo, T. Convenient and quantitative esterification of poly(gamma-glutamic acid) produced by microorganism. *J. Polym. Sci. A Polym. Chem*. **1993**, *31*, 2877-2878.

7. Kunioka, M.; Furusawa, K. Poly(γ-glutamic acid) hydrogel prepared from microbial poly(γ-glutamic acid) and alkanediamine with water-soluble carbodiimide. *J. Appl. Polym. Sci.* **1997**, *65*, 1889-1896.

8. Morillo, M.; Martínez de Ilarduya, A.; Muñoz-Guerra, S. Comblike alkyl esters of biosynthetic poly (γ-glutamic acid). 1. Synthesis and characterization. *Macromolecules* **2001**, *34*, 7868–7875.

9. Yoshida, H.; Klinkhammer, K.; Matsusaki, M.; Moller, M.; Klee, D.; Akashi, M. Disulfide-crosslinked electrospun poly(γ-glutamic acid) nonwovens as reduction-responsive scaffolds. *Macromol. Biosci.* **2009**, *9*, 568-574.

10. Tachibana, Y.; Kurisawa, M.; Uyama, H.; Kobayashi, S. Thermo- and pH-responsive biodegradable poly (α-N-substituted γ-glutamine)s. *Biomacromolecules* **2003**, *4*, 1132-1134.

11. Akagi, T.; Higashi, M.; Kaneko, T.; Kida, T.; Akashi, M. Hydrolytic and enzymatic degradation of nanoparticles based on amphiphilic poly(γ-glutamic acid)-graft-L-phenylalanine copolymers. *Biomacromolecules* **2006**, *7*, 297-303.

12. Kim, H.; Akagi, T.; Akashi, M. Preparation of size tunable amphiphilic poly(amino acid) nanoparticles. *Macromol. Biosci.* **2009**, *9*, 842-848.

13. Portilla-Arias, J. A.; Camargo, B.; García-Alvarez, M.; Martínez de Ilarduya, A.; Muñoz-Guerra, S. Nanoparticles made of microbial poly(γ-glutamate)s for encapsulation and delivery of drugs and proteins. *J. Biomater. Sci. Polym. Ed.* **2009**, *20*, 1065-1079.

14. Akagi, T.; Piyapakorn, P.; Akashi, M. Formation of unimer nanoparticles by controlling the self-association of hydrophobically modified poly(amino acid)s. *Langmuir* **2012**, *28*, 5249–5256.

15. Kang, H. S.; Park, S. H.; Lee, Y. G.; Son, T. I. Polyelectrolyte complex hydrogel composed of chitosan and poly(γ-glutamic acid) for biological application: Preparation, physical properties, and cytocompatibility. *J. Appl. Polym. Sci.* **2007**, *103*, 386-394.

19. Mi, F. L.; Wu, Y.Y.; Lin, Y. H.; Sonaje, K.; Ho, Y. C.; Chen, C. T.; Juang, J. H.; Sung, H. W. Oral delivery of peptide drugs using nanoparticles self-assembled by poly(γ-glutamic acid) and a chitosan derivative functionalized by trimethylation. *Bioconjug. Chem.* **2008**, *19*, 1248-1255.

17. Sonaje, K.; Chen, Y. J.; Chen, H. L.; Wey, S. P.; Juang, J. H.; Nguyen, H. N.; Hsu, C.W.; Lin, K. J.; Sung, H. W. Enteric-coated capsules filled with freeze-dried chitosan/poly(γ-glutamic acid) nanoparticles for oral insulin delivery. *Biomaterials* **2010***, 31*, 3384-3394.

18. Kunioka, M.; Choi, H. J. Preparation conditions and swelling equilibria of biodegradable hydrogels prepared from microbial poly(γ-glutamic acid) and poly(ε-lysine). *J. Environ. Polym. Degrad.* **1996**, *4*, 123-129.

19. Pérez-Camero, G.; García-Alvarez, M., Martínez De Ilarduya, A.; Fernández, C., Campos, L., Muñoz-Guerra, S. Comblike complexes of bacterial poly(γ,D-glutamic acid) and cationic surfactants. *Biomacromolecules*. **2004**, *5*, 144–152.

20. García-Alvarez, M.; Alvarez, J.; Alla, A.; Martínez de Ilarduya, A.; Muñoz-Guerra, S. Comb-like ionic complexes of cationic surfactants with bacterial poly(γ-glutamic acid) of racemic composition. *Macromol. Biosci.* **2005**, *5*, 30–38.

21. Zanuy, D.; Alemán, C.; Muñoz-Guerra, S. A molecular dynamics study of the stoichiometric complex formed by poly (α,L-glutamate) and octyltrimethylammonium ions in chloroform solution. *Biopolymers* **2002**, *63*, 151–162.

22. Zanuy, D.; Alemán, C. Molecular dynamics study of complexes of poly (glutamate) and dodecyltrimethylammonium. *Biomacromolecules* **2007**, *8*, 663–671.

23. Pérez-Camero, G.; Martínez de Ilarduya, A.; García-Álvarez, M., Muñoz-Guerra, S. Stoichiometric complexes made of naturally occurring poly (γ,D-glutamic acid) and cationic surfactants. *Polym. Preprints Amer. Chem. Soc.* **1999**, *40*, 1142-1143.

24. Sinha Ray, S.; Okamoto, M. Polymer/layered silicate nanocomposites: a review from preparation to processing. *Progr. Polym. Sci.* **2003**, *28*, 1539–1641.

25. Krikorian, V.; Kurian, M.; Galvin, M. E.; Nowak, A. P.; Deming, T. J.; Pochan, D. J. Polypeptide-based nanocomposite: Structure and properties of poly(L-lysine)/Na+-montmorillonite. *J. Polym. Sci. B Polym. Phys.* **2002**, *40*, 2576-2586.

26. Hule, R. A.; Pochan, D. J. Poly(L-lysine) and clay nanocomposite with desired matrix secondary structure: Effects of polypeptide molecular weight. *J. Polym. Sci. B Polym. Phys.* **2007**, *45*, 239-252.

27. Gougeon, R. D.; Soulard, M.; Reinholdt, M.; Miehe-Brendle, J.; Chezeau, J. M.; Le Dred, R.; Marchal, R.; Jeandet, P. Polypeptide adsorption on a synthetic montmorillonite: A combined solid-state NMR spectroscopy, X-ray diffraction, thermal analysis and N-2 adsorption study. *Eur. J. Inorg. Chem.* **2003**, *7*, 1366-1372.

28. Gougeon R. D.; Reinholdt M.; Delmotte L.; Miehe-Brendle J.; Jeandet P. Solid-state NMR investigation on the interactions between a synthetic montmorillonite and two homopolypeptides. *Solid State Nucl. Magnet. Res.* **2006**, *29*, 322–329.

29. Chiang, M. F.; Wu, T. M. Intercalation of γ-PGA in Mg/Al layered double hydroxides: An in situ WAXD and FTIR investigation. *Appl. Clay Sci.* **2011**, *51*, 330-334.

30. Chiang, M. F.; Wu, F. M.; Chen, E. C.; Wu, T. M. Preparation, mechanical properties and thermal stability of poly(L-lactide)/γ-polyglutamate-modified layered double hydroxide nanocomposites. *Polym. Degrad. Stabil.* **2012**, *97*, 995-1001.

31. Kodona, E. K.; Alexopoulos, C.; Panou, E.; Pomonis, P. J. Self-organized meso- and hybridic phases of poly(aspartic acid) and poly(glutamic amino acid) with cationic surfactants (CnTAB, n=14, 16) and a silica source (TEOS). *Chem. Mater.* **2007**, *19*, 1853-1861.

32. Tolentino, A.; Alla, A.; Muñoz-Guerra, S. Nanocomposites of comb-like ionic complexes of bacterial poly(glutamic acid) with nanoclays. *Eur. Polym. J.* **2012**, *48*, 1838–1845.

33. Hendrix, W. T.; von Rosenberg, J. L. The mechanism of the rearrangement of the hydrocobalt carbonyl catalyzed isomerization of 3-phenylpropene. *J. Am. Chem. Soc.* **1976**, *98*, 4850–4852.

34. Ponomarenko, E. A.; Waddon, A. J.; Tirrell, D. A.; Macknight, W. J. Structure and properties of stoichiometric complexes formed by sodium poly (α,L-glutamate) and oppositely charged surfactants. *Langmuir* **1996**, *12*, 2169–2172.

35. Ponder, J. W.; Richards, F. M. An efficient Newton-like method for molecular mechanics energy minimization of large molecules. *J. Comp. Chem.* **1987**, *8*, 1016-1024.

36. Kundrot, C. E.; Ponder, J. W.; Richards, F. M. Algorithms for calculation excluded volume and its derivatives as a function of molecular-conformation and their use in energy minimization. *J. Comp. Chem.* **1991**, *12*, 402-409.

37. Dudek, M. J.; Ponder, J. W. Accurate modeling of the intramolecular electrostatic energy of proteins. *J. Comp. Chem.* **1995**, *16*, 791-816.

38. Allinger, N. L.; Yuh, Y. H.; Lii, J. H.. Molecular mechanics. The MM3 force-field for hydrocarbons .1. *J. Amer. Chem. Soc.* **1989**, *111*, 8551-8566.

39. Melis, J.; Zanuy, D.; Aleman, C.; García-Álvarez, M.; Muñoz-Guerra, S. On the crystal structure of poly(α-benzyl-γ-D,L-glutamate)s. Macromolecules **2002**, *35*, 8774-8780.

40. Chen, B.; Evans, J. R. G.; Greenwell, H. C.; Boulet, P.; Coveney, P. V; Bowden, A. A.; Whiting, A. A critical appraisal of polymer-clay nanocomposites. *Chem. Soc. Rev.* **2008**, *37*, 568–94.

41. Zerda, A. S.; Lesser, A. J. Intercalated clay nanocomposites : Morphology, mechanics, and fracture behavior. *J. Polym. Sci. B Polym. Phys.* **2001**, *39*, 1137–1146.

42. Dunkerley, E.; Koerner, H.; Vaia, R. a.; Schmidt, D. Structure and dynamic mechanical properties of highly oriented PS/clay nanolaminates over the entire composition range. *Polymer* **2011**, *52*, 1163–1171.

43. Wen, X.; He, H.; Zhu, J.; Jun, Y.; Ye, C.; Deng, F. Arrangement, conformation, and mobility of surfactant molecules intercalated in montmorillonite prepared at different pillaring reagent concentrations as studied by solid-state NMR spectroscopy. *J. Colloid Interface Sci.* **2006**, *299*, 754–60.

44. Zeng, Q. H.; Yu, A. B.; Lu, G. Q. Molecular dynamics simulation of organic-inorganic nanocomposites: Layering behavior and interlayer structure of organoclays. *Chem. Mater.* **2003**, *15*, 4732-4738.

45. Zeng, Q. H.; Yu, A. B.; Lu, G. Q.; Standish, R. K. Molecular dynamics simulation of the structural and dynamic properties of dioctadecyldimethyl ammoniums in organoclays. *J. Phys. Chem. B* **2004**, *108*, 10025-10033.

2.6. Supporting information

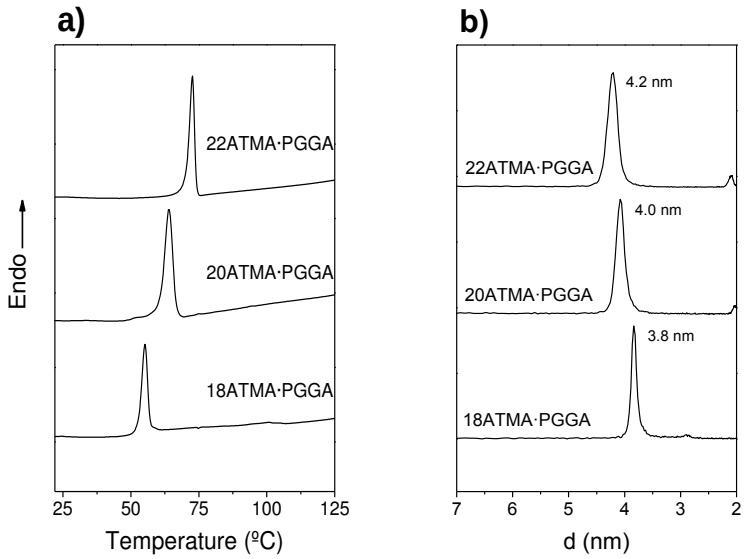

SI Figure 1. DSC traces (a) and SAXS profiles (b) of *n*ATMA·PGGA complexes.

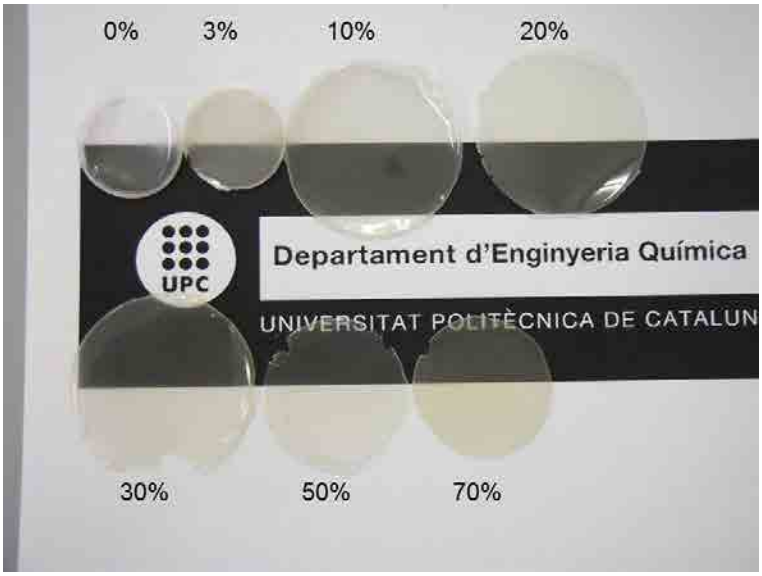

SI Figure 2. Photographs of 22ATMA·PGGA.X%CL films prepared by casting.

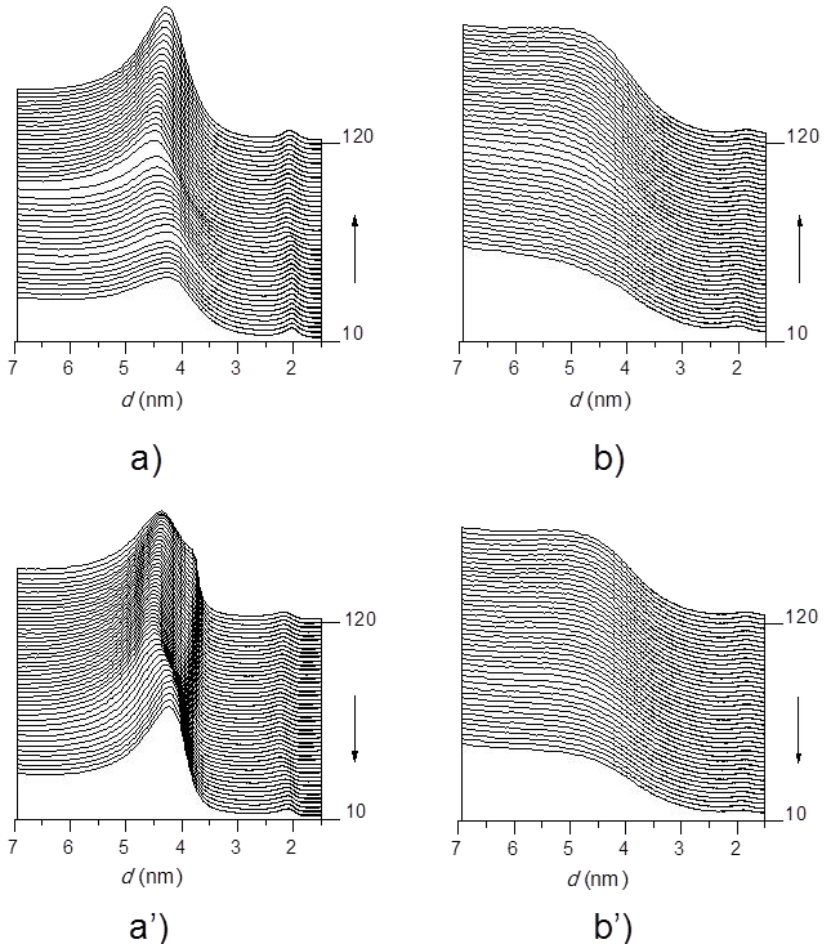

SI Figure 3. Time resolved SAXS profiles recording at heating and cooling from 18ATMA·PGGA·50%CL (a, a') and 18ATMA·PGGA·70%CL (b, b') nanocomposites.

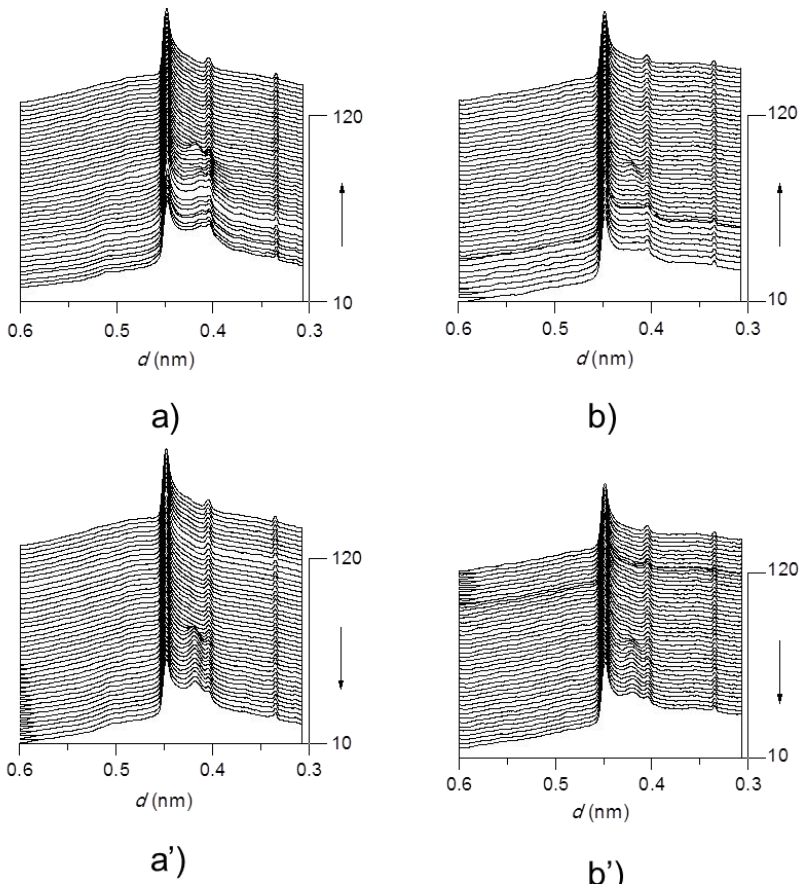

SI Figure 4. Time resolved WAXS profiles recording at heating and cooling from 18ATMA·PGGA·50%CL (a, a') and 18ATMA·PGGA·70%CL (b, b') nanocomposites.

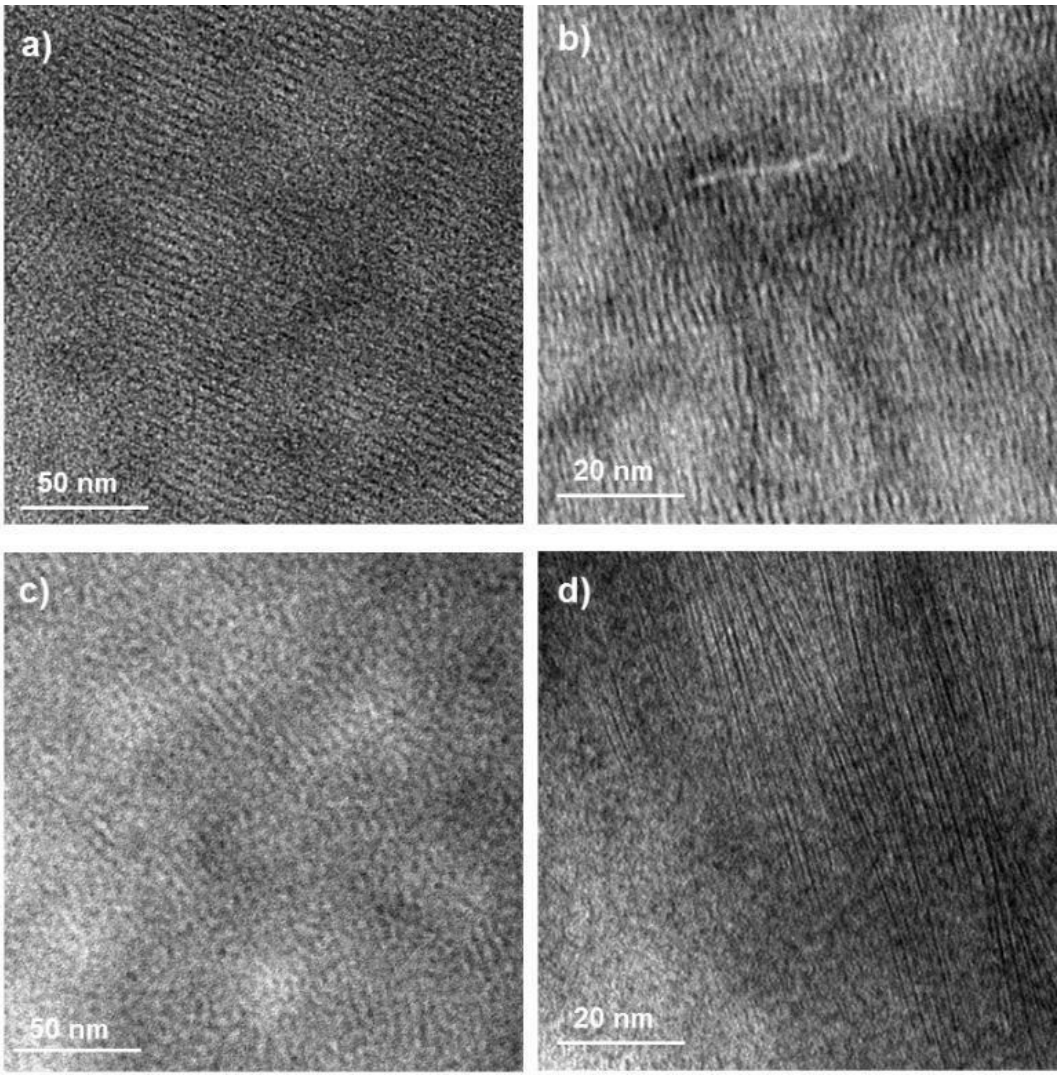

SI Figure 5. TEM micrographs of 18ATMA·PGGA·3%CL (a), 22ATMA·PGGA·3%CL (b), 18ATMA·PGGA·10% CL(c) and 18ATMA·PGGA 50%CL (d).

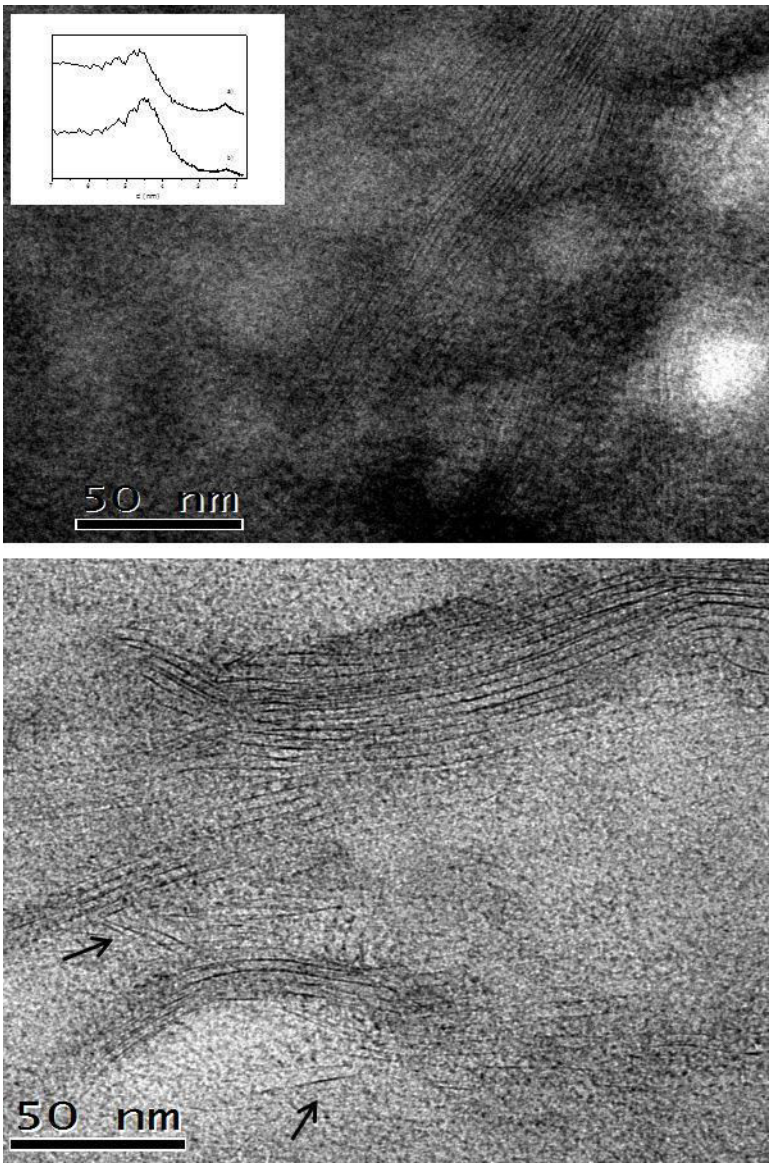

SI Figure 6. TEM micrographs of 22ATMA·PGGA-50% before a), and after thermal treatment b). Arrows in b) point to single lamellae. Inset in a): SAXS of the sample showing the increasing of intersheet spacings as a consequence of the thermal treatment.

Chapter V: General conclusions

Stoichiometric ionic complexes with a comb-like architecture were prepared by coupling the polyuronic acids PGaA and coPGuMnA with alkyltrimethylammonium surfactants bearing alkyl chains of 18, 20 and 22 carbon atoms. The complexes were insoluble in either water and common organic solvents. In the solid-state, they adopted a biphasic layered arrangement with an interlayer repeating distance of 3-4.5 nm according to the length of the alkyl side chain. They displayed one reversible thermal transition within the 50-80 ºC range involving the melting-crystallization of the paraffinic phase but with the layered structure remaining essentially unaltered.

Thermal decomposition of neat PGaA and coPGuMnA happened in one single stage with almost quantitative decarboxylation and dehydratation, and generation of furfural and formic acid. Their stoichiometric complexes alkyltrimethylammonium surfactants followed a three-stage decomposition pattern very similar for the two families. The degradation process initiated with dissociation of the complex and decomposition of the ammonium counterpart in amines and alcohols, and proceeded with decomposition of the polysaccharide. Decomposition temperatures were considerably lower than for the separated components revealing certain unfavourable mutual interaction between the polymer and the surfactant.

Stoichiometric ionic complexes with a comb-like architecture were prepared by coupling hyaluronic acid with alkyltrimethylammonium surfactants bearing alkyl chains of 18, 20 and 22 carbon atoms. The complexes were non-soluble in water but they dissolved in common organic solvents and were thermally stable up to temperatures around 200 ºC. The layered arrangement adopted by these complexes showed a repeating distance of 4.5 nm independent of the length of the alkyl side chain. They showed melting in the 50-70 ºC range depending on the number of methylene units in the alkyl side chain.

n-Alkanoylcholine iodides surfactants (***n***ACh·I) were synthesized from saturated fatty acids of 12, 14, 16 and 18 carbon atoms. They were thermally stable up to 200 ºC and showed Krafft temperatures in the 30-60 ºC range. Upon crystallization from solution they adopted a bilayered crystal structure with a monoclinic lattice in the ***P***1 space group. Three thermotropic phases were identified in ***n***ACh·I upon heating, all they consisting of a bilayered arrangement with the alkanoyl chains interdigitated in a more or less extent. The two transitions implied in the thermotropic interconversion took place in the 30-60 ºC and 160-170 ºC ranges, and they entailed melting-crystallization of either the polymethylene segments or the choline iodide groups, respectively.

Stoichiometric ionic complexes ***n***ACh·PGGA with a comb-like architecture were prepared by coupling poly(γ-glutamic acid) with ***n***-alkanoylcholine iodides surfactants bearing alkyl chains of 18, 20 and 22 carbon atoms. These complexes were found to be soluble in organic solvents and to decompose at temperatures above 200ºC. ***n***ACh·PGGA with alkyl tails of n≥14 displayed a reversible melting-crystallization process in the 40-65 ºC range. Owing to the higher mobility of the alkanoyl chain provided by the ester linkage group, the biphasic layered structures adopted by these systems achieved a higher order degree than in complexes based on trimethylalkylammonium surfactants.

The hydrolytic degradation of ***n***ACh·PGGA complexes under physiological conditions required months and took place by complex dissociation and hydrolysis of the alkanoylcholine moiety in fatty acid and choline. The biocompatible nature of the degradation products of ***n***ACh·PGGA ensure their suitability for drug store and delivery. Nanoparticles of 50-100 nm diameter were prepared from these complexes with a surfactant/polymer ratio of 0.75 Neutral drugs, theophiline and carbamazepine, were entrapped in the nanoparticles with low efficiency and released in hours upon incubation. On the contrary, the ionic drug doxorubicine could be loaded at 30% and its release took place in parallel to complex degradation with a discharge of less than 10% in one month.

Nanocomposites of ***n***ATMA·PGGA complexes with Cloisite 30B were obtained by mixing complexes of ***n***= 18, 20 and 22 carbon atoms and the modified nanoclay at different proportions. These hybrid systems degraded at temperatures above 200 ºC through a mechanism involving depolymerisation and decomposition of the alkylammonium moiety by Hoffmann elimination. Elastic modulus of nanocomposite films increased with the content in Cloisite 30B whereas the elongation to break was drastically reduced. Nanocomposites containing 3% of nanoclay showed an exceptional mechanical behaviour distinguished by a remarkable ductility, which was due to the high dispersion degree attained by the clay platelets in the polymeric matrix for such concentration.

The structure of ***n***ATMA·PGGA·X%CL nanocomposites was found to be highly dependent on composition. At low clay contents, a good dispersion of the clay platelets into the polymeric matrix was attained with retention of the layered structure typical of the ***n***ATMA·PGGA complex. At higher clay contents, nanocomposites consisted of a heterogeneous mixture of isolated clay platelets, bundles of intercalated clay and complex sheets, in addition to compact clay aggregates, or homogeneous complex domains depending on composition. A remarkable increasing in clay/PGGA intercalation resulted upon annealing which indicates that the mixing process is kinetically controlled, and that a fully intercalated structure would be achievable by application of the appropriate heating treatment.

Acknowledgments

En este espacio me gustaría mostrar mi agradecimiento a todas aquellas personas que de alguna manera han contribuido a la culminación de este trabajo y han sido una parte importante profesional o personalmente durante estos años.

En primer lugar quiero agradecer especialmente al Prof. Sebastián Muñoz Guerra su labor como director de la presente tesis, así como su confianza, apoyo y dedicación durante todo este periodo; especialmente en la última y más complicada etapa.

Deseo agradecer también al Dr. Abdelilah Alla y al Dr. Antxon Martínez de Ilarduya su inestimable ayuda, predisposición para resolver cualquier duda o problema, además de su importante participación en esta investigación.

A todos los miembros del grupo de *Polímeros Industriales, Polímeros Avanzados y Biopolímeros Tecnológicos*, por su ayuda durante este periodo. Y a Irene, por su orientación con los trámites administrativos.

A Montserrat Marsal e Isaac López-Insa por su paciencia y dedicación con el SEM. A Lourdes Campos por guiarme y aconsejarme amablemente en la obtención de monocristales.

I wish to express my gratitude to Prof. Axel Müller and his group for all their kindness, generosity and support during my stay at Bayreuth. Thanks to Dr. Markus Drexler and Melanie Förtsch for their patience and technical support with TEM. To all the mc2 staff for the great time I spent there (and in Barcelona), with the BBQs, parties, biergartens, the “kein bock” and the “I know” joke. Ramón, tu amiga “catalasca” agradece enormemente haberte tenido allí, tanto dentro como fuera del laboratorio.

A mis compañeros de tesis más antiguos Romina, Nathalie, y Robert, a los más contemporáneos Cristina Japu y Mayka; también a Giuseppe, Javier, Angélica, Bruno y resto de compañeros de máster; además de Yani, Sejin y Laura. Gracias por toda la ayuda ofrecida, los buenos momentos que hemos pasado juntos, las reuniones espontáneas en el laboratorio de las Cristinas, los ánimos y las quejas e indignaciones que también hemos compartido.

A mi compañero de laboratorio Alberto, gracias por estar siempre dispuesto a ayudar y por tu paciencia con el caos que invariablemente me acompaña. A

mis amigos Cristina Lavilla y Javier; además de vuestro apoyo, os agradezco esos cafés surrealistas en la planta 10, las cartas heredadas, las bromas y todas nuestras conversaciones. A todos, os echaré de menos.

A los frikis del tetris David (el vinagres por excelencia), Guillem (y sus ya míticas pieles de naranja y pedidos de cuadros que jamás verán la luz), Franki (el exponente máximo de la veteranía), Dani (y sus recomendaciones musicales), Georgina, Esther y Mar. A Mireia, con quien, junto con Guillem, siempre acabo reencontrándome de una u otra manera y con quienes es un placer haber compartido máster, tesis y empresa. Todos ellos, los de *abajo*, que venían a buscarnos a los de *arriba* en un alarde de ingenio y logística, para volver a ir *abajo* a comer. A todos vosotros, gracias por vuestra amistad, las entrañables conversaciones sobre el tritema política-religión-fútbol, los altos grados de surrealismo que manejábamos y lo bien que nos los hemos pasado juntos.

Quisiera agradecer también a mis amigos, mi cuadrilla donostiarra, Kit, Ainara, Estitxu, Tzo y Amaia, que se han mostrado siempre interesados en saber la evolución de esta eterna tesis *nuestra*; e incluso haciendo el esfuerzo de comprender de qué va. Gracias por vuestra amistad y todo lo compartido, desde vacaciones y cenas a charlas sobre cómo arreglar el mundo durante estos mil años.

Así como a mis amigos de Barcelona Ignacio, Judit, Mauro, Ignasi, Alexis, Eric, Iban, Claudio, Iñaki, Sara, Andrés, Esther, Laura y compañía que, además de interesarse por mis avances, me han ayudado tanto a desconectar y divertirme en medio de este batiburrillo de hipsters, picateclas y modernas.

A Juncal, Mikel, Ander, Hodei y resto de compañeros de la carrera (Sheila, Erlea, Leire…), por compartir aquellos años donde empezamos a amar (u odiar) la química, y esas cenas en petit comité que permanecen desde entonces.

A mis compis del ICIQ, que a pesar de haber sufrido mis despistes derivados de la falta de sueño, han seguido mostrando interés por "¿cómo va la tesis?"

A mis padres, por su ejemplo, afecto y continuo apoyo. Cualquiera de los logros que he conseguido es gracias a la educación que me ofrecieron. Al resto de mi familia, tanto el clan de los Chivis como los Tolentino-gen T, que tanto ánimo y apoyo me han brindado siempre mostrando un especial interés por todos mis avances.

A Joseba, mi apoyo incondicional y mi alma gemela. Gracias por tus conversaciones científicas y grandes ideas en general, tu sentido del humor y bailes, tu ayuda ilimitada y sin rechistar, por ser mi válvula de escape y soportar la enorme presión que ha acarreado esta tesis. Gracias por compartir tu vida conmigo. A Mila y José Mari por su ánimo y gran interés, con los que también han contribuido a la realización de este trabajo (ordenadores y UPS incluidos).

Finalmente, agradecer también al Gobierno Vasco la concesión de la beca de Formación de Personal Investigador con la que ha sido posible realizar esta tesis.

The author

Ainhoa Tolentino Chivite was born on 6th of October 1984 in San Sebastián, Spain. In 2002 she started her bachelor studies on Chemistry Science at the faculty of Chemistry of the Universidad del País Vasco (UPV) in San Sebastián and graduated in 2007 in Polymer Science specialty.

In 2007 she started her master studies on Polymers and Biopolymers at the faculty of Industrial Engineering (ETSEIB) of the Universitat Politécnica de Catalunya (UPC) in Barcelona, Spain. Her master dissertation titled "Study of biodegradable polyelectrolyte ionic complexes" was based on her research carried out within the group "Advanced and Biotechnological Industrial Polymers" under the supervision of Prof. Sebastián Muñoz Guerra. Ainhoa obtained a FPI Basque Government Research Fellowship and continued the research on her PhD project entitled "Ionic complexes of biodegradable polyelectrolytes." During the PhD she performed an international stay for 3 months in the Makromolekulare Chemie II group of Prof. Axel Müller at Universität Bayreuth (Germany). The results of her research studies are described in this Thesis.

Currently she is working as Project Researcher at Institut Català d'Investigació Química (ICIQ)-Henkel Joint Unit (Tarragona, Spain) developing the project "New water-based polyurethane-based dispersions for adhesive applications."

Scientific production derived from the Thesis

Scientific papers

1. Tolentino, A.; Martínez de Ilarduya, A.; Alla, A.; Muñoz-Guerra, S. Ionic complexes of polyacids and cationic surfactants. *Macromol. Symp*. **2010**, *296*, 265-271**.**

2. Tolentino, A.; Alla, A.; Martínez de Ilarduya, A.; Muñoz-Guerra, S. Comb-like ionic complexes of pectinic and alginic acids with alkyltrimetylammonium surfactants*. Carbohydr. Polym.* **2011**, *86*, 484-490.

3. Tolentino, A.; Alla, A.; Muñoz-Guerra, S. Nanocomposites of comb-like ionic complexes of bacterial poly(glutamic acid) with nanoclays. *Eur. Polym. J.* **2012**, *48*, 1838-1845.

4. Tolentino, A.; Alla, A.; Martínez de Ilarduya, A.; Muñoz-Guerra, S. Comb-like ionic complexes of hyaluronic acid with alkyltrimethylammonium surfactants. *Carbohydr. Polym.* **2013**, *92*, 691-696.

5. Tolentino, A.; León, S.; Alla, A.; Martínez de Ilarduya, A.; Muñoz-Guerra, S. Comblike ionic complexes of poly (γ-glutamic acid) and alkanoylcholines derived from fatty acids. *Macromolecules* **2013**, *46*, 1607-1617.

6. Tolentino, A.; León, S.; Alla, A.; Martínez de Ilarduya, A.; Muñoz-Guerra, S. The structure of poly (γ-glutamic acid)/nanoclay hybrids compatibilized by alkylammonium surfactants. *Eur. Polym. J.* **2013**, *49*, 2596–2609.

7. Tolentino, A.; Alla, A.; Martínez de Ilarduya, A.; Font-Bardia, M.; León, S.; Muñoz-Guerra, S. Thermal behavior of long-chain alkanoylcholine soaps. *RSC Advances* **2014**, *4*, 10738-10750.

8. Tolentino, A.; Alla, A.; Martínez de Ilarduya, A.; Muñoz-Guerra, S. Complexes of polyglutamic acid and long-chain alkanoylcholines: Nanoparticle formation and drug release. *Int. J. Biol. Mol.* **2014**. *Accepted.*

Conference proceedings

1. Tolentino, A.; Martínez de Ilarduya, A.; Alla, A.; Muñoz-Guerra, S. Ionic complexes of polyacids and cationic surfactants. Oral Communication (Muñoz-Guerra, S.) at European Polymer Congress EPF. Graz (Austria), 12^{th}-17^{th} July 2009.

2. Tolentino, A.; Alla, A.; Martínez de Ilarduya, A.; Muñoz-Guerra, S. Ionic complexes of polyuronic acids with cationic surfactants. Poster at X Reunión del Grupo Especializado de Polímeros GEP. Valladolid (Spain) 20^{th}-24^{th} September 2009.

3. Tolentino, A.; Alla, A.; Martínez de Ilarduya A, Muñoz-Guerra S. Hybrid nanocomposites made of bacterial poly (gamma-glutamic acid), cationic surfactants and modified clays. Poster at 6th Conference on Nanostructured Polymers and Nanocomposites ECNP. Madrid (Spain) 28^{th}-30^{th} April 2010.

4. Tolentino, A.; Alla, A.; Martínez de Ilarduya, A.; Muñoz-Guerra, S. Complejos iónicos de ácidos poliurónicos y surfactantes catiónicos. Oral communication at V Congreso de Jóvenes Investigadores en Polímeros JIP. Calella de Palafrugell (Spain) 2^{nd}-6^{th} May 2010.

5. Tolentino, A.; Alla, A.; Martínez de Ilarduya, A.; Muñoz-Guerra, S. Hybrid nanocomposites made of poly(γ-glutamic acid), cationic surfactants and modified clays. Poster at Hybrid Materials. Strasbourg (France) 6^{th}-10^{th} March 2011.

6. Tolentino, A.; Alla, A.; Martínez de Ilarduya, A.; Muñoz-Guerra, S. Ionic complexes of polyuronic acids with cationic surfactants. Poster at Hybrid Materials. Strasbourg (France) 6^{th}-10^{th} March 2011.

7. Tolentino, A.; Alla, A.; Martínez de Ilarduya, A.; Muñoz-Guerra, S. Thermal degradation of polyuronic acids and their ionic complexes. Poster at European Polymer Congress EPF, XII Grupo Especializado de Polímeros (GEP) Congress. Granada (Spain) 26^{th} June-1^{st} July 2011.

8. Tolentino, A.; León, S.; Alla, A.; Martínez de Ilarduya, A.; Muñoz Guerra, S. Comb-like ionic complexes of poly(γ- glutamic acid) and fatty acid choline esters. Poster at Frontiers in Polymer Science. Sitges (Spain) 21^{st}-23^{rd} May 2013.

9. Tolentino, A.; Alla, A.; Martínez de Ilarduya, A.; León, S.; Muñoz Guerra, S. Complexes of poly glutamic acid and choline surfactants for drug delivery. Poster at European Polymer Congress EPF. Pisa (Italy) 16^{th}-21^{st} June, 2013.